

TURKISH JOURNAL OF PHARMACEUTICAL SCIENCES



TURKISH JOURNAL OF PHARMACEUTICAL SCIENCES

Editor-in-Chief

Prof. Terken BAYDAR, Ph.D., E.R.T.
orcid.org/0000-0002-5497-9600
Hacettepe University, Faculty of Pharmacy,
Department of Toxicology, Ankara, TURKEY
tbaydar@hacettepe.edu.tr

Associate Editors

Prof. Samiye YABANOĞLU ÇİFTÇİ, Ph.D.
orcid.org/0000-0001-5467-0497
Hacettepe University, Faculty of Pharmacy,
Department of Biochemistry, Ankara, TURKEY
samiye@hacettepe.edu.tr

Assoc. Prof. Pınar ERKEKOĞLU, Ph.D., E.R.T.
orcid.org/0000-0003-4713-7672
Hacettepe University, Faculty of Pharmacy,
Department of Toxicology, Ankara, TURKEY
erkekp@hacettepe.edu.tr

Editorial Board

Prof. Fernanda BORGES, Ph.D.
orcid.org/0000-0003-1050-2402
Porto University, Faculty of Sciences, Department of
Chemistry and Biochemistry, Porto, PORTUGAL
fborges@fc.up.pt

Prof. Bezhan CHANKVETADZE, Ph.D.
orcid.org/0000-0003-2379-9815
Ivane Javakishvili Tbilisi State University, Institute
of Physical and Analytical Chemistry, Tbilisi,
GEORGIA
jpba_bezhan@yahoo.com

Prof. Dietmar FUCHS, Ph.D.
orcid.org/0000-0003-1627-9563
Innsbruck Medical University, Center for Chemistry
and Biomedicine, Institute of Biological Chemistry,
Biocenter, Innsbruck, AUSTRIA
dietmar.fuchs@i-med.ac.at

Prof. Satyajit D. Sarker, Ph.D.
orcid.org/0000-0003-4038-0514
Liverpool John Moores University, Liverpool,
UNITED KINGDOM
S.Sarker@ljmu.ac.uk

Prof. Luciano SASO, Ph.D.
orcid.org/0000-0003-4530-8706
Sapienze University, Faculty of Pharmacy
and Medicine, Department of Physiology and
Pharmacology "Vittorio Ersamer", Rome, ITALY
luciano.saso@uniroma1.it

Prof. Rob VERPOORTE, Ph.D.
orcid.org/0000-0001-6180-1424
Leiden University, Natural Products Laboratory,
Leiden, NETHERLANDS
verpoort@chem.leidenuniv.nl

Advisory Board

Prof. Nurettin ABACIOĞLU, Ph.D.
Kyrenia University, Faculty of Pharmacy,
Department of Pharmacology, Girne, TRNC,
CYPRUS

Prof. Kadriye BENKLİ, Ph.D.
Girne American University, Faculty of Pharmacy,
Department of Pharmaceutical Chemistry, Girne,
TRNC, CYPRUS

Prof. Arzu BEŞİKCİ, Ph.D.
Ankara University, Faculty of Pharmacy,
Department of Pharmacology, Ankara, TURKEY

Prof. Erem BİLENSOY, Ph.D.
Hacettepe University, Faculty of Pharmacy, Department
of Pharmaceutical Technology, Ankara, TURKEY

Prof. Hermann BOLT, Ph.D.
Dortmund University, Leibniz Research Centre, Institute
of Occupational Physiology, Dortmund, GERMANY

Prof. Erdal CEVHER, Ph.D.
İstanbul University Faculty of Pharmacy,
Department of Pharmaceutical Technology,
İstanbul, TURKEY

Prof. Nevin ERK, Ph.D.
Ankara University, Faculty of Pharmacy,
Department of Analytical Chemistry, Ankara,
TURKEY

Prof. Jean-Alain FEHRENTZ, Ph.D.
Montpellier University, Faculty of Pharmacy,
Institute of Biomolecules Max Mousseron,
Montpellier, FRANCE

Prof. Joerg KREUTER, Ph.D.
Johann Wolfgang Goethe University, Faculty of
Pharmacy, Institute of Pharmaceutical Technology,
Frankfurt, GERMANY

Prof. Christine LAFFORGUE, Ph.D.
Paris-Sud University, Faculty of Pharmacy,
Department of Dermopharmacology and
Cosmetology, Paris, FRANCE

Prof. Şule APIKOĞLU RABUŞ, Ph.D.
Marmara University, Faculty of Pharmacy,
Department of Clinical Pharmacy, İstanbul,
TURKEY

Prof. Robert RAPOPORT, Ph.D.
Cincinnati University, Faculty of Pharmacy,
Department of Pharmacology and Cell Biophysics,
Cincinnati, USA

Prof. Wolfgang SADEE, Ph.D.
Ohio State University, Center for
Pharmacogenomics, Ohio, USA

Prof. Hildebert WAGNER, Ph.D.
Ludwig-Maximilians University, Center for
Pharmaceutical Research, Institute of Pharmacy,
Munich, GERMANY

Assoc. Prof. Hande SİPAHİ, Ph.D.
Yeditepe University, Faculty of Pharmacy,
Department of Toxicology, İstanbul, TURKEY

Assoc. Prof. İpek SÜNTAR, Ph.D.
Gazi University, Faculty of Pharmacy, Department
of Pharmacognosy, Ankara, TURKEY

TURKISH JOURNAL OF PHARMACEUTICAL SCIENCES

Baş Editör

Terken BAYDAR, E.R.T. , Prof. Dr. E.R.T.
orcid.org/0000-0002-5497-9600
Hacettepe Üniversitesi, Eczacılık Fakültesi,
Toksikoloji Anabilim Dalı, Ankara, TÜRKİYE
tbaydar@hacettepe.edu.tr

Yardımcı Editörler

Samiye YABANOĞLU ÇİFTÇİ, Prof. Dr.
orcid.org/0000-0001-5467-0497
Hacettepe Üniversitesi, Eczacılık Fakültesi ,
Biyokimya Anabilim Dalı, Ankara, TÜRKİYE
samiye@hacettepe.edu.tr

Pınar ERKEKOĞLU, Doç. Dr. E.R.T.
orcid.org/0000-0003-4713-7672
Hacettepe Üniversitesi, Eczacılık Fakültesi,
Toksikoloji Anabilim Dalı, Ankara, TÜRKİYE
erkekp@hacettepe.edu.tr

Editörler Kurulu

Fernanda BORGES, Prof. Dr.
orcid.org/0000-0003-1050-2402
Porto Üniversitesi, Fen Fakültesi, Kimya ve
Biyokimya Anabilim Dalı, Porto, PORTEKİZ
fborges@fc.up.pt

Bezhan CHANKVETADZE, Prof. Dr.
orcid.org/0000-0003-2379-9815
Ivane Javakishvili Tiflis Devlet Üniversitesi, Fiziksel
ve Analitik Kimya Enstitüsü, Tiflis, GÜRCİSTAN
jpba_bezhan@yahoo.com

Dietmar FUCHS, Prof. Dr.
orcid.org/0000-0003-1627-9563
Innsbruck Tıp Üniversitesi, Kimya ve Biyotıp Merkezi,
Biyolojik Kimya Enstitüsü, Biocenter, Innsbruck,
AVUSTURYA
dietmar.fuchs@i-med.ac.at

Satyajit D. Sarker, Prof. Dr.
orcid.org/0000-0003-4038-0514
Liverpool John Moores Üniversitesi, Liverpool,
BİRLEŞİK KRALLIK
S.Sarker@ljmu.ac.uk

Luciano SASO, Prof. Dr.
orcid.org/0000-0003-4530-8706
Sapienza Üniversitesi, Eczacılık ve Tıp Fakültesi,
Fizyoloji ve Farmakoloji Anabilim Dalı "Vittorio
Erspamer", Roma, İTALYA
luciano.saso@uniroma1.it

Rob VERPOORTE, Prof. Dr.
orcid.org/0000-0001-6180-1424
Leiden Üniversitesi, Doğal Ürünler Laboratuvarı,
Leiden, HOLLANDA
verpoort@chem.leidenuniv.nl

Danışma Kurulu

Nurettin ABACIOĞLU, Prof. Dr.
Girne Üniversitesi, Eczacılık Fakültesi, Farmakoloji
Anabilim Dalı, Girne, TRNC, KIBRIS

Kadriye BENKLİ, Prof. Dr.
Girne Amerikan Üniversitesi, Eczacılık Fakültesi,
Farmasötik Anabilim Dalı, Girne, TRNC, KIBRIS

Arzu BEŞİKCİ, Prof. Dr.
Ankara Üniversitesi, Eczacılık Fakültesi,
Farmakoloji Anabilim Dalı, Ankara, TÜRKİYE

Erem BİLENSOY, Prof. Dr.
Hacettepe Üniversitesi, Eczacılık Fakültesi,
Farmasötik Anabilim Dalı, Ankara, TÜRKİYE

Hermann BOLT, Prof. Dr.
Dortmund Üniversitesi, Leibniz Araştırma Merkezi,
Mesleki Fizyoloji Enstitüsü, Dortmund,
ALMANYA

Erdal CEVHER, Prof. Dr.
İstanbul Üniversitesi Eczacılık Fakültesi,
Farmasötik Anabilim Dalı, İstanbul, TÜRKİYE

Nevin ERK, Prof. Dr.
Ankara Üniversitesi, Eczacılık Fakültesi, Analitik
Kimya Anabilim Dalı, Ankara, TÜRKİYE

Jean-Alain FEHRENTZ, Prof. Dr.
Montpellier Üniversitesi, Eczacılık Fakültesi,
Biyomoleküller Enstitüsü Max Mousseron,
Montpellier, FRANSA

Joerg KREUTER, Prof. Dr.
Johann Wolfgang Goethe Üniversitesi, Eczacılık
Fakültesi, Farmasötik Teknoloji Enstitüsü,
Frankfurt, ALMANYA

Christine LAFFORGUE, Prof. Dr.
Paris-Sud Üniversitesi, Eczacılık Fakültesi,
Dermofarmakoloji ve Kozmetoloji Bölümü, Paris,
FRANSA

Şule APİKOĞLU RABUŞ, Prof. Dr.
Marmara Üniversitesi, Eczacılık Fakültesi, Klinik
Eczacılık Anabilim Dalı, İstanbul, TÜRKİYE

Robert RAPOPORT, Prof. Dr.
Cincinnati Üniversitesi, Eczacılık Fakültesi,
Farmakoloji ve Hücre Biyofiziği Bölümü, Cincinnati,
ABD

Wolfgang SADEE, Prof. Dr.
Ohio Eyalet Üniversitesi, Farmakogenomik
Merkezi, Ohio, ABD

Hildebert WAGNER, Prof. Dr.
Ludwig-Maximilians Üniversitesi, Farmasötik
Araştırma Merkezi, Eczacılık Enstitüsü, Münih,
ALMANYA

Hande SİPAHİ, Doç. Dr.
Yeditepe Üniversitesi, Eczacılık Fakültesi,
Toksikoloji Anabilim Dalı, İstanbul, TÜRKİYE

İpek SÜNTAR, Doç. Dr.
Gazi Üniversitesi, Eczacılık Fakültesi,
Farmakognози Anabilim Dalı, Ankara, TÜRKİYE

TURKISH JOURNAL OF PHARMACEUTICAL SCIENCES

AIMS AND SCOPE

The Turkish Journal of Pharmaceutical Sciences is the only scientific periodical publication of the Turkish Pharmacists' Association and has been published since April 2004.

Turkish Journal of Pharmaceutical Sciences journal is regularly published 6 times in a year (February, April, June, August, October, December). The issuing body of the journal is Galenos Yayınevi/Publishing House level.

The aim of Turkish Journal of Pharmaceutical Sciences is to publish original research papers of the highest scientific and clinical value at an international level. The target audience includes specialists and professionals in all fields of pharmaceutical sciences.

The editorial policies are based on the "Recommendations for the Conduct, Reporting, Editing, and Publication of Scholarly Work in Medical Journals (ICMJE Recommendations)" by the International Committee of Medical Journal Editors (2013, archived at <http://www.icmje.org/>) rules.

Editorial Independence

Turkish Journal of Pharmaceutical Sciences is an independent journal with independent editors and principles and has no commercial relationship with the commercial product, drug or pharmaceutical company regarding decisions and review processes upon articles.

ABSTRACTED/INDEXED IN

PubMed Central
Web of Science-Emerging Sources Citation Index (ESCI)
SCOPUS SJR
TÜBİTAK/ULAKBİM TR Dizin
Directory of Open Access Journals (DOAJ)
ProQuest
Chemical Abstracts Service (CAS)
EBSCO
EMBASE
GALE
Index Copernicus
Analytical Abstracts
International Pharmaceutical Abstracts (IPA)
Medicinal & Aromatic Plants Abstracts (MAPA)
British Library
CSIR INDIA
GOALI
Hinari
OARE
ARDI
AGORA
Türkiye Atıf Dizini
Türk Medline
UDL-EDGE
J- Gate
Ideonline
ROOTINDEXING

OPEN ACCESS POLICY

This journal provides immediate open access to its content on the principle that making research freely available to the public supports a greater global exchange of knowledge.

Open Access Policy is based on the rules of the Budapest Open Access Initiative (BOAI) <http://www.budapestopenaccessinitiative.org/>. By "open access" to peer-reviewed research literature, we mean its free availability on the public internet, permitting any users to read, download, copy, distribute, print, search, or link to the full texts of these articles, crawl them for indexing, pass them as data to software, or use them for any other lawful purpose, without financial, legal, or technical barriers other than those inseparable from gaining access to the internet itself. The only constraint on reproduction and distribution, and the only role for copyright in this domain, should be to give authors control over the integrity of their work and the right to be properly acknowledged and cited.

CORRESPONDENCE ADDRESS

All correspondence should be directed to the Turkish Journal of Pharmaceutical Sciences editorial board;

Post Address: Turkish Pharmacists' Association, Mustafa Kemal Mah 2147.Sok No:3 06510 Çankaya/Ankara, TURKEY
Phone: +90 (312) 409 81 00
Fax: +90 (312) 409 81 09
Web Page: <http://turkjps.org>
E-mail: teb@teb.org.tr

PERMISSIONS

Requests for permission to reproduce published material should be sent to the publisher.

Publisher: Erkan Mor
Address: Molla Gürani Mah. Kaçamak Sok. 21/1 Fındıkzade, Fatih, İstanbul, Turkey
Telephone: +90 212 621 99 25
Fax: +90 212 621 99 27
Web page: <http://www.galenos.com.tr/en>
E-mail: info@galenos.com.tr

ISSUING BODY CORRESPONDING ADDRESS

Issuing Body : Galenos Yayınevi
Address: Molla Gürani Mah. Kaçamak Sk. No: 21/1, 34093 İstanbul, Turkey
Phone: +90 212 621 99 25 Fax: +90 212 621 99 27
E-mail: info@galenos.com.tr

MATERIAL DISCLAIMER

The author(s) is (are) responsible for the articles published in the JOURNAL. The editor, editorial board and publisher do not accept any responsibility for the articles.

This work is licensed under a Creative Commons Attribution-NonCommercial-NoDerivatives 4.0 International License.



Galenos Publishing House
Owner and Publisher
Derya Mor
Erkan Mor
Publication Coordinator
Burak Sever
Web Coordinators
Fuat Hocalar
Turgay Akpınar
Graphics Department
Ayda Alaca
Çiğdem Birinci
Gülşah Özgül

Project Coordinators
Hatice Sever
Gamze Aksoy
Saliha Tuğçe Evin
Melike Eren
Duygu Yıldırım
Pınar Akpınar

Project Assistants
Gülşay Akın
Özlem Çelik
Rabia Palazoğlu
Research&Development
Mert Can Köse
Mevlûde Özlem Akgüney
Finance Coordinator
Sevinç Çakmak

Publisher Contact

Address: Molla Gürani Mah. Kaçamak Sk. No: 21/1
34093 İstanbul, Turkey
Phone: +90 (212) 621 99 25 Fax: +90 (212) 621 99 27
E-mail: info@galenos.com.tr/yayin@galenos.com.tr
Web: www.galenos.com.tr | Publisher Certificate Number: 14521

Printing at: Özgün Basım Tanıtım San. Tic. Ltd. Şti.
Yeşilce Mah. Aytakin Sok. Oto Sanayi Sitesi No: 21 Kat: 2
Seyrantepe Sanayi, Kağıthane, İstanbul, Türkiye
Telefon/Phone: +90 (212) 280 00 09 Sertifika No: 48150

Printing Date: August 2020

ISSN: 1304-530X

International scientific journal published quarterly.

TURKISH JOURNAL OF PHARMACEUTICAL SCIENCES

INSTRUCTIONS TO AUTHORS

Turkish Journal of Pharmaceutical Sciences journal is published 6 times (February, April, June, August, October, December) per year and publishes the following articles:

- Research articles
- Reviews (only upon the request or consent of the Editorial Board)
- Preliminary results/Short communications/Technical notes/Letters to the Editor in every field of pharmaceutical sciences.

The publication language of the journal is English.

The Turkish Journal of Pharmaceutical Sciences does not charge any article submission or processing charges.

A manuscript will be considered only with the understanding that it is an original contribution that has not been published elsewhere.

The Journal should be abbreviated as "Turk J Pharm Sci" when referenced.

The scientific and ethical liability of the manuscripts belongs to the authors and the copyright of the manuscripts belongs to the Journal. Authors are responsible for the contents of the manuscript and accuracy of the references. All manuscripts submitted for publication must be accompanied by the Copyright Transfer Form [copyright transfer]. Once this form, signed by all the authors, has been submitted, it is understood that neither the manuscript nor the data it contains have been submitted elsewhere or previously published and authors declare the statement of scientific contributions and responsibilities of all authors.

Experimental, clinical and drug studies requiring approval by an ethics committee must be submitted to the JOURNAL with an ethics committee approval report including approval number confirming that the study was conducted in accordance with international agreements and the Declaration of Helsinki (revised 2013) (<http://www.wma.net/en/30publications/10policies/b3/>). The approval of the ethics committee and the fact that informed consent was given by the patients should be indicated in the Materials and Methods section. In experimental animal studies, the authors should indicate that the procedures followed were in accordance with animal rights as per the Guide for the Care and Use of Laboratory Animals (<http://oacu.od.nih.gov/regs/guide/guide.pdf>) and they should obtain animal ethics committee approval.

Authors must provide disclosure/acknowledgment of financial or material support, if any was received, for the current study.

If the article includes any direct or indirect commercial links or if any institution provided material support to the study, authors must state in the cover letter that they have no relationship with the commercial product, drug, pharmaceutical company, etc. concerned; or specify the type of relationship (consultant, other agreements), if any.

Authors must provide a statement on the absence of conflicts of interest among the authors and provide authorship contributions.

All manuscripts submitted to the journal are screened for plagiarism using the 'iThenticate' software. Results indicating plagiarism may result in manuscripts being returned or rejected.

The Review Process

This is an independent international journal based on double-blind peer-review principles. The manuscript is assigned to the Editor-in-Chief, who reviews the manuscript and makes an initial decision based on manuscript quality and editorial priorities. Manuscripts that pass initial evaluation

are sent for external peer review, and the Editor-in-Chief assigns an Associate Editor. The Associate Editor sends the manuscript to at least two reviewers (internal and/or external reviewers). The Associate Editor recommends a decision based on the reviewers' recommendations and returns the manuscript to the Editor-in-Chief. The Editor-in-Chief makes a final decision based on editorial priorities, manuscript quality, and reviewer recommendations. If there are any conflicting recommendations from reviewers, the Editor-in-Chief can assign a new reviewer.

The scientific board guiding the selection of the papers to be published in the Journal consists of elected experts of the Journal and if necessary, selected from national and international authorities. The Editor-in-Chief, Associate Editors may make minor corrections to accepted manuscripts that do not change the main text of the paper.

In case of any suspicion or claim regarding scientific shortcomings or ethical infringement, the Journal reserves the right to submit the manuscript to the supporting institutions or other authorities for investigation. The Journal accepts the responsibility of initiating action but does not undertake any responsibility for an actual investigation or any power of decision.

The Editorial Policies and General Guidelines for manuscript preparation specified below are based on "Recommendations for the Conduct, Reporting, Editing, and Publication of Scholarly Work in Medical Journals (ICMJE Recommendations)" by the International Committee of Medical Journal Editors (2013, archived at <http://www.icmje.org/>).

Preparation of research articles, systematic reviews and meta-analyses must comply with study design guidelines:

CONSORT statement for randomized controlled trials (Moher D, Schultz KF, Altman D, for the CONSORT Group. The CONSORT statement revised recommendations for improving the quality of reports of parallel group randomized trials. *JAMA* 2001; 285: 1987-91) (<http://www.consort-statement.org/>);

PRISMA statement of preferred reporting items for systematic reviews and meta-analyses (Moher D, Liberati A, Tetzlaff J, Altman DG, The PRISMA Group. Preferred Reporting Items for Systematic Reviews and Meta-Analyses: The PRISMA Statement. *PLoS Med* 2009; 6(7): e1000097.) (<http://www.prisma-statement.org/>);

STARD checklist for the reporting of studies of diagnostic accuracy (Bossuyt PM, Reitsma JB, Bruns DE, Gatsonis CA, Glasziou PP, Irwig LM, et al., for the STARD Group. Towards complete and accurate reporting of studies of diagnostic accuracy: the STARD initiative. *Ann Intern Med* 2003;138:40-4.) (<http://www.stard-statement.org/>);

STROBE statement, a checklist of items that should be included in reports of observational studies (<http://www.strobe-statement.org/>);

MOOSE guidelines for meta-analysis and systemic reviews of observational studies (Stroup DF, Berlin JA, Morton SC, et al. Meta-analysis of observational studies in epidemiology: a proposal for reporting Meta-analysis of observational Studies in Epidemiology (MOOSE) group. *JAMA* 2000; 283: 2008-12).

GENERAL GUIDELINES

Manuscripts can only be submitted electronically through the Journal Agent website (<http://journalagent.com/tjps/>) after creating an account. This system allows online submission and review.

TURKISH JOURNAL OF PHARMACEUTICAL SCIENCES

INSTRUCTIONS TO AUTHORS

Format: Manuscripts should be prepared using Microsoft Word, size A4 with 2.5 cm margins on all sides, 12 pt Arial font and 1.5 line spacing.

Abbreviations: Abbreviations should be defined at first mention and used consistently thereafter. Internationally accepted abbreviations should be used; refer to scientific writing guides as necessary.

Cover letter: The cover letter should include statements about manuscript type, single-Journal submission affirmation, conflict of interest statement, sources of outside funding, equipment (if applicable), for original research articles.

ETHICS COMMITTEE APPROVAL

The editorial board and our reviewers systematically ask for ethics committee approval from every research manuscript submitted to the Turkish Journal of Pharmaceutical Sciences. If a submitted manuscript does not have ethical approval, which is necessary for every human or animal experiment as stated in international ethical guidelines, it must be rejected on the first evaluation.

Research involving animals should be conducted with the same rigor as research in humans; the Turkish Journal of Pharmaceutical Sciences asks original approval document to show implements the 3Rs principles. If a study does not have ethics committee approval or authors claim that their study does not need approval, the study is consulted to and evaluated by the editorial board for approval.

SIMILARITY

The Turkish Journal of Pharmaceutical Sciences is routinely looking for similarity index score from every manuscript submitted before evaluation by the editorial board and reviewers. The journal uses iThenticate plagiarism checker software to verify the originality of written work. There is no acceptable similarity index; but, exceptions are made for similarities less than 15 %.

REFERENCES

Authors are solely responsible for the accuracy of all references.

In-text citations: References should be indicated as a superscript immediately after the period/full stop of the relevant sentence. If the author(s) of a reference is/are indicated at the beginning of the sentence, this reference should be written as a superscript immediately after the author's name. If relevant research has been conducted in Turkey or by Turkish investigators, these studies should be given priority while citing the literature.

Presentations presented in congresses, unpublished manuscripts, theses, Internet addresses, and personal interviews or experiences should not be indicated as references. If such references are used, they should be indicated in parentheses at the end of the relevant sentence in the text, without reference number and written in full, in order to clarify their nature.

References section: References should be numbered consecutively in the order in which they are first mentioned in the text. All authors should be listed regardless of number. The titles of Journals should be abbreviated according to the style used in the Index Medicus.

Reference Format

Journal: Last name(s) of the author(s) and initials, article title, publication title and its original abbreviation, publication date, volume, the inclusive page numbers. Example: Collin JR, Rathbun JE. Involitional entropion: a review with evaluation of a procedure. Arch Ophthalmol. 1978;96:1058-1064.

Book: Last name(s) of the author(s) and initials, book title, edition, place of publication, date of publication and inclusive page numbers of the extract cited.

Example: Herbert L. The Infectious Diseases (1st ed). Philadelphia; Mosby Harcourt; 1999:11;1-8.

Book Chapter: Last name(s) of the author(s) and initials, chapter title, book editors, book title, edition, place of publication, date of publication and inclusive page numbers of the cited piece.

Example: O'Brien TP, Green WR. Periocular Infections. In: Feigin RD, Cherry JD, eds. Textbook of Pediatric Infectious Diseases (4th ed). Philadelphia; W.B. Saunders Company;1998:1273-1278.

Books in which the editor and author are the same person: Last name(s) of the author(s) and initials, chapter title, book editors, book title, edition, place of publication, date of publication and inclusive page numbers of the cited piece. Example: Solcia E, Capella C, Kloppel G. Tumors of the exocrine pancreas. In: Solcia E, Capella C, Kloppel G, eds. Tumors of the Pancreas. 2nd ed. Washington: Armed Forces Institute of Pathology; 1997:145-210.

TABLES, GRAPHICS, FIGURES, AND IMAGES

All visual materials together with their legends should be located on separate pages that follow the main text.

Images: Images (pictures) should be numbered and include a brief title. Permission to reproduce pictures that were published elsewhere must be included. All pictures should be of the highest quality possible, in JPEG format, and at a minimum resolution of 300 dpi.

Tables, Graphics, Figures: All tables, graphics or figures should be enumerated according to their sequence within the text and a brief descriptive caption should be written. Any abbreviations used should be defined in the accompanying legend. Tables in particular should be explanatory and facilitate readers' understanding of the manuscript, and should not repeat data presented in the main text.

MANUSCRIPT TYPES

Original Articles

Clinical research should comprise clinical observation, new techniques or laboratories studies. Original research articles should include title, structured abstract, key words relevant to the content of the article, introduction, materials and methods, results, discussion, study limitations, conclusion references, tables/figures/images and acknowledgement sections. Title, abstract and key words should be written in both Turkish and English. The manuscript should be formatted in accordance with the above-mentioned guidelines and should not exceed 16 A4 pages.

Title Page: This page should include the title of the manuscript, short title, name(s) of the authors and author information. The following descriptions should be stated in the given order:

TURKISH

JOURNAL OF PHARMACEUTICAL SCIENCES

INSTRUCTIONS TO AUTHORS

1. Title of the manuscript (Turkish and English), as concise and explanatory as possible, including no abbreviations, up to 135 characters
2. Short title (Turkish and English), up to 60 characters
3. Name(s) and surname(s) of the author(s) (without abbreviations and academic titles) and affiliations
4. Name, address, e-mail, phone and fax number of the corresponding author
5. The place and date of scientific meeting in which the manuscript was presented and its abstract published in the abstract book, if applicable

Abstract: A summary of the manuscript should be written in both Turkish and English. References should not be cited in the abstract. Use of abbreviations should be avoided as much as possible; if any abbreviations are used, they must be taken into consideration independently of the abbreviations used in the text. For original articles, the structured abstract should include the following sub-headings:

Objectives: The aim of the study should be clearly stated.

Materials and Methods: The study and standard criteria used should be defined; it should also be indicated whether the study is randomized or not, whether it is retrospective or prospective, and the statistical methods applied should be indicated, if applicable.

Results: The detailed results of the study should be given and the statistical significance level should be indicated.

Conclusion: Should summarize the results of the study, the clinical applicability of the results should be defined, and the favorable and unfavorable aspects should be declared.

Keywords: A list of minimum 3, but no more than 5 key words must follow the abstract. Key words in English should be consistent with "Medical Subject Headings (MESH)" (www.nlm.nih.gov/mesh/MBrowser.html). Turkish key words should be direct translations of the terms in MESH.

Original research articles should have the following sections:

Introduction: Should consist of a brief explanation of the topic and indicate the objective of the study, supported by information from the literature.

Materials and Methods: The study plan should be clearly described, indicating whether the study is randomized or not, whether it is retrospective or prospective, the number of trials, the characteristics, and the statistical methods used.

Results: The results of the study should be stated, with tables/figures given in numerical order; the results should be evaluated according to the statistical analysis methods applied. See General Guidelines for details about the preparation of visual material.

Discussion: The study results should be discussed in terms of their favorable and unfavorable aspects and they should be compared with the literature. The conclusion of the study should be highlighted.

Study Limitations: Limitations of the study should be discussed. In addition, an evaluation of the implications of the obtained findings/results for future research should be outlined.

Conclusion: The conclusion of the study should be highlighted.

Acknowledgements: Any technical or financial support or editorial contributions (statistical analysis, English/Turkish evaluation) towards the study should appear at the end of the article.

References: Authors are responsible for the accuracy of the references. See General Guidelines for details about the usage and formatting required.

Review Articles

Review articles can address any aspect of clinical or laboratory pharmaceuticals. Review articles must provide critical analyses of contemporary evidence and provide directions of or future research. Most review articles are commissioned, but other review submissions are also welcome. Before sending a review, discussion with the editor is recommended.

Reviews articles analyze topics in depth, independently and objectively. The first chapter should include the title in Turkish and English, an unstructured summary and key words. Source of all citations should be indicated. The entire text should not exceed 25 pages (A4, formatted as specified above).

TURKISH JOURNAL OF PHARMACEUTICAL SCIENCES

CONTENTS

Letter to Editor

- 357 Can Pharmacists be More Effective Regarding the Proper Use of Face Masks by the Public During the COVID-19 Pandemic?
Eczacılar COVID-19 Salgını Sırasında Yüz Maskelerinin Toplum Tarafından Doğru Kullanılmasında Daha Etkili Olabilir mi?
Nesliğül ÖZDEMİR, Melda BAHAP, Ayçe ÇELİKLER

Original Articles

- 359 Development and Statistical Optimization of Solid Lipid Nanoparticle Formulations of Fluticasone Propionate
Flutikazon Propiyonatının Katı Lipit Nanopartikül Formülasyonlarının Geliştirilmesi ve İstatistiksel Optimizasyonu
Gülin AMASYA, Ceyda Tuba ŞENGEL TÜRK, Ulya BADILLI, Nilüfer TARIMCI
- 367 Evaluation of Lactose-Based Direct Tableting Agents' Compressibility Behavior Using a Compaction Simulator
Sıkıştırma Simülatörü Kullanarak Laktoz Bazlı Doğrudan Tabletleme Ajanlarının Sıkıştırılabilir Davranışlarının Değerlendirilmesi
Yıldız ÖZALP, Motunrayo M. ONAYO, Nailla JIWA
- 372 Determining the Best Poloxamer Carrier for Thiocolchicoside Solid Dispersions
Tiyokolşikosid Katı Dispersiyonları İçin En İyi Poloksamer Taşıyıcının Belirlenmesi
Hemanth ANNEPOGU, Hindustan Abdul AHAD, Devanna NAYAKANTI
- 381 The Formulation of Methylene Blue Encapsulated, Tc-99m Labeled Multifunctional Liposomes for Sentinel Lymph Node Imaging and Therapy
Sentinel Lenf Nodu Görüntüleme ve Tedavisi İçin Metilen Mavisi Enkapsüle Edilmiş, Tc-99m İşaretli Çok-Fonksiyonlu Lipozomların Formülasyonu
Mine SİLİNDİR GÜNAY
- 388 Development of Bioadhesive Buccal Tablets of Nicorandil Using a Factorial Approach
Faktöriyel Yaklaşım ile Nikorandil İçeren Biyoadeziv Bukkal Tabletlerin Geliştirilmesi
Rajendra KOTADIYA, Karan SHAH
- 398 Electrochemical Determination of Rifampicin Based on Its Oxidation Using Multi-Walled Carbon Nanotube-Modified Glassy Carbon Electrodes
Çok Duvarlı Karbon Nanotüp Modifiye Camı Karbon Elektrot Kullanılarak Rifampisin Oksidasyonuna Dayalı Elektrokimyasal Tayini
Dilek KUL
- 408 Investigation of the Peripheral Analgesic Activity of Oxicams and Their Combinations with Caffeine
Oksikamların ve Kafein ile Kombinasyonlarının Periferik Analjezik Aktivitelerinin İncelenmesi
Anna SYROVA, Larisa LUKYANOVA, Svetlana KOZUB, Oksana ZAVADA, Olga LEVASHOVA, Viktor SHAPOSHNIK
- 412 Green Synthesis and Characterization of Copper Nanoparticles and Their Effects on Liver Function and Hematological Parameters in Mice
Bakır Nanopartiküllerinin Yeşil Sentezi, Karakterizasyonu, Farelerde Karaciğer İşlevi ve Hematolojik Parametreler Üzerine Etkileri
Mehrdad KHATAMI, Katrin EBRAHIMI, Nasrin GALEHDAR, Mohammad Nabi MORADI, Alireza MOAYYEDKAZEMI
- 417 Molecular Docking Simulation Studies of Curcumin and Its Derivatives as Cyclin-Dependent Kinase 2 Inhibitors
Siklin Bağımlı Kinaz 2 İnhibitörü Olarak Kurkumin ve Türevlerinin Moleküler Kenetlenme Simülasyonları
Riyadi SUMIRTANURDIN, Shafira SUNGKAR, Yasarah HISPRASTIN, Kenny Dwi SIDHARTA, Dea Dian NURHIKMAH
- 424 Ferulic Acid Prevents Angiogenesis Through Cyclooxygenase-2 and Vascular Endothelial Growth Factor in the Chick Embryo Chorioallantoic Membrane Model
Ferulik Asitin Tavuk Embriyo Koriyoallantoik Membran Modelinde Siklooksijenaz 2 ve Vasküler Endotel Büyüme Faktörü Üzerinden Anjiyojenezi Önlemesi
Juni EKOWATI, Iwan Sahrial HAMID, Nuzul Wahyuning DIYAH, Siswandono SISWANDONO
- 432 Safety Assessment of Vanillic Acid: Subacute Oral Toxicity Studies in Wistar Rats
Vanilik Asitin Güvenlik Değerlendirmesi: Wistar Sıçanlarında Subakut Oral Toksikite Çalışmaları
Anwarbaig Chandbaig MIRZA, Shital Sharad PANCHAL
- 440 The Effect of *Rusa unicolor* Antler Deer Extracts from East Kalimantan in Bone Turnover Cell Model
Doğu Kalimantan'dan Rusa unicolor Geyiği Boynuzu Ekstraktlarının Kemik Dönüşümü Hücre Modelleri Üzerine Etkisi
Retno WIDYOWATI, Suciati SUCIATI, Dewi Melani HARYADI, Hsin-I CHANG, IPG Ngurah SURYAWAN, Agung Widi UTAMA
- 446 Cytotoxic, Genotoxic, and Apoptotic Effects of Nickel Oxide Nanoparticles in Intestinal Epithelial Cells
Nikel Oksit Nanopartiküllerinin Bağırsak Epitel Hücreleri Üzerine Sitotoksik, Genotoksik ve Apoptotik Etkileri
Mahmoud ABUDAYYAK, Elif GÜZEL, Gül ÖZHAN

TURKISH

JOURNAL OF PHARMACEUTICAL SCIENCES

CONTENTS

- 452 Evaluation of the Possible Role of miRNAs in Chemical Allergen Potency
miRNA'ların Kimyasal Alerjen Potansiyellerinin Olası Rollerinin Değerlendirilmesi
Hatice Gül ANLAR, Valentina GALBIATI, Emanuela CORSINI, Nurşen BAŞARAN

Review

- 457 Toxicological Evaluation of Bisphenol A and Its Analogues
Bisfenol A ve Analoglarının Toksikolojik Değerlendirilmesi
İrem İYİGÜNDOĞDU, Aylin ÜSTÜNDAĞ, Yalçın DUYDU

PUBLICATION NAME	Turkish Journal of Pharmaceutical Sciences
TYPE OF PUBLICATION	Vernacular Publication
PERIOD AND LANGUAGE	Bimonthly-English
OWNER	Erdoğan ÇOLAK on behalf of the Turkish Pharmacists' Association
EDITOR-IN-CHIEF	Prof.Terken BAYDAR, Ph.D.
ADDRESS OF PUBLICATION	Turkish Pharmacists' Association, Mustafa Kemal Mah 2147.Sok No:3 06510 Çankaya/ Ankara, TURKEY

TURKISH JOURNAL OF PHARMACEUTICAL SCIENCES

Volume: 17, No: 4, Year: 2020

CONTENTS

Letter to Editor

- Can Pharmacists be More Effective Regarding the Proper Use of Face Masks by the Public During the COVID-19 Pandemic?
Neslişül ÖZDEMİR, Melda BAHAP, Ayçe ÇELİKİR 357

Original Articles

- Development and Statistical Optimization of Solid Lipid Nanoparticle Formulations of Fluticasone Propionate
Gülin AMASYA, Ceyda Tuba ŞENGEL TÜRK, Ulya BADILLI, Nilüfer TARIMCI 359
- Evaluation of Lactose-Based Direct Tableting Agents' Compressibility Behavior Using a Compaction Simulator
Yıldız ÖZALP, Motunrayo M. ONAYO, Nailla JIWA 367
- Determining the Best Poloxamer Carrier for Thiocolchicoside Solid Dispersions
Hemanth ANNEPOGU, Hindustan Abdul AHAD, Devanna NAYAKANTI 372
- The Formulation of Methylene Blue Encapsulated, Tc-99m Labeled Multifunctional Liposomes for Sentinel Lymph Node Imaging and Therapy
Mine SİLİNDİR GÜNAY 381
- Development of Bioadhesive Buccal Tablets of Nicorandil Using a Factorial Approach
Rajendra KOTADIYA, Karan SHAH 388
- Electrochemical Determination of Rifampicin Based on Its Oxidation Using Multi-Walled Carbon Nanotube-Modified Glassy Carbon Electrodes
Dilek KUL 398
- Investigation of the Peripheral Analgesic Activity of Oxicams and Their Combinations with Caffeine
Anna SYROVA, Larisa LUKYANOVA, Svetlana KOZUB, Oksana ZAVADA, Olga LEVASHOVA, Viktor SHAPOSHNIK 408
- Green Synthesis and Characterization of Copper Nanoparticles and Their Effects on Liver Function and Hematological Parameters in Mice
Mehrdad KHATAMI, Katrin EBRAHIMI, Nasrin GALEHDAR, Mohammad Nabi MORADI, Alireza MOAYYEDKAZEMI 412
- Molecular Docking Simulation Studies of Curcumin and Its Derivatives as Cyclin-Dependent Kinase 2 Inhibitors
Riyadi SUMIRTANURDIN, Shafira SUNGKAR, Yasarah HISPRASTIN, Kenny Dwi SIDHARTA, Dea Dian NURHIKMAH 417
- Ferulic Acid Prevents Angiogenesis Through Cyclooxygenase-2 and Vascular Endothelial Growth Factor in the Chick Embryo Chorioallantoic Membrane Model
Juni EKOWATI, Iwan Sahrial HAMID, Nuzul Wahyuning DIYAH, Siswandono SISWANDONO 424
- Safety Assessment of Vanillic Acid: Subacute Oral Toxicity Studies in Wistar Rats
Anwarbaig Chandbaig MIRZA, Shital Sharad PANCHAL 432
- The Effect of *Rusa unicorn* Antler Horn Extracts from East Kalimantan in Bone Turnover Cell Model
Retno WIDYOWATI, Suciati SUCIATI, Dewi Melani HARYADI, Hsin-I CHANG, IPG Ngurah SURYAWAN, Agung Widi UTAMA 440
- Cytotoxic, Genotoxic, and Apoptotic Effects of Nickel Oxide Nanoparticles in Intestinal Epithelial Cells
Mahmoud ABUDAYYAK, Elif GÜZEL, Gül ÖZHAN 446
- Evaluation of the Possible Role of miRNAs in Chemical Allergen Potency
Hatice Gül ANLAR, Valentina GALBIATI, Emanuela CORSINI, Nurşen BAŞARAN 452

Review

- Toxicological Evaluation of Bisphenol A and Its Analogues
İrem İYİGÜNDOĞDU, Aylin ÜSTÜNDAĞ, Yalçın DUYDU 457



Can Pharmacists be More Effective Regarding the Proper Use of Face Masks by the Public During the COVID-19 Pandemic?

Eczacılar COVID-19 Salgını Sırasında Yüz Maskelerinin Toplum Tarafından Doğru Kullanılmasında Daha Etkili Olabilir mi?

© Nesligül ÖZDEMİR*, © Melda BAHAP, © Ayçe ÇELİKER

Hacettepe University Faculty of Pharmacy, Department of Clinical Pharmacy, Ankara, Turkey

Key words: Face mask, pharmacist, COVID-19

Anahtar Kelimeler: Yüz maskesi, eczacı, COVID-19

Dear Editor,

COVID-19 disease has spread quickly throughout the world after it was first identified in Wuhan, China. Since the outbreak was accepted as a pandemic by the World Health Organization, governments/health authorities have started to announce and implement preventive and protective measures against the disease. Using face masks is one of these methods of protection. At this point, at the beginning some governments/health authorities recommended face masks only for those who have respiratory symptoms or are vulnerable to infections.¹ Currently, increasing numbers of agencies and governments are advocating that the general population should wear masks, besides health professionals. The use of a face mask has become common whether the authorities have recommended it or not. For effective prevention and protection from respiratory diseases wearing a face mask in the correct way is an important issue. When the public's behavior during this pandemic is evaluated, it is seen that many do not use masks correctly. Touching the front of the mask, touching the face and other surfaces without washing the hands after removing the mask, and using disposable masks repeatedly are incorrect practices seen among the public. Many bacteria, viruses, and

fungi accumulate on the outer surface, especially the inner side of the mask.² In the study conducted by Chughtai et al.² when surgical masks used by healthcare workers were examined, 10% of the mask users had respiratory virus contamination and the most contamination was observed with adenovirus, bocavirus, and influenza virus. Contamination possibility increased 6 hours after wearing the mask. Although healthcare workers are knowledgeable about the vital function of protective equipment and use it correctly, the public's knowledge and ability regarding correct equipment use appear insufficient. Therefore, incorrect use increases the risk of contamination to both the wearer and those around. When we observe population behavior towards compliance with protective measures for pandemic diseases we see that as well as unchangeable factors such as age and sex, comparable factors such as perceived susceptibility have important impacts. According to Sim et al.³ perceived susceptibility appears to be the most significant factor influencing compliance with mask wearing. They suggest that, to increase the public's perceived susceptibility, they should be educated about contagious diseases. Eastwood et al.⁴ stated that the community was more likely to seek information about the outbreak from general practitioners

*Correspondence: E-mail: nesliozdmr@hotmail.com, Phone: +90 536 978 72 51 ORCID-ID: orcid.org/0000-0003-2551-9549

Received: 19.06.2020, Accepted: 22.07.2020

©Turk J Pharm Sci, Published by Galenos Publishing House.

and other healthcare professionals than the national health hotline set up for rapid information dissemination during the H1N1 pandemic. Pharmacists, as healthcare professionals effective in providing preventive public health services by delivering necessary health interventions about lifestyle changes in chronic diseases, vaccination, sexual health, and stopping smoking and alcohol consumption, play an important role in consulting during extraordinary situations such as pandemics as well. They can prevent incorrect use of masks by explaining preventive measures to the public during the current pandemic.⁵ They should prioritize giving the necessary information about mask use to the public and make sure that people use masks correctly, which would be of importance especially during shortages. There is no study on this role of pharmacists. We think that pharmacists' contribution to the public as a whole through education about taking preventive measures will improve compliance with preventive measures, and therefore we recommend that studies should be conducted in this direction.

Conflicts of interest: No conflict of interest was declared by the authors. The authors alone are responsible for the content and writing of the paper.

REFERENCES

1. Feng S, Shen C, Xia N, Song W, Fan M, Cowling BJ. Rational use of face masks in the COVID-19 pandemic. *Lancet Respir Med.* 2020;8:434-436.
2. Chughtai AA, Stelzer-Braid S, Rawlinson WD, Pontivivo G, Wang Q, Pan Y, Zhang D, Zhang Y, Li L, MacIntyre CR. Contamination by respiratory viruses on outer surface of medical masks used by hospital healthcare workers. *BMC Infect Dis.* 2019;19:491.
3. Sim SW, Moey KS, Tan NC. The use of facemasks to prevent respiratory infection: a literature review in the context of the Health Belief Model. *Singapore Med J.* 2014;55:160-167.
4. Eastwood K, Durrheim DN, Butler M, Jon A. Responses to pandemic (H1N1) 2009, Australia. *Emerg Infect Dis.* 2010;16:1211-1216.
5. Ou HT, Yang YK. Community Pharmacists in Taiwan at the Frontline Against the Novel Coronavirus Pandemic: Gatekeepers for the Rationing of Personal Protective Equipment. *Ann Intern Med.* 2020;173:149-150.



Development and Statistical Optimization of Solid Lipid Nanoparticle Formulations of Fluticasone Propionate

Flutikazon Propiyonatinın Katı Lipit Nanopartikül Formülasyonlarının Geliştirilmesi ve İstatistiksel Optimizasyonu

© Gülin AMASYA*, © Ceyda Tuba ŞENGEL TÜRK, © Ulya BADILLI, © Nilüfer TARIMCI

Ankara University Faculty of Pharmacy, Department of Pharmaceutical Technology, Ankara, Turkey

ABSTRACT

Objectives: The aim of this study was to develop fluticasone propionate (FP)-loaded solid lipid nanoparticle (SLN) formulations by using factorial design approach.

Materials and Methods: Tristearin percentages (X1) (1%, 2%, and 4%) and homogenization cycles (X2) (2, 4, and 8 cycles) were selected as independent variables in the factorial design. SLN formulations were optimized by multiple linear regression (MLR) to evaluate the influence of the selected process and formulation independent variables on SLNs' characteristics, namely as encapsulation efficiency (Q1) and particle size (Q2). The polydispersity index and surface charge of the SLNs were also evaluated in this research. Moreover, transmission electron microscopy, differential scanning calorimetry, and *in vitro* drug release studies were carried out on the optimum SLN formulation.

Results: The MLR analysis indicated that as the homogenization cycle (X2) increased in the production process, the mean particle size decreased.

Conclusion: This research showed that FP-encapsulated SLNs with desired characteristics can be produced by varying the production and content variables of the formulations.

Key words: Experimental design, fluticasone propionate, nanoparticles

ÖZ

Amaç: Bu çalışmanın amacı, faktöriyel tasarım yaklaşımını kullanarak flutikazon propiyonat (FP)-yükü katı lipit nanopartikül formülasyonları (SLN) geliştirmektir.

Gereç ve Yöntemler: Faktöriyel tasarımda tristearin yüzdeleri (X1) (%1, %2 ve %4) ve homojenizasyon döngüleri (X2) (2, 4 ve 8 döngü) bağımsız değişkenler olarak seçilmiştir. SLP formülasyonlarının çoklu regresyon analizi (MLR) ile optimize edilmiş, seçilen işlemin ve formülasyonun etkisini SLN'lerin karakteristikleri üzerinde değerlendirmek için bağımsız değişkenleri olarak enkapsülasyon etkinliği (Q1) ve partikül boyutları (Q2) seçilmiştir. Bu çalışmada nanopartiküllere ait polidispersite indeksi ve yüzey yükleri de değerlendirilmiştir. Bunun yanı sıra, optimum SLN formülasyonu için transmisyon elektron mikroskopisi, diferansiyel taramalı kalorimetri ve *in vitro* etkin madde salım çalışmaları da yapılmıştır.

Bulgular: MLR analizi, üretim sürecinde homojenizasyon döngüsü (X2) arttıkça, ortalama partikül boyutunun azaldığını göstermiştir.

Sonuç: Bu araştırma, istenen özelliklere sahip FP ile enkapsüle edilmiş SLN'lerin, formülasyonların üretim ve içerik değişkenleri değiştirilerek üretilebileceğini göstermiştir.

Anahtar kelimeler: Deneysel tasarım, flutikazon propiyonat, nanopartiküller

*Correspondence: E-mail: glnmsy@gmail.com, Phone: +90 505 818 74 28 ORCID-ID: orcid.org/0000-0002-0491-450X

Received: 26.03.2019, Accepted: 12.04.2019

©Turk J Pharm Sci, Published by Galenos Publishing House.

INTRODUCTION

Topical corticosteroids are regularly used drugs in the practice of dermatology, especially for the treatment of inflammatory skin disorders. However, the long-term application of them is restricted due to their local or systemic adverse effects. Several studies have been performed to enhance the anti-inflammatory efficiency of these active substances and to reduce their side effects.¹⁻³

Fluticasone propionate (FP), which is a potent anti-inflammatory, immunosuppressive, and antiproliferative drug, is a synthetic trifluorinated topical corticosteroid and is used for the therapy of skin conditions like atopic dermatitis and psoriasis.^{4,5} It is a highly lipophilic substance and highly glucocorticoid receptor binding and activation is its main characteristic.² FP is available in 0.005% ointment and 0.05% cream formulations for the treatment of inflammatory skin disorders that are responsive to corticosteroids.^{5,6}

The purpose of dermal drug delivery is to deliver the active molecules to the skin layers with minimum systemic absorption. One of the most important issues regarding the therapy of skin disorders such as atopic dermatitis, psoriasis, and skin cancer is the accumulation of the active substances in skin layers.^{7,8} In other words, drugs should reach the skin layers at a sufficient concentration and stay there for a particular duration. However, the stratum corneum, the outermost layer of the epidermis, considerably restricts the penetration of active substances into the skin.⁹ Nanosized drug delivery systems come into play at this point since they offer several advantages for dermal drug application. These advantages can be summarized as improving the skin penetration and reducing the adverse effects of active substances, achieving site-specific drug targeting into the skin, providing sustained and/or controlled drug release, and enhancing the chemical stability of molecules.⁹⁻¹¹ Dermal drug delivery by liposomes,¹² niosomes,¹³ nanoemulsions,¹⁴ polymeric nanoparticles,¹⁵ and lipid nanoparticles¹⁶⁻¹⁸ has been extensively researched by several groups.

Solid lipid nanoparticles (SLNs) were investigated at the beginning of the 90s for the elimination of the drawbacks of pre-existing colloidal systems such as nanoemulsions, liposomes, and polymeric nanoparticles.^{19,20} SLNs are produced by physiologically tolerated lipids or a mixture of lipids that are in solid form at body and room temperature. SLNs have several advantages like biocompatibility, protection of drugs against degradation, modification of the drug release rate, and the possibility of large scale production without the use of organic solvents. Moreover, the structural similarity and interactions between the epidermal lipids and the lipid matrix of SLNs could enhance the skin permeation of encapsulated drugs. The nanosize, narrow size distribution, and greater surface area of SLNs also facilitate drug penetration into the skin.²¹⁻²³ The controlled release of drugs can be achieved because of the considerably lower mobility of drug in a solid matrix than in a droplet. Several types of solid lipids including fatty acids, triglycerides, partial glycerides, waxes, and steroids can be used as the main ingredients of SLNs. The most

frequently used surfactants are nonionic triblock copolymers of polyoxypropylene and polyoxyethylene, nonionic surfactant, and emulsifiers such as polysorbates, lecithins, or polyvinyl alcohol for providing the stabilization of nanodispersions.^{24,25}

There are various methods for the production of SLNs such as high pressure homogenization, microemulsion, high shear homogenization and/or ultrasonication, solvent emulsification/evaporation, solvent emulsification/diffusion, electrospraying, solvent injection, and the use of membrane contactors and supercritical fluids. High pressure homogenization is the most desirable production technique for SLNs since it exhibits several advantages compared to the other techniques, such as suitability for large scale industrial production, the possibility of avoiding use of organic solvents, and the quite short processing time.^{26,27}

Factorial design is an approach that provides a statistical perspective to determine the effects and effect levels of input factors on the final product. The main objective in the factorial design approach is to obtain the maximum information between the minimum sample size and the cause-effect relationship for optimization of the formulation.²⁸ For this purpose, the factorial design approach makes controlled changes in input variables. The factorial design helps to scale the replies of the dependent variables based on the defined goals. Response surface methodology provides a graphical evaluation of the effects of input variables on response variables.^{29,30} The aim of the present investigation was to develop FP-loaded SLNs using the factorial design approach. A 3² full factorial design through design expert 6.0.8 software was used to optimize the various physico-chemical characteristics of SLNs. Two formulation parameters, tristearin percentages (1%, 2%, and 4%) and homogenization cycles (2, 4, and 8 cycles) were chosen as input factors. The output (response) factors selected to evaluate the particles *in vitro* were the encapsulation efficiency percentage (Q1) and particle size (Q2) of the SLNs.

MATERIALS AND METHODS

Materials

FP was kindly supplied as a gift from Deva Drug Company (Istanbul, Turkey). Tristearin was obtained from Sigma Aldrich (USA). Tween 80 was purchased from Fluka (USA). All other materials were of analytical grade.

Analytical validation of the high performance liquid chromatography (HPLC) method

The FP was analyzed by HPLC and the method was validated by means of the linearity, accuracy, precision, limit of detection (LOD), and limit of quantification (LOQ).

Optimization by 3² factorial design

Multiple linear regression (MLR) was carried out to examine the variables influencing the final characteristics of SLNs.³¹ Nine SLN formulations were produced as per a 3² factorial design to investigate the effect of two input factors, namely tristearin percentages (X1) and homogenization cycle (X2), on the two output factors, namely entrapment efficiency percentage (Q1)

and mean particle size (Q2), of the FP-loaded SLNs. Three levels were determined in order to evaluate each factor: -1, 0, and 1. The fitted models' regression equation for the output variables is presented in Equation 1 below.

$$Q = b_0 + b_1X_1 + b_2X_2 + b_3X_1^2 + b_4X_2^2 + b_5X_1X_2 \text{ (Equation 1)}$$

In the model, Q is the output factor, b_0 is the arithmetic average value of the tests, and b_1 , b_2 , b_3 , b_4 , and b_5 are the forecasted coefficients for the factors X_1 and X_2 . Nonlinearity is analyzed through the polynomial terms (X_1^2 and X_2^2). The outcomes were investigated statistically using analysis of variance (ANOVA)⁴. The variable levels and the actual values are tabulated in Table 1.

Preparation of solid lipid nanoparticle formulations

FP-loaded SLN formulations were manufactured using a high pressure homogenizer. Tristearin was melted and 50 mg of FP was added to the melted lipid. Aqueous Tween 80 (1%) solution was also heated to the same temperature. After an Ultraturrax T25 (IKA, Germany) at 13,500 rpm was used to mix the lipid phase and aqueous phase for 3 min, the hot pre-emulsion was subsequently homogenized by a Microfluidics M110L (USA) at a pressure of 18,000 Psi. Three different tristearin percentages (1%, 2%, and 4%) and three different cycle numbers (2, 4, and 8 cycles) were investigated based on two responses: encapsulation efficiency (Q1) and particle size (Q2). SLN dispersions were centrifuged using a Vivaspin (MWCO=10,000) at 4500 rpm for 30 min (Sigma 3K30, Germany) and then lyophilized.

Particle size and zeta potential analysis

Particle size measurements were obtained by a dynamic light scattering technique. For this purpose, a Malvern Zetasizer (Malvern, UK) was used to measure the mean particle size, polydispersity index, and the zeta potential values of FP-loaded SLNs. Dry powder of lipid nanoparticles was dispersed in ultrapure water before analysis.

Table 1. Actual values and variable levels designed through 3² factorial design of FP-loaded SLNs

Formulation codes	Actual values		Variable levels in coded form				
	X1	X2	X1	X2	X1 ²	X2 ²	X1X2
SLN1	1%	2	-1	-1	1	1	1
SLN2	1%	4	-1	0	1	0	0
SLN3	1%	8	-1	1	1	1	-1
SLN4	2%	2	0	-1	0	0	0
SLN5	2%	4	0	0	0	1	0
SLN6	2%	8	0	1	0	0	0
SLN7	4%	2	1	-1	1	1	-1
SLN8	4%	4	1	0	1	0	0
SLN9	4%	8	1	1	1	1	1

FP: Fluticasone propionat, SLN: Solid lipid nanoparticle

Determination of encapsulation efficiency

For the determination of the encapsulation efficiency of SLN formulations, 10 mg of SLN was dissolved in methanol at 75°C. The solution was stirred using a magnetic stirrer in a tightly sealed vial. After that, the solution was ultrasonicated with 50% power for 5 min (Bandelin Sonoplus HD 2070, Germany) and then cooled to room temperature. It was centrifuged at 26,000 rpm for 20 min at 4°C (Sigma 3K30, Germany) and then the supernatant was filtered using a 0.22 µm cellulose acetate membrane filter. The amount of FP was determined using an HPLC system (Agilent 1260 Infinity). Separation was carried out using a NovaPak® C18 column (4 µm, 150x3.9 mm) (Waters, Ireland). The column temperature was set to 35°C. The mobile phase composition was acetonitrile:water (60:40 v/v) and the flow rate was 1 mL/min. A 10-µL sample was injected into the system and the samples were analyzed at a wavelength of 236 nm.

In vitro drug release study

The dialysis bag method was used to determine the *in vitro* release profile of FP from the SLN formulation. SLN formulation corresponding to 5 mg of FP was placed into hydrated dialysis membranes (MWCO=12-14 kDa, Spectrapor-2). A mixture of 100 mL of phosphate buffered saline pH 7.4 and ethanol (70:30) was used as dissolution medium at 37°C and under constant stirring (100 rpm). The samples were taken at particular times over 24 h. The medium was completely removed and replaced with 100 mL of fresh dissolution medium at each time point to provide a sink condition. Samples taken were filtered through 0.45 µm regenerated cellulose membrane filters and the amount of FP was determined by HPLC.

Transmission electron microscopy (TEM) analysis

The shapes of the lipid nanoparticles were examined by FEI Tecnai G2 S Twin TEM (Osaka, Japan) at an acceleration voltage of 120 kV. After dry powder of lipid nanoparticles was dispersed in ultrapure water the dispersion was dropped on a copper grid.

Differential scanning calorimetry (DSC) analysis

The thermal properties and crystallinity of pure FP, bulk lipid, and FP-loaded SLNs were determined by DSC (Shimadzu DSC-60, Japan). Five milligrams of sample was placed in hermetically sealed aluminum pans and a DSC thermogram was obtained at a scanning rate of 5°C/min while the samples were heated from room temperature to 300°C. Moreover, for the calibration of the instrument indium was used as a reference.

Statistical analysis

All results were statistically analyzed using one-way ANOVA through design expert 6.0.8 software.

RESULTS AND DISCUSSION

Analytical validation of the HPLC method

Linearity

After analyzing the eight different concentration of FP six times by HPLC, the average peak areas were plotted against

concentrations. A linear relationship between peak area and concentration was observed. The best linearity was obtained between concentrations of 0.25 and 10 µg/mL in methanol since the correlation coefficient was found to be 0.9996.

Accuracy

After FP solutions in methanol at concentrations of 0.5 µg/mL, 4 µg/mL, and 10 µg/mL were injected 6 times as a test sample, the detector responses were used to calculate the concentrations of FP. The accuracy of the analytical method was determined with the help of the variation coefficient [relative standard deviation (RSD)] of the percent recovery values. Since the RSD values obtained were close to or less than 2%, the method was assumed to be accurate (Table 2).

Table 2. The RSD % values obtained for the analytical validation parameters

	0.5 µg/mL	4 µg/mL	10 µg/mL
Accuracy (RSD %)	1.43	2.34	0.55
Repeatability (RSD %)	1.92	1.55	1.30
Intermediate precision (RSD %)	1.89	1.80	1.19

RSD: Relative standard deviation

Precision

The repeatability and intermediate precision of the method were evaluated. The repeatability of the method was determined by analysis of 6 repetitive injections of FP-methanol solutions and was shown as the RSD of measured concentrations. The RSD values were less than 2% as can be seen in Table 2. The intermediate precision of the HPLC method was defined by the RSD value of 12 injections performed on two different days and the RSD values were less than 2% (Table 2). On the other hand, there was no statistically significant difference between the means of the measured concentrations obtained on two different days for each FP solution ($p > 0.05$).

LOD and LOQ values

The LOD and LOQ values were calculated in accordance with the equations below. The standard deviation (s) of the response and the slope (m) of the calibration curve were used. While the LOD value was 0.09 µg/mL, the LOQ value was 0.28 µg/mL.

$$\text{LOD} = 3.3 \times s/m$$

$$\text{LOQ} = 10 \times s/m$$

Formulation optimization by 3² factorial design

Tristearin percentages were varied (1%, 2%, and 4%). These three different ratios were tested at three different numbers of homogenization cycles: 2, 4, and 8. In this way, nine SLNs were produced as per the 3² factorial design. The magnitude and sign of the main influence indicate the relative effect of each factor on the response by means of polynomial equations. Table 3 gives the predicted and the observed values of responses (Q1, Q2). The predicted values were derived from the equations and the observed values were determined from experimental results.

Table 4 shows the results of model coefficients estimated by MLR and the ANOVA of the investigated model for all responses. The quality of the model developed was evaluated based on the regression coefficient values. The determination coefficient (r^2 value) for the response Q2 was nearer to 1, indicating that there was a good correlation between the observed and the response measures from the model. The negative sign in front of the coefficients indicated that the response of the nanoparticles increased when the independent factor was decreased, and the positive sign for the coefficients showed the positive effect of the independent factors on the observed replies. The model F-value of 3.87 for Q1 response implied there was a 5.30% probability that a "Model F-Value" of this magnitude could be caused by noise. On the other hand, the "Model F-value" of 57.71 for Q2 response indicated that the model was statistically meaningful. The possibility of such a large "Model F-Value" due to noise is only 0.01%,^{28,31,32}

Figure 1 shows the linearity plots between the Q1 and Q2 values. The correlation graphs that show linearity between actual and predicted response variables indicated that the fit to the model was at an excellent level for Q2 ($p < 0.05$), whereas the linear correlation plots showed a low compliance to the model for Q1 ($p > 0.05$) (Figure 1). This situation is also evidenced by the F-value calculated for the Q1 model. The F-value of the Q1 model ($F = 3.87$) is smaller than the tabulated F-value ($F_{\text{tab}} = 4.46$). This situation indicates statistical nonsignificance of the model (Figure 1 and also the p values in Table 4).

As seen from Table 3, drug entrapment efficiency of all factorial formulations was produced within a broad range of 27.07-94.65%. Drug entrapment efficiency was not affected significantly by the level of X1 or X2 ($p > 0.05$). Generally, as seen in p values that indicated the significance of the coefficients (Table 4), neither of the independent factors (X1 and X2) had a strong effect on the drug entrapment efficiency (Q1) ($p > 0.05$).

Table 3. Observed and predicted responses of FP-loaded SLNs

Formul code	Responses			
	Observed values		Predicted values	
	Q1± SD (%)	Q2± SD (nm)	Q1± SD (%)	Q2± SD (nm)
SLN1	52.02	352.9	43.51	334.3
SLN2	37.70	203.8	47.55	223.5
SLN3	33.31	130.9	31.97	112.7
SLN4	35.70	243.5	36.36	253.4
SLN5	38.11	190.7	34.68	196.8
SLN6	27.07	131.2	13.39	140.1
SLN7	71.32	177.1	79.17	172.5
SLN8	94.65	178.4	71.78	170.0
SLN9	29.74	171.6	44.76	167.5

FP: Fluticasone propionate, SLN: Solid lipid nanoparticle, SD: Standard deviation

When the average size of the SLNs was investigated depending on the variation in homogenization cycles (X2) at each tristearin percentage (X1), it was observed that as X2 increased from 2 to 8 the mean particle size decreased significantly ($p < 0.05$). The average particle size of SLNs ranged from 130.9 ± 3.30 to 352.9 ± 10.93 nm. Generally, from the p values of the coefficients presented in Table 4, it was concluded that both of the investigated variables (X1 and X2) had a major influence on the output Q2 ($p < 0.05$). The biggest average size was observed in the lowest level of X1 (1%) and the lowest level of X2 (2 cycles) in factorial formulation SLN1.

PDI, which is the indicator of homogeneity of the size distribution in colloidal drug delivery systems, is generally expressed as less than 0.3 for narrow size distribution.^{28,32} The PDI values of all factorial formulations were between 0.181 and 0.497 (Figure 2). It was observed that the factorial formulations that contain tristearin with a percentage of 1 or 2 showed a wide size distribution ($PDI > 0.2$) based on the homogenization cycles investigated except in the formulations that contained 2% tristearin at homogenization cycle 8 (SLN6 coded formulation). As tristearin percentage increased from 1% or 2% to 4%, the PDI values were less than 0.3, indicating a uniform size distribution.

The surface charge of nanosized particles is the potential at the

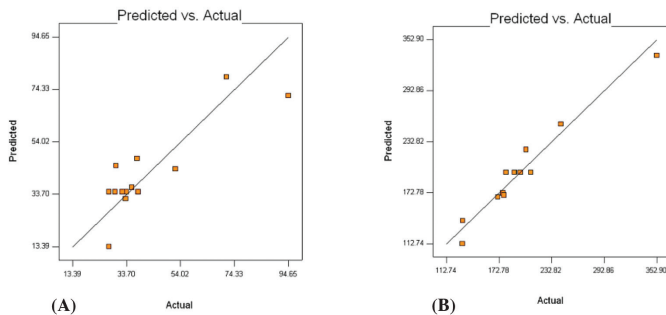


Figure 1. Linearity correlation graphs between actual and predicted values of (A) Q1, (B) Q2

hydrodynamic shear plane and indicates the particle stability in dispersions.³¹ All of the SLNs exhibited negative surface charge between -19.5 and -29.7 mV. The surface charge of SLNs was not affected significantly by the variation in tristearin percentages or the homogenization cycles (Figure 3).

Simplified models were also utilized to draw contour plots for analyzing the effect of independent variables. The contour plots give a diagrammatical demonstration of the values of

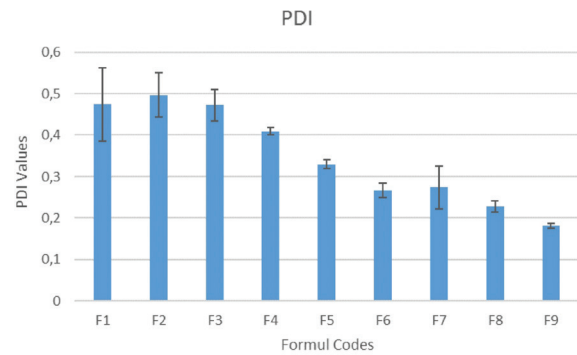


Figure 2. PDI values of the FP-loaded SLN formulations
PDI: Polydispersity index, FP: Fluticasone propiyonat, SLN: Solid lipid nanoparticle

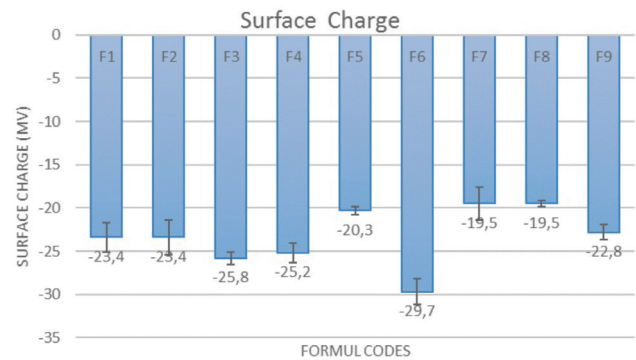


Figure 3. Surface charge of the FP-encapsulated SLN formulations
FP: Fluticasone propiyonat, SLN: Solid lipid nanoparticle

Table 4. Results of model coefficients estimated by MLR and the ANOVA of the fitted model for all responses

Responses	Model coefficients			Regression analysis of variance			
	Factor	Coefficients	p value	F	p value	R ²	Adjusted R ²
Q1	Intercept	34,6844		3.87	0.0530	0.7345	0.5449
	X1	+12,1133	0.0638				
	X2	-11,4867	0.0755				
	X1 ²	+24,9931	0.0179				
	X2 ²	-9,81070	0.2662				
	X1X2	-5,71750	0.4248				
Q2	Intercept	+196,7462		57.71	<0.0001	0.9506	0.9341
	X1	-26,7500	0.0013				
	X2	-56,6333	<0.0001				
	X1X2	+54,1250	<0.0001				

MLR: Multiple linear regression, ANOVA: Analysis of variance

the response. Since the contour plot of Q1 (Figure 4A) was nonlinear, it demonstrates a nonlinear relationship between input factors. As can be seen from the contour plot of Q2 (Figure 4B), the indicator of the linear relationship between X1 and X2 input factors is the linearity of the graph.

According to the release profile study of FP-loaded SLNs as shown in Figure 5, prolonged release was obtained without any initial burst effect. The nature of the lipid matrix affects the release profile of the active substance. It is thought that FP-loaded SLNs formed in a core-shell model with a drug-enriched core. This may be responsible for the slow release.

TEM micrographs of FP-loaded SLNs are shown in Figure 6. TEM analysis confirmed the colloidal sizes of the FP-loaded SLNs with spherical shapes.

Differential scanning calorimetry analysis

The DSC thermograms given in Figure 7 show that pure FP is decomposed by a small exothermic peak at 271.72°C. This outcome is in agreement with previous research by El-Gendy et al.³³ and Dai et al.³⁴ The peak of the active agent thus observed also indicated that the FP was a crystal structure. When the thermogram of the pure form of tristearin was evaluated, it was seen that tristearin produced a small exothermic shoulder peak at 49.89°C at first and then it gave a large endothermic peak at 60.73°C, which indicated the presence of a crystal structure in tristearin.³⁵ When the thermogram of the optimum SLN was examined, it was seen that the exothermic peak of FP disappeared. This indicated that FP's crystal structure was turned into an amorphous structure within the SLN matrix.

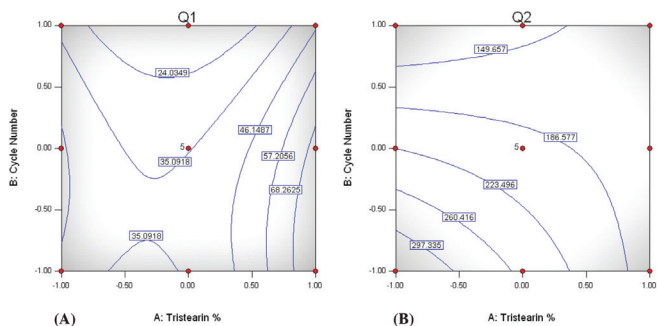


Figure 4. Contour plots of FP-loaded SLNs showing the influence of X1 and X2 on A) Q1, B) Q2
 FP: Fluticasone propiionat, SLN: Solid lipid nanoparticle

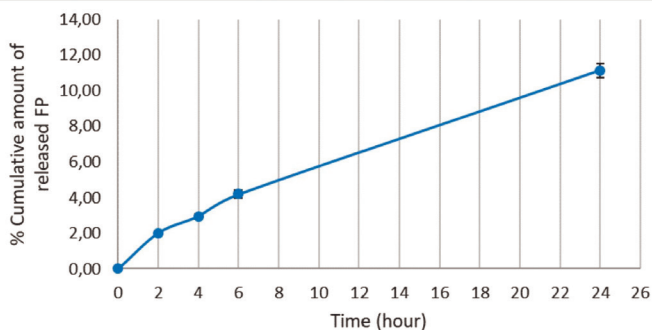


Figure 5. *In vitro* drug release profile of FP-loaded SLNs
 FP: Fluticasone propiionat, SLN: Solid lipid nanoparticle

When the optimum formulation's thermogram was examined for tristearin peaks, it was seen that the exothermic shoulder peak of tristearin disappeared where the main endothermic main peak at 57.02°C remained the same shape with the same sharpness. This situation was interpreted as showing that tristearin in the SLN formulation preserved a large proportion of its crystal structure.

CONCLUSION

FP-loaded SLNs were successfully fabricated using high pressure homogenization. A 3² experimental design and contour plot analysis were used with software to set up the best formulation conditions with a limited number of experiments. This study showed that tristearin percentages and the number of homogenization cycles used in the SLN formulations significantly affected the physico-chemical characteristics

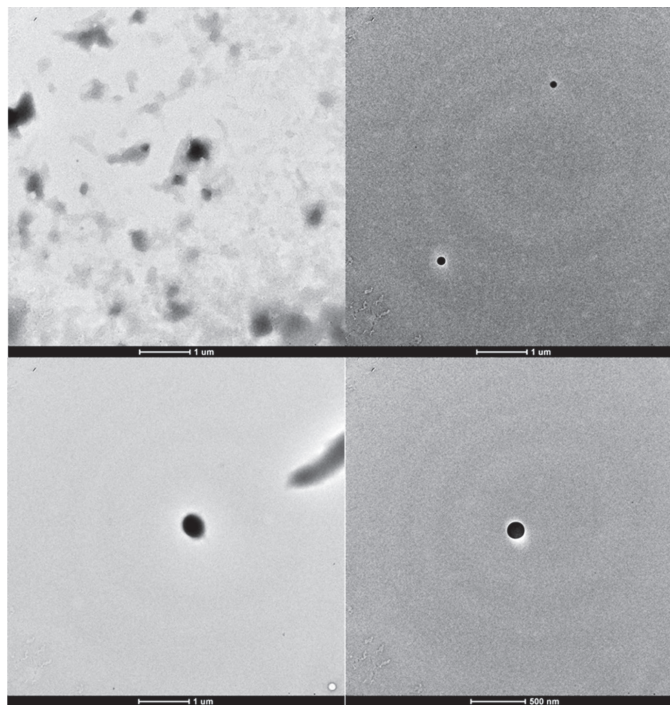


Figure 6. TEM micrograph of the optimal formulation
 TEM: Transmission electron microscopy

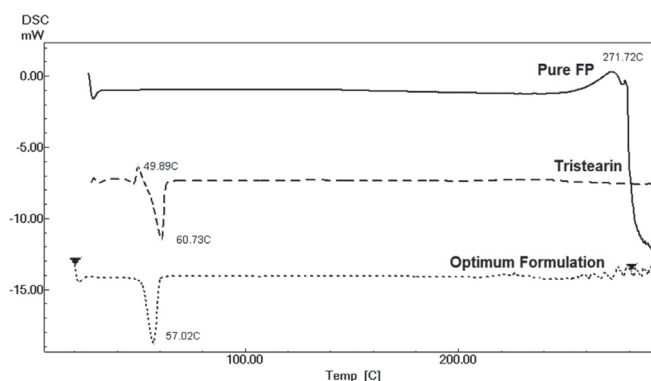


Figure 7. DSC thermograms of pure FP, tristearin, and optimum formulation
 DSC: Differential scanning calorimetry, FP: Fluticasone propiionat

of FP-loaded SLNs. According to the factorial design study performed in this research, the optimum formulation could be achieved with the content of 4% tristearin and 4 homogenization cycles.

Conflicts of interest: No conflict of interest was declared by the authors. The authors alone are responsible for the content and writing of the paper.

REFERENCES

- Brazzini B, Pimpinelli N. New and established topical corticosteroids in dermatology: clinical pharmacology and therapeutic use. *Am J Clin Dermatol.* 2002;3:47-58.
- Roeder A, Schaller M, Schäfer-Korting M, Korting HC. Safety and efficacy of fluticasone propionate in the topical treatment of skin diseases. *Skin Pharmacol Physiol.* 2005;18:3-11.
- Gual A, Pau-Charles I, Abeck D. Topical corticosteroids in dermatology: from chemical development to galenic innovation and therapeutic trends. *J Clin Exp Dermatol Res.* 2015;6:1-5.
- Doktorová S, Araújo J, Garcia ML, Rakovský E, Souto EB. Formulating fluticasone propionate in novel PEG-containing nanostructured lipid carriers (PEG-NLC). *Colloids Surf B Biointerfaces.* 2010;75:538-542.
- Korting HC, Schöllmann C. Topical fluticasone propionate: intervention and maintenance treatment options of atopic dermatitis based on a high therapeutic index. *J Eur Acad Dermatol Venereol.* 2012;26:133-140.
- Spencer CM, Wiseman LR. Topical fluticasone propionate: a review of its pharmacological properties and therapeutic use in the treatment of dermatological disorders. *BioDrugs.* 1997;7:318-334.
- Brown MB, Martin GP, Jones SA, Akomeah FK. Dermal and transdermal drug delivery systems: current and future prospects. *Drug Deliv.* 2006;13:175-187.
- Badilli U, Gumustas M, Uslu B, Ozkan SA. Lipid Based Nanoparticles for Dermal Drug Delivery, In: Grumezescu AM, Andrew W, eds. *Organic Materials as Smart Nanocarriers for Drug Delivery*; Applied Science Publishers-Elsevier; 2018;9:369-413.
- Gupta M, Agrawal U, Vyas SP. Nanocarrier-based topical drug delivery for the treatment of skin diseases. *Expert Opin Drug Deliv.* 2012;9:783-804.
- Papakostas D, Rancan F, Sterry W, Blume-Peytavi U, Vogt A. Nanoparticles in dermatology. *Arch Dermatol Res.* 2011;303:533-550.
- Zhang Z, Tsai PC, Ramezanli T, Michniak-Kohn BB. Polymeric nanoparticles-based topical delivery systems for the treatment of dermatological diseases. *Wiley Interdiscip Rev Nanomed Nanobiotechnol.* 2013;5:205-218.
- López-Pinto JM, González-Rodríguez ML, Rabasco AM. Effect of cholesterol and ethanol on dermal delivery from DPPC liposomes. *Int J Pharm.* 2005;298:1-12.
- Manconi M, Sinico C, Valenti D, Lai F, Fadda AM. Niosomes as carriers for tretinoin. III. A study into the *in vitro* cutaneous delivery of vesicle-incorporated tretinoin. *Int J Pharm.* 2006;311:11-19.
- Shakeel F, Haq N, Al-Dhfyan A, Alanazi FK, Alsarra IA. Double w/o/w nanoemulsion of 5-fluorouracil for self-nanoemulsifying drug delivery system. *Journal of Molecular Liquids.* 2014;200:183-190.
- Alvarez-Román R, Naik A, Kalia YN, Guy RH, Fessi H. Skin penetration and distribution of polymeric nanoparticles. *J Control Release.* 2004;99:53-62.
- Souto EB, Wissing SA, Barbosa CM, Müller RH. Development of a controlled release formulation based on SLN and NLC for topical clotrimazole delivery. *Int J Pharm.* 2004;278:71-77.
- Gainza G, Pastor M, Aguirre JJ, Villullas S, Pedraz JL, Hernandez RM, Igartua M. A novel strategy for the treatment of chronic wounds based on the topical administration of rhEGF-loaded lipid nanoparticles: *In vitro* bioactivity and *in vivo* effectiveness in healing-impaired db/db mice. *J Control Release.* 2014;185:51-61.
- Pradhan M, Singh D, Murthy SN, Singh MR. Design, characterization and skin permeating potential of Fluocinolone acetonide loaded nanostructured lipid carriers for topical treatment of psoriasis [published correction appears in *Steroids.* 2016 Feb;106:93]. *Steroids.* 2015;101:56-63.
- Gasco MR. Method for producing solid lipid microspheres having a narrow size distribution. *US Patent.* 1993;5:250-236.
- Müller RH, Radtke M, Wissing SA. Solid lipid nanoparticles (SLN) and nanostructured lipid carriers (NLC) in cosmetic and dermatological preparations. *Adv Drug Deliv Rev.* 2002;54(Suppl 1):S131-S155.
- Zhai Y, Zhai G. Advances in lipid-based colloid systems as drug carrier for topic delivery. *J Control Release.* 2014;193:90-99.
- Sala M, Diab R, Elaissari A, Fessi H. Lipid nanocarriers as skin drug delivery systems: Properties, mechanisms of skin interactions and medical applications. *Int J Pharm.* 2018;535:1-17.
- Garcês A, Amaral MH, Sousa Lobo JM, Silva AC. Formulations based on solid lipid nanoparticles (SLN) and nanostructured lipid carriers (NLC) for cutaneous use: A review. *Eur J Pharm Sci.* 2018;112:159-167.
- Gastaldi L, Battaglia L, Peira E, Chirio D, Muntoni E, Solazzi I, Gallarate M, Dosio F. Solid lipid nanoparticles as vehicles of drugs to the brain: current state of the art. *Eur J Pharm Biopharm.* 2014;87:433-444.
- Ganesan P, Narayanasamy D. Lipid nanoparticles: Different preparation techniques, characterization, hurdles, and strategies for the production of solid lipid nanoparticles and nanostructured lipid carriers for oral drug delivery. *Sustainable Chemistry and Pharmacy.* 2017;6:37-56.
- Mehnert W, Mader K. Solid lipid nanoparticles: production, characterization and applications. *Advanced Drug Delivery Reviews.* 2012;64:83-101.
- Muller RH, Mader K, Gohla S. Solid lipid nanoparticles (SLN) for controlled drug delivery: a review of the state of the art. *Eur J Pharm Biopharm.* 2000;50:161-177.
- Sengel-Turk CT, Hascicek C. Design of lipid-polymer hybrid nanoparticles for therapy of BPH: Part I. Formulation optimization using a design of experiment. *J Drug Deliv Sci Technol.* 2017;39:16-27.
- Blasi P, Giovagnoli S, Schoubben A, Puglia C, Bonina F, Rossi C, Ricci M. Lipid nanoparticles for brain targeting I. Formulation optimization. *Int J Pharm.* 2011;419:287-295.
- Kumar Das S, Yuvaraja K, Khanam J, Nanda A. Formulation development and statistical optimization of Ibuprofen-loaded polymethacrylate microspheres using response surface methodology. *Chem Eng Res Des.* 2015;96:1-14.
- Gu B, Burgess DJ. Prediction of dexamethasone release from PLGA microspheres prepared with polymer blends using a design of experiment approach. *Int J Pharm.* 2015;495:393-403.
- Sengel Turk CT, Oz UC, Serim TM, Hascicek C. Formulation and optimization of nonionic surfactants emulsified nimesulide-loaded PLGA-

- based nanoparticles by design of experiments. *AAPS PharmSciTech*. 2014;15:161-176.
33. El-Gendy N, Pornputtapitak W, Berkland C. Nanoparticle agglomerates of fluticasone propionate in combination with albuterol sulfate as dry powder aerosols. *Eur J Pharm Sci*. 2011;44:522-533.
34. Dai J, Ruan BH, Zhu Y, Liang X, Su F, Su W. Preparation of Nanosized Fluticasone Propionate Nasal Spray With Improved Stability and Uniformity. *Chem Ind Chem Eng. Q*. 2015;21:457-464.
35. Amasya G, Badilli U, Aksu B, Tarimci N. Quality by design case study 1: Design of 5-fluorouracil loaded lipid nanoparticles by the W/O/W double emulsion - Solvent evaporation method. *Eur J Pharm Sci*. 2016;84:92-102.



Evaluation of Lactose-Based Direct Tableting Agents' Compressibility Behavior Using a Compaction Simulator

Sıkıştırma Simülatörü Kullanarak Laktoz Bazlı Doğrudan Tabletleme Ajanlarının Sıkıştırılabilir Davranışlarının Değerlendirilmesi

Yıldız ÖZALP*, Motunrayo M. ONAYO, Nailla JIWA

Near East University Faculty of Pharmacy, Department of Pharmaceutical Technology, Nicosia, Cyprus

ABSTRACT

Objectives: A compaction simulator (CS) is a single-punch instrument that records data during the powder compaction process. The aim of the study was to determine the behavior of lactose-based direct tableting agents (DTAs) by CS. The data recorded were used to evaluate the flowability and compressibility of powders. The focus of the study was on comparing the compressibility of StarLac® [alpha lactose monohydrate (85%) and white maize starch (15%)] and FlowLac®100 (spray-dried alpha lactose monohydrate) in order to make tablets containing poorly flowable paracetamol.

Materials and Methods: Two lactose-based DTAs were used. Physical characterization of these powders was done by measuring bulk, tapped, and true densities alongside scanning electron microscopy analysis. Flow properties were then calculated by the angle of repose, Hausner ratio, and Carr's compressibility index. Force, in-die thickness, and punch displacement data produced by the CS were captured during in-die compression. Compressibility was calculated using the Heckel equation.

Results: The physical characterization test results showed no significant difference between the two DTAs. Hardness results revealed that tablet formulations containing FlowLac® had higher sensitivity to an increase in compression force in comparison with StarLac®. From the Heckel plots generated by the CS during the compression cycle, yield pressure (P_y) values were calculated for FlowLac®100 and StarLac®. The Heckel parameter (P_y) for FlowLac®100 and StarLac® was calculated as 87.5 MPa and 85.2 MPa, respectively, during the compaction cycle at 5 kN. These data indicated that both powders are compressible and have brittle behavior.

Conclusion: StarLac® is less brittle, which was shown by its lower sensitivity to compression force. P_y values obtained from the Heckel equation described the plasticity of particles, which gives distinct information on the compressibility of both DTAs in real time during the compaction cycle.

Key words: Compaction simulator, compressibility, tablet, FlowLac®100, StarLac®

ÖZ

Amaç: Sıkıştırma simülatörü (CS) toz sıkıştırma prosesi sırasında veri kaydı yapan tek zımbalı bir cihazdır. Bu çalışmanın amacı laktoz bazlı doğrudan tabletleme ajanlarının (DTA) davranışlarını CS kullanarak belirlemektir. Kaydedilen veriler tozların basılabilir ve akış özelliklerini değerlendirmede kullanılmıştır. Çalışmanın odağı zayıf akış özelliğine sahip parasetamol içeren tabletler yapmak için StarLac® [alfa laktoz monohidrat (%85) ve mısır nişastası %15] ve FlowLac® 100 (püskürterek kurutulmuş alfa laktoz monohidrat) basılabilirliğini karşılaştırmaktır.

Gereç ve Yöntemler: İki laktoz bazlı DTA kullanılmıştır. Bu tozların bulk, sıkıştırılmış ve gerçek yoğunlukları yansira fiziksel özellikleri taramalı elektron mikroskopu analiziyle birlikte görüntülenmiştir. Daha sonra akış özellikleri yığın açısı, Hausner oranı ve Carr basılabilirlik indeksleri hesaplanmıştır. CS tarafından üretilen kuvvet, sıkışmış tozun zımba içindeki kalınlığı ve zımba deplasmanı verileri iç kompresyon esnasında elde edilmiştir. Basılabilirlik Heckel eşitliği kullanılarak hesaplanmıştır.

Bulgular: Fiziksel karakterizasyon test sonuçları iki DTA arasında anlamlı bir fark göstermemiştir. Sertlik sonuçları FlowLac® içeren tablet formülasyonların StarLac® içeren formülasyonlara göre baskı gücünün artmasına karşı daha yüksek hassasiyet gösterdiklerini açığa çıkarmıştır. Baskı döngüsü esnasında, CS tarafından oluşturulan Heckel plotlarından FlowLac®100 and StarLac® için verim basıncı (P_y) hesaplanmıştır. kM' de sıkıştırma döngüsü esnasında FlowLac®100 and StarLac® için Heckel parametreleri (P_y) sırasıyla 87,5 MPa ve 85,2 MPa olarak hesaplanmıştır. Bu veriler iki tozun da sıkıştırılabilir olduğunu ve kırılma davranış gösterdiğine işaret etmiştir.

*Correspondence: E-mail: yildiz.ozalp@neu.edu.tr, Phone: +90 532 463 00 08 ORCID-ID: orcid.org/0000-0001-7928-1666

Received: 12.04.2019, Accepted: 16.04.2019

©Turk J Pharm Sci, Published by Galenos Publishing House.

Sonuç: StarLac®'in daha az kırılğan olduğu baskı kuvveti uygulamasına karşı daha az duyarlı olduğu ile gösterilmiştir. Heckel eşitliğinden elde edilen partiküllerin plastisitesini tarif etmektedir ve bu da sıkıştırma döngüsü esnasında her iki DTA'nın da sıkıştırılabilirlikleri hakkında belirgin bilgi vermektedir.

Anahtar kelimeler: Sıkıştırma simülatorü, sıkıştırılabilirlik, tablet, FlowLac®100, StarLac®

INTRODUCTION

A compaction simulator (CS) works by mimicking the exact cycle of any tableting process in real time and records all important parameters during a single compression cycle. It has a wide range of advantages in industrial production and pharmaceutical research, having the ability to perform scale-up, understand compaction behavior, and characterize powders.¹ Data obtained from measurements of forces and displacement of upper and lower punches as well as plastic and elastic energies are used to evaluate the deformation characteristics of pharmaceutical powders.

Direct tableting agents (DTAs) are incorporated into formulations to improve the flow and compressibility of poorly flowable paracetamol. The primary function of DTAs in a tablet is to act as a carrier for the active pharmaceutical ingredient (API).² The focus of the present study was on lactose-based powders, which are generally used to enhance the bulk of a tablet, flow, and tableting properties. The two DTAs evaluated in our study were FlowLac®100 (spray-dried alpha lactose monohydrate) and StarLac® (co-processed maize starch and lactose). Lactose is a commonly used agent in tablet formulations. Lactose exhibits poor binding properties as a result of particle fragmentation, which is considered the main consolidation mechanism of lactose.³

Characterization of powders can be achieved using various compression equations that have been derived by many researchers.⁴⁻¹⁰ The Heckel equation, proposed by Heckel in 1961, which characterizes materials according to plastic and brittle properties, has been widely used in compaction studies.¹¹ The yield pressure, which is calculated from the Heckel equation, follows first-order kinetics. Yield pressure (P_y) is the stress at which a material begins to plastically deform. A low P_y value indicates that a material will deform plastically and higher P_y values indicate brittle deformation.¹² Attempts have been made by mechanical descriptors to set limits on these values, allowing materials to be categorized.¹³ Although these limits are present, it has been reported that there may be factors that affect the yield pressure, which may give rise to variations in the P_y values for the same material.¹⁴⁻¹⁷

The target of the present study was to see how both DTAs improve the compactibility characteristics of the model API with the aid of data produced by a compaction simulator.

MATERIALS AND METHODS

Paracetamol USP grade (Kimetsan) was used with the DTA StarLac® (Meggler AG). StarLac® is co-processed by the spray-drying of α -lactose monohydrate and corn starch. For comparison, FlowLac®100 (spray-dried alpha lactose monohydrate, Meggler AG) was used. Stearic acid (Kimetsan) was added to all formulations as lubricant.

Material characterization

The bulk and tapped densities of the dry sieved raw materials were determined. Bulk and tapped densities were measured using an ERWEKA® tapped volumeter (type: SMV 101/SMV 102, Germany). First the powder was transferred to a 50 mL graduated glass cylinder with the aid of a funnel. After that the sample was weighed on an analytical balance. The glass cylinder was placed on the tapped volumeter and tapped up to 100 times. The volume of the substance was visually detected and the tapped and bulk densities were calculated. The true densities of substances were determined using a helium pycnometer.

Microscopy

Particle morphology of the powders used was assessed by scanning electron microscopy (SEM).

Formulation design

The tablet formulations in this study are shown in Table 1. Formulations were made to compare the compressibility of StarLac® [alpha lactose monohydrate (85%) and white maize starch (15%)] and FlowLac®100 (spray-dried alpha lactose monohydrate) in order to make tablets containing poorly flowable paracetamol.

Preparation of powder blends and granulation

The process of dry granulation was employed in the present study to ensure a uniform granulated powder ready for tableting. Slugging was performed in place of roller compaction. The API was fed into a large capacity tablet press (Korsch XP 1) and was compacted by means of flat punches 18 mm in diameter. The slugs were then milled and screened through a 0.63-mm mesh sieve. Four formulations were prepared, and a fixed amount of FlowLac®100 or StarLac® was weighed and mixed with 300 mg of API granules and 10 mg of lubricant in a cubic mixer (ERWEKA® Heusenstamm Germany, type KB 15, serial no. 73876. 1070) for 5 min at a mixing speed of 50 rpm.

Compression procedures

The tablets were compressed on a Stylcam 200R Compaction Simulator (Medepharma, France). Flat-faced punches 11.28 mm in diameter were used. The tablets were compressed using 15

Table 1. Formulation composition

Formulations for tableting (mg)				
Formulation	Paracetamol	FlowLac®100	StarLac®	Stearic acid
F01	-	500	-	10
F02	-	-	500	10
F03	300	200	-	10
F04	300	-	200	10

kN and 30 kN force to determine the compressibility of the API. The CS recorded upper and lower punch displacement data, which were analyzed using the software ANALIS.

Determining tablet properties

Ten tablets were made for each formulation at 5, 10, 15, and 20 kN. Physical tests were carried out on an average of three of them. The crushing strength for each formulation was measured with an ERWEKA® tablet hardness tester (TBH 225 series). Thickness and diameter were also measured.

Heckel analysis

The Heckel equation is an experimental equation that interprets the relationship between the densification of a powder bed and applied stress.

$$\ln\left(\frac{1}{1-D}\right) = KP + \text{Intercept}$$

D is the relative density of the powder, P is pressure, and K is a constant and the slope of the linear portion of the graph. The Heckel parameter, denoted by 1/K (inverse of the slope), is thought to be related to the P_y of the powder and has the unit of pressure. The arch at low pressure often seen before the linear region on a Heckel plot is due to rearrangement or fracture.^{4,11,18}

Statistical analysis

The study data were analyzed using One-Way ANOVA. The software package IBM SPSS statistics v26 was used. The level of significance was p<0.05.

RESULTS

The powder flowability was determined by measuring and calculating the angle of repose, the Hausner ratio, and Carr’s index. As expected, the results in Table 2 show that the flow properties of paracetamol granules were poor. FlowLac®100 and StarLac® showed excellent flow properties as indicated by the Hausner ratio (1.14 and 1.17, respectively).

In Figures 1a and 1b the SEM images show the similarity in particle structure between FlowLac®100 and StarLac®. Both the fillers appeared to have spherical particles with rough surfaces and their particle sizes are within close range (Meggler).

Figures 2a and 2b illustrate the in-die Heckel plots, which were obtained for F01 and F02. ln(1/1-D) was calculated for the formulations within a range of compaction forces and these were plotted against each other to determine P_y.

The variations observed in P_y for both materials can be attributed to the effect of compaction pressure as shown in Tables 3a and 3b. Yield stress (P_y) showed a progressive increase with

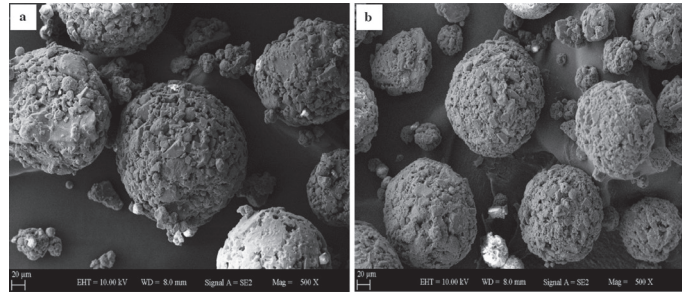


Figure 1a, 1b. Scanning electron microscopy images of the DTAs used in this study (500x):

a) StarLac® b) FlowLac®100
DTAs: Direct tableting agents

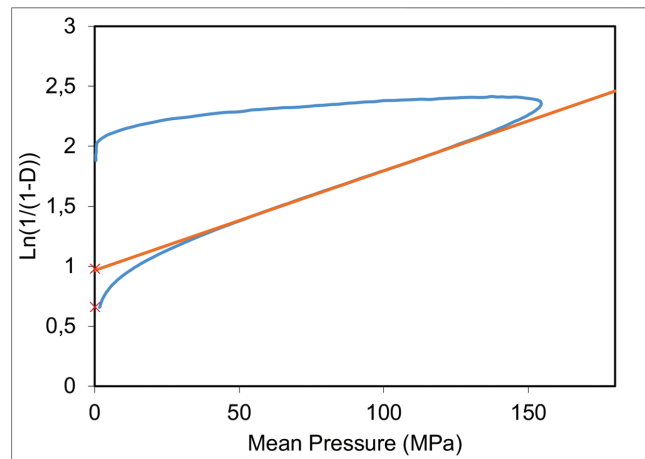


Figure 2a. In-die Heckel plot for 510 mg of StarLac® compressed at 15 kN

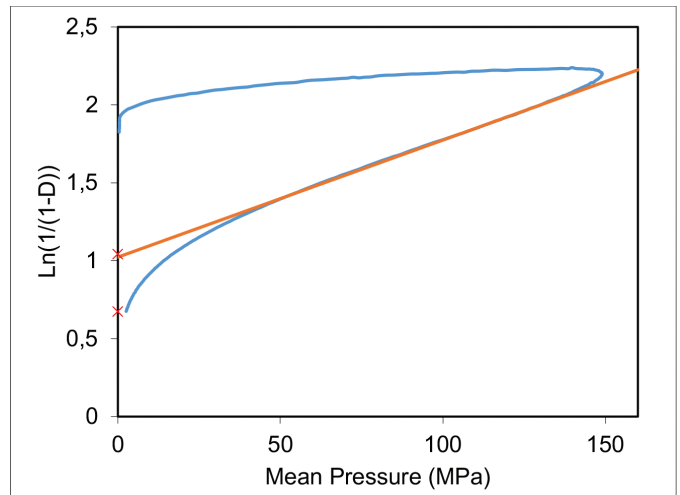


Figure 2b. In-die Heckel plot for 510 mg of FlowLac®100 compressed at 15 kN

Table 2. Powder physical properties

Powders	Bulk density (g/L)	Tapped density (g/L)	Hausner ratio	Flow character	Carr’s index (%)	Angle of repose (°)	Flow properties
Granulated paracetamol	44	80	1.8	Very, very poor	44	50	Poor
FlowLac® 100	625	714	1.14	Good	12.5	21.15	Excellent
StarLac®	609	714	1.17	Good	14.6	19.79	Excellent

increase in compression force. This indicated that yield stress is pressure dependent.

The Heckel analysis showed that for both formulations, F01 and F02, an increase in compaction pressure resulted in an increase in relative densities, thus signifying that a higher degree of densification occurred at higher pressures.

Figure 3 shows the hardness profiles for the formulations made. There was a greater decrease in crushing strength for FlowLac®100 containing formulations as the compression force increased. However, the sensitivity of StarLac® to change in compression force was less.

DISCUSSION

The calculated yield pressures for both formulations from Figures 2a and 2b were greater than 80 MPa. In accordance with the limits set by Roberts and Rowe¹⁴ both powders would be considered brittle materials. Generally, a lower P_y value (higher slope) reflects lower resistance to pressure, better densification, higher plastic deformation ability, and improved compressibility.¹⁹

Duberg and Nyström²⁰ divided the Heckel plot into two phases: compression and decompression. For an elastic material the curve shows a noticeable deviation from the horizontal in the decompression phase, which then leads to a low P_y value. As expected, the lactose-based excipients showed no deviation from the horizontal.

The Heckel analysis showed that for both formulations, F01 and F02, as the compaction pressure increased, values of relative density increased. Hence, a higher degree of densification

occurred at higher pressures. In concurrence with previous studies,^{18,21} StarLac® had lower P_y when compared to FlowLac®100; therefore, the values of P_y were higher for F01 at all compaction pressures compared to F02. These findings also indicate that more densification was exhibited by F02 and this could be attributed to the low resistance to force as seen in Figure 3. This may also be attributed to the different physical properties of the DTAs.

The confidence level of 95% gives a clear indication of variation between P_y of both DTAs, with a significant difference value ($p < 0.05$).

The reduced densification of F01 (FlowLac®100) can be associated with increased frictional and cohesive forces, which tend to restrain particle sliding. This leads to a relatively small amount of fragmentation and thus formation of less dense compacts.¹⁴

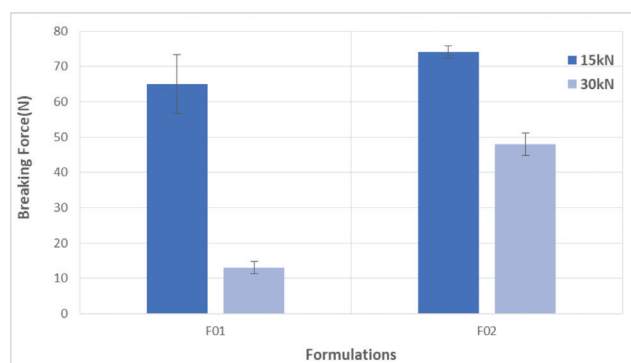


Figure 3. Hardness profiles of formulations at different compaction forces

Table 3a. Mean yield pressure, densification due to initial die filling, elastic energy, plastic energy, and R^2 values obtained from in-die Heckel analysis for FlowLac®100

Compression force (kN)	P_y (MPa)	R^2	D_{0^*}	EE	PE	EE/PE ratio
5 (0.2)	87.5 (0.95)	0.995 (0.001)	0.300 (0.066)	0.083 (0.009)	3.662 (0.064)	0.023 (0.002)
10 (1.8)	119.5 (9.25)	0.997 (0.002)	0.363 (0.066)	0.202 (0.020)	6.828 (0.053)	0.030 (0.002)
15 (0.3)	138.0 (2.57)	0.996 (0.002)	0.383 (0.046)	0.385 (0.017)	9.736 (0.171)	0.041 (0.001)
20 (0.4)	145.5 (1.78)	0.996 (0.000)	0.408 (0.013)	0.617 (0.100)	12.249 (0.10)	0.050 (0.001)

$n=3$ with standard deviations in parentheses, *values of D_{0^*} are derived from the subtraction of densification due to slippage and rearrangement of primary particles (D_{0^*}) from densification due to initial particle rearrangement (D_0)

P_y : Yield pressure, EE: Elastic energy, PE: Plastic energy

Table 3b. Mean yield pressure, densification due to initial die filling, elastic energy, plastic energy, and R^2 values obtained from in-die Heckel analysis for StarLac®

Compression force (kN)	P_y (MPa)	R^2	D_{0^*}	EE	PE	EE/PE ratio
5 (0.2)	85.2 (1.115)	0.998 (0.001)	0.223 (0.006)	0.078 (0.004)	3.529 (0.091)	0.022 (0.001)
10 (1.8)	112.1 (1.553)	0.999 (0.000)	0.330 (0.000)	0.196 (0.012)	6.686 (0.119)	0.028 (0.001)
15 (0.3)	121.3 (1.595)	0.996 (0.001)	0.320 (0.030)	0.340 (0.026)	9.493 (0.215)	0.035 (0.002)
20 (0.4)	118.7 (2.476)	0.995 (0.000)	0.337 (0.031)	0.572 (0.067)	12.398 (0.01)	0.047 (0.005)

$n=3$ with standard deviations in parentheses *values of D_{0^*} are derived from the subtraction of densification due to slippage and rearrangement of primary particles (D_{0^*}) from densification due to initial particle rearrangement (D_0)

P_y : Yield pressure, EE: Elastic energy, PE: Plastic energy

The data illustrated in Tables 3a and 3b indicated that at different compaction forces the StarLac® tablets exhibited lower elastic energies than FlowLac®100 tablets did.

As observed from the hardness profiles of F03 and F04, both formulations were compressible and gave suitable crushing strengths at 15 kN. Due to the difference in composition of the DTAs, StarLac® gave rise to a combination of deformation mechanisms. This indicates that there was a reduction in the brittle behavior of StarLac®.

Study limitation

A limitation of the study is that slugging may not generate reproducible results and therefore the use of a roller compactor may improve reliability.

To obtain an optimized formulation using the same materials, the study can be expanded by implementing more tablet tests to help design a more robust formulation with the aid of a compaction simulator.

CONCLUSION

A CS can precisely and efficiently characterize the compressibility of DTAs in a single compression cycle in real time. The low P_y of the StarLac® formulation indicated better compressibility in comparison to FlowLac®100. Initial characterization of both DTAs used led to understanding of their deformation behavior from the Heckel parameter (P_y) depicting a brittle nature.

Conflicts of interest: No conflict of interest was declared by the authors. The authors alone are responsible for the content and writing of the paper.

REFERENCES

1. Çelik M, Marshall K. Use of a Compaction Simulator System in Tableting Research. *Drug Dev Ind Pharm.* 1989;15:759-800.
2. Khan K A, Rhodes CT. Effect of Variation in Compaction Force on Properties of Six Direct Compression Tablet Formulation. *J Pharm Sci.* 1976;65:1835-1837.
3. Bolhuis GK, de Waard H. Compaction properties of directly compressible materials. *Pharmaceutical Powder Compaction Technology.* CRC Press. 2016;143-204.
4. Klevan I, Nordström J, Bauer-Brandl A, Alderborn G. On the physical interpretation of the initial bending of a Shapiro-Konopicky-Heckel compression profile *Eur J Pharm Biopharm.* 2009;71:395-401.
5. Adams MJ, McKeown R. Micromechanical analyses of the pressure-volume relationship for powders under confined uniaxial compression. *Powder Technology.* 1996;88:155-163.
6. Adams MJ, Mullier MA, Seville JPK. Agglomerate strength measurement using a uniaxial confined compression test. *Powder Technology.* 1994;78:5-13.
7. Denny PJ. Compaction equations: a comparison of the Heckel and Kawakita equations. *Powder Technology.* 2002;127:162-172.
8. Kawakita K, Lüdde KH. Some considerations on powder compression equations. *Powder technology.* 1971;4:61-68.
9. Nordström J, Klevan I, Alderborn G. A particle rearrangement index based on the Kawakita powder compression equation. *Journal of pharmaceutical sciences.* 2009;98:1053-1063.
10. Sonnergaard JM. Investigation of a new mathematical model for compression of pharmaceutical powders. *Eur J Pharm Sci.* 2001;14:149-157.
11. Hooper D, Clarke FC, Mitchell JC, Snowden MJ. A modern approach to the Heckel Equation: The effect of compaction pressure on the yield pressure of ibuprofen and its sodium salt. *J Nanomed Nanotechnol.* 2016;7:3.
12. Alderborn G. *Tablets and compaction* Churchill Livingstone. 2007.
13. Rowe RC, Roberts RJ. *Mechanical Properties: Pharmaceutical Powder Compaction Technology,* Marcel Dekker, Inc;1996.
14. Roberts RJ, Rowe RC. The effect of punch velocity on the compaction of a variety of materials. *J Pharm Pharmacol.* 1985;37:377-384.
15. Denny PJ. Compaction equations: a comparison of the Heckel and Kawakita equations. *Powder Technology.* 2002;127:162-172.
16. Fell JT, Newton JM. Effect of particle size and speed of compaction on density changes in tablets of crystalline and spray-dried lactose. *J Pharm Sci.* 1971;60:1866-1869.
17. Patel S, Kaushal AM, Bansal AK. Effect of particle size and compression force on compaction behavior and derived mathematical parameters of compressibility. *Pharm Res.* 2007;24:111-124.
18. Mahmoodi F, Klevan I, Nordström J, Alderborn G, Frenning G. A comparison between two powder compaction parameters of plasticity: the effective medium A parameter and the Heckel 1/K parameter. *Int J Pharm.* 2013;453:295-299.
19. Kilicarslan M, Çamca R, Imamoglu S, Antep MN, Ocak B, Yuksel N. Investigation on the flow properties and compressibilities of different direct tableting agents by using pyridoxine hydrochloride as a model drug. *J Fac Pharm.* 2009;38:331-344.
20. Duberg M, Nyström C. Studies on direct compression of tablets. XVII. Porosity-pressure curves for the characterization of volume reduction mechanisms in powder compression. *Powder Technol.* 1986;46:67-75.
21. Hauschild K, Picker-Freyer KM. Evaluation of a new co-processed compound based on lactose and maize starch for tablet formulation. *AAPS pharmSci.* 2004;6:e16.



Determining the Best Poloxamer Carrier for Thiocolchicoside Solid Dispersions

Tiyokolşikosid Katı Dispersiyonları için En İyi Poloksamer Taşıyıcının Belirlenmesi

© Hemanth ANNEPOGU¹, © Hindustan Abdul AHAD^{2*}, © Devanna NAYAKANTI³

¹Jawaharlal Nehru Technological University, Research and Development, Ananthapuramu, India

²Raghavendra Institute of Pharmaceutical Education and Research (RIPER), Department of PG Industrial Pharmacy, Ananthapuramu, India

³Jawaharlal Nehru Technological University, Oil Technological and Pharmaceutical Research Institute, Ananthapuramu, India

ABSTRACT

Objectives: The aim of this study of this study was to discover the best poloxamer as a solid dispersion carrier for thiocolchicoside (TCS).

Materials and Methods: The compatibility of TCS with excipients was studied by differential scanning calorimetry and fourier transform infrared spectroscopy. Different formulations of solid dispersions (SDs) were made with poloxamer carriers, i.e. poloxamer-108, poloxamer-188, poloxamer-237, poloxamer-338, and poloxamer-407 were made by taking TCS:poloxamer in ratios of 1:1, 1:2, 1:4, and 1:6. The SDs were made by a novel microwave fusion method and compressed using an 8-station tablet compression machine. The fabricated SD tablets were characterized by physicochemical constraints and drug release rates. The release of TCS from the prepared SDs was later analyzed by kinetic models.

Results: TCS was observed to be compatible with the poloxamer carriers. The SD formulations showed satisfactory physicochemical constraints and TCS release following first-order release.

Conclusion: Among the poloxamer carriers used, poloxamer-188 was the best for increasing the solubility and release rate of TCS from the SDs.

Key words: Thiocolchicoside, poloxamer, solid dispersion, evaluation

ÖZ

Amaç: Bu çalışmanın amacı tiyokolşikosid için en iyi poloksamer katı dispersiyon taşıyıcısını bulmaktır.

Gereç ve Yöntemler: Tiyokolşikosidin eksipyanlarla geçimliliği diferansiyel tarama kolorimetrisi ve fourier transform infrared spektroskopisi ile çalışılmıştır. Katı dispersiyonların (SD) farklı formülasyonları poloksamer-108, poloksamer-188, poloksamer-237, poloksamer-338 ve poloksamer-407 gibi poloksamer taşıyıcılarını tiyokolşikosid: poloksamer oranı 1:1, 1:2, 1:4 ve 1:6 olacak şekilde yapılmıştır. SD'ler yeni bir mikrodalga füzyon metoduyla yapılmıştır ve 8-istasyonlu tablet kompresyon makinesi kullanılarak basılmıştır. Üretilen SD tabletleri fizikokimyasal kısıtlama ve ilaç salım oranları ile karakterize edilmiştir. Hazırlanan SD'lerden salınan tiyokolşikosid daha sonra kinetik modellerle analiz edilmiştir.

Bulgular: Tiyokolşikosid poloksamer taşıyıcılarla geçimli bulunmuştur. SD formülasyonları fizikokimyasal kısıtlamalar açısından ve tek basamaklı salımı takiben tatmin eden tiyokolşikosid salımı göstermiştir.

Sonuç: Kullanılan poloksamer taşıyıcılar arasında, poloksamer-188 çözünürlük artışı ve SD'lerde tiyokolşikosid salımı açısından en iyisi olarak belirlenmiştir.

Anahtar kelimeler: Tiyokolşikosid, poloksamer, katı dispersiyon, değerlendirme

*Correspondence: E-mail: abdulhindustan@gmail.com, Phone: +91 9440944899 ORCID-ID: orcid.org/0000-0001-5329-6878

Received: 19.01.2019, Accepted: 18.04.2019

©Turk J Pharm Sci, Published by Galenos Publishing House.

INTRODUCTION

Industrial pharmacists make many attempts to enhance the solubility of drugs economically. Among the various approaches for enhancing solubility, the solid dispersion (SD) approach is gaining in importance as it is simpler and requires less effort than the other approaches.¹

Thiocolchicoside (TCS) is a colchicoside derivative from *Gloriosa superba* and *Colchicum autumnale*. TCS is a muscle relaxant used to tackle sore muscle shrinkages, acute and arthritic problems, and pains, and it lacks sedative side effects, unlike other muscle relaxants. It is also given with many nonsteroidal anti-inflammatory drugs.²⁻⁵ TCS is a yellow crystalline powder that is slightly soluble in ethyl alcohol and insoluble in chloroform.

The traditional method of preparing SDs is by fusion, in which the polymer-carriers used for SDs are not exposed to a uniform heat from the heat source. To overcome this, a novel microwave (MW) melting technique is adopted. Electromagnetic irradiation was applied in an MW oven with 0.3 to 300 GHz of infrared and radio frequencies equivalent to wavelengths of 1 mm to 1 m. This technique can be adopted for obtaining fast and continuous heating even in materials presenting low heat conductivity (e.g., polymers), because the relocation of energy does not depend on heat diffusion.^{6,7} Thus, this novel MW melting method was adopted in the preparation of SDs.

Much research has been performed on enhancing the solubility of drugs using poloxamers, i.e. poloxamer-108,⁸ poloxamer-188,⁹ poloxamer-237,¹⁰ poloxamer-338,¹¹ and poloxamer-407.¹²

Therefore, it is important to enhance the solubility of TCS, with faster discharge, absorption, and action to relieve acute patients. It also helps researchers to know which poloxamer carrier is best for releasing TCS among poloxamer-108, poloxamer-188, poloxamer-237, poloxamer-338, and poloxamer-407. The current investigation aimed to enhance the solubility of TCS with poloxamer carriers and find out the best among the better poloxamers.

MATERIALS AND METHODS

Materials

TCS was gifted from Yarrow Chemicals. Poloxamer-108, poloxamer-188, poloxamer-237, poloxamer-338, and poloxamer-407 were from Amrutha Organics, Hyderabad. Microcrystalline cellulose, talc, and magnesium stearate were obtained from Colorcon, India. Double distilled water (DW) was utilized whenever appropriate.

Statistical analysis

Solubility studies

Pure TCS was examined for solubility in 0.1 N HCl, water, pH 4.5 acetate buffer, and pH 6.8 and pH 7.4 phosphate buffers.¹³

Drug-excipient compatibility studies

Differential scanning calorimetry (DSC) and fourier transform infrared (FTIR) spectroscopy were used to explore the interaction among the TCS and carriers used in the study.

Differential scanning calorimetry

Pure drug (TCS) and 1:1 ratio of TCS and carriers (SDs) were included in the analysis. About 10 mg of mix (in a DSC aluminum pan) was examined between 50 and 300°C (DSC-50, Shimadzu, Japan).

Fourier transform infrared spectroscopic study

The relations between the ingredients of the SDs were investigated using FTIR spectroscopy. The FTIR spectra of the TCS alone and together with carriers were logged using an FTIR spectrometer (Bruker) by scanning at 4000-400 cm⁻¹ range.

Designing of solid dispersions (physical mixture)

TCS and carrier SDs were prepared by MW induced heating technique.¹⁴ Different percentages of TCS and carrier (Table 1) were put into a glass beaker in CATA- 2R MW oven (Catalytic Systems, Pune, India) at 560 W. In the oven, one beaker containing drug excipient blend was kept in an accurate site every time. The mixture was exposed to MW radiation for prearranged periods (3, 4, 5, and 6 min). Then the beakers with mixtures were left at room temperature to solidify.¹⁵ The SDs were kept in a desiccator for 24 h and smashed in a mortar. The pulverized blends were passed through an 80# sieve (Table 1).

Table 1. Drug (thiocolchicoside):carrier (poloxamer) ratios in various formulations

Drug:carrier	Ratio	Formulation code
TCS: poloxamer-108	1:1	TP108-1
	1:2	TP108-2
	1:4	TP108-3
	1:6	TP108-4
TCS: poloxamer-188	1:1	TP188-1
	1:2	TP188-2
	1:4	TP188-3
	1:6	TP188-4
TCS: poloxamer-237	1:1	TP237-1
	1:2	TP237-2
	1:4	TP237-3
	1:6	TP237-4
TCS: poloxamer-338	1:1	TP338-1
	1:2	TP338-2
	1:4	TP338-3
	1:6	TP338-4
TCS: poloxamer-407	1:1	TP407-1
	1:2	TP407-2
	1:4	TP407-3
	1:6	TP407-4

TCS: Thiocolchicoside

Evaluation of solid dispersions

Flow properties for solid dispersions

The designed SDs were evaluated in terms of their micromeritic characteristics, i.e. angle of repose, true and tapped densities, Carr's index, and the Hausner ratio.^{16,17}

Yield

The % recovery of SDs were determined after full removal of moisture. Thus it includes the weight of dried SDs in the total of the TCS and excipients necessary for making SDs.

$$\% \text{ Yield} = \frac{\text{Actual weight of the SDs}}{\text{Total weight of the TCS and excipients}} \times 100$$

Tablet preparation and depiction

SDs equivalent to TCS were made by direct compression¹⁸ into tablets, after mixing with prerequisite amounts of all ingredients (Table 2) with the aid of a tablet compression machine (8 station-Karnavati Engineering, Ahmedabad, India).

Evaluation of tablets

The following parameters were tested for the TCS SDs tablets.¹⁹⁻²²

Morphological constraints

The tablets were assessed for their uniformity in size and shape.

Thickness

The thickness of the tablets was measured using vernier calipers (Qumos Enterprises, Mumbai, India). They were measured three times.

Hardness

The force needed to fragment the tablets was recorded with a Monsanto tablet hardness tester (Vinsyst Technologies, Mumbai) to determine the physical strength. These tests were performed three times.

Uniformity in weight

Individual lots of 20 tablets were weighed with an electronic digital balance (Citizen, CY-104, Mumbai, India) and the mean was determined. The % change in weight was determined and then compared with IP specifications (limit $\pm 7.5\%$).

Table 2. formulation of a tablet containing solid dispersions

Ingredients	Quantity per tablet (mg)
SDs equivalent to 4 mg of TCS	125
Lactose	50
Starch	15
Microcrystalline cellulose	50
Magnesium stearate	5
Talc	5
The weight of the tablets	250

SDs: Solid dispersions, TCS: Thiocolchicoside

Friability

This test was done with a Roche Friabilator to determine the physical strength of the prepared tablets and to check their intactness when subjected to physical stresses. W_{initial} was recorded for 10 tablets before the test, and they were placed in the drum and spun at 25 rpm for 4 min and W_{final} was recorded. The loss on friability was then determined by the following equation:

$$F = \frac{W_{\text{initial}} - W_{\text{final}}}{W_{\text{initial}}} \times 100$$

Thiocolchicoside calibration curve

The practice of finding TCS by ultraviolet (UV) spectrophotometer at 259 nm was standardized and the TCS was observed to obey the Beer-Lambert law in 2-10 $\mu\text{g/mL}$ concentration.²³

Uniformity of thiocolchicoside content

Tablets from every lot ($n=5$) were taken, weighed, and smashed in a mortar. Then 4 mg of TCS was dissolved in 100 mL of 0.1 M HCl. Next, 0.2 mL of solution was made up to 10 mL with 0.1 M HCl. The absorbance was determined²⁴ at 259 nm with a UV-visible spectrophotometer (Double Beam-lab India, Mumbai). The content evenness was determined from the TCS standard calibration graph.

Dissolution rate/in vitro thiocolchicoside discharge

The dissolution conditions were as below:²⁵

- Apparatus: USP XXIII dissolution test apparatus
- Dissolution medium: 0.1 M HCl
- Volume: 900 mL
- Temperature: $37 \pm 0.5^\circ\text{C}$
- Paddle speed: 50 rpm
- Sampling times: every 5 min
- Sample withdrawn: 10 mL
- Absorbance: 259 nm

Kinetic modeling of TCS discharge

The mechanisms of the TCS discharge from the tablets were examined and the rate kinetics of the SDs was attained with the formula shown below:^{26,27}

- Cumulative % of drug discharged vs time (zero-order plots)
- Log cumulative % of drug enduring vs time (first-order plots)
- Cube root of drug remaining vs time (Hixson-Crowell plots)

Accelerated stability studies

The TCS-SDs tablets were subjected to stability studies for 6 months in different storage environments to determine their sustainability in these storage conditions (Environmental Chamber Model 5532).²⁸

RESULTS

Novel and efficient SDs of TCS with poloxamer carriers using MW fusion (MWF) were prepared. In contrast, TCS matching with the carriers used was confirmed by the DSC thermograms (Figure 1).

The matching of the TCS drug with the poloxamer carriers was established by FTIR studies and the FTIR spectra of the TCS with poloxamer carriers used (Figure 2).

The SDs were checked for flow properties to confirm their free movement from hopper to tableting machine die wall without adhesion. The flow properties of the fabricated TCS-SDs are given in Table 3.

The fabricated TCS tablets were observed to be uniform in size and shape, off white, and odorless with a smooth surface. The prepared formulations' thickness, uniformity of weight, hardness, friability, percent yield, and TCS amount uniformity are given in Table 4.

The main reason for preparing SDs is to increase the solubility of drugs. The solubility of the prepared SDs was studied in various solvents. The solubility of the prepared tablets was high in DW and 0.1 N HCl. These values are shown in Figure 3.

Later TCS discharge was assessed by *in vitro* drug dissolution. The TCS discharge from the tablets was determined by plotting a calibration curve of TCS as per the procedure described before and the calibration curve (Figure 4).

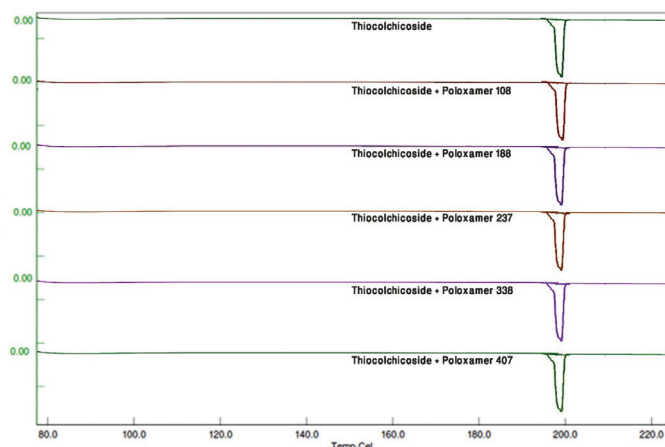


Figure 1. DSC thermograms of thiocolchicoside with poloxamer bases
DSC: Differential scanning calorimetry

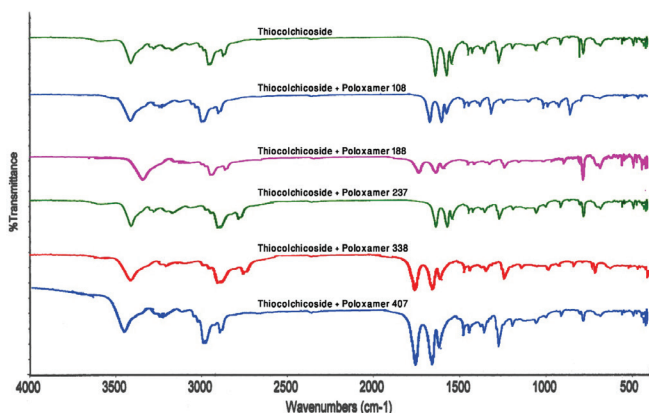


Figure 2. FTIR spectrum of thiocolchicoside with poloxamer
FTIR: Fourier transform infrared

The solubility of TCS SDs was further demonstrated by *in vitro* testosterone dissolution studies. All the SDs showed satisfactory drug discharge. The SDs containing TCS:poloxamer (1:6) showed better discharge than the other formulations (Figure 5).

The TCS discharge mechanism from the tablets was determined by kinetic treatment of *in vitro* drug dissolution data. The correlation (R^2) values are given in Table 5. The first-order and Hixson-Crowell's plots are shown in Figures 6 and 7.

DISCUSSION

DSC is a vital tool for obtaining evidence quickly about suitability among the TCS and the carrier by the presence, swing, or vanishing of endothermic/exothermic peaks.²⁹ DSC gives an insight into the melting and recrystallization activities of SDs. Neither loss of characteristic peaks nor appearance of new peaks were documented upon DSC analyses and confirms the lack of incompatibility between the TCS and the carrier used.³⁰ The DSC points were attained on pure TCS and physical blend. The thermograms of TCS with poloxamer combinations were shifted towards the left, indicating proper impregnation of TCS with the carriers used. The characteristic peaks and stretches of pure TCS were also seen in the TCS-poloxamer carrier combinations, indicating no incompatibility of TCS with the carriers used.

FTIR spectroscopy is another significant approach to determine possible chemical interactions among TCS and the excipients. The orientation of new absorption bands gives the main signals of the interaction among TCS and the active substance.³¹ The FTIR spectra showed that typical TCS bands and carrier separately were not rehabilitated in the mixtures, which indicates no interactions between TCS and poloxamer.

The spectra of TCS show prominent bands at 1556.6 cm^{-1} , attributed to the C=O stretching, tropane ring at 1647.6 cm^{-1} , Amide II band (N-H stretching) at 3326.98 cm^{-1} , and -OH stretching band at 3413.77 cm^{-1} . All these bands were seen undisturbed even in TCS-poloxamer blends and are given in Figure 2.

The free flow of SDs from the hopper was confirmed by the micromeritic properties. The fabricated TCS SDs showed very good flow properties in terms of the angle of repose (34.52 ± 0.02 to $25.21 \pm 0.03^\circ$) and nearly spherical particles. The compressibility index was 0.877 ± 0.05 to 10.552 ± 0.09 , signifying good compression properties while tableting. The fabricated TCS tablets were uniform in size and shape, off white, and odorless, with a smooth surface.

The TCS tablets appeared to be uniform in thickness (4.5 mm) and weight, indicating the TCS and excipients used were added and blended properly. The loss on friability was <1% and the hardness was more than 4 kg/cm^2 , indicating that the tablets have good mechanical strength, and that means good cohesive properties of SDs for compressing them into tablets. The yield was observed to be good (>90%) and TCS content was uniform.

Pure TCS was checked for solubility in various media, i.e. water, 0.1 N HCl, pH 4.5 acetate buffer, pH 6.8 phosphate buffer, and

Table 3. Flow character specifications

Formulation	Flow properties				
	Angle of repose (°)	Bulk density	Tapped density	Carr's index	Hausner ratio
TP108-1	33.95±0.03	0.785±0.05	0.799±0.06	1.752±0.01	1.017±0.01
TP108-2	29.64±0.05	0.458±0.02	0.466±0.01	1.716±0.08	1.017±0.01
TP108-3	28.45±0.02	0.635±0.01	0.654±0.06	2.905±0.02	1.029±0.02
TP108-4	29.05±0.05	0.258±0.01	0.268±0.01	3.731±0.05	1.038±0.01
TP188-1	27.37±0.09	0.528±0.03	0.536±0.04	1.492±0.01	1.015±0.01
TP188-2	31.22±0.06	0.568±0.07	0.578±0.04	1.730±0.03	1.017±0.03
TP188-3	31.55±0.05	0.258±0.01	0.268±0.01	3.731±0.07	1.038±0.09
TP188-4	25.84±0.06	0.269±0.05	0.287±0.02	6.271±0.05	1.066±0.05
TP237-1	26.37±0.05	0.356±0.03	0.398±0.01	10.552±0.09	1.117±0.01
TP237-2	30.50±0.05	0.524±0.05	0.545±0.03	3.853±0.04	1.040±0.03
TP237-3	29.41±0.03	0.425±0.03	0.457±0.01	7.002±0.09	1.075±0.03
TP237-4	29.15±0.04	0.546±0.04	0.555±0.06	1.621±0.05	1.016±0.07
TP338-1	30.50±0.06	0.365±0.05	0.389±0.02	6.169±0.06	1.065±0.08
TP338-2	29.12±0.06	0.358±0.01	0.364±0.02	1.648±0.01	1.016±0.01
TP338-3	25.21±0.03	0.452±0.03	0.456±0.05	0.877±0.05	1.008±0.01
TP338-4	26.09±0.06	0.254±0.08	0.259±0.01	1.930±0.01	1.019±0.07
TP407-1	26.27±0.04	0.524±0.01	0.541±0.03	3.142±0.02	1.032±0.02
TP407-2	30.28±0.06	0.658±0.05	0.666±0.01	1.201±0.01	1.012±0.01
TP407-3	34.52±0.02	0.524±0.05	0.566±0.01	7.420±0.09	1.080±0.08
TP407-4	28.46±0.02	0.425±0.01	0.433±0.01	1.847±0.01	1.018±0.01

All values given as mean ± SD, trials (n=3), SD: Standard deviation

Table 4. Physical characteristics of prepared solid dispersions

Physical parameter						
Formulation	Uniformity of weight (mg)	Hardness (cm ²)	Thickness (mm)	Friability (%)	Yield (%)	Assay (%)
TP108-1	250.2±2.01	6.5±0.21	4.50±0.01	0.18±0.02	88.2±0.85	102.5±1.23
TP108-2	254.3±1.25	5.2±0.09	4.53±0.02	0.62±0.07	89.3±0.65	96.7±0.44
TP108-3	255.2±0.12	6.9±0.08	4.50±0.03	0.53±0.04	90.5±0.94	99.5±0.77
TP108-4	255.2±0.98	5.3±0.06	4.51±0.04	0.45±0.03	99.2±0.32	100.6±0.48
TP188-1	255.1±0.65	4.9±0.07	4.51±0.02	0.51±0.01	96.8±0.65	97.8±0.05
TP188-2	250.9±0.54	4.5±0.01	4.53±0.02	0.62±0.09	98.8±1.25	97.3±0.85
TP188-3	252.3±0.96	5.7±0.01	4.50±0.04	0.53±0.03	97.8±1.95	96.2±0.06
TP188-4	253.8±0.08	6.3±0.02	4.51±0.06	0.55±0.04	98.6±3.26	99.0±2.25
TP237-1	250.5±0.17	5.3±0.03	4.50±0.02	0.61±0.01	95.6±0.68	100.6±0.08
TP237-2	250.1±0.07	4.5±0.04	4.50±0.06	0.82±0.01	92.5±0.84	97.1±0.84
TP237-3	254.2±0.84	5.2±0.02	4.51±0.01	0.45±0.02	95.6±1.39	96.8±0.16
TP237-4	252.2±0.63	6.0±0.01	4.50±0.04	0.35±0.03	98.5±1.28	97.3±0.08
TP338-1	251.3±0.83	5.3±0.02	4.50±0.02	0.51±0.05	92.3±0.94	96.1±0.09
TP338-2	252.3±0.10	4.5±0.01	4.51±0.03	0.72±0.01	90.7±0.83	98.5±0.09
TP338-3	251.2±0.54	7.2±0.07	4.52±0.08	0.63±0.02	97.4±0.64	97.8±0.75
TP338-4	250.2±1.28	8.3±0.04	4.50±0.03	0.25±0.03	98.3±0.88	96.6±0.84
TP407-1	250.2±2.26	4.5±0.03	4.51±0.05	0.41±0.03	92.8±1.23	98.9±0.99
TP407-2	251.2±2.39	4.2±0.02	4.52±0.03	0.52±0.01	96.8±1.29	100.9±2.25
TP407-3	250.1±1.25	6.3±0.01	4.50±0.04	0.53±0.03	97.9±0.36	97.8±0.23
TP407-4	252.1±1.24	5.2±0.01	4.51±0.03	0.65±0.07	99.1±0.35	99.6±0.09

All values given as mean ± SD, trials (n=3), SD: Standard deviation

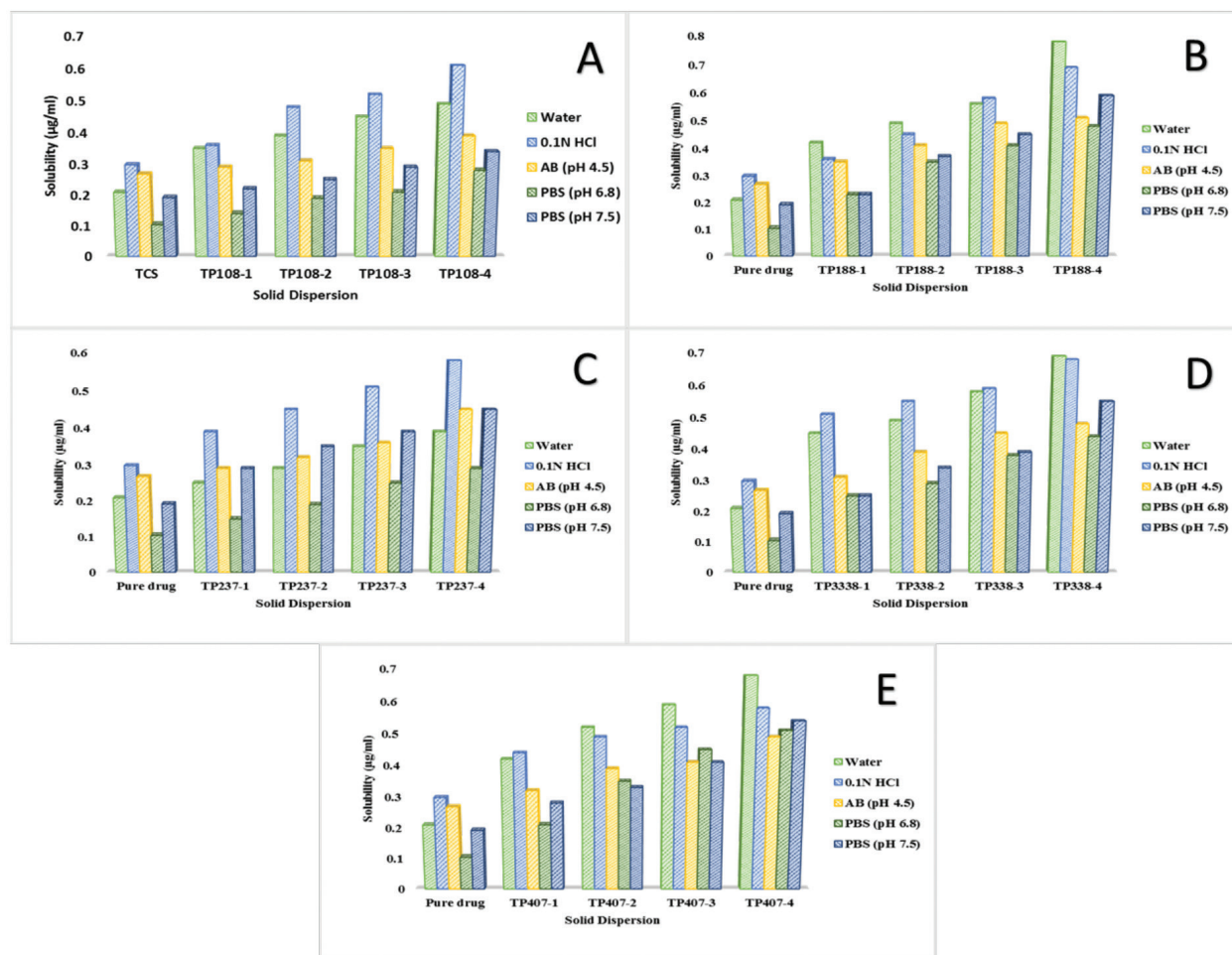


Figure 3. Solubility of thiocolchicoside and solid dispersions in various media with A) poloxamer-108; B) poloxamer-188; C) poloxamer-237; D) poloxamer-338; E) poloxamer-407
TCS: Thiocolchicoside

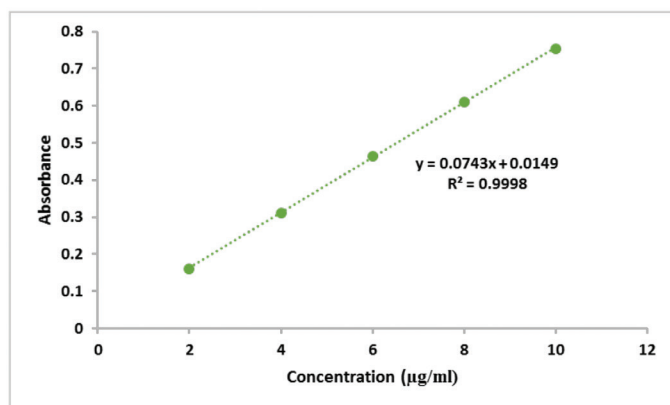


Figure 4. Calibration curve for the estimation of thiocolchicoside

pH 7.4 phosphate buffer. The solubility in these was $<0.3 \mu\text{g/mL}$, indicating poor solubility of the drug.

The SD tablets with poloxamer-108 (TP108-1, TP108-2, TP108-3, and TP108-4) showed good solubility in 0.1 N HCl (up to $0.61 \pm 0.05 \mu\text{g/mL}$) and in DW (up to $0.49 \pm 0.03 \mu\text{g/mL}$). The tablets with poloxamer-188 (TP188-1, TP188-2, TP188-3, and

TP188-4) showed good solubility in DW (up to $0.78 \pm 0.04 \mu\text{g/mL}$) and in 0.1 N HCl (up to $0.69 \pm 0.05 \mu\text{g/mL}$). The SDs tablets with poloxamer P-237 (TP237-1, TP237-2, TP237-3, and TP237-4) showed good solubility in 0.1 N HCl (up to $0.58 \pm 0.04 \mu\text{g/mL}$) and in acetate buffer (pH 6.8) (up to $0.45 \pm 0.03 \mu\text{g/mL}$). The tablets with poloxamer-338 (TP338-1, TP338-2, TP338-3, and TP338-4) showed good solubility in DW (up to $0.69 \pm 0.04 \mu\text{g/mL}$) and in 0.1 N HCl (up to $0.68 \pm 0.05 \mu\text{g/mL}$). The tablets with poloxamer-407 (TP407-1, TP407-2, TP407-3, and TP407-4) showed good solubility in DW (up to $0.68 \pm 0.05 \mu\text{g/mL}$) and in 0.1 M HCl (up to $0.58 \pm 0.03 \mu\text{g/mL}$). The nonionic surfactant component of poloxamer enhances the solubility of TCS in solvents.^{32,33}

TCS followed the Beer-lambert law at the concentration of 2 to 10 $\mu\text{g/mL}$. The regression produced $R^2=0.9998$; slope= $0.0743x+0.0149$. The dissolution of the tablets was good in a lot of TCS:poloxamer (1:6) with all carriers, i.e. poloxamer-108, poloxamer-188, poloxamer-237, poloxamer-338, and poloxamer-407.

Furthermore, the hydrophilic polyoxyethylene part of the copolymer prevented aggregation of individual drug particles,

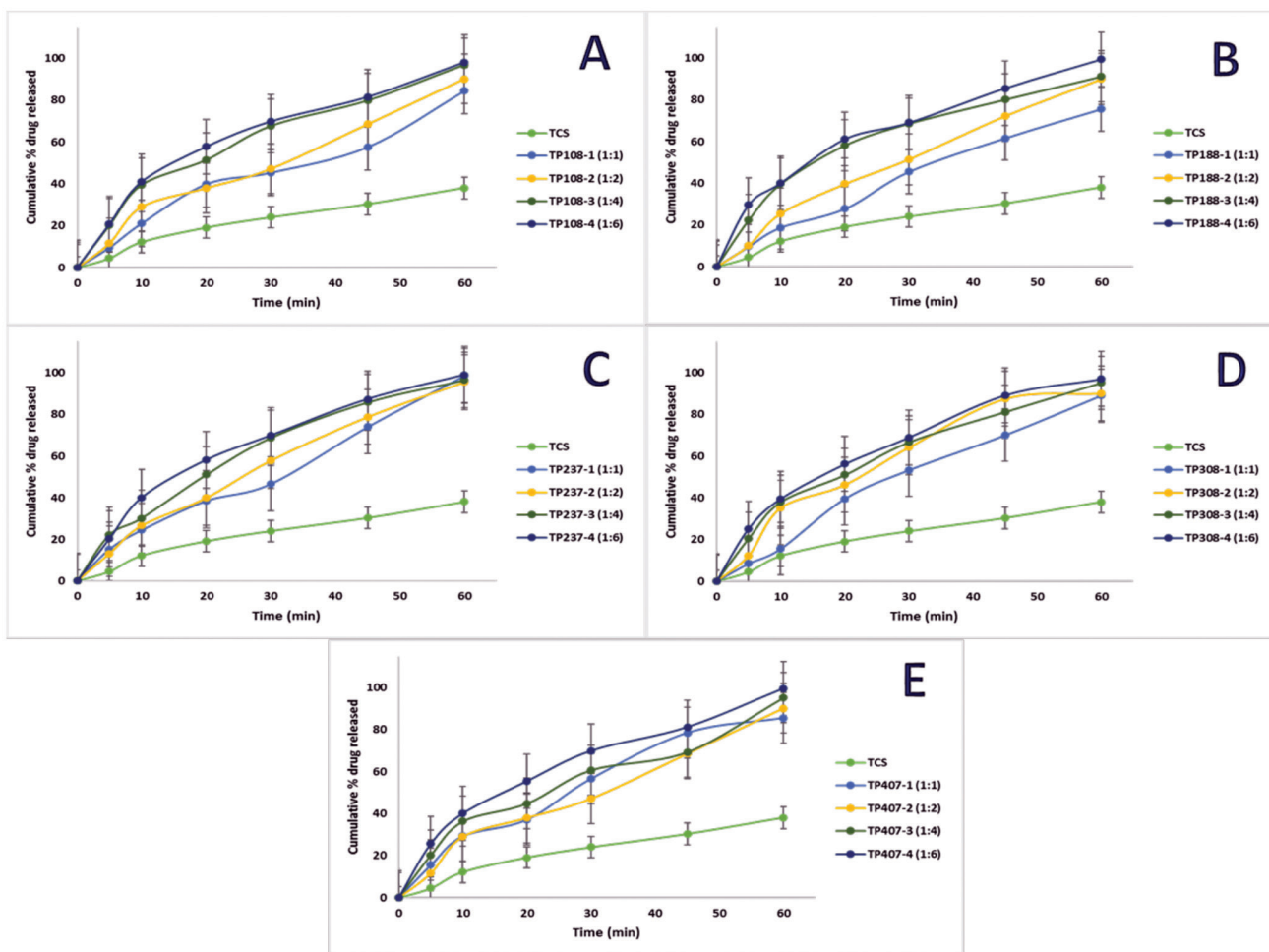


Figure 5. *In vitro* drug dissolution plots of thiocolchicoside solid dispersions with A) poloxamer-108; B) poloxamer-188; C) poloxamer-237; D) poloxamer-338; E) poloxamer-407
TCS: Thiocolchicoside

Table 5. Correlation coefficients (R²) for different release kinetics of thiocolchicoside solid dispersions

Formulation	Zero order	First order	Hixson-Crowell
TP108-4	0.9738	0.9936	0.9979
TP188-4	0.5025	0.9885	0.9868
TP237-4	0.8823	0.9494	0.9206
TP338-4	0.9785	0.9868	0.9860
TP407-4	0.9738	0.9666	0.9804

exhibiting high solid-liquid surface tension. Hence, it acted on the hydrodynamic layer adjacent to the TCS particles, resulting in an *in situ* inclusion progression that augmented dissolution. Similar observations have been reported for SDs by Viraj and Praveen.³⁴

The regression gave R²=0.9930, 0.9869, 0.9868, 0.8869 and 0.9980 for the first-order plots and 0.9979, 0.9868, 0.9206, 0.9860 and 0.9804 for the Hixson-Crowell models for formulations TP108-4, TP188-4, TP237-4, TP338-4, and TP407-

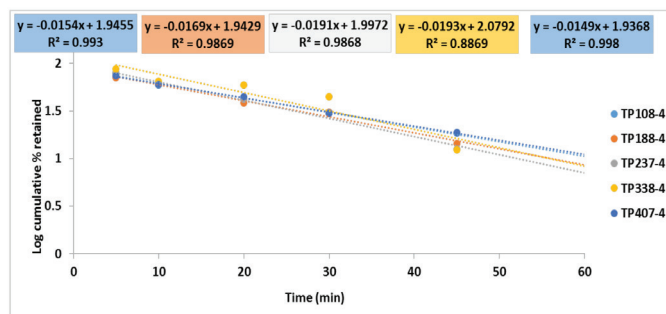


Figure 6. First-order plots for formulations with the drug:carrier ratio 1:6

4. Accelerated stability studies for the optimized formulation (TP188-4) revealed that these formulations retained their physical parameters even after extreme storage environments.

CONCLUSION

The attempt at elevating solubility was successful using various poloxamer carriers in 1:6 ratios of drug and carrier (TP108-4, TP188-4, TP237-4, TP338-4, and TP407-4) by making them into SD formulations. The MWF method was better than the

other techniques of making SDs as MWF enables the exposure of drug and polymers to a uniform temperature and prevents overheating. TCS and poloxamer interactions studied using DSC and FTIR confirmed the suitability of polymer carrier with TCS. All the SDs were found to raise the solubility of TCS. Among the SDs the preparations with 1:6 ratios of TCS and poloxamer-188 (TP188-4) had better solubility and drug dissolution constraints compared to poloxamer-108, poloxamer-237, poloxamer-338, and poloxamer-407. This advance in formulation technology, MWF, is better than other conventional SDs preparation

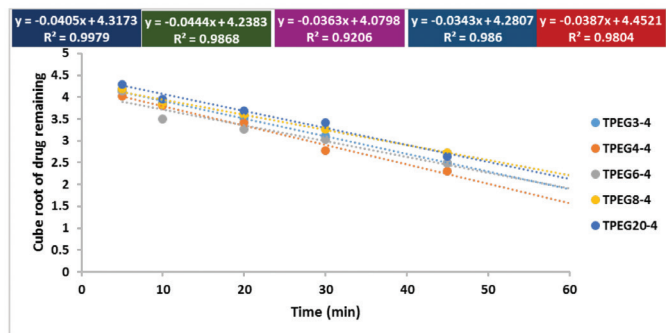


Figure 7. Hixson-Crowell plots for formulations with the drug:carrier ratio 1:6

techniques in terms of preparation and drug release. Hence we can conclude that poloxamer-188 is a better poloxamer carrier compared to poloxamer-108, poloxamer-237, poloxamer-338, and poloxamer-407 for preparing TCS SDs.

ACKNOWLEDGMENTS

The authors are thankful to Prof. N. Devanna, director, JNTUA-OTPRI, Ananthapuramu, AP, India, for providing lab facilities for doing this research work.

Conflicts of interest: No conflict of interest was declared by the authors. The authors alone are responsible for the content and writing of the paper.

REFERENCES

- Den Mooter GV. The use of amorphous solid dispersions: a formulation strategy to overcome poor solubility and dissolution rate. *Drug Discovery Today Technologies*. 2011;9:79-85.
- Tüzün F, Unalan H, Oner N, Özgüzel H, Kirazlı Y, İçağasioğlu A, Kuran B, Tüzün S, Başar G. Multicenter, randomized, double-blinded, placebo-controlled trial of Thiocolchicoside in acute low back pain. *Joint Bone Spine*. 2003;70:356-361.
- Soonawalla DF, Joshi N. Efficacy of Thiocolchicoside in Indian patients suffering from low back pain associated with muscle spasm. *J Indian Med Assoc*. 2008;106:331-335.
- Maryadele J. *The Merck Index*; Thirteenth edition; Merck & Co Inc. White house Station, NJ, USA; 2001:1662-1663.
- Janbroers JM. Review of the toxicology, PD and PK of Thiocolchicoside, a GABA-agonist muscle-relaxant with anti-inflammatory and analgesic actions. *Acta Ther*. 1987;13:221-250.
- Zawar L, Bari S. Microwave induced solid dispersion as a novel technique for enhancing dissolution rate of Repaglinide. *Adv Pharmacol Pharm*. 2013;1:95-101.
- Moneghini M, Bellich B, Baxa P, Princivalle F. Microwave generated solid dispersions containing Ibuprofen. *Int J Pharm*. 2008;361:125-130.
- Rashmika B, Veena V, Kachhwaha S, Bhikshapathi DVRN. Formulation development and in vivo evaluation of Fexofenadine HCl solid dispersions by spray drying technique. *Der Pharmacia Lettre*. 2013;5:73-82.
- Xifeng Zhai, Li C, Lenon GB, Xue CCL, Li W. Preparation and characterisation of solid dispersions of tanshinone IIA, cryptotanshinone and total tanshinones. *Asian J of Pharm Sci*. 2017;12:85-97.
- Orlandi S, Priotti J, Diogo HP, Leonardi D, Salomon CJ, Nunes TG. Structural Elucidation of Poloxamer 237 and Poloxamer 237/Praziquantel Solid Dispersions: Impact of Poly (Vinylpyrrolidone) over Drug Recrystallization and Dissolution. *AAPS Pharm Sci Tech*. 2018;19:1274-1286.
- Moneghini M, Zordi N, Grassi M, Zingone G. Sustained-release solid dispersions of ibuprofen prepared by microwave irradiation. *Journal of Drug Delivery Science and Technology*. 2008;18:327-333.
- Seetha D, Peddinti D, Pinnika A. Formulation and evaluation of solid dispersion tablets of poorly water soluble drug candesartan cilexetil using poloxamer 407. *Int J of Pharm Sci Review and Research*. 2014;29:67-73.
- Zhao Y, Xin T, Ye T, Yang X, Pan W. Solid dispersion in the development of a Nimodipine delayed-release tablet formulation. *Asian J Pharm Sci*. 2014;9:35-41.
- Papadimitriou SA, Bikiaris DN, Avgoustakis K. Microwave-Induced Enhancement of the Dissolution Rate of Poorly Water-Soluble Tibolone from Poly (ethylene glycol) Solid Dispersions. *Journal of Applied Polymer Science*. 2008;108:1249-1258.
- Mourya D, Belamwar V, Tekade A. Microwave induced solubility enhancement of poorly water soluble atorvastatin calcium. *J Pharm Pharmacol*. 2010;62:1599-1606.
- Martin A. *Physical Pharmacy*. 4th ed. Maryland, USA: Lippincott Williams and Wilkins; 1991:423.
- Shah RB, Tawakkul MA, Khan MA. Comparative evaluation of flow for pharmaceutical powders and granules. *Aaps Pharmscitech*. 2008;9:250-258.
- Chiou WL, Riegelman S. Preparation and dissolution characteristics of several fast-release solid dispersions of Griseofulvin. *J Pharm Sci*. 1969;58:1505-1510.
- Gu B, Linehan B, Tseng YC. Optimization of the Buchi B-90 sprays drying process using a central composite design for preparation of solid dispersions. *Int J Pharm*. 2015;491:208-217.
- Annepogu H, Hindustan AA, Devanna N. Assessing the best polyvinyl pyrrolidone as a carrier for Etoricoxib solid Dispersions: fabrication and evaluation. *J Pharm Sci Innov*. 2018;7:208-214.
- Lachman L, Liberman HA, Kanig JL *The Theory and Practice of Industrial Pharmacy*. Philadelphia, PA: Lea and Febiger; 1987:317-318.
- Faheem B, Ahad HA, Shameena S, Asif M, Meena M, Abdul Riyaz S. Determining the Best Poly Ethylene Glycol as Solid Dispersion Carrier for Improvement of Solubility and Dissolution Rate of Ofloxacin. *Int J Chem Pharm Sci*. 2017;5:72-76.

23. Annapurna MM, Priya NK, Anusha N, Purneshwar PB. New derivative spectrophotometric methods for the determination of thiocolchicoside - A semisynthetic derivative of colchicoside, *International Journal of Green Pharmacy*. 2018;12(Suppl):149-153.
24. Ayman A. Spectrophotometric and spectrofluorometric methods for the determination of NSAIDs. *Arabian J Chemistry*. 2013;6:145-163.
25. Indian Pharmacopoeia, Volume III; Government of India, Ministry of Health & Family Welfare; the Indian Pharmacopoeia Commission; Ghaziabad. 2010:2213.
26. Chen ZP, Sun J, Chen HX, Xiao YY, Liu D, Chen J, Cai H, Cai BC. Comparative pharmacokinetics and bioavailability studies of quercetin, kaempferol and isorhamnetin after oral administration of Ginkgo biloba extracts, Ginkgo biloba extract phospholipid complexes and Ginkgo biloba extract solid dispersions in rats. *Fitoterapia*. 2010;81:1045-1052.
27. Lheritier AC, Abramovici JM. Improvement of the dissolution kinetics of SR 33557 by means of solid dispersions containing PEG 6000. *International Journal of Pharmaceutics*. 1995;123:273-279.
28. Remunan C, Bretal MJ, Nunez A, Jato JV. Accelerated stability of sustained release tablet prepared with Gelucire. *Int J Pharm*. 1992;80:151-159.
29. Daniel JSP, Veronez IP, Rodrigues LL, Trevisan MG, Garcia JS. Risperidone-solid-state characterization and pharmaceutical compatibility using thermal and non-thermal techniques. *Thermochimica Acta*. 2013;568:148-155.
30. Kolasinac N, Kachrimanis K, Homsek I, Grujic B, Duric Z, Ibric S. Solubility enhancement of desloratadine by solid dispersion in poloxamers. *Int J Pharm*. 2012;436:161-170.
31. Veronez IP, Daniel JSP, Junior CEC, Garcia JS, Trevisan MG. Development, characterization, and stability studies of ethinyl estradiol solid dispersion. *J Therm Anal Calorim*. 2014;120:573-581.
32. Suhagia BN, Patel HM, Shah SA, Rathod I, Parmar VK. Preparation and characterization of Etoricoxib-polyethylene glycol 4000 plus polyvinyl pyrrolidone K30 solid dispersions. *Acta Pharm*. 2006;56:285-298.
33. Barzegar-Jalalia M, Valizadeha H, Dastmalchi S, Shadbada MRS, Barzegar-Jalalie A, Adibkia K, Mohammadia G. Enhancing dissolution rate of Carbamazepine via co-grinding with crospovidone and hydroxypropylmethylcellulose. *Iranian J Pharm Res*. 2007;6:159-165.
34. Viraj VK, Praveen DC. Characterization of Etoricoxib Solid Dispersions Prepared By Spray Drying Technique. *Research J Pharm and Tech*. 2010;3:1158-1166.



The Formulation of Methylene Blue Encapsulated, Tc-99m Labeled Multifunctional Liposomes for Sentinel Lymph Node Imaging and Therapy

Sentinel Lenf Nodu Görüntüleme ve Tedavisi İçin Metilen Mavisi Enkapsüle Edilmiş, Tc-99m İşaretli Çok-Fonksiyonlu Lipozomların Formülasyonu

© Mine SİLİNDİR GÜNAY

Hacettepe University Faculty of Pharmacy, Department of Radiopharmacy, Ankara, Turkey

ABSTRACT

Objectives: Methylene blue (MB) is a commonly used dye that can be used for near-infrared (NIR) imaging and photodynamic therapy (PDT) by producing reactive oxygen species after light exposure, inducing apoptosis. The limiting factor of MB is its poor penetration through cell membranes. Its decreased cellular uptake can be prevented by encapsulation in drug delivery systems such as liposomes. Additionally, the enhanced permeability and retention effect of tumors enables enhanced accumulation of nanocarriers at the target site.

Materials and Methods: Nanosized, MB encapsulated, Tc-99m radiolabeled Lipoid S PC:PEG2000-PE:Chol: DTPA-PE and DPPC:PEG2000-PE:Chol:DTPA-PE liposomes were formulated to design multifunctional theranostic nanocarriers for: 1) NIR imaging, 2) gamma probe detection of sentinel lymph nodes (SLNs), and 3) PDT, which can provide accurate imaging and therapy helping surgery with a single liposomal system. The characterization of liposomes was performed by measuring particle size, zeta potential, phospholipid content, and encapsulation efficiency. Additionally, the *in vitro* release profile of MB and physical stability were also evaluated over 6 months at determined time intervals by measuring the mean particle size, zeta potential, encapsulation efficiency, and phospholipid content of liposomes kept at room temperature (25°C) and 4°C.

Results: Tc-99m radiolabeled, nanosized Lipoid S PC:PEG2000-PE:Chol:DTPA-PE and DPPC:PEG2000-PE:Chol:DTPA-PE liposomes showed suitable particle size (around 100 nm), zeta potential (-9 to -13 mV), encapsulation efficiency (around 10%), phospholipid efficiency (around 85-90%), and release profiles. Additionally, the liposomes found stable for 3 months especially when kept at 4°C.

Conclusion: MB encapsulated, Tc-99m radiolabeled, nanosized Lipoid S PC:PEG2000-PE:Chol:DTPA-PE and DPPC:PEG2000-PE:Chol:DTPA-PE liposomes were found to have potential for SLN imaging by gamma probe detection, NIR imaging, and PDT. *In vitro* and *in vivo* imaging and therapeutic efficiency should be definitely evaluated to enable a final decision and our studies on this research topic are continuing.

Key words: Sentinel lymph node, methylene blue, theranostic nanomedicine, diagnosis

ÖZ

Amaç: Metilen mavisi (MV) yakın infrared (NIR) görüntüleme ve foto-dinamik tedavi (PDT) için, ışığa maruziyet sonrası reaktif oksijen radikalleri üreterek apoptozu indükleyen sıklıkla kullanılan bir boyadır. MV'nin hücre membranlarından zayıf penetrasyonu etkinliğini kısıtlayan bir faktördür. Azalmış hücresel alımı lipozomlar gibi ilaç taşıyıcı sistemlere enkapsülasyonu ile önlenir. Ek olarak, tümörlerin artmış geçirgenlik ve tutulum özellikleri nanotaşıyıcıların hedef bölgede tutulumunu sağlar.

Gereç ve Yöntemler: Nanoboyutlu, MV enkapsüle edilmiş, Tc-99m radyo-işaretli Lipoid S PC:PEG2000-PE:Chol:DTPA-PE ve DPPC:PEG2000-PE:Chol:DTPA-PE multifonksiyonel teranostik lipozomları daha kesin görüntüleme ve cerrahiye yardımcı olabilecek tedavi sağlayabilmek amacıyla; 1) NIR görüntüleme, 2) sentinel lenf nodlarının (SLN) gama prob ile tayini ve 3) PDT'yi aynı lipozomal sistemde dizayn edilebilen formülasyonlar olarak hazırlanmıştır. Lipozomların karakterizasyonu partikül boyutu, zeta potansiyeli, fosfolipit içeriği ve enkapsülasyon etkinliği ölçülerek yapılmıştır. Ayrıca, MV'sinin *in vitro* salım profili ve fiziksel stabilitesi altı aylık sürede belirli zaman aralıklarında ortalama partikül boyutu, zeta potansiyeli, enkapsülasyon etkinliği ve fosfolipit içeriği oda sıcaklığında (25°C) ve 4°C'de ölçülerek değerlendirilmiştir.

*Correspondence: E-mail: mines@hacettepe.edu.tr, Phone: +90 312 305 21 52 ORCID-ID: orcid.org/0000-0002-5291-810X

Received: 08.04.2019, Accepted: 27.06.2019

©Turk J Pharm Sci, Published by Galenos Publishing House.

Bulgular: Tc-99m radyo-işaretli, nanoboyutlu Lipoid S PC:PEG2000-PE:Chol:DTPA-PE ve DPPC:PEG2000-PE:Chol:DTPA-PE lipozomları uygun partikül boyutu (100 nm civarında), zeta potansiyeli (-9 mV'den -13 mV'e dek), enkapsülasyon etkinliği (%10 civarında), fosfolipit etkinliği (%85-90 civarında) ve salım profili göstermiştir. Ayrıca, 4°C'de saklandıklarında lipozomlar 3 ay boyunca stabil kalmıştır.

Sonuç: MV enkapsüle, Tc-99m radyo-işaretli, nanoboyutlu Lipoid S PC:PEG2000-PE:Chol:DTPA-PE ve DPPC:PEG2000-PE:Chol:DTPA-PE lipozomlarının SLN'nin gama proba tayin edilebilmesi, NIR görüntüleme ve PDT için potansiyellerinin olduğu bulunmuştur. *In vitro* ve *in vivo* görüntüleme ve tedavi etkinliklerinin daha kesin sonuca ulaşmak için değerlendirilmesi gerekmektedir ve bu konudaki çalışmalarımız devam etmektedir.

Anahtar kelimeler: Sentinel lenf nodu, metilen mavisi, teranostik nanotıp, teşhis

INTRODUCTION

The identification and mapping of sentinel lymph nodes (SLNs) for biopsy or imaging are commonly used for staging of many cancers especially breast cancer. SLNs are important as they are the first nodes draining the primary tumor to which a malignancy is likely to metastasize. Various dyes have been used for SLN identification such as isosulfan blue and methylene blue (MB). MB is a cheap and easily accessible dye that is approved by the Food and Drug Administration. Additionally, its side effects are less serious than those of isosulfan blue.^{1,2} The limiting factor of MB is its poor penetration through cell membranes.

Radiopharmaceuticals have been used as an alternative or in addition to dyes for external imaging and/or radiation detector monitoring for SLN detection and mapping before surgery. Intraoperative use of gamma probe detectors enables confirmation of external sampling procedures by directly counting the various lymph nodes discovered through a small incision. By the use of these methods, various advantages can be achieved: 1) a significant reduction in the duration of the surgical procedure, 2) a significant increase in the accuracy of SLN identification, and 3) a significant decrease in morbidity due to the staging procedure.³

MB is used to diagnose breast tumors with near-infrared (NIR) fluorescence imaging injection after i.v. administration.² NIR imaging is a relatively new field for the investigation of preclinical and clinical applications in cancer imaging with its high spatial resolution and real-time display. The NIR light range (wavelength: 650-900 nm) provides tissue penetration and less autofluorescence from neighboring tissues.^{4,5}

Photodynamic therapy (PDT) has been investigated as a therapeutic approach for a variety of cancers.⁶⁻⁸ Its mechanism depends on photooxidation of biological matter. For this purpose, a photosensitizer is illuminated with a light having an appropriate wavelength to excite and induce photochemical reactions that generate reactive oxygen species inducing cell death.^{9,10} PDT has been used as an experimental treatment approach for different cancer types in many countries^{11,12} and it is generally approved as an effective therapy for some small and localized tumors.¹³ Reduced long-term morbidity is the most important advantage of PDT.^{9,14}

Encapsulation or modification of active pharmaceutical ingredients and/or contrast/radiocontrast agents in nanosystems is desirable due to the enhancement of bioavailability and organ/tissue accumulation by specific targeting, and decrease side effects and dose. Liposomes still attract significant attention for both diagnostic imaging¹⁵ and therapy¹⁶ due to their advantages of encapsulation of different kinds of drugs and modification

with target specific ligands.¹⁷⁻¹⁹ By the effect of reducing particle size to nanometer ranges, polymer modification of surfaces such as PEG steric stabilization can be achieved and rapid removal of liposomes can be prevented from circulation by opsonization with a reticulo-endothelial system (RES) such as plasma proteins and macrophages.¹⁹⁻²¹ Therefore, enhanced circulation time, bioavailability, and especially for diseases related to damaged vessel integrity enhanced drug delivery accumulation and targeting in the desired disease area by enhanced permeability and retention (EPR) effect such as in tumors can be achieved at the end.²¹

Recently, NIR imaging has been used with PDT for a theranostic approach by using appropriate photosensitizer dyes. MB, a cheap and safe dye, has both NIR fluorescence (excitation: 668 nm, emission: 688 nm) and photosensitizer properties. To evaluate SLN detection, MB, isosulfan blue, radioisotopes, and nanocarriers have been used alone or in combination in some previous studies for lymphoscintigraphy and SLN biopsy as a promising approach.^{3,22-24} However, the poor penetration of MB through cell membranes is a limiting factor. Its decreased cellular uptake can be prevented by encapsulating MB in delivery systems such as liposomes. Combining a radionuclide and photosensitizer dye (MB) in one injection can allow both lymphoscintigraphy and lymphatic mapping by nuclear imaging and NIR imaging and also PDT by application of a light giving suitable illumination, which can help in SLN surgery.

The aim of the present study was to formulate MB encapsulated, Tc-99m radiolabeled, PEGylated liposomes to design a multifunctional theranostic nanocarrier for NIR imaging and detection by gamma probe of SLNs and PDT that can be combined with surgery with a single vesicular system. The characterization of liposomes was performed by measurement of particle size, zeta potential, phospholipid content, radiolabeling efficiency, and encapsulation efficiency. The *in vitro* release profile of MB was determined. The *in vitro* stability of the liposomes was also evaluated over 6 months, which were stored at room temperature (25°C) and 4°C.

MATERIALS AND METHODS

Materials

Lipoid S phosphatidylcholine [(PC) from soybean (98%)] and dipalmitoylphosphatidylcholine (DPPC) were kind gifts from Lipoid GmbH (Germany) and Phospholipon GmbH (Germany), respectively. Cholesterol (Chol) was obtained from Sigma-Aldrich (USA). "1,2-Distearoyl-sn-glycero-3-phosphoethanolamine-N-[methoxy(polyethylene glycol)-2000] (ammonium salt) (PEG2000-DSPE) and 1,2-dioleoyl-sn-

glicero-3-phosphoethanolamine (DOPE) were obtained from Avanti Polar Lipids (USA). Diethylenetriaminepentaacetic acid anhydride (DTPA) and MB were obtained from Sigma-Aldrich (Germany). Dimethyl sulfoxide (DMSO) was obtained from Merck (Germany).

DTPA-PE synthesis

DTPA-PE is used for Tc-99m radiolabeling. For its synthesis, 30 μ L of triethylamine was added to 0.1 mM of DOPE in 4 mL of chloroform. This solution was added to 1 mM of DTPA anhydride in 20 mL of DMSO slowly. It was then mixed for 3 h at 25°C under argon gas. Afterwards, the mixed solution was dialyzed against water at 4°C for 2 days and freeze-dried.²⁵⁻²⁹

Preparation of MB encapsulated, PEGylated, DTPA-PE containing liposomes

MB encapsulated, nanosized liposomes were prepared by film hydration.³⁰ Lipid S PC:PEG2000-PE:Chol:DTPA-PE (60:0.9:39:0.1% molar ratio) were used. For this purpose, Lipid S PC, PEG2000-PE, Chol, and DTPA-PE were dissolved in chloroform. The chloroform was then evaporated and the dry lipid film was hydrated with 0.5 mM MB solution in HEPES (1 M, pH 7.4) buffer at 35°C. The liposomes were then extruded twice through polycarbonate membranes having 0.6, 0.4, and 0.2 μ m pore sizes. Afterwards, the liposomes were dialyzed through a cellulose membrane (3500 Da cut-off size) for 12 h.¹

For the preparation of DPPC as phospholipid containing liposomes DPPC:PEG2000-PE:Chol:DTPA-PE (60:0.9:39:0.1% molar ratio) were used for the mixture. The same procedure was also used for the preparation of MB encapsulated DPPC:PEG2000-PE:Chol:DTPA-PE liposomes; the only difference was that the hydration procedure was performed at 60°C.

Characterization of MB encapsulated, PEGylated, DTPA-PE containing liposomes

The characterization of MB encapsulated, liposomal formulations was performed by measuring their mean particle size, zeta potential, phosphate content, and encapsulation efficiency %.

Mean particle size and zeta potential

It was determined by using a Zetasizer Nano ZS (Malvern Instruments UK).³¹

Encapsulation efficiency (%)

After the removal of unencapsulated MB by dialysis, the liposomes were lysed with ethanol. Encapsulated MB amount was determined spectrophotometrically at 660 nm. Encapsulation efficiency (%) was calculated with the help of the standard line and line equation obtained previously. The percentage of entrapped drug was determined by applying Equation 1:

$$\text{Entrapment efficiency (\%)} = (D_e \times 100) / (D_i), \quad (1)$$

where D_e is the amount of entrapped drug and D_i is the initial amount of drug.

Liposomal phospholipid amount

The phosphate content of MB encapsulated liposomes was obtained by a modified method.³² This method depends on the detection of phosphorus content after perchloric acid destruction of liposomes at 797 nm spectrophotometrically (Shimadzu UV-1280, Germany).

Physical stability of liposomes

Any alterations in the mean particle size, zeta potential, and encapsulation efficiency of liposomes were evaluated. The liposomes were kept at two different temperatures (4°C and 25°C) for 6 months and changes in these parameters were evaluated at fixed time intervals (0, 3, 5, 7, 14, 21, 30, 60, 90, 120, 150, 180 days) over 6 months.²⁹

In vitro release studies

The *in vitro* release profile of MB was evaluated by dialysis.²⁷ For this purpose, 1 mL samples of the liposomes were put in dialysis bags (MW cut-off: 2000) in 10 mL of HEPES (1 M, pH 7.4) buffer, and agitated in a shaking water bath (SWB 5050, Labnet International, Canada) (100 oscillations.min⁻¹), which was incubated at 37°C. Then 1 mL of formulations was taken for the measurement of MB concentrations at specific time points. Release of MB in HEPES (1 M, pH 7.4) buffer was determined spectrophotometrically (Shimadzu UV-1280, Germany).

Radiolabeling of MB encapsulated, PEGylated, DTPA-PE containing liposomes

MB encapsulated, DTPA-PE containing liposomes were radiolabeled by tin reduction. For this, 0.5 mL of SnCl₂.2H₂O (1 mg.mL⁻¹) and 1.5 mCi of Tc-99m were mixed with liposomes for 30 min by shaking to allow transchelation.^{28,29} After incubation, the liposomes were dialyzed against HEPES (1 M, pH 7.4) buffer for 5 h at 4°C to remove free Tc-99m by dialysis membrane (3500-Da cut-off size). After removal of unchelated Tc-99m, the radioactivity of liposomes was measured by a gamma counter.

Statistical analysis

All data are given as mean \pm standard deviation. To evaluate the statistical significance of differences among the results, statistical analysis was performed. Depending on the numbers of data, which are less than 30, nonparametric test methods were applied for evaluation. Due to the group number, the Mann-Whitney U test and Kruskal-Wallis test were applied for comparison of two groups and three or more groups, respectively. The significance level was accepted as $p \leq 0.05$.

RESULTS

Tc-99m labeled, MB encapsulated liposomes were formulated for the purpose of SLN detection by gamma probe, NIR imaging, and also PDT of SLNs to perform better detection, mapping, and also a treatment option helping during surgery.

MB encapsulated liposomes were characterized and the results are given in Table 1.

The mean particle sizes of all liposomes were about 100 nm. DPPC containing liposomal dispersions had smaller particle size than Lipid S PC liposomes ($p > 0.05$). The MB

Table 1. Characterization of MB encapsulated liposomal dispersions (n=6)

Liposome formulation	Mean particle size (nm)	PDI	Zeta potential (mV)	Encapsulation efficiency (%)	Phospholipid efficiency (%)
Lipoid S PC:PEG2000-PE:Chol:DTPA-PE	116±0.14	0.17	-13.75±0.21	9.51±0.01	86.8±2.1
DPPC:PEG2000-PE:Chol:DTPA-PE	121±0.19	0.12	-9.81±0.16	11.84±0.02	91.7±3.2

MB: Methylene blue, PC: Phosphatidylcholine, Chol: Cholesterol, DTPA: Diethylenetriaminepentaacetic acid anhydride, DPPC: Dipalmitoylphosphatidylcholine

encapsulation amount of liposomes was higher than that of Lipoid S PC liposomes ($p>0.05$). The liposomes' phosphate content was high, about 85-90%. DPPC containing liposomes had higher phosphate content than Lipoid S PC containing ones did ($p>0.05$).

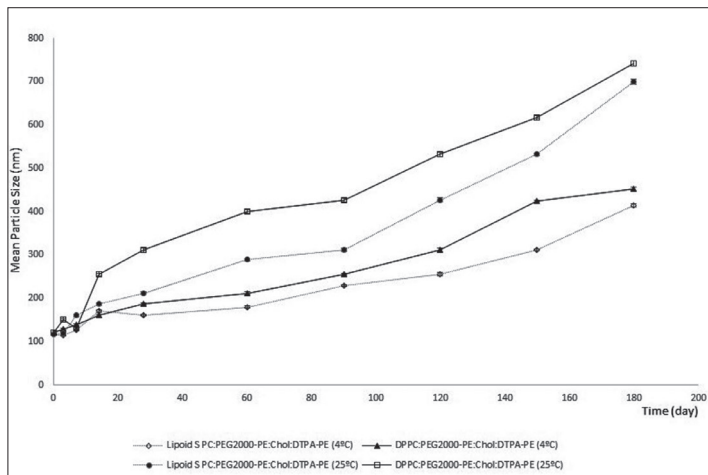


Figure 1. Alterations in mean particle size of MB encapsulated, nanosized liposomes over 6 months of storage at both 4°C and 25°C
MB: Methylene blue, Chol: Cholesterol, DTPA: Diethylenetriaminepentaacetic acid anhydride

Alterations in mean particle size, zeta potential, and MB encapsulation efficiency of liposomes stored at both 4°C and 25°C for 6 months are given in Figures 1-3, respectively. Only slight increases were observed in these parameters of both formulations stored at 4°C at the end of 3 months ($p>0.05$). Higher alterations were observed in these parameters of both liposomes stored at 25°C when compared with those stored at 4°C at the end of 3 months ($p<0.05$). Significant increases were observed in these parameters for all formulations stored at both 4°C and 25°C for 6 months ($p<0.05$). On the other hand, MB encapsulated liposomes were stable due to mean particle size, zeta potential and MB encapsulation efficiency when stored at 25°C for 1 month. When the effect of phospholipid was

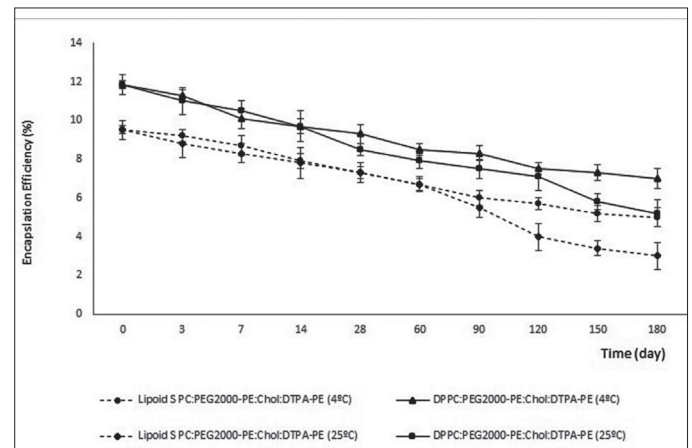


Figure 3. Alterations in MB encapsulation efficiency of nanosized liposomes over 6 months of storage at both 4°C and 25°C
MB: Methylene blue, Chol: Cholesterol, DTPA: Diethylenetriaminepentaacetic acid anhydride

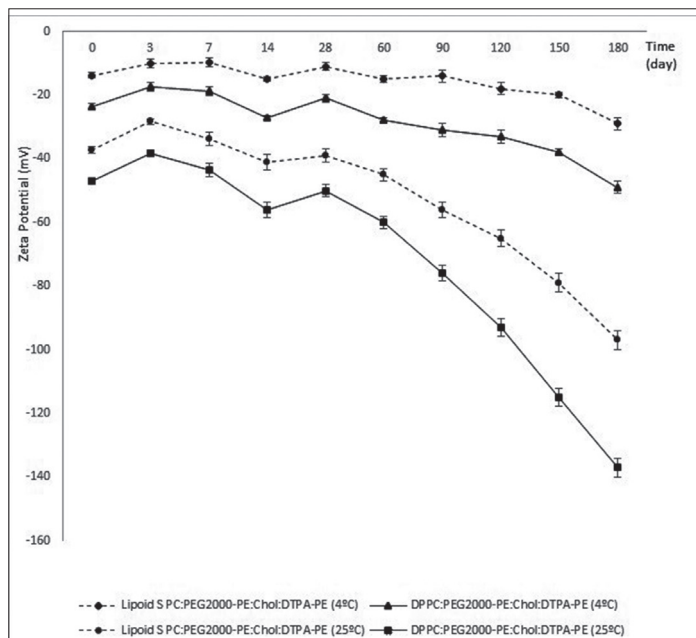


Figure 2. Alterations in zeta potential of nanosized, MB encapsulated liposomes over 6 months of storage at both 4°C and 25°C
MB: Methylene blue, Chol: Cholesterol, DTPA: Diethylenetriaminepentaacetic acid anhydride

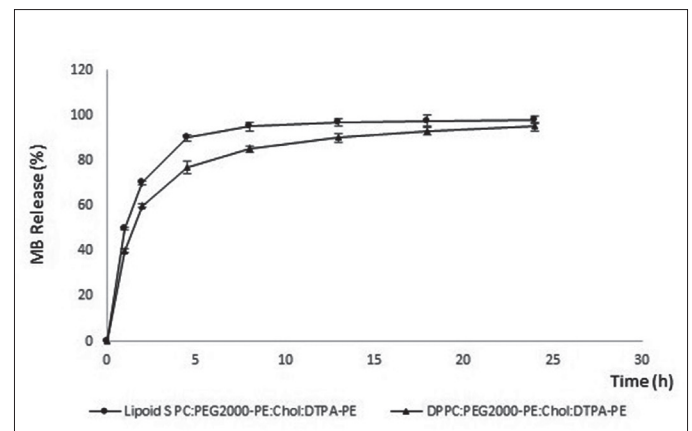


Figure 4. *In vitro* release of nanosized, MB encapsulated liposomes at 37°C
MB: Methylene blue, Chol: Cholesterol, DTPA: Diethylenetriaminepentaacetic acid anhydride

compared, no significant difference was seen between Lipoid S PC containing liposomes and DPPC containing ones stored in the same conditions ($p > 0.05$). These results are compatible with those of previous studies.^{28,29,33}

The *in vitro* release of both MB encapsulated, nanosized liposomes were evaluated by dialysis.²⁷ Lipoid S PC containing liposomes showed slightly faster release of MB when compared with DPPC containing ones ($p > 0.05$). As shown in Figure 4, the two formulations exhibited similar release profiles. A number of studies were found in the literature supporting our data.^{34,35}

DISCUSSION

Both liposomes were formulated to combine a radionuclide and photosensitizer dye (MB) in one injection to achieve both lymphoscintigraphy by nuclear and NIR imaging and also PDT, which can help in surgery.

All formulations exhibited nanosize (around 100 nm) significant for long-circulation and passive targeting by PEGylation to obtain “stealth” formulations, which is essential for EPR effect in tumor accumulation.³⁶ Lipoid S PC containing liposomes have smaller particle size than DPPC containing ones ($p > 0.05$). This may be due to the liquid crystalline structure of Lipoid S PC, which may easily be reduced by extrusion because of greater elasticity than gel state phospholipids. Furthermore, PDI values, which are a significant indicator for the homogeneity of particle size distribution in a dispersion, of MB encapsulated, Lipoid S and DPPC containing liposomes were very small, around approximately 0.1. Surface modification was performed by PEG2000-DSPE coating for all formulations for passive targeting of SLNs and surrounding tumor tissue by EPR effect, which prevents opsonization by RES cells and increasing blood circulation time.

DTPA-PE was synthesized for Tc-99m radiolabeling of formulations due to its metal chelator properties. DTPA is one of the most commonly used chelator agents nowadays for efficient radiolabeling of liposomes for imaging.^{26,28,29} The chelating agent DTPA conjugates to the amino head group with a -COOH group and in this way while PE was incorporated with the lipid bilayer of liposomes, Tc-99m was incorporated with DTPA with high efficiency.^{25,26}

Zeta potential exhibits the magnitude of the electrostatic repulsion/attraction between particles. Therefore, it affects the stability and shelf-life of formulations and provides detailed information about dispersion, aggregation, and flocculation. The zeta potentials of liposomes are suitable (-9 to -13 mV) to prevent aggregation.³⁵ The zeta potential of Lipoid S PC:PEG2000-PE:Chol:DTPA-PE liposomes was slightly higher when compared with DPPC liposomes ($p > 0.05$) due to the different nature of the phospholipids. The MB encapsulation efficiency of DPPC liposomes was slightly higher than that of Lipoid S PC containing ones ($p > 0.05$), due to the gel state of DPPC phospholipid providing less leakage of encapsulated drug through the vesicles. Although the ability to encapsulate hydrophilic drugs within the liposome vesicles was very limited

(5-10%),³⁶ both formulations exhibited about 10% encapsulation efficiency. The phosphate content of all liposomes was very high (around 85-90%), which is essential for obtaining intact liposome vesicles. The phosphate content loss was smaller in DPPC liposomes than in Lipoid S PC liposomes, but this difference was statistically insignificant ($p > 0.05$). This may have been due to the gel state phospholipid content of DPPC liposomes, which is a saturated synthetic lipid and generally forms stable and intact vesicles.

Alterations in the characterization parameters of Lipoid S PC and DPPC liposomes were evaluated over 6 months during storage at both temperatures. Changes in these parameters are essential for evaluating the stability of liposomes. Alterations in zeta potential are also crucial for physical stability, in which any alteration may cause aggregation. Leakage of encapsulated drug is essential for physical stability of liposomes during storage because vesicles should stay stable during storage. Only a slight increase was observed for each measurement in mean particle size, zeta potential, and encapsulation efficiency of both MB encapsulated liposomes stored at 4°C for 3 months ($p > 0.05$). Higher alterations were observed in these parameters of both liposomes stored at 25°C when compared with those stored at 4°C for 3 months ($p < 0.05$). Lipoid S PC and DPPC liposomes were stable when stored at 25°C for 1 month. When the effect of phospholipid amount was compared, no significant difference was evaluated between Lipoid S PC and DPPC containing liposomes stored in the same conditions ($p > 0.05$). This may be because of the liquid crystalline state structure of Lipoid S PC and its low phase transition temperature.^{29,36} As a result, leakage of MB from Lipoid S PC liposomes was higher than that from DPPC liposomes, which is compatible with previous studies.²⁸⁻³³

In vitro release profiles of liposomes are meaningful for predicting an efficient therapeutic effect. The release of MB is faster from liposomes composed of liquid-crystalline type phospholipids, depending on the distance within the polar head groups of liquid crystalline-type phospholipids, and is also faster than in gel state phospholipids.^{34,35} Liposomes comprising DPPC exhibited slightly better *in vitro* MB release amounts than Lipoid S PC containing liposomes. However, this difference was not significant. These results were comparable with previously published results.^{33,36}

Study limitations

Further studies are needed in order to reach to a clearer decision on this topic.

CONCLUSION

MB encapsulated, nanosized, PEGylated, Tc-99m radiolabeled liposomes were designed as potential formulations to accumulate in SLNs due to EPR effect by PEGylation for prolonged blood circulation time and nanosize for imaging and therapy. MB encapsulated, nanosized, PEGylated, Tc-99m radiolabeled Lipoid S PC:PEG2000-PE:Chol:DTPA-PE

and DPPC:PEG2000-PE:Chol:DTPA-PE (60:0.9:39:0.1% molar ratio) liposomes were evaluated as potential carriers for SLN imaging, mapping by gamma probe, NIR imaging, and therapy by PDT, which may help during surgery in terms of vesicular characteristics, release profile, and physical stability. Further studies should be surely performed to enable certain decisions to be made. This study may lead to the design of more specific radiocontrast agents for both imaging and therapy of many cancers.

Conflicts of interest: No conflict of interest was declared by the authors. The authors alone are responsible for the content and writing of the paper.

REFERENCES

- Özdemir A, Mayir B, Demirbakan K, Oygür N. Efficacy of methylene blue in sentinel lymph node biopsy for early breast cancer. *J Breast Health*. 2014;10:88-91.
- Zhang C, Mao Y, Kun Wang, Jie Tian. The identification of breast cancer by Near-Infrared fluorescence imaging with methylene blue. *J Clin Oncol*. 2018;36:15-17.
- Hinkle GH. Lymphoscintigraphy and Sentinel Node Biopsy in The Staging of Cancer. Correspondence Continuing Education Courses for Nuclear Pharmacists and Nuclear Medicine Professionals, 11th ed. The University of New Mexico Health Sciences Center College of Pharmacy Albuquerque, New Mexico; 2005:1-43.
- Kosaka N, Ogawa M, Choyke PL, Kobayashi H. Clinical implications of near-infrared fluorescence imaging in cancer. *Future Oncol*. 2009;5:1501-1511.
- Silindir-Gunay M, Sarcan ET, Ozer AY. Near-infrared imaging of diseases: A nanocarrier approach. *Drug Dev Res*. 2019.
- Rizvi I, Celli JP, Evans CL, Abu-Yousif AO, Muzikansky A, Pogue BW, Finkelstein D, Hasan T. Synergistic enhancement of carboplatin efficacy with photodynamic therapy in a three-dimensional model for micrometastatic ovarian cancer. *Cancer Res*. 2010;70:9319-9328.
- Ahn TG, Lee BR, Choi EY, Kim DW, Han SJ. Photodynamic therapy for breast cancer in a BALB/c mouse model. *J Gynecol Oncol*. 2012;23:115-119.
- Montazerabadi AR, Sazgarnia A, Bahreyni-Toosi MH, Ahmadi A, Shakeri-Zadeh A, Aledavood A. Mitoxantrone as a prospective photosensitizer for photodynamic therapy of breast cancer. *Photodiagnosis Photodyn Ther*. 2012;9:46-51.
- Acedo P, Stockert JC, Cañete M, Villanueva A. Two combined photosensitizers: a goal for more effective photodynamic therapy of cancer. *Cell Death Dis*. 2014;5:1122-1134.
- Sarcan ET, Silindir-Gunay M, Ozer AY. Theranostic polymeric nanoparticles for NIR imaging and photodynamic therapy. *Int J Pharm*. 2018;551:329-338.
- Agostinis P, Berg K, Cengel KA, Foster TH, Girotti AW, Gollnick SO, Hahn SM, Hamblin MR, Juzeniene A, Kessel D, Korbelik M, Moan J, Mroz P, Nowis D, Piette J, Wilson BC, Golab J. Photodynamic therapy of cancer : An update. *Am Cancer J Clin*. 2011;61:250-281.
- Simone CB 2nd, Friedberg JS, Glatstein E, Stevenson JP, Serman DH, Hahn SM, Cengel KA. Photodynamic therapy for the treatment of non-small cell lung cancer. *J Thorac Dis*. 2012;4:63-75.
- Marchal S, Dolivet G, Lassalle HP, Guillemin F, Bezdetnaya L. Targeted photodynamic therapy in head and neck squamous cell carcinoma: heading into the future. *Lasers Med Sci*. 2015;30:2381-2387.
- Dos Santos AF, Terra LF, Wailemann RA, Oliveira TC, Gomes VM, Mineiro MF, Meotti FC, Bruni-Cardoso A, Baptista MS, Labriola L. Methylene blue photodynamic therapy induces selective and massive cell death in human breast cancer cells. *BMC Cancer*. 2017;17:1-15.
- Guenoun J, Koning GA, Doeswijk G, Bosman L, Wielopolski PA, Krestin GP, Bernsen MR. Cationic Gd-DTPA liposomes for highly efficient labeling of mesenchymal stem cells and cell tracking with MRI. *Cell Transplant*. 2012;21:191-205.
- Nisini R, Poerio N, Mariotti S, De Santis F, Fraziano M. The multirole of liposomes in therapy and prevention of infectious diseases. *Front Immunol*. 2018;9:1-23.
- Seleci M, Ag Seleci D, Scheper T, Stahl F. Theranostic liposome-nanoparticle hybrids for drug delivery and bioimaging. *Int J Mol Sci*. 2017;18:1415-1426.
- Silindir M, Erdoğan S, Özer AY, Maia S. Liposomes and their applications in molecular imaging. *J Drug Target*. 2012;20:401-415.
- Silindir-Gunay M, Ozer AY. Liposomes and Micelles as Nanocarriers for Diagnostic and Imaging Purposes. In: Grumezescu AM, ed. *Design of Nanostructures for Theranostics Applications* 1st ed. USA, Elsevier; 2018:305-340.
- Kwon G, Suwa S, Yokoyama M, Okano T, Sakurai Y, Kataoka K. Enhanced tumor accumulation and prolonged circulation times of micelle-forming poly (ethylene oxide)aspartate block copolymers-andriamycin conjugates. *J Control Release*. 1994;29:17-23.
- Maruyama K. Peg-immunoliposomes. *Biosci Rep*. 2002;22:251-266.
- Osborne MP, Richardson VJ, Jeyasingh K, Ryman BE. Potential applications of radionuclide-labelled liposomes in the detection of the lymphatic spread of cancer. *Int J Nucl Med Biol*. 1982;9:47-51.
- Phillips WT, Klipper R, Goins B. Use of ^{99m}Tc-labeled liposomes encapsulating blue dye for identification of the sentinel lymph node. *J Nucl Med*. 2001;42:446-451.
- Bao A, Goins B, Klipper R, Negrete G, Mahindaratne M, Phillips WT. A novel liposome radiolabeling method using ^{99m}Tc-“SNS/S” complexes: *In vitro* and *in vivo* evaluation. *J Pharm Sci*. 2003;92:1893-1904.
- Grant CW, Karlik S, Florio E. A Liposomal MRI contrast agent: phosphatidylethanolamine-DTPA. *Magn Reson Med*. 1989;11:236-243.
- Elbayoumi TA, Torchilin VP. Enhanced accumulation of longcirculating liposomes modified with the nucleosome-specific monoclonal antibody 2C5 in various tumours in mice: Gamma imaging studies. *Eur J Nucl Med Mol Imaging*. 2006;33:1196-1205.
- Zheng J, Perkins G, Kirilova A, Allen C, Jaffray DA. Multimodal contrast agent for combined computed tomography and magnetic resonance imaging applications. *Invest Radiol*. 2006;41:339-348.
- Silindir M, Erdoğan S, Özer AY, Doğan AL, Tuncel M, Ugur Ö, Torchilin VP. Nanosized multifunctional liposomes for tumor diagnosis and molecular imaging by SPECT/CT. *J Liposome Res*. 2013;23:20-27.
- Silindir-Gunay M, Karpuz M, Ozturk N, Ozer AY, Erdogan S, Tuncel M. Radiolabeled, folate-conjugated liposomes as tumor imaging agents: Formulation and *in vitro* evaluation. *J Drug Deliv Sci Technol*. 2019;50:321-328.
- Bangham AD, Standish MM, Watkins JC. Diffusion of univalent ions across the lamellae of swollen phospholipids. *J Mol Biol*. 1965;13:238-252.

31. Silindir-Gunay M, Ozer AY. ^{99m}Tc-Radiolabeled Levofloxacin and micelles as infection and inflammation imaging agents. *J Drug Deliv Sci Technol.* 2020;56:101571.
32. Rouser G, Fleischer S, Yamamoto A. Two dimensional thin layer chromatographic separation of polar lipids and determination of phospholipids by phosphorus analysis of spots. *Lipids.* 1970;5:494-496.
33. Mutlu NB, Değim Z, Yılmaz Ş, Eşsiz D, Nacar A. New perspective for the treatment of Alzheimer diseases: Liposomal rivastigmine formulations. *Drug Dev Ind Pharm.* 2011;37:775-789.
34. Wu PT, Lin CL, Lin CW, Chang NC, Tsai WB, Yu J. Methylene-blue-encapsulated liposomes as photodynamic therapy nano agents for breast cancer cells. *Nanomaterials (Basel).* 2019;9:14.
35. NonoComposix. Zeta potential analysis of nanoparticles. 2012;1:1-6.
36. Shashi K, Satinder K, Bharat P. A complete review on: liposomes. *Int Res J Pharm.* 2012;3:10-17.



Development of Bioadhesive Buccal Tablets of Nicorandil Using a Factorial Approach

Faktöriyel Yaklaşım ile Nikorandil İçeren Biyoadeziv Bukkal Tabletlerin Geliştirilmesi

© Rajendra KOTADIYA^{1*}, © Karan SHAH²

¹Charotar University of Science and Technology, Ramanbhai Patel College of Pharmacy, Changa, India

²Sigma Institute of Pharmacy, Vadodara, India

ABSTRACT

Objectives: In the present investigation, bioadhesive buccal tablets were prepared using the sustained-release polymer hydroxypropyl methylcellulose (HPMC) K100M, bioadhesive polymer neem gum, and an impervious backing layer of ethyl cellulose. Nicorandil is sensitive to the first-pass effect; therefore, a buccal-adhesive dosage form can avoid this effect.

Materials and Methods: We used the direct compression technique to prepare the tablet formulation. A 3² full factorial design was composed in which the amounts of HPMC K100M (X1) and neem gum (X2) were chosen as the independent variables and the dependent variables were the percentage drug release at 6 h (Y1) and mucoadhesive strength in grams (Y2). Various *in vitro* parameters, i.e. thickness, friability, hardness, weight variation, surface pH, moisture absorption ratio, dissolution studies, and drug release kinetics, and *ex vivo* parameters like mucoadhesive strength and mucoadhesion time were determined for the prepared tablets. We subjected the optimized batch to a comparison with the marketed formulation and stability studies were performed.

Results: The formulation containing a 50:50 ratio of neem gum and HPMC K100M (F5) was considered optimum. The zero-order release kinetics model best fitted the optimized batch release profile, suggesting the system would release the drug at a constant rate.

Conclusion: The release by the optimized formulation of the drug at a sustained rate along with its bioadhesive nature showed that the buccal route can be an option for the administration of nicorandil.

Key words: Nicorandil, neem gum, buccal tablets, factorial design

ÖZ

Amaç: Bu araştırmada, biyoadesif bukkal tabletler sürekli salımlı polimer hidroksipropil metilselüloz (HPMC) K100M, biyoadesif polimer neem sakızı ve geçirimsiz etil selüloz arka tabaka kullanılarak hazırlanmıştır. Nikorandil ilk geçiş etkisine karşı duyarlıdır. Bu nedenle, bukkal adesif dozaj formu bu etkiyi önleyebilir.

Gereç ve Yöntemler: Tablet formülasyonu hazırlamak için doğrudan sıkıştırma tekniği kullanılmıştır. HPMCK 100M (X1) ve neem sakızı (X2) miktarları bağımsız değişken olarak ve 6. saat (Y1) ilaç salımı yüzdesi ve gram biriminde mukoadhesif güç yüzde bağımlı değişkenler olarak seçilerek 3² tam faktöriyel tasarımı oluşturulmuştur. Hazırlanan tabletler için farklı *in vitro* parametreler (kalınlık, ufalanma, sertlik, ağırlık sapması, yüzeysel pH'sı, nem absorpsiyon oranı, çözünme çalışmaları ve ilaç salım kinetikleri) ve *ex vivo* parametreler (mukoadesif güç ve mukoadesif zaman) belirlenmiştir. Optimize edilen seri piyasadaki formülasyon ile karşılaştırılmış ve stabilite çalışmaları yapılmıştır.

Bulgular: 50:50 oranında neem zamkı ve HPMC K100M içeren formülasyon (F5)'in en uygun olduğu kabul edilmiştir. Sıfır derece salım kinetiği modeli optimize seri salım profiline en iyi düzeyde uymuştur ve bu sistemin ilacı sabit bir hızda salım sağlayacağını belirtmektedir.

Sonuç: İlacın optimize edilmiş formülasyonunun biyoadesif özelliğinin yanında sürdürülebilir hızla salımı nikorandilin bukkal yol ile uygulanmasının bir seçenek olacağını göstermiştir.

Anahtar kelimeler: Nikorandil, neem sakızı, bukkal tabletler, faktöriyel tasarım

*Correspondence: E-mail: rajendrakotadiya.ph@charusat.ac.in, Phone: +912697265146 ORCID-ID: orcid.org/0000-0002-5484-874X

Received: 30.04.2019, Accepted: 18.07.2019

©Turk J Pharm Sci, Published by Galenos Publishing House.

INTRODUCTION

Hypertension and angina pectoris are cardiovascular diseases for which constant monitoring is crucial. Angina pectoris is a medical condition that causes chest pain by reduced blood flow to the heart. Potassium channel openers are currently regarded as an important drug class for the treatment of such conditions. A primary medicinal agent that possesses an ability to tackle such a situation is nicorandil, a vasodilatory drug.¹⁻³ It appears to be active in all types of angina pectoris and has the twin properties of nitrate and K⁺ adenosine triphosphate channel agonist. The major problem with orally administered nicorandil is its first-pass metabolism, which gives about 75% systemic bioavailability. Moreover, it has a short elimination half-life (1 h), which necessitates frequent administration of the drug (10 to 20 mg twice daily).⁴⁻⁶ Thus, higher fluctuation of drug concentration may give rise to undesirable side effects. In summary, there is a strong requirement for a patient-friendly sustained-release formulation of nicorandil to reduce the frequency of administration.

Such a requirement for an oral dosage form can be fulfilled by employing a buccal bioadhesive drug delivery system. It is a captivating substitute to the oral route of drug administration that overcomes the deficiencies associated with the latter mode of administration. Precisely it prevents any chance of reductant hepatic metabolism, avoiding unneeded drug degradation in the upper GIT, and also it increases the contact between drug and absorbing surface.⁷⁻¹¹ Moreover, such type of delivery is considered safer since drug absorption can be concluded any time if toxicity occurs due to it by removal of the formulation from the site of application.¹²⁻¹⁴

Thus, in the present research, buccal bioadhesive tablets of nicorandil were prepared using the sustained-release polymer hydroxypropyl methylcellulose (HPMC) K100M,^{10,15} bioadhesive polymer neem gum,¹⁶ and an impermeable backing layer of ethyl cellulose. Buccal bioadhesive tablets were prepared by direct compression method employing a 3² factorial design in which the amounts of HPMC K100M (X₁) and neem gum (X₂) were selected as independent variables and their effects on dependent variables, i.e. percentage drug release at 6 h (Y₁) and mucoadhesive strength in grams (Y₂), were studied.

MATERIALS AND METHODS

Materials

Nicorandil was a gratis sample from Sun Pharma Laboratories Ltd. (East Sikkim). Neem gum was purchased from the local market and the remaining materials were purchased from Chem Dyes Corporation (Vadodara, Gujarat, India).

Methods

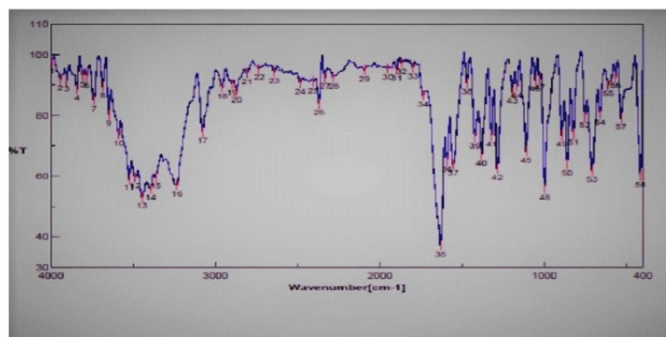
Drug-excipients compatibility study

Accurately weighed (3 mg) nicorandil was taken and mixed thoroughly with 100 mg of potassium bromide (dried at 40-50°C). The mixture was compressed into pellets (under 10-t pressure) using a hydraulic press followed by scanning between 4000 and 400 cm⁻¹ using an fourier transform-infrared (FT-IR)

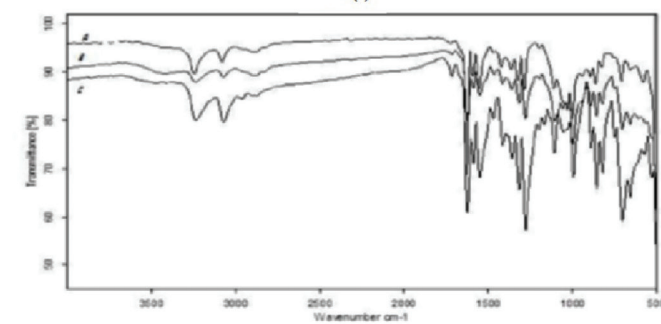
410 PC spectrophotometer. The obtained IR spectra of pure drug (Figure 1a) were compared with those of the reference standard (Figure 1b) taken from Indian Pharmacopoeia as well as with the IR spectra (Figure 1c) of the prepared nicorandil tablet formulation to check the drug excipient compatibility.

Preparation of buccal tablets

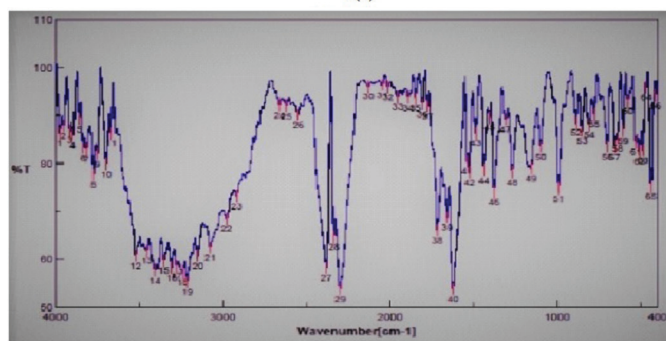
Initially, the drug was accurately measured and mixed thoroughly with mannitol on butter paper using a stainless-steel spatula. Except the lubricant, all the additives were blended for 10 min by geometric dilution. After uniform blending of the additives, lubricant was added followed by mixing for 2 min. Next, 100 mg of such blends of each formulation was pre-compressed on a 10-station rotary tablet punching machine at a low compression force, resulting in single-layered core tablets 8 mm in diameter. The prepared core tablet was placed in the center of the 12-mm lower punch and the backing layer of 100 mg of ethyl cellulose was added around and over the core tablet; the two layers were then compressed into a mucoadhesive bilayer tablet. A tablet (200 mg) was formed whose thickness was 1.6 to 1.8



1(a)



1(b)



1(c)

Figure 1 a, b, c. FT-IR spectra
FT-IR: Fourier transform-infrared

mm. Table 1 shows the results of preliminary trials to evaluate the bioadhesive polymers and Table 2 depicts formulations to evaluate the sustained-release characteristics of various compositions.

Factorial batches

Based on the preliminary studies, a 3² full factorial design was constructed in which the amounts of HPMC K100M (X₁) and

Table 1. Preliminary trial for selection of bioadhesive polymer (B1-B5)

Ingredients	B1	B2	B3	B4	B5
Core tablet					
Nicorandil	10	10	10	10	10
Neem gum	30	-	-	-	-
Guar gum	-	30	-	-	-
Na alginate	-	-	30	-	-
Carbopol 934	-	-	-	30	-
Xanthan gum	-	-	-	-	30
PVP K30	10	10	10	10	10
Mannitol	68	68	68	68	68
Magnesium stearate	1	1	1	1	1
Aspartame	1	1	1	1	1
Backing layer					
Ethyl cellulose	80	80	80	80	80
Total (mg)	200	200	200	200	200

PVP: Polyvinylpyrrolidone

Table 2. Compositions of formulation for optimization of sustained release polymer (S1-S3)

Ingredients	S1	S2	S3
Core tablet			
Nicorandil		10	10 10
Neem gum		30	30 30
HPMC K4 100M	30	-	-
HPMC K4 M	-	30	-
HPMC K15 LV	-	-	30
PVP K30	10	10	10
Mannitol	38	38	38
Magnesium stearate	1	1	1
Aspartame	1	1	1
Backing layer			
Ethyl cellulose	80	80	80
Total (mg)	200	200	200

HPMC: Hydroxypropyl methylcellulose, PVP: Polyvinylpyrrolidone

neem gum (X₂) were selected as independent variables and their levels were defined. The dependent variables were % drug release at 6 h (Y₁) and mucoadhesive strength in grams (Y₂). Table 3 gives details regarding the employed factorial design. ANOVA was performed using the software Design Expert 11.0 demo version (State-ease) and the responses were studied.

Evaluation of buccal tablets

Thickness

A vernier caliper was used to calculate the thickness of tablets (n=10) and the mean tablet thickness was calculated.

Friability and hardness

Friability (n=20) and hardness (n=3) were measured by a Roche friabilator and a Monsanto type hardness tester, respectively.¹⁷

Weight variation

Tablets (n=20) were weighed individually and their weight variation was found by comparing these weights to the label claim.¹⁷

Drug contents

The prepared tablets (n=10) were powdered and an amount corresponding to 10 mg of nicorandil was accurately weighed. The powder was extracted with a volume of buffer solution (phosphate buffer saline, pH 6.8) and analyzed using a spectrophotometer at 262 nm after appropriate dilution.

Surface pH

To evaluate the possibility of the prepared tablets causing irritation to the oral mucosa, surface pH studies were performed. Tablets were soaked in 12 mL of buffer solution (phosphate buffer saline, pH 6.8) and allowed to swell for 2 h at room temperature. A pH meter containing a glass electrode was utilized to find out the pH of the resultant swelled tablets

Table 3. 3² Experimental design for buccal tablet formulation

Ingredients	F1	F2	F3	F4	F5	F6	F7	F8	F9
Core tablet									
Nicorandil	10	10	10	10	10	10	10	10	10
Neem gum	20	20	20	30	30	30	40	40	40
HPMC K4100M	20	30	40	20	30	40	20	30	40
Mannitol	58	48	38	48	38	28	38	28	18
PVP K30	10	10	10	10	10	10	10	10	10
Magnesium stearate	1	1	1	1	1	1	1	1	1
Aspartame	1	1	1	1	1	1	1	1	1
Backing layer									
Ethyl cellulose	80	80	80	80	80	80	80	80	80
Total weight in mg	200	200	200	200	200	200	200	200	200

HPMC: Hydroxypropyl methylcellulose, PVP: Polyvinylpyrrolidone

by bringing the glass electrode into contact with the surface of the tablet and allowing it to equilibrate for 1 min.¹⁸

Moisture absorption ratio

Hot water was taken and the required quantity of agar (5% w/v) was added to it. The resultant solution was added to petri plates and inducted to solidify. Previously, vacuum dried nicorandil buccal tablets (n=6) were taken, weighed individually, and one was laminated with cellophane tape (impermeable backing membrane). The tablets were then placed individually in petri plates so that their other side was in contact with the agar medium, followed by incubation at 37°C for 1 h. After incubation, the buccal tablets were reweighed, and the percentage of moisture absorption was calculated using the following formula:

$$\% \text{ Moisture absorption} = \frac{(\text{Final weight} - \text{Initial weight})}{\text{Initial weight}} \times 100$$

Ex vivo mucoadhesive strength

Ex vivo mucoadhesive strength was determined using a modified balance method. On the day of the experiment, the authors visited a nearby slaughterhouse and collected surgically cut out goat buccal mucosa, which can be used within 2 h of slaughter, a model substrate used for the present study. To prevent it going rotten, a piece of buccal mucosa was kept in Krebs buffer and stored at 4°C for 2 h. The goat mucosa reached room temperature before further use. This model substrate was then tied to a glass slide to provide it with mechanical strength. On that membrane a tablet was gently put with manual pressure for 5 min after moistening with fluid, which led to bioadhesion. To that biologically attached tablet water was added to detach it from the model substrate, and the amount of water (in grams) needed to detach the tablet from the surface was determined as mucoadhesive strength. Such a procedure was repeated three times and the average mucoadhesive strengths were reported.^{19,20}

Ex vivo mucoadhesion time

Freshly cut goat buccal mucosa was used for the measurement of ex vivo mucoadhesion time (n=3) according to the reported method. Fresh goat buccal mucosa was collected and maintained as described above. A glass slide was taken and excised goat buccal mucosa was tied onto it. Upon this goat buccal membrane a bioadhesive side of the tablet, previously wetted with fluid, was pasted and light force was applied with a fingertip for 30 s. The glass slide along with the pasted tablet was placed in a beaker containing 200 mL of phosphate buffer (pH 6.8) and it was kept at 37±1°C. The beaker containing the entire assembly was slowly stirred similar to the buccal cavity and the entire assembly was monitored for 12 h. The ex vivo mucoadhesion time was calculated as the time required to detach the tablet from the goat membrane that was tied to a glass slide.^{19,20}

Drug release studies

A method previously reported by Daravath et al.²¹ for furosemide sustained release bilayered buccal tablets was simply followed in the present drug release studies using the

US Pharmacopeia XXIII rotating paddle apparatus. An instant adhesive (cyanoacrylate adhesive) was used for pasting the backing layer of the buccal tablet on a glass slide. The slide was then placed at the bottom of the dissolution vessel containing 250 mL of phosphate buffer saline (pH 6.8), which was maintained at 37±0.5°C and rotated at 50 rpm throughout the experiment. Samples (10 mL) were withdrawn at predetermined time intervals in sink condition, followed by filtering through Whatman filter (0.45 µm) paper and analysis by ultraviolet (UV) spectrophotometer at 262 nm.

Ex vivo permeation of drug from buccal tablets

Ex vivo permeation of drug from buccal tablets was performed using a Franz diffusion cell through porcine buccal mucosa at 37±0.5°C and at 50 rpm. Fresh porcine buccal mucosa was obtained from a local slaughterhouse and used within 2 h of slaughter. The mucosal membrane was separated by removing the underlying fat and loose tissues, and washed with distilled water and then with phosphate buffer (pH 6.8) at 37°C. The fresh porcine buccal mucosa was cut into pieces and washed with phosphate buffer (pH 6.8). The membrane was collected and was stored at 4°C in Krebs buffer. This membrane was arranged between the two chambers and phosphate buffer saline (pH 6.8) was used to fill the receiver chamber. To the donor chamber was added 1 mL of phosphate buffer saline and a buccal tablet was suspended there. Aliquots of 5 mL samples were collected at predefined times. The collected samples were filtered, suitably diluted, and the amount of drug permeated was determined using a double beam UV spectrophotometer at $\lambda_{\text{max}}=262$ nm. The flux (J) and permeability coefficient (P) were calculated using the following formulae:

$$J = \frac{dQ}{dt} \div \Delta CA$$

$$P = \frac{dQ}{dt} \div A$$

Here J is flux (mg/h cm²), P is a permeability coefficient (cm/h), dQ/dt is the slope of the steady-state portion of the curve, ΔC is the difference in concentration across the membrane, and A is the area of diffusion (cm²).²²

ANOVA studies

To evaluate the effect of independent variables on the responses, ANOVA was applied to the nine formulations prepared using Design Expert software. The p values for the respective responses were also calculated to check whether the effect was statistically significant or not.

Drug release kinetics

To define the kinetics of drug release, the dissolution profile of the optimized batch (F5) was fitted to various models such as zero order, first order, Higuchi, Hixon Crowell, Korsmeyer, and Peppas.²³

Stability studies

To determine the change in bioadhesive strength and in vitro release profile during storage, a 3-month short-term stability study for the optimized batch was performed at 40±2°C in a stability chamber with 75±5% relative humidity (RH). Tablets

were taken out at 1-month intervals and evaluated for any change in bioadhesive strength and *in vitro* drug release pattern. The difference factor (f_1) and similarity index (f_2) were calculated to find out the similarity between the dissolution profile of batch F5 before and after storage at the level of significant ($p < 0.05$) by using the paired *t*-test.

The formulae to calculate difference factor (f_1) and similarity index (f_2) are as follows:

$$f_1 = \left\{ \sum |R_t - T_t| \div \sum R_t \right\} \times 100$$

$$f_2 = 50 \log \left\{ \left[1 + \sum_{n=1}^n (R_t - T_t)^2 \right]^{0.5} \times 100 \right\}$$

Here t is 1 to n , n is the dissolution time, and R_t and T_t are the reference and test dissolution value at time t .^{24,25}

RESULTS AND DISCUSSION

Drug excipient compatibility study

FT-IR spectroscopy was employed to study any kind of interaction between the drug and additives used in the formulation. As per the FT-IR graph, no significant shift in the positions of the wave numbers was found for the formulation (F5) when compared to that of the pure drug values, which inferred no interaction between the drug and the employed additives in the formulation (Figure 1).

Preliminary study

Initially, the study was started with the preparation of preliminary tablets using various natural polymers to check their bioadhesive properties along with tableting properties and the same were compared with synthetic polymer (Carbopol 934). Table 4 shows the evaluation results for these formulations, which indicated that batch B1, which contained neem gum, has better bioadhesive strength as well as hardness. Hence, neem gum was chosen as a bioadhesive polymer for further study. To assess the synergistic sustained-release characteristics of neem gum along with different grades of HPMC, tablet formulations (S1, S2, and S3) were prepared and checked with respect to drug release for 12 h. It was found that formulations S2 and S3 (containing HPMC K4M and HPMC K15 LV) were not able to sustain drug release for 12 h, whereas S1 (containing neem gum and HPMC K4 100M) showed sustained drug release for 12 h as depicted in Table 5. Such sustained effect would be needed for our study and hence was selected for further study.

Table 4. Evaluation of preliminary batches for selection of bioadhesive polymer

Batches	Hardness (kg/cm ²) (n=3)	Mucoadhesive strength (gram force) (n=3)
B1	5.74±0.75	19.07±1.12
B2	5.86±0.67	17.45±1.14
B3	5.34±0.47	17.01±1.11
B4	6.47±0.42	21.24±0.99
B5	5.14±0.33	16.67±1.10

Full factorial design

Physico-chemical parameters

The prepared factorial formulations were evaluated for various physicochemical parameters. From the results, it was found that the weight variation within 7.5% deviation, hardness (4.33-5.71 kg/cm²), thickness (1.69-1.86 mm), friability LT 1%, and drug contents (98.97-101.21%) were within the specified limits.

Surface pH of all the formulations was found to be between 5.5 and 7.5 (Figure 2), which seemed within the acceptable salivary pH range (5.5-7.0). It was inferred that the tablets would not produce local irritation to the mucosal surface.

Moisture absorption ratio

The moisture absorption ratio was calculated to assess the relative moisture absorption potential of polymers as well as their strengths to maintain the integrity of the formulation after that absorption. The prepared tablets were subjected to such studies and the results are shown in Figure 3. Formulation F4

Table 5. Evaluation of preliminary batches for optimization of sustained release polymer

Time (h)	Cumulative percentage drug release		
	S1	S2	S3
0	0	0	0
1	18.23±0.56	22.14±0.64	30.23±0.54
2	26.60±0.64	39.89±0.84	36.02±0.64
3	35.11±0.68	47.02±0.24	41.05±0.66
4	46.12±0.67	57.64±0.26	56.31±0.52
5	57.46±0.62	63.74±0.34	71.26±0.34
6	64.34±0.54	73.23±0.28	83.27±0.25
7	73.23±0.45	83.37±0.94	98.63±0.47
8	79.26±1.20	90.54±0.34	-
9	86.23±0.87	91.23±0.67	-
10	90.14±0.67	101.2±0.84	-
11	95.46±0.75	-	-
12	100.47±0.84	-	-

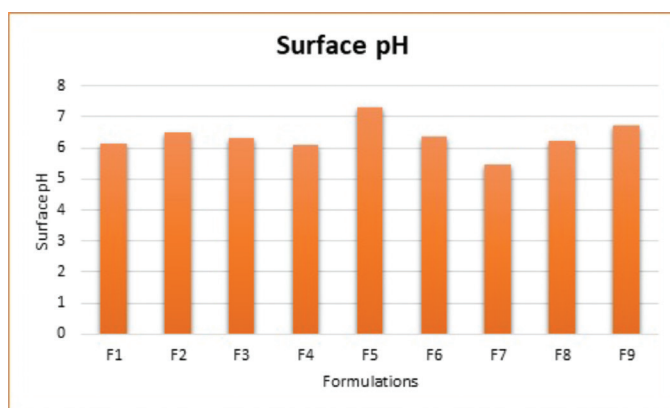


Figure 2. Surface pH of factorial batches

was found to have the minimum value (28%), whereas F8 had the maximum value (51%), which may be attributed to the high concentration of hydrophilic neem gum.

Ex vivo mucoadhesive strengths and time

The *ex vivo* mucoadhesive strengths and time of the tablets were determined for all formulations using goat buccal mucosa. The mucoadhesive strengths and time were found to be increased with increased concentrations of polymers. The best bioadhesive strength was found for F9 (21.28 g) and the lowest for F1 (17.25 g). The mucoadhesion was attributed to the formation of a hydrogen bond between polymers due to swelling and mucin of the mucus membrane. F9 was prepared with higher concentrations of neem gum and HPMC, which might have resulted in high swelling and ultimately higher values of mucoadhesion. Figure 4 shows the results obtained from the test. This test indicated the mucoadhesive potential of polymers used in formulations.

In vitro drug release studies

The prepared factorial tablets were subjected to *in vitro* dissolution studies for 12 h to check the effect of the various concentrations of neem gum with HPMC K100M and the results are given in Figure 5. The dissolution pattern was found to be F1<F2<F4<F8<F3<F6<F5<F9. Based on the criteria selected according to the theoretical drug release profile of nicorandil at 1 h (12%), 5 h (50%), and 8 h (80%), F5 is considered to be

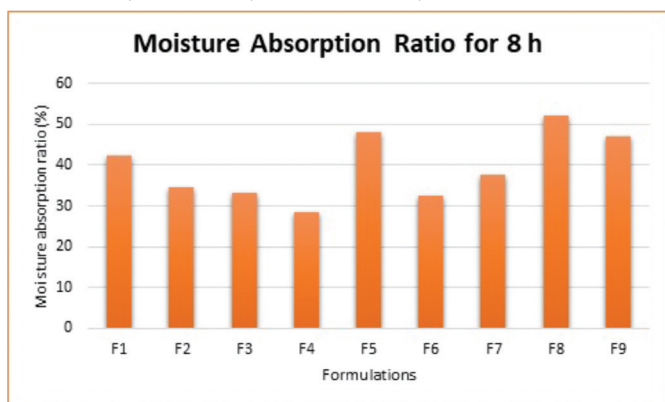


Figure 3. Moisture absorption ratio for 8 h of factorial batches

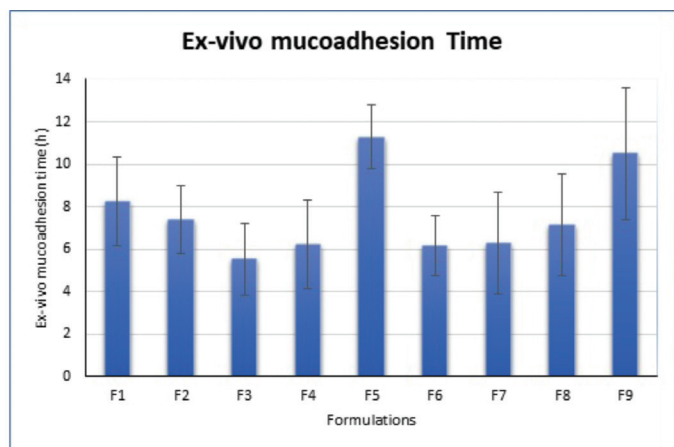


Figure 4. Ex vivo mucoadhesion time of factorial batches

promising as it had drug release of 11.25% at 1 h, 51.81% at 5 h, and 79.20% at 8 h. Additionally, it sustained the drug release for 12 h, which was attributed to the synergistic effect that occurred due to the presence of HPMC K100M as well as neem gum. To ensure the drug release kinetics from the optimized buccal tablet, the dissolution profile was fitted to different release kinetic models: zero-order, first-order, Hixson-Crowell, Higuchi, and Weibull's equations. The regression analysis was performed for batch F5 and residual values were used to analyze the best fit of the experimental data to the predicted models ($r^2 > 0.99$ and minimum residual mean square and model parameters). The results are shown in Figure 6. As can be seen, the zero-order model was suited best to the dissolution data for F5, which suggested that the rate of drug release was perpetual over the course of time independent of the drug concentration.

Ex vivo permeation studies

Ex vivo permeation studies ($n=3$) were performed for the optimized buccal tablet (F5). The slope, flux, and permeability coefficient for various formulations were 0.623, 0.889 ± 0.12 , and 0.241 ± 0.07 , respectively. Cumulative percentage of drug permeated from the prepared formulation is shown in Figure 7. The results of the permeation study affirmed that the drug was liberated controllably from the tablet and impregnated steadily through the porcine buccal membrane and could possibly be infiltrated through the human buccal membrane as well.

Statistical analysis

ANOVA studies

A total of nine formulations were advised by the 3^2 factorial design for two independent variables: the amount of neem gum (X_1 , mg) and HPMC K100M (X_2 , mg). The effect of these factors on Y_{60} (release in 60 min), Y_{240} (release in 240 min), $T_{50\%}$ (time in min required for 50% release), and mucoadhesive strength in gram force (MS) was examined as response parameters in the study. Summaries of the variables and observed responses are given in Tables 6 and 7. The software Design Expert 7.0

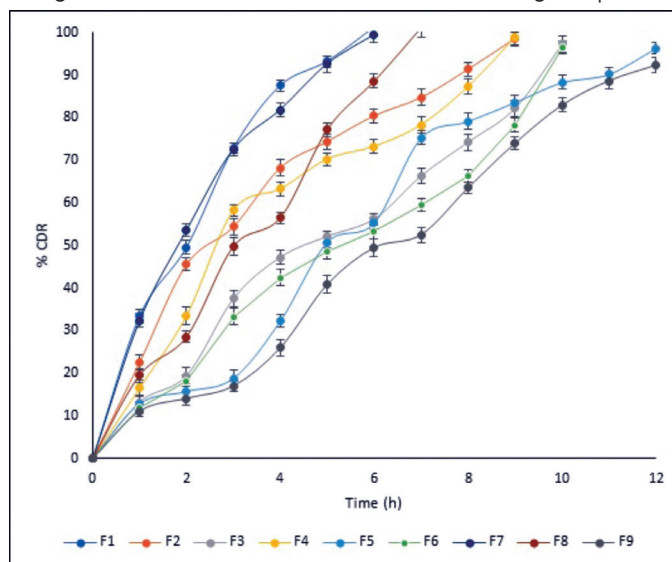


Figure 5. Cumulative percentage drug release profiles

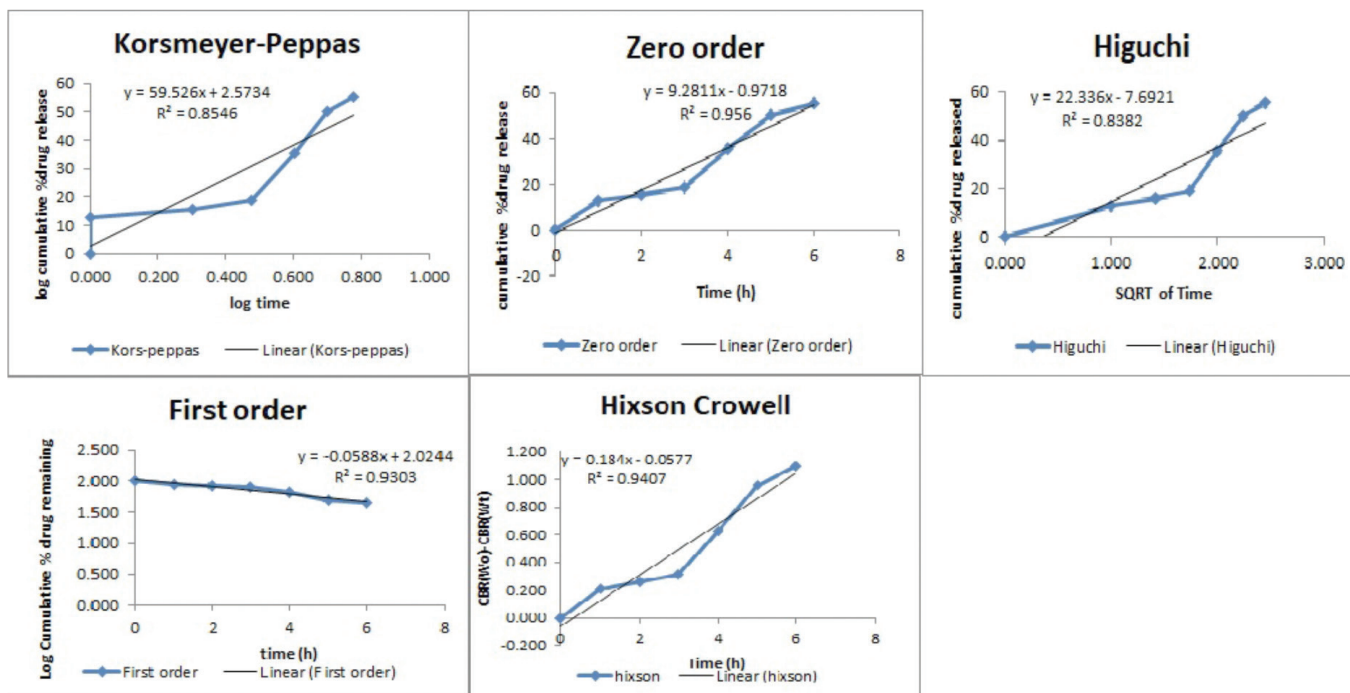


Figure 6. Release kinetics results of the optimized formulation (F5)

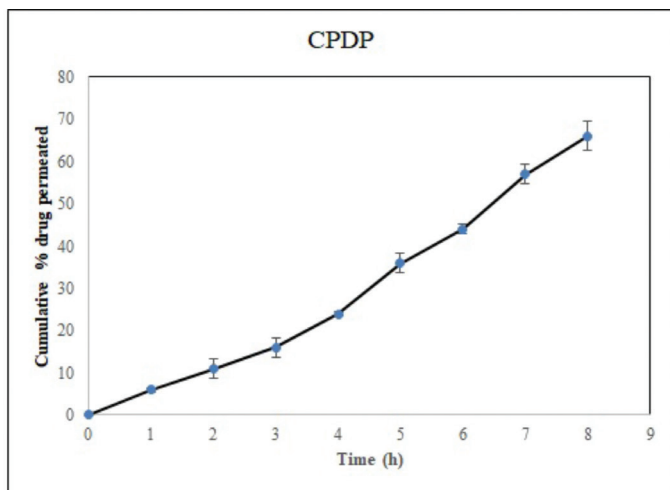


Figure 7. Cumulative percentage drug permeation of F5

calculated suitable model equations after fitting these data. According to the ANOVA results, all the models were significant ($p < 0.05$). Model simplification was carried out by eliminating nonsignificant terms ($p > 0.05$) in the equations, giving the model equation relating

$$Y_{60} = 20.60 - 8.95X_1 + 0.6050X_2 \quad \text{Equation no (1)}$$

$$Y_{240} = 56.61 - 18.74X_1 - 5.88X_2 \quad \text{Equation no (2)}$$

$$T_{50\%} = 221.22 + 88.67X_1 + 14.50X_2 \quad \text{Equation no (3)}$$

$$MS = 18.99 + 0.8183X_1 + 1.07X_2 \quad \text{Equation no (4)}$$

The data obviously demonstrated that the response values are strongly dependent on the independent variables chosen. From the equations (1-4), it was established that the independent

Table 6. Response values for buccal tablet formulations as per experimental design

Batch code	Y_{60} (%)	Y_{240} (%)	T_{50} (min)	Mucoadhesive strength (gram force)
F1	33.42	87.52	120	17.25
F2	22.56	68.24	145	18.12
F3	11.32	47.56	275	18.23
F4	22.31	63.26	162	18.49
F5	12.83	32.3	350	18.42
F6	12.01	42.56	312	20.36
F7	32.38	81.81	110	19.22
F8	27.45	56.24	180	19.52
F9	11.10	30.01	337	21.28

variables (X_1 and X_2) have significant effects on the chosen responses. The effects of factors (X_1 and X_2) on responses were demonstrated by plotting 3D surface plots and contour plots as shown in Figure 8. It was found that responses may be changed by a convenient choice of the levels of X_1 and X_2 . The results of dependent variables were selected to check the suitability of the prepared tablets as a mucoadhesive sustained-release formulation. Based on the theoretical requirement to prepare a sustained-release tablet formulation of nicorandil, Y_{60} should be 11.25%, Y_{240} should be 35%, and $T_{50\%}$ should be 300 min. F5 was found to have results similar to the theoretically calculated requirements. Hence, it is considered to be the optimized formulation and can be explored further in future research.

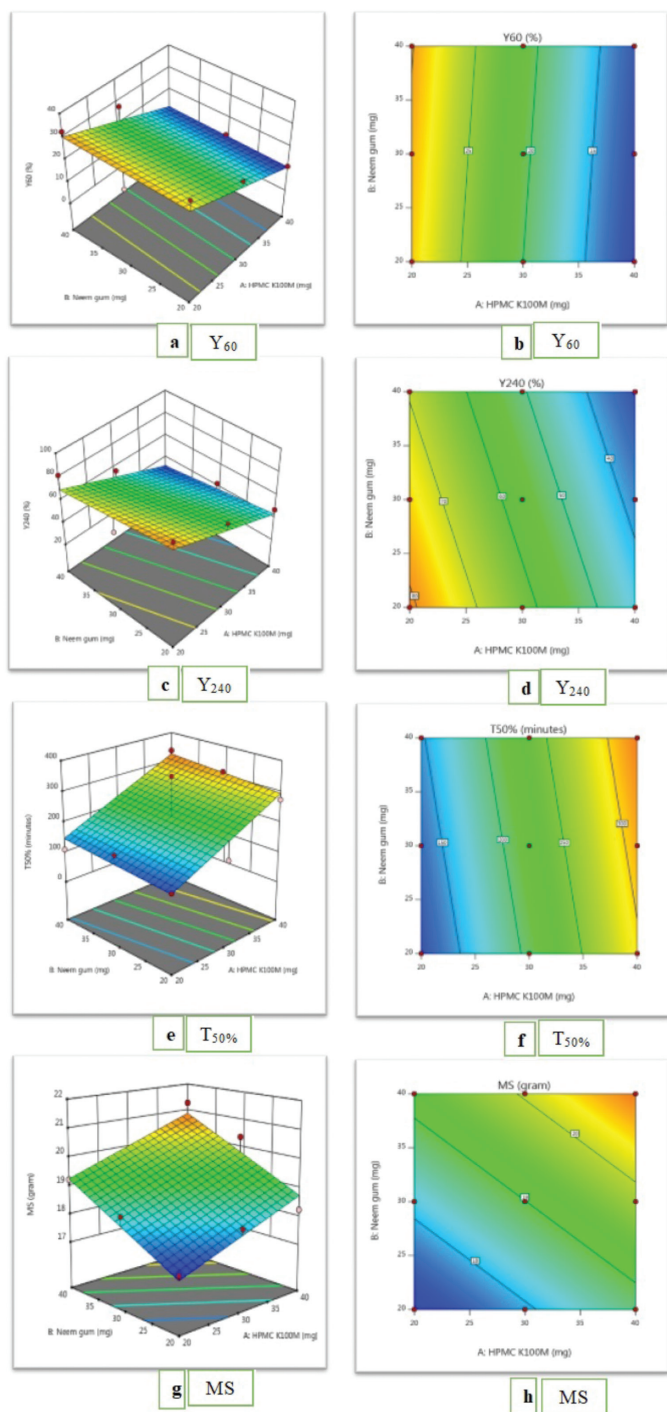


Figure 8. Surface plots (a, c, e, g) and contour plots (b, d, f, h)
MS: Gram force

Stability studies

To assess the physicochemical nature of the optimized formulation (F5) with respect to dissolution characteristics and mucoadhesive strength, it was wrapped in aluminum foil and kept in the stability chamber with well-controlled conditions of temperature (40±2°C) and humidity (75±5% RH). After storage, dissolution parameters and mucoadhesive strength were determined and the results are depicted in Table 8. The precise way to find similarities between dissolution curves is to find

Table 7. ANOVA for linear model

Y ₆₀					
Source	Sum of squares	df	Mean square	F value	p value
Model	482.45	2	241.23	7.83	0.0213 Significant
A-HPMC K100M	480.26	1	480.26	15.59	0.0076
B-neem gum	2.20	1	2.20	0.0713	0.7984
Residual	184.89	6	30.81		
Cor total	667.34	8			
Y ₂₄₀					
Source	Sum of squares	df	Mean square	F value	p value
Model	2315.09	2	1157.54	6.72	0.0294 Significant
A-HPMC K100M	2107.88	1	2107.88	12.25	0.0128
B-neem gum	207.21	1	207.21	1.20	0.3146
Residual	1032.84	6	172.14		
Cor total	3347.93	8			
T _{50%}					
Source	Sum of squares	df	Mean square	F value	p value
Model	48432.17	2	24216.08	5.52	0.0437 Significant
A-HPMC K100M	47170.67	1	47170.67	10.75	0.0168
B-neem gum	1261.50	1	1261.50	0.2876	0.6111
Residual	26321.39	6	4386.90		
Cor total	74753.56	8			
Mucoadhesive strength					
Source	Sum of squares	df	Mean square	F value	p value
Model	10.89	2	5.44	21.71	0.0018 Significant
A-HPMC K100M	4.02	1	4.02	16.03	0.0071
B-neem gum	6.87	1	6.87	27.40	0.0019
Residual	1.50	6	0.2507		
Cor total	12.39	8			

HPMC: Hydroxypropyl methylcellulose

out the similarity factor f_2 and the difference factor f_1 . According to the food and drug administration, f_1 values less than 15 and f_2 values greater than 50 should establish an agreement between the dissolution curves, demonstrating an average disparity

Table 8. Evaluation of stability studies of formulation (F5) for 3 months (mean \pm SD, n=3)

Batch F5	<i>In vitro</i> drug release at 12 h (%)	Mucoadhesive strength (grams)
Before storage	96.35 \pm 1.54	18.42 \pm 0.54
After storage at 40 \pm 2°C and 75 \pm 5% relative humidity	98.25 \pm 2.03	20.56 \pm 1.20
Similarity and dissimilarity (f_1 & f_2) factor	$f_1=4$ $f_2=77$	Not applicable

SD: Standard deviation

of no more than 10% at the sample time points. According to this guideline, the dissolution curves corresponding to F5 before storage were similar to those obtained with the same formulation after storage. No significant changes were found according to the results, which indicated that the prepared tablet formulation is stable.

CONCLUSION

To prevent the first-pass metabolism and provide sustained drug release, buccal drug delivery of nicorandil is considered to be one of the best surrogate routes of administration. Additionally, it will lead to patient compliance as well by reducing the frequency of administration. To attain this, a factorial approach was used with a combination of HPMC K100M and neem gum to prepare sustained-release buccal tablets of nicorandil that resulted in a sustained formulation, which can be used in a once a day tablet.

ACKNOWLEDGMENTS

The authors are thankful to Sun Pharma Laboratories Ltd., East Sikkim, for providing nicorandil as a gratis sample to carry out this research work.

Conflicts of interest: No conflict of interest was declared by the authors. The authors alone are responsible for the content and writing of this article.

REFERENCES

- Ahmed AB, Nath LK. Design and development of controlled release floating matrix tablet of Nicorandil using hydrophilic cellulose and pH-independent acrylic polymer: *in-vitro* and *in-vivo* evaluations. *Expert Opin Drug Deliv.* 2016;13:315-324.
- Falase B, Easaw J, Youhana A. The role of nicorandil in the treatment of myocardial ischaemia. *Expert Opin Pharmacother.* 2001;2:845-856.
- Singh B, Garg T, Goyal AK, Rath G. Development, optimization, and characterization of polymeric electrospun nanofiber: a new attempt in sublingual delivery of nicorandil for the management of angina pectoris. *Artif Cells Nanomed Biotechnol.* 2016;44:1498-1507.
- Krishnaiah YS, Al-Saidan SM, Chandrasekhar DV, Satyanarayana V. Controlled *in vivo* release of nicorandil from a carvone-based transdermal therapeutic system in human volunteers. *Drug Deliv.* 2006;13:69-77.
- Prajapati G, Patel R. Design and *in vitro* evaluation of novel nicorandil sustained release matrix tablets based on combination of hydrophilic and hydrophobic matrix systems. *International Journal of Pharmaceutical Sciences Review and Research.* 2010;1:33-38.
- Tamilvanan S, Babu VR, Nappinai A, Sivaramakrishnan G. *In vitro* and *in vivo* evaluation of hydrophilic and hydrophobic polymers-based nicorandil-loaded peroral tablet compared with its once-daily commercial sustained-release tablet. *Drug Development and Industrial Pharmacy.* 2011;37:436-445.
- Boddupalli BM, Mohammed ZN, Nath RA, Banji D. Mucoadhesive drug delivery system: An overview. *J Adv Pharm Technol Res.* 2010;1:381-387.
- Chinna Reddy P, Chaitanya KS, Madhusudan Rao Y. A review on bioadhesive buccal drug delivery systems: current status of formulation and evaluation methods. *Daru.* 2011;19:385-403.
- Hoogstraate JAJ, Wertz PW, Wertz PW. Drug delivery via the buccal mucosa. *Pharmaceutical Science Technology Today.* 1998;1:309-316.
- Mohamed FAA, Roberts M, Seton L, Ford JL, Levina M, Rajabi-Siahboomi AR. Production of extended release mini-tablets using directly compressible grades of HPMC. *Drug Dev Ind Pharm.* 2013;39:1690-1697.
- Nafee NA, Ismail FA, Boraie NA, Mortada LM. Mucoadhesive delivery systems. II. Formulation and *in-vitro/in-vivo* evaluation of buccal mucoadhesive tablets containing water-soluble drugs. *Drug Dev Ind Pharm.* 2004;30:995-1004.
- Peh KK, Wong CF. Polymeric films as vehicle for buccal delivery: swelling, mechanical, and bioadhesive properties. *J Pharm Pharm Sci.* 1999;2:53-61.
- Wong CF, Yuen KH, Peh KK. Formulation and evaluation of controlled release Eudragit buccal patches. *Int J Pharm.* 1999;178:11-22.
- Yamsani VV, Gannu R, Kolli C, Rao ME, Yamsani MR. Development and *in vitro* evaluation of buccoadhesive carvedilol tablets. *Acta Pharm.* 2007;57:185-197.
- Vueba ML, Batista de Carvalho LA, Veiga F, Sousa JJ, Pina ME. Influence of cellulose ether mixtures on ibuprofen release: MC25, HPC and HPMC K100M. *Pharm Dev Technol.* 2006;11:213-228.
- Krishna LNV, Kulkarni PK, Dixit M, Lavanya D, Raavi PK. Brief introduction of natural gums, mucilages and their applications in novel drug delivery systems-a review. *IJDFR.* 2011;2:54-71.
- Saha RN, Sajeev C, Sahoo J. A comparative study of controlled release matrix tablets of diclofenac sodium, ciprofloxacin hydrochloride, and theophylline. *Drug Deliv.* 2001;8:149-154.
- Mohamad SA, Abdelkader H, Elrehany M, Mansour HF. Vitamin B12 buccoadhesive tablets: auspicious non-invasive substitute for intra muscular injection: formulation, *in vitro* and *in vivo* appraisal [published correction appears in *Drug Dev Ind Pharm.* 2019;45:x]. *Drug Dev Ind Pharm.* 2019;45:244-251.
- Gupta A, Garg S, Khar RK. Measurement of bioadhesive strength of mucoadhesive buccal tablets: Design of an *in-vitro* assembly. *Indian Drugs.* 1993;30:152-155.

20. Patel DM, Shah PM, Patel CN. Formulation and evaluation of bioadhesive buccal drug delivery of repaglinide tablets. *Asian Journal of Pharmaceutics*. 2014;6:171-179.
21. Daravath B, Swathi D, Rao BB. Formulation Development and Evaluation of Sustained Release Bioadhesive Bilayered Buccal Tablets of Furosemide. *Analytical Chemistry Letters*. 2017;7:215-277.
22. Biswal B, Karna N, Bhavsar B. Formulation and Evaluation of Repaglinide Buccal Tablet: *Ex Vivo* Bioadhesion Study and *Ex Vivo* Permeability Study. *Journal of Applied Pharmaceutical Science*. 2014;4:96-103.
23. Costa P, Sousa Lobo JM. Modeling and comparison of dissolution profiles. *Eur J Pharm Sci*. 2001;13:123-133.
24. Malaterre V, Ogorka J, Loggia N, Gurny R. Evaluation of the tablet core factors influencing the release kinetics and the loadability of push-pull osmotic systems. *Drug Dev Ind Pharm*. 2009;35:433-439.
25. Simionato LD, Petrone L, Baldut M, Bonafede SL, Segall AI. Comparison between the dissolution profiles of nine meloxicam tablet brands commercially available in Buenos Aires, Argentina. *Saudi Pharm J*. 2018;26:578-584.



Electrochemical Determination of Rifampicin Based on Its Oxidation Using Multi-Walled Carbon Nanotube-Modified Glassy Carbon Electrodes

Çok Duvarlı Karbon Nanotüp Modifiye Camı Karbon Elektrot Kullanılarak Rifampisin Oksidasyonuna Dayalı Elektrokimyasal Tayini

© Dilek KUL

Karadeniz Technical University Faculty of Pharmacy, Department of Analytical Chemistry, Trabzon, Turkey

ABSTRACT

Objectives: The aim of the study was to investigate the electrochemical behavior of rifampicin (RIF) in the anodic direction using multi-walled carbon nanotube (MWCNT)-modified glassy carbon electrodes.

Materials and Methods: The anodic investigation of RIF was carried out with cyclic, differential pulse, and square wave voltammetry. A three-electrode system consisting of a glassy carbon electrode with a modification by MWCNTs as the working electrode, a platinum wire as the counter electrode, and an Ag/AgCl electrode as reference was used for the experiments.

Results: The anodic process of RIF was irreversible and diffusion controlled. Linear responses were obtained between 0.04 and 10 μM for both techniques in acetate buffer (pH 3.5) as supporting electrolyte. The limit of detection values were 7.51 and 11.3 nM for differential pulse and square wave voltammetry, respectively. The repeatability, reproducibility, precision, and accuracy of the proposed methods were also investigated. Determination of RIF was carried out on its pharmaceutical dosage forms and the results were compared with those from other electrochemical sensors and the liquid chromatographic and spectrophotometric methods in the literature.

Conclusion: These validated techniques provided selective, rapid, sensitive, precise, and cheap determination of RIF as alternative techniques to the liquid chromatographic and spectrophotometric methods in therapeutic drug monitoring.

Key words: Rifampicin, voltammetry, multi-walled carbon nanotubes, glassy carbon electrode, pharmaceuticals

ÖZ

Amaç: Bu çalışmanın amacı, rifampisin (RIF) elektrokimyasal davranışını çok duvarlı karbon nanotüp (MWCNT) ile modifiye edilmiş camı karbon elektrotlar kullanarak anodik yönde incelemektir.

Gereç ve Yöntemler: RIF'nin anodik incelemesi dönüşümlü, diferansiyel puls ve kare dalga voltametri teknikleri ile yapılmıştır. Çalışma elektrotu olarak MWCNT'nin bir modifikasyonuna sahip camı bir karbon elektrot, karşı elektrot olarak bir platin tel ve referans olarak bir Ag/AgCl elektrotundan oluşan üç elektrotlu sistem, deneyler için kullanılmıştır.

Bulgular: RIF'nin anodik süreci geri dönüşümsüz ve difüzyon kontrollüydü. Destek elektrolit olarak asetat tamponunda (pH 3,5) her iki teknik için de 0,04 ila 10 μM arasında doğrusal cevaplar elde edilmiştir. Tespit limiti değerleri diferansiyel puls ve kare dalga voltametri teknikleri için sırasıyla 7,51 ve 11,3 nM olarak bulunmuştur. Önerilen yöntemlerin tekrarlanabilirliği, tekrar üretilebilirliği, kesinliği ve doğruluğu da incelenmiştir. RIF'in tayini, farmasötik dozaj formlarından yapılmıştır ve sonuçlar, literatürdeki diğer elektrokimyasal sensörler ve ayrıca sıvı kromatografik ve spektrofotometrik yöntemlerle karşılaştırılmıştır.

Sonuç: Bu valide edilmiş teknikler, terapötik ilaç izlemede sıvı kromatografik ve spektrofotometrik yöntemlere alternatif teknikler olarak rifampisin seçici, hızlı, hassas, kesin ve ucuz bir şekilde tayinini sağlamıştır.

Anahtar kelimeler: Rifampisin, voltametri, çok duvarlı karbon nanotüp, camı karbon elektrot, farmasötikler

*Correspondence: E-mail: dilekk@ktu.edu.tr, Phone: +90 462 377 88 21 ORCID-ID: orcid.org/0000-0002-8665-9417

Received: 25.02.2019, Accepted: 20.06.2019

©Turk J Pharm Sci, Published by Galenos Publishing House.

INTRODUCTION

Rifampicin (RIF), a semisynthetic derivative of rifamycin, is a macrocyclic antibiotic used to treat bacterial infections such as tuberculosis, leprosy, and Legionnaire's disease.¹ This drug, whose major activity is against mycobacteria, inhibits DNA-dependent RNA polymerase in susceptible bacteria by forming a stable complex with the enzyme. Inhibition of the initiation of RNA synthesis by binding to the β -subunit of RNA polymerase results in the death of the cell.² It is generally used with other antibiotics to expand the antibacterial effect and thus various infections originating from both intracellular and extracellular organisms can be treated.^{3,4} Although RIF is one of the most potent antibiotics used for the treatment of tuberculosis, the bacteria quickly develop resistance to RIF. In order to prevent the development of resistance, RIF is used in combination with other effective antimycobacterial agents such as isoniazid and ethambutol.² RIF is not used for the treatment of viral infections such as colds and flu.

RIF has some adverse effects such as nausea, vomiting, loss of appetite, diarrhea, liver problems, and allergic reactions. The most serious adverse effect of RIF is hepatotoxicity, causing liver damage. In addition, RIF causes orange coloration of body fluids such as urine, sweat, and tears.

RIF has a heterocyclic structure containing naphthoquinone, giving it its characteristic orange color. Its chemical name is 3-(4-methylpiperazinyl)imino-methyl rifamycin SV (Figure 1). RIF binds the bacterial RNA polymerase with the four hydroxyl groups forming hydrogen bonds with amino acid residues on the protein.²

RIF is usually administered orally, rapidly absorbed, and distributed to the body. The half-life of RIF is 2-3 h. Taking RIF with meals significantly decreases its absorption. RIF is quickly hydrolyzed after absorption and completely eliminated from the body through urine and mostly feces after about 6 h.⁵

Some studies are found in the literature for the determination of RIF using high performance liquid chromatography (HPLC),⁶⁻¹⁰ LC-mass spectrometry,¹¹ Raman spectroscopy,¹² Nuclear magnetic resonance spectroscopy,¹³ and ultraviolet-visible spectrophotometry.¹⁴ Electrochemical studies of RIF have also been performed, which studied both in the direction of oxidation using some unmodified^{15,16} and modified electrodes.¹⁷⁻²¹

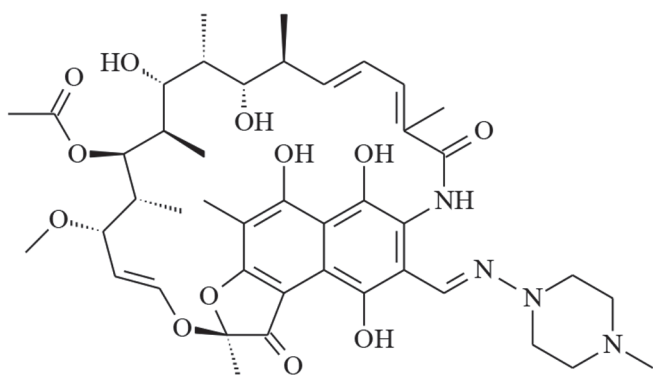


Figure 1. Molecular structure of rifampicin

and in the direction of reduction.^{22,23} The older studies on RIF were based on its electrochemical reduction using a mercury drop electrode by differential pulse polarography²² and differential pulse adsorptive stripping voltammetry (DPAdSV).²³ In later years (between 2004 and 2017), RIF was studied in the direction of oxidation. In one previous study,¹⁵ a carbon paste electrode was used for the determination of RIF and isoniazid by cyclic and square wave voltammetry. Adsorptive stripping voltammetry was also used for both RIF and rifamycin at renewable pencil graphite electrodes.¹⁶ Some modifications such as a hollow manganese oxide@mesoporous silica oxide core-shell nanohybrid at a disposable carbon paste microelectrode,¹⁷ nickel hydroxide nanoparticles-reduced graphene oxide nanosheets film at a glassy carbon (GC) electrode,¹⁹ and polyvinyl pyrrolidone capped CoFe_2O_4 @CdSe core shell at a GC electrode²⁰ were also used for the sensitive determination of RIF.

Most of the chromatographic and spectrophotometric methods in the literature require expensive instrumentation and involve high running costs. Electrochemical methods ensure simple, sensitive, cheap, and fast analysis and determination of drugs. In addition, the electrochemical properties of drugs help us to understand their metabolic fate or *in vivo* redox processes and pharmacological activity. Although modified electrodes provide highly sensitive determination of drugs, it is important that procedures for the modification of electrodes are easy to prepare and stable. For this reason, new modification methods for electrodes and voltammetric methods are constantly investigated to find the best results for the electroactive components.

Carbon nanotubes (CNTs) were discovered in 1991 and have fascinating electronic, magnetic, and mechanical properties. Their unique structure making them strong and rigid means they are suitable for use in the fields of medicine (drug delivery, treatments of diseases, monitoring of cells), manufacturing, electronics, optics, nanotechnology, and other materials science and technology.²⁴ In addition, electrically conductive CNTs can also be used as a carrier of some specific drugs by attaching to the drugs and targeting certain types of cells such as cancer cells.²⁵ CNTs are generally categorized as single-walled CNTs and multiwalled CNTs (MWCNTs).²⁶ MWCNTs were used in the present study since they are well-known materials widely used since 1991 due to their superior chemical and physical properties mentioned above. In addition, MWCNTs have a very strong and elastic structure due to the sp^2 bonds between carbon atoms. These strong bonds ensure that MWCNTs have very high electric conductivity and resistance to high temperatures.²⁶

The aim of the present study was to conduct electrochemical analysis and sensitive determination of the antibacterial drug RIF through its oxidation with a functionalized MWCNT-modified GC electrode by using cyclic voltammetry (CV), differential pulse voltammetry (DPV), and square wave voltammetry (SWV). Developing fully validated and rapid methods using a simply modified GC electrode will ensure more sensitive

determination of RIF based on its oxidation compared to the studies in the literature providing the direct determination of RIF from pharmaceutical dosage forms without any sample pretreatment.

MATERIALS AND METHODS

Materials

RIF and its pharmaceutical dosage form (Rifcap[®], including 300 mg of RIF per capsule) were kindly supplied by Koçak Farma (Istanbul, Turkey). COOH functionalized MWCNTs were from NanoLab, U.S.A., with >95% purity, 15±5 nm diameter, and 1–5 µm length. The other chemicals were analytical grade (Merck or Sigma) and used without any purification.

Stock solutions of RIF (1.0×10^{-3} M) were prepared in ultrapure water and stored in the dark at +4°C. Voltammetric experiments for RIF were performed using working solutions of RIF prepared by direct dilution of the stock solution with the selected supporting electrolyte. The supporting electrolytes were phosphate buffer (PB, 0.1 M NaH₂PO₄·2 H₂O; 0.1 M Na₂HPO₄; pH 5.5–8.0), Britton-Robinson buffer [(BRB), 0.04 M H₃BO₃; 0.04 M H₃PO₄; 0.04 M CH₃COOH; pH 2.0–8.0], and acetate buffer [(AcB), 0.5 M CH₃COOH; pH 3.5–5.5].

Apparatus

Voltammetric measurements were recorded using a computer-controlled Autolab type 2 potentiostat/galvanostat with Nova 1.10 software (Metrohm, the Netherlands) at room temperature. The three-electrode system consisted of a GC electrode (BASi, f: 3.0 mm diameter) with modification by MWCNTs as the working electrode, a platinum wire as the counter electrode (BASi), and a Ag/AgCl electrode (BASi, 3.0 M KCl) as reference. The bare GC electrode was polished with aqueous slurry of alumina powder (f: 0.01 µm) on a damp smooth polishing cloth before the modification.

The operating conditions for DPV were as follows: pulse amplitude, 50 mV; pulse width, 50 ms; scan rate, 2 mV s⁻¹; for SWV: pulse amplitude, 25 mV; frequency, 10 Hz; step potential, 1 mV.

The surface morphology of the bare GC and MWCNT-modified GC electrodes was determined using scanning electron microscopy (SEM) with a LEO 438 VP (LEO Instruments, UK) in high vacuum mode at 20 keV.

The pH measurements were made using a model HI2211 pH-meter (Hanna, Romania) with a combined electrode (glass/reference electrodes) with an accuracy of ±0.05 pH at room temperature.

Sartorius Arium[®] ProUV ultrapure water (resistivity ≥18 MΩ cm) was used for the preparation of all solutions.

Preparation of MWCNT-modified electrodes

Functionalized MWCNTs were weighed and dispersed in dimethyl formamide (DMF) as 0.2% (mg mL⁻¹). The dispersion was sonicated for 4 h to ensure a homogeneous mixture. Before the coating, the bare GC electrode was polished with Al₂O₃ slurry on a polishing pad and rinsed with nanopure water.

Then a specified amount of MWCNT/DMF dispersion, 1.5, 2.5, 3.5, and 5.0 µL, was dropped on the surface of the GC electrode and it was left to dry overnight at room temperature to obtain the MWCNT-modified GC electrode, labeled as MWCNT/GC electrode.

Voltammetric studies

All working solutions of RIF were prepared freshly just before the experiments and protected from light. The calibration equations were obtained from both DP and SW voltammograms by plotting the peak current against RIF concentration. The ruggedness, precision, and accuracy of the methods were checked by assaying five replicate samples on the same day and different days over a week. The ruggedness and the precision of the methods were checked with relative standard deviations (RSD%). The relative errors (Bias%), which describe the deviation from the expected results, were also calculated to check the accuracy and the precision of the developed methods.^{27,28}

Capsule assay procedure

The contents of ten capsules of Rifcap[®], including 300 mg of RIF per capsule, were weighed. An appropriate amount of the contents was taken and diluted to 25 mL with ultrapure water to prepare a stock solution of 1.0×10^{-3} M RIF. The solution was sonicated for 15 min to complete dissolution and then left for 10 min to allow the insoluble parts to settle to the bottom. The working solutions were prepared by taking from the clear supernatant liquor and diluting with the selected supporting electrolyte.²⁹ The RIF amount per capsule was calculated using the corresponding calibration plots of both DPV and SWV.

The other components of the matrix of the pharmaceutical dosage forms can show any interference during the determination of RIF. For this purpose, recovery studies were carried out to check the accuracy of the developed methods using the standard addition method.²⁷ A known amount of RIF was added to the preanalyzed RIF capsule and then the calculations were conducted using the related regression equations of the calibration plots for both techniques.

Statistical analysis

Validation of the proposed method was carried out by statistical analysis of data obtained during the experiments to define the performance and limitations of the method. Based on the statistical analysis, the analytical limits, precision, and accuracy of the proposed methods were determined.

RESULTS AND DISCUSSION

An easily modified GC was used to ensure more sensitive determination of RIF based on its oxidation in comparison to the studies in the literature. In the first step, coating of the GC electrode was performed using 0.2% (mg mL⁻¹) MWCNT/DMF dispersion. For this purpose, an amount of the dispersion was dropped using a micropipette on the surface of the GC electrode. After the electrode dried, the surface was activated by cycling the potential in the region from -0.8 to +1.2 V vs. Ag/AgCl at a scan rate of 100 mV s⁻¹ for 15 cycles in BRB solution at pH 5.0.

The electrochemical responses of 20 μM RIF were compared for both the bare GC electrode and 2.5 μL of 0.2% MWCNT/DMF-coated GC electrode using CV and DPV in BRB solution at pH 5.0. The peak currents of RIF obtained with the MWCNT/GC electrode were 1.86 times and 4.52 times higher than those bare GC electrodes for CV and DPV (Figure 2), respectively.

The coating amount of MWCNT/DMF dispersion was selected for the best electrochemical analysis of RIF. For this purpose, 1.5, 2.5, 3.5, and 5.0 μL of the 0.2% MWCNT/DMF dispersion were dropped on the surface of the GC electrode and the peak currents of RIF were analyzed by CV, DPV, and SWV. The highest peak current with the best peak shape was obtained with 1.5 μL of 0.2% MWCNT/DMF dispersion; thus, the GC electrode was modified with this amount for the further studies of RIF.

Surface characterization

SEM was used to investigate the surface morphology of both the bare GC and MWCNT-modified GC electrodes. Figures 3A and 3B show SEM images of the bare GC electrode and GC electrode coated with 1.5 μL of 0.2% MWCNT/DMF dispersion, respectively. As can be seen in Figure 3B, densely packed and popcorn-like MWCNTs were used for coating and formed a porous structure onto the surface of the GC electrode.

Effect of pH and scan rate

Electrochemical characterization of RIF was carried out with the MWCNT/GC electrode. For this purpose, cyclic voltammograms of RIF were obtained at a scan rate of 100 mV s^{-1} in the potential

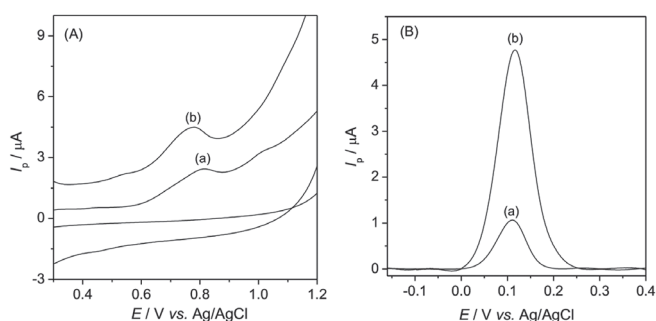


Figure 2. (A) Cyclic and (B) differential pulse voltammograms of 20 μM of RIF in BRB solution at pH 5.0 obtained at (a) bare GC and (b) 2.5 μL of 0.2% MWCNT/DMF-coated GC electrodes

RIF: Rifampicin, BRB: Britton-Robinson buffer, GC: Glassy carbon, MWCNT: Multi-walled carbon nanotube, DMF: Dimethyl formamide

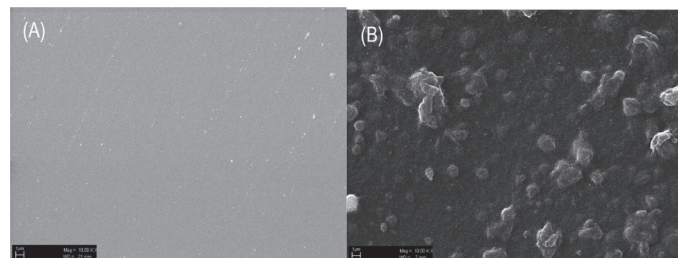


Figure 3. SEM images of (A) bare GC and (B) 1.5 μL of 0.2% MWCNT/DMF-coated GC electrodes, scale bar: 1 μm

SEM: Scanning electron microscopy, GC: Glassy carbon, MWCNT: Multi-walled carbon nanotube, DMF: Dimethyl formamide

range from -0.6 to +1.1 V in different buffer solutions at pH values between 2.0 and 8.0. Buffer solutions with pH values higher than 8.0 were not used in order to prevent the loss of MWCNT coatings on the surface of the GC electrode.

According to the cyclic voltammograms (Figure 4A), an anodic peak having a high peak current at all pHs was observed at around +0.9 V (labeled as Ox1), showing an irreversible oxidation process. At around +0.3 V, another anodic peak having a relatively high peak current was also seen (labeled as Ox2), showing a reversible redox process. With increasing pH, additional anodic and cathodic waves appeared at the peak potentials between -0.2 and +0.2 V. Differential pulse (Figure 4B) and square wave (Figure 4C) voltammograms were also obtained at all pHs to investigate the anodic peaks of RIF for its quantitative determination. The Ox1 peak was not observed at around +0.9 V in DP or SW voltammograms. However, the Ox2 peak at around +0.3 V was seen as a symmetrical and well-defined anodic peak with a high peak current. Another anodic peak separated well from the Ox2 peak was observed at around -0.1 V at pHs lower than 5.0, whereas this peak was intercalated with the Ox2 peak and observed as a shoulder at pHs higher than 5.0.

The reversible redox process including the Ox2 anodic peak (Figure 4A) may be due to the hydroquinone-quinone redox system of the 6,9-dihydroxynaphthalene moiety to the corresponding naphthoquinone of RIF.¹⁵ The irreversible oxidation peak labeled Ox1 (Figure 4A) may be attributed to the irreversible oxidation of the piperazinyl-imino moiety.²¹

Peak potentials of both Ox1 and Ox2 peaks shifted to less positive potentials with increasing pH from 2.0 to 8.0 for all voltammetric techniques. The shift values were 0.285 V for the Ox1 peak with CV and 0.256 V, 0.266 V, and 0.275 V for the Ox2 peak with CV, DPV, and SWV, respectively. These negative shifts showed that the decrease in the concentration of H_3O^+ in the buffer solutions allowed easier oxidation of RIF due to its weak acidic nature.

The relationship between pH and peak potential and peak current of 40 μM RIF was studied using CV for the Ox1 peak and using CV, DPV, and SWV for the Ox2 peak. Graphs of E_p -

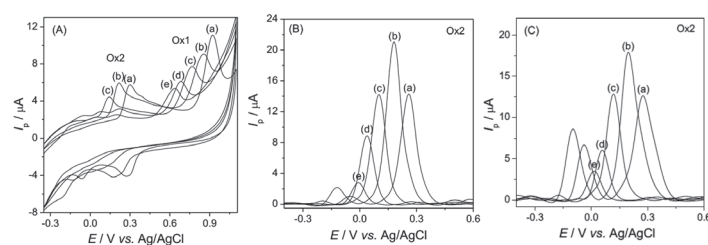


Figure 4. Voltammograms of 40 μM RIF obtained with (A) CV, (B) DPV (for Ox2 peak, baseline corrected), and (C) SWV (for Ox2 peak, baseline corrected) in (a) BRB at pH 2.0, (b) AcB at pH 3.5, (c) PB at pH 5.5, (d) PB at pH 7.0, and (e) BRB at pH 8.0 at the MWCNT/GC electrode. Scan rate: 100 mV s^{-1} for CV

RIF: Rifampicin, CV: Cyclic voltammetry, DPV: Differential pulse voltammetry, SWV: Square wave voltammetry, BRB: Britton-Robinson buffer, MWCNT: Multi-walled carbon nanotube, GC: Glassy carbon

pH for both Ox1 and Ox2 peaks using CV are given in Figures 5A and 5B, respectively. The graphs obtained with DPV and SWV for the Ox2 peak were similar; thus, their graphs are not shown. According to all graphs, linear plots were obtained for both Ox1 and Ox2 peaks at pHs between 2.0 and 8.0, expressed by equations 1-4.

$$E_p \text{ (V)} = 1.030 - 0.048 \text{ pH}; r = 0.990, n = 10 \text{ (for Ox1, obtained with CV)} \quad (1)$$

$$E_p \text{ (V)} = 0.365 - 0.041 \text{ pH}; r = 0.991, n = 10 \text{ (for Ox2, obtained with CV)} \quad (2)$$

$$E_p \text{ (V)} = 0.335 - 0.042 \text{ pH}; r = 0.996, n = 10 \text{ (for Ox2, obtained with DPV)} \quad (3)$$

$$E_p \text{ (V)} = 0.345 - 0.042 \text{ pH}; r = 0.992, n = 10 \text{ (for Ox2, obtained with SWV)} \quad (4)$$

The negative slope values of the linear plots of the E_p -pH graphs in the pH range between 2.0 and 8.0 were between -41 and -48 mV pH^{-1} , showing that the numbers of electrons and protons might not be equal in the redox process of RIF. The slope of 59 mV pH^{-1} is the theoretical value showing that the numbers of protons and electrons are equal.²⁹

The effect of pH on the peak current (I_p) of RIF was also investigated using CV, DPV and SWV for the Ox2 peak. Since the Ox1 peak was not observed in DP or SW voltammograms, quantitative determination of RIF was studied with only the Ox2 peak. According to the I_p -pH graphs of the Ox2 peak, a single, well-defined, sharp, and symmetrical anodic peak (Figures 4B and 4C) having the highest peak current was obtained in AcB at pH 3.5 for both DPV (Figure 5C) and SWV. For this reason, AcB solution at pH 3.5 was selected as the supporting electrolyte for further studies.

The redox process of RIF was determined with scan rate studies using CV in the sweep range from 5 to 200 mV s^{-1} for 40 μM RIF in AcB at pH 3.5. The linear relationship between the square root of the scan rate ($v^{1/2}$, mV s^{-1}) and the peak current (I_p , μA) of RIF for the Ox2 peak demonstrated the diffusional behavior of RIF on the MWCNT/GC electrode (Equation 5). The graph between the logarithm of scan rate ($\log v$) and the logarithm of peak current ($\log I_p$) gave a straight line with a slope of 0.667 for the Ox2 peak (Equation 6). Theoretical values of 0.5 and 1.0 for the $\log v$ vs. $\log I_p$ graph express diffusion and adsorption controlled electrode process, respectively.³⁰ The obtained slope of 0.667 showed that the process was diffusion controlled under some adsorptive effects. Due to the adsorptive effects, DPAdSV and square wave adsorptive stripping voltammetry were tested with the parameters of accumulation potential and accumulation time for the determination of RIF. However, these parameters could not be optimized and linear calibration graphs could not be obtained. For this reason, DPV and SWV were used for the determination studies of RIF.

$$I_p \text{ (}\mu\text{A)} = 0.172 v^{1/2} \text{ (mV s}^{-1}\text{)} - 0.197; r = 0.996, n = 8 \text{ (for Ox2)} \quad (5)$$

$$\log I_p \text{ (}\mu\text{A)} = 0.667 \log v \text{ (mV s}^{-1}\text{)} - 1.154; r = 0.993, n = 8 \text{ (for Ox2)} \quad (6)$$

Determination of RIF by MWCNT/GC electrode

Determination of RIF was studied with the MWCNT/GC

electrode using both DPV and SWV having good selectivity, high sensitivity, and low detection limits. All measurements were made for the anodic Ox2 peak in AcB at pH 3.5 as the supporting electrolyte. Calibration graphs were obtained between the concentration of RIF and the peak current of Ox2 for DPV and SWV. Figure 6 shows DP and SW voltammograms obtained with different concentrations of RIF.

The plots of the calibration graphs were linear in the range between 0.04 and 10 μM for both DPV and SWV. At concentrations higher than 10 μM , the linearity was lost, probably due to the increase in the adsorption effect of RIF on the surface of the MWCNT/GC electrode. Besides linearity ranges, the values of slope, correlation coefficient, limits of detection (LOD) and quantification (LOQ), repeatability (within day), reproducibility (between days), and precision were calculated for both techniques at MWCNT/GC electrodes.^{27,28} All values are listed in Table 1. Calibration graphs gave a linear plot with a slope of 0.799 $\mu\text{A } \mu\text{M}^{-1}$ for DPV and two linear plots with slope values of 1.503 $\mu\text{A } \mu\text{M}^{-1}$ and 0.714 $\mu\text{A } \mu\text{M}^{-1}$ for SWV.

The LOD and LOQ values were calculated from the peak current of RIF using $\text{LOD} = 3 s/m$ and $\text{LOQ} = 10 s/m$ equations, where s is the standard deviation of the peak currents (three runs) and m is the slope of the related calibration equation.^{27,31} The repetitive five DPV and SWV experiments in the same day (repeatability) and on different days over a week (reproducibility) obtained from different solutions containing RIF at the same concentration (4 μM) gave the precision of the techniques. These within-day and

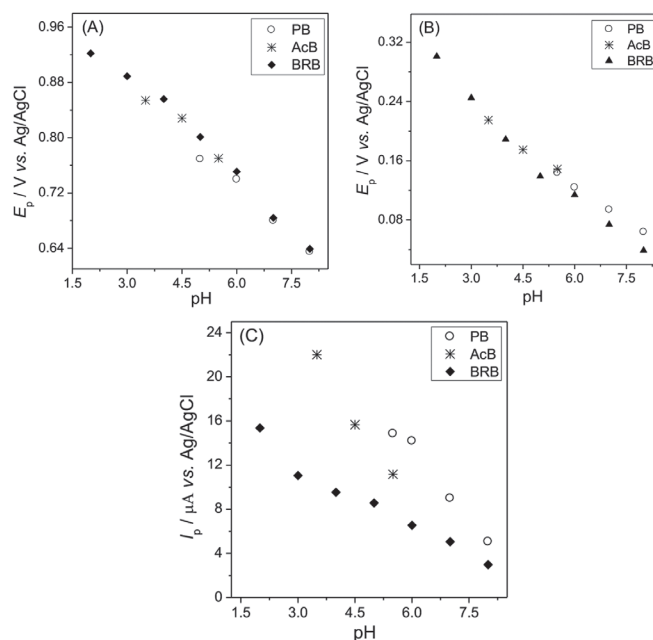


Figure 5. Effects of pH on the peak potentials for Ox1 (A) and Ox2 (B) and the peak currents for Ox2 (C) of RIF obtained with CV (A and B) and DPV (C) at the MWCNT/GC electrode. RIF concentration 40 μM in 0.1 M PB (o), 0.5 M AcB (x), and 0.04 M BRB (♦)

RIF: Rifampicin, CV: Cyclic voltammetry, DPV: Differential pulse voltammetry, MWCNT: Multi-walled carbon nanotube, GC: Glassy carbon, o PB: Phosphate buffer, x AcB: Acetate buffer, ♦ BRB: Britton-Robinson buffer

between-day precision, accuracy, and reproducibility values are presented as RSD% (Table 1). RSD% values lower than 1.5% demonstrated good precision, accuracy, and reproducibility.

Stability of RIF

The stability of RIF solutions was also studied over a month. Stock solution of RIF dissolved in ultrapure water was stored in the dark at +4°C. DP and SW voltammograms of the prepared

solutions containing the same RIF concentration in AcB at pH 3.5 were obtained. According to the voltammograms, decreases of 2.68% for DPV and 2.37% for SWV were observed at the peak currents of RIF after 4 weeks of storage. These low decrease values show that the solutions of RIF prepared by dissolving in ultrapure water can be used for up to 4 weeks. However, all solutions were freshly prepared every week to ensure the stability of RIF in the working solutions.

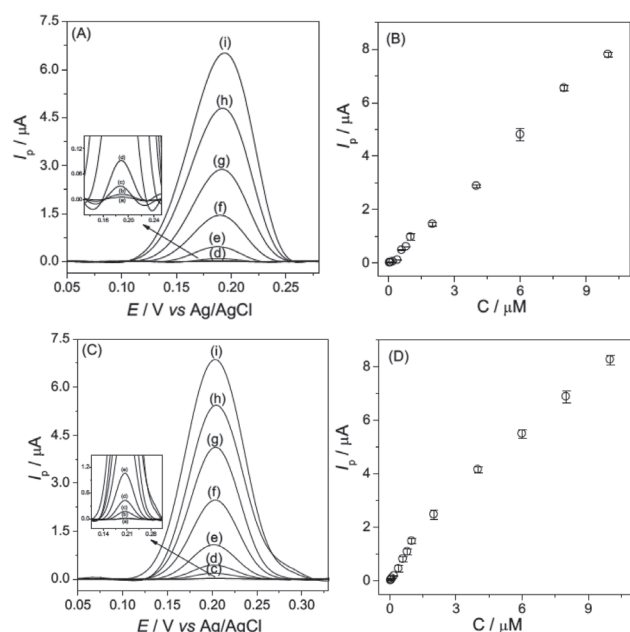


Figure 6. Baseline corrected (A) differential pulse and (C) square wave voltammograms obtained for the determination of (a) blank, (b) 0.06 μM , (c) 0.2 μM , (d) 0.4 μM , (e) 0.8 μM , (f) 2.0 μM , (g) 4.0 μM , (h) 6.0 μM , and (i) 8.0 μM of RIF in pH 3.5 AcB. Plots of the peak current (I_p) vs. the concentration of RIF with error bars representing standard deviations for each concentration, calculated from (B) differential pulse and (D) square wave voltammograms

RIF: Rifampicin, AcB: Acetate buffer

Determination of RIF from pharmaceutical dosage forms

The determination of RIF from its pharmaceutical dosage forms was studied to investigate the accuracy, selectivity, and precision of the developed voltammetric techniques with MWCNT/GC electrodes. For this purpose, the proposed DPV and SWV techniques were used to determine RIF in its capsules (300 mg RIF per capsule) for the prepared MWCNT/GC electrode. Pretreatment steps such as extraction and evaporation were not used before the voltammetric measurements. Recovery studies showed whether the excipients in pharmaceutical dosage forms caused any interference in the analysis of RIF. These studies were carried out by adding known amounts of standard RIF solution to the preanalyzed capsule solutions. The results are listed in Table 2. These results showed that the proposed methods for the prepared MWCNT/GC electrode could be applied for the sensitive anodic determination of RIF from pharmaceutical dosage forms without any interference from the excipients.

The bias % values were calculated to see the differences between the expected values obtained with DPV and SWV measurements and the true value (labeled RIF amount per capsule). Positive values of bias% indicated overestimation bias, meaning that the true value was slightly lower than the calculated values for both DPV and SWV (Table 2).

Table 1. Regression data of the calibration lines for quantitative determination of RIF in pH 3.5 AcB with DPV and SWV at the MWCNT/GC electrode

	DPV	SWV	
Measured potential (V)	0.193	0.203	
Linearity range (μM)	0.04-10	0.04-1.6 and 1.6-10	
Slope of the calibration graph ($\mu\text{A } \mu\text{M}^{-1}$)	0.799 \pm 0.01	1.503 \pm 0.04 and 0.714 \pm 0.01	
Intercept (μA)	-0.059 \pm 0.04	-0.078 \pm 0.02 and 1.169 \pm 0.11	
Correlation coefficient	0.997	0.994 and 0.998	
LOD (μM)	7.51 $\times 10^{-3}$	1.13 $\times 10^{-2}$	
LOQ (μM)	2.50 $\times 10^{-2}$	3.78 $\times 10^{-2}$	
4 μM RIF	Repeatability of peak current (RSD%)	1.01	0.84
	Repeatability of peak potential (RSD%)	0.56	0.35
	Reproducibility of peak current (RSD%)	1.07	1.42
	Reproducibility of peak potential (RSD%)	0.60	0.42

RIF: Rifampicin, AcB: Acetate buffer, SWV: Square wave voltammetry, MWCNT: Multi-walled carbon nanotube, GC: Glassy carbon, LOD: Limits of detection, LOQ: Limit of quantitation, RSD: Relative standard deviations, DPV: Differential pulse voltammetry, SWV: Square wave voltammetry

Table 2. The results for the determination of RIF from capsule form and recovery experiments achieved in pH 3.5 AcB using the MWCNT/GC electrode

Parameters	DPV	SWV
Labeled claim (mg)	300.00	300.00
Amount found* (mg)	300.32	300.36
RSD%	1.11	1.38
Bias%	0.11	0.12
Added (mg)	1.640x10 ⁻²	1.640x10 ⁻²
Found* (mg)	1.656x10 ⁻²	1.660x10 ⁻²
Average recovered (%)	100.98	101.22
RSD% of recovery	1.68	2.40
Bias%	0.98	1.22

*Obtained from five experiments, RIF: Rifampicin, AcB: Acetate buffer, MWCNT: Multi-walled carbon nanotube, GC: Glassy carbon, DPV: Differential pulse voltammetry, SWV: Square wave voltammetry, RSD: Relative standard deviations

Comparison of the proposed methods

The parameters of the validated DPV and SWV techniques for the MWCNT/GC electrode were compared with those of other sensors in the literature obtained for the determination of RIF in both the anodic^{15-18,21,32-35} and cathodic^{21,22,36-38} directions (Table 3). According to the results obtained in the anodic direction, a wider linear range was obtained in the present study compared to the studies in Table 3. Lower LODs were found only in two studies;^{18,32} however, the linear ranges of those studies were narrower. In addition, the electrode preparation procedures were long and complicated in some previous studies^{17,33-35} compared to the MWCNT/GC electrode used in the present study.

The results for RIF obtained in the direction of reduction in Table 3 showed that a wider linear range was found in the present study compared to the studies in the literature.^{21,37,38} Although a carbon paste electrode gave a wider linear range in a previous study,²² the LOD was higher than that in the present study. In another previous study,³⁶ there was no information

Table 3. Compared parameters obtained using different electrochemical sensors for the determination of RIF in the anodic direction

	Electrode	Method	Medium	Linear range, μM	LOD, μM
Anodic direction	Carbon paste electrode ¹⁵	SWV	Britton-Robinson buffer, pH 4.0	0.5-50	0.235
	Renewable pencil graphite electrode ¹⁶	DPAdSV	-	-	0.013
	Disposable carbon paste microelectrode modified with a hollow manganese oxide@mesoporous silica oxide core-shell nanohybrid ¹⁷	SWAdSV	Citric acid - Na ₂ HPO ₄ buffer, pH 6.0	0.03-3.0	10.8x10 ⁻³
	Lead film-modified glassy carbon electrode ¹⁸	AdSV	Acetate buffer, pH 5.0	2.5x10 ⁻⁴ -1.0x10 ⁻²	9.0x10 ⁻⁵
	Surfactant-modified carbon paste electrode ²¹	DPAdSV	0.1 M KCl, pH 2.0 or 0.2 M HCl	3.5x10 ⁻⁴ -5.4x10 ⁻³	-
	Carbon paste electrode ³²	AdSV	Acetate buffer, pH 4.9	0.1-2	5x10 ⁻³
	Iron oxide nanoparticles (Fe ₃ O ₄ NPs) and multiwalled carbon nanotubes (MWCNTs) composite-modified glassy carbon electrode ³³	DPV	Phosphate buffer, pH 7.5	2-20	0.032
Cathodic direction	Poly-melamine and gold nanoparticles-modified glassy carbon electrode ³⁴	LSV	Phosphate buffer, pH 7.0	0.08-15	0.030
	Carbon-dots@CuFe ₂ O ₄ nanocomposite-modified carbon paste electrode ³⁵	SWV	Britton-Robinson buffer, pH 7.0	0.07-8.0	0.022
	Surfactant-modified carbon paste electrode ²¹	DPAdSV	0.1 M KCl, pH 2.0 or 0.2 M HCl	9.0x10 ⁻⁵ -2.9x10 ⁻³	-
	Carbon paste electrode ²²	DPP	Acetate buffer, pH 4.5	0.1-100	0.010
	Hanging mercury drop electrode ³⁶	DPAdSV SWAdSV	-	-	6.14x10 ⁻³ 9.83x10 ⁻³
	Hanging mercury drop electrode ³⁷	DPAdSV	Carbonate buffer, pH 9.5	1.99-2.78	0.170
	Hanging mercury drop electrode ³⁸	DPV	Mcllvaine buffer, pH 7.0	0.49-2.4	85x10 ⁻³
MWCNT/GCE (this work)	DPV SWV	AcB, pH 3.5	0.04-10	7.51x10 ⁻³ 1.13x10 ⁻²	

RIF: Rifampicin, AdSV: Adsorptive stripping voltammetry, DPAdSV: Differential pulse adsorptive stripping voltammetry, SWAdSV: Square wave adsorptive stripping voltammetry, LSV: Linear sweep voltammetry, DPP: Differential pulse polarography, LOD: Limits of detection, MWCNT: Multi-walled carbon nanotube, AcB: Acetate buffer

about the linear range and the LOD was at the nM level as in the present study. The detection limits of the other studies in Table 3^{37,38} were higher compared to that of the MWCNT/GC electrode in the present study.

The linear range and LOD values obtained in the present study were also compared with those of the liquid chromatographic and spectrophotometric methods used for the determination of RIF (Table 4). According to the results, the linear range was wider and LOD values were lower for both DPV and SWV compared to the studies in Table 4.³⁹⁻⁴⁴

CONCLUSION

The electrochemical behavior of RIF was studied in the anodic direction by using MWCNT-modified GC electrodes. Modification was done by coating of 1.5 μL of 0.2% (mg mL^{-1}) MWCNT/DF dispersion on the surface of a GC electrode. The anodic process of RIF was irreversible and diffusion controlled in AcB at pH 3.5 as supporting electrolyte. Determination studies were carried out with DPV and SWV. These validated techniques

enabled selective, rapid, sensitive, and cheap determination of RIF. RIF was also sensitively determined in its pharmaceutical dosage forms without any separation steps. The results showed that the inactive excipients caused no interference during the voltammetric measurements. The results obtained in the present study were compared with those of both other electrochemical sensors and the liquid chromatographic and spectrophotometric methods proposed for RIF. The proposed DPV and SWV techniques using MWCNT-modified GC electrodes were more sensitive, cheaper, simpler, and faster determination methods for RIF. They might be alternatives to the liquid chromatographic and spectrophotometric methods in therapeutic drug monitoring.

Table 4. Compared parameters obtained using different analytical methods for the determination of RIF

Method	Medium	Linear range, $\mu\text{g/mL}$	LOD, $\mu\text{g/mL}$
RP-HPLC ³⁹	Methanol:acetonitrile: water (60:20:20, v/v)	40-100	0.5
HPLC ⁴⁰	20 mM monobasic sodium phosphate buffer with 0.2% triethylamine (pH 7.0):acetonitrile (96+4, v/v)	105-195	-
RP-HPLC ⁴¹	Acetonitrile:methanol:water (30:5:65, v/v, pH 5.2)	60-150	0.13
UV spectrophotometry ⁴²	Folin-Ciocalteu reagent (FCR)	1.0-35	0.32
UV spectrophotometry ⁴³	Methanol	5-50	2.30
UV spectrophotometry ⁴⁴	Ethyl acetate solution	2.5-35.0	0.83
DPV (this work)	AcB, pH 3.5	0.033-8.23	6.18×10^{-3}
SWV			9.11×10^{-3}

RIF: Rifampicin, RP-HPLC: Reversed phase-high performance liquid chromatography, UV: Ultraviolet, DPV: Differential pulse voltammetry, SWV: Square wave voltammetry, LOD: Limits of detection, AcB: Acetate buffer

REFERENCES

- Hardman JG, Limbird LE. Goodman and Gilman's The Pharmacological Basis of Therapeutics (9th ed). In: Molinoff PB, Ruddon RW, eds. New York; Mc-Graw-Hill; 1996:1160.
- Campbell EA, Korzheva N, Mustaev A, Murakami K, Nair S, Goldfarb A, Darst SA. Structural mechanism for rifampicin inhibition of bacterial RNA polymerase. *Cell*. 2001;104:901-912.
- Takahashi K, Tatsumi N, Fukami T, Yokoi T, Nakajima M. Integrated analysis of rifampicin-induced microRNA and gene expression changes in human hepatocytes. *Drug Metab Pharmacokinet*. 2014;29:333-340.
- Eswaran S, Adhikari AV, Chowdhury IH, Pal NK, Thomas KD. New quinoline derivatives: Synthesis and investigation of antibacterial and antituberculosis properties. *Eur J Med Chem*. 2010;45:3374-3383.
- World Health Organization, WHO Model Prescribing Information: Drugs Used in Mycobacterial Diseases. Geneva; 1991.
- Liu J, Sun J, Zhang W, Gao K, He Z. HPLC determination of rifampicin and related compounds in pharmaceuticals using monolithic column. *J Pharm Biomed Anal*. 2008;46:405-409.
- Allanson AL, Cotton MM, Tettey JNA, Boyter AC. Determination of rifampicin in human plasma and blood spots by high performance liquid chromatography with UV detection: A potential method for therapeutic drug monitoring. *J Pharm Biomed Anal*. 2007;44:963-969.
- Goutal S, Auvity S, Legrand T, Hauquier F, Cisternino S, Chapy H, Saba W, Tournier N. Validation of a simple HPLC-UV method for rifampicin determination in plasma: Application to the study of rifampicin arteriovenous concentration gradient. *J Pharm Biomed Anal*. 2016;123:173-178.
- Grégoire M, Leroy AG, Bouquié R, Malandain D, Dailly E, Boutoille D, Renaud C, Jolliet P, Caillon J, Deslandes G. Simultaneous determination of ceftaroline, daptomycin, linezolid and rifampicin concentrations in human plasma by on-line solid phase extraction coupled to high-performance liquid chromatography-tandem mass spectrometry. *J Pharm Biomed Anal*. 2016;118:17-26.
- Fang PF, Cai HL, Li HD, Zhu RH, Tan QY, Gao W, Xu P, Liu YP, Zhang WY, Chen YC, Zhang F. Simultaneous determination of isoniazid, rifampicin, levofloxacin in mouse tissues and plasma by high performance

- liquid chromatography-tandem mass spectrometry. *J Chromatogr B*. 2010;878:2286-2291.
- Vu DH, Koster RA, Bolhuis MS, Greijdanus B, Altena RV, Nguyen DH, Brouwers JRB, Uges DRA, Alffenaar JWC. Simultaneous determination of rifampicin, clarithromycin and their metabolites in dried blood spots using LC-MS/MS. *Talanta*. 2014;121:9-17.
 - Chellini PR, Mendes TO, Franco PHC, Porto BLS, Tippavajhala VK, César IC, Oliveira MAL, Pianetti GA. Simultaneous determination of rifampicin, isoniazid, pyrazinamide and ethambutol in 4-FDC tablet by Raman spectroscopy associated to chemometric approach. *Vib Spectrosc*. 2017;90:14-20.
 - Salem AA, Mossa HA, Barsoum BN. Quantitative determinations of levofloxacin and rifampicin in pharmaceutical and urine samples using nuclear magnetic resonance spectroscopy. *Spectrochim Acta A Mol Biomol Spectrosc*. 2005;62:466-472.
 - Benetton SA, Kedor-Hackmann ER, Santoro MI, Borges VM. Visible spectrophotometric and first-derivative UV spectrophotometric determination of rifampicin and isoniazid in pharmaceutical preparations. *Talanta*. 1998;47:639-643.
 - Hammam E, Beltagi AM, Ghoneim MM. Voltammetric assay of rifampicin and isoniazid drugs, separately and combined in bulk, pharmaceutical formulations and human serum at a carbon paste electrode. *Microchem J*. 2004;77:53-62.
 - Kawde AN, Temerk Y, Farhan N. Adsorptive stripping voltammetry of antibiotics rifamycin SV and rifampicin at renewable pencil electrodes. *Acta Chim Slov*. 2014;61:398-405.
 - Gan T, Shi Z, Wang K, Sun J, Lv Z, Liu Y. Rifampicin determination in human serum and urine based on a disposable carbon paste microelectrode modified with a hollow manganese oxide@mesoporous silica oxide core-shell nanohybrid. *Can J Chem*. 2015;93:1061-1068.
 - Tyszczyk K, Korolczyk M. New protocol for determination of rifampicin by adsorptive stripping voltammetry. *Electroanalysis*. 2009;21:101-106.
 - Rastgar S, Shahrokhian S. Nickel hydroxide nanoparticles-reduced graphene oxide nanosheets film: Layer-by-layer electrochemical preparation, characterization and rifampicin sensory application. *Talanta*. 2014;119:156-163.
 - Asadpour-Zeynali K, Mollarasouli F. Novel electrochemical biosensor based on PVP capped CoFe_2O_4 @CdSe core-shell nanoparticles modified electrode for ultra-trace level determination of rifampicin by square wave adsorptive stripping voltammetry. *Biosens Bioelectron*. 2017;92:509-516.
 - Gutierrez-Fernandez S, Blanco-Lopez MC, Lobo-Castanon MJ, Miranda-Ordieres AJ, Tunon-Blanco P. Adsorptive stripping voltammetry of rifampicin at unmodified and surfactant-modified carbon paste electrodes. *Electroanalysis*. 2004;16:1660-1666.
 - Hahn Y, Shin S. Electrochemical behavior and differential pulse polarographic determination of rifampicin in the pharmaceutical preparations. *Arch Pharm Res*. 2001;24:100-104.
 - Alonso Lomillo MA, Dominguez Renedo O, Arcos Martinez MJ. Optimization of the experimental parameters in the determination of rifampicin by adsorptive stripping voltammetry. *Electroanalysis*. 2002;14:634-637.
 - Balasubramanian K, Burghard M. Chemically functionalized carbon nanotubes. *Small*. 2005;1:180-192.
 - Rivas GA, Rubianes MD, Rodriguez MC, Ferreyra NF, Luque GL, Pedano ML, Miscoria SA, Parrado C. Carbon nanotubes for electrochemical biosensing. *Talanta*. 2007;74:291-307.
 - Iijima S. Carbon nanotubes: Past, present, and future. *Physica B*. 2002;323:1-5.
 - Method Validation in Pharmaceutical Analysis. In: Ermer J, Miller JH, eds. *Veinheim; Wiley-VCH*; 2005.
 - Bievre P, Günzler H. *Validation in Chemical Measurements*. New York; Springer; 2005.
 - Kul D. Sensitive and selective determination of tolterodine tartrate and its electrochemical investigation on solid carbon based electrodes. *J Anal Chem*. 2014;69:970-981.
 - Laviron E, Roullier L, Degrand C. A multilayer model for the study of space distributed redox modified electrodes: Part II. Theory and application of linear potential sweep voltammetry for a simple reaction. *J Electroanal Chem Interfacial Electrochem*. 1980;112:11-23.
 - Validation of Active Pharmaceutical Ingredients (2nd ed). In: Berry IR, Harpaz D, eds. *Washington; CRC Press*; 2001.
 - Yi LH, Li JN, Gao P. Anodic adsorptive voltammetric determination of rifampicin at a carbon paste electrode. *Nat Sci J Xiangnan Univ*. 2005;27:108-111.
 - Chokkareddy R, Bhajanthri NK, Redhi GG. A novel electrode architecture for monitoring rifampicin in various pharmaceuticals. *Int J Electrochem Sci*. 2017;12:9190-9203.
 - Amidi S, Hosseinzadeh Ardakani Y, Amiri-Aref M, Ranjbari E, Sepehri Z, Bagheri H. Sensitive electrochemical determination of rifampicin using gold nanoparticles/poly-melamine nanocomposite. *RSC Advances*. 2017;7:40111-40118.
 - Shiri S, Pajouheshpoor N, Khoshshafar H, Amidi S, Bagheri H. An electrochemical sensor for the simultaneous determination of rifampicin and isoniazid using a C-dots@CuFe₂O₄ nanocomposite modified carbon paste electrode. *New J Chem*. 2017;41:15564-15573.
 - Lomillo MAA, Renedo OD, Martinez MJA. Optimization of the experimental parameters in the determination of rifampicin by adsorptive stripping voltammetry. *Electroanalysis*. 2001;14:634-637.
 - Lomillo MAA, Renedo OD, Martinez MJA. Optimization procedure, applying the experimental-design methodology, for the determination of rifampicin after metal complexation by differential pulse adsorptive stripping voltammetry. *Helv Chim Acta*. 2002;85:2430-2439.
 - Leandro KC, de Carvalho JM, Giovanelli LF, Moreira J. Development and validation of an electroanalytical methodology for determination of isoniazid and rifampicin content in pharmaceutical formulations. *Braz J Pharm Sci*. 2009;45:331-337.
 - Kumari MK, Kasthuri JK, Babu BH, Satyanarayana PVV, Tchaleu BN. A validated liquid chromatographic method for the determination of rifampicin and isoniazid in pharmaceutical formulations. *Brit J Pharm Res*. 2015;7:299-307.
 - Chellini PR, Lages EB, Franco PHC, Nogueira FHA, César IC, Pianetti GA. Development and validation of an HPLC method for simultaneous determination of rifampicin, isoniazid, pyrazinamide, and ethambutol hydrochloride in pharmaceutical formulations. *J AOAC Int*. 2015;98:1234-1239.
 - Prasanthi B, Vijaya Ratna J, Ch. Phani RS. Development and validation of RP-HPLC method for simultaneous estimation of rifampicin, isoniazid and pyrazinamide in human plasma. *J Anal Chem*. 2015;70:1015-1022.

-
42. Swamy N, Basavaiah K. Spectrophotometric determination of rifampicin in bulk drug and pharmaceutical formulations based on redox and complexation reactions. *J Appl Spectros.* 2017;84:694-703.
 43. Tilinca M, Hancu G, Mircia E, Irimescu D, Rusu A, Vlad RA, Barabas E. Simultaneous determination of isoniazid and rifampicin by UV spectrophotometry. *Farmacia.* 2017;65:219-224.
 44. Khan MF, Rita SA, Kayser MS, Islam MS, Asad S, Bin Rashid R, Bari MA, Rahman MM, Al Aman DAA, Setu NI, Banoo R, Rashid MA. Theoretically guided analytical method development and validation for the estimation of rifampicin in a mixture of isoniazid and pyrazinamide by UV spectrophotometer. *Front Chem.* 2017;5:27.



Investigation of the Peripheral Analgesic Activity of Oxycams and Their Combinations with Caffeine

Oksikamların ve Kafein ile Kombinasyonlarının Periferel Analjezik Aktivitelerinin İncelenmesi

Anna SYROVA¹, Larisa LUKYANOVA¹, Svetlana KOZUB¹, Oksana ZAVADA¹, Olga LEVASHOVA^{1*}, Viktor SHAPOSHNIK²

¹Kharkiv National Medical University, Department of Medical and Bioorganic Chemistry, Kharkiv, Ukraine

²Kharkiv National Medical University, Kharkiv, Ukraine

ABSTRACT

Objectives: Therapy of pain syndromes involves exposure to its source, receptors, and peripheral fibers. Treatment of acute pain and inflammation involves the use of nonsteroidal anti-inflammatory drugs and nonnarcotic analgesics. An alternative to obsolete analgesics is combined compositions. Experimental results clearly indicates that caffeine effectively enhances the peripheral analgesic activity when combined in an analgesic. The aim of the present study was to evaluate the peripheral analgesic activity of meloxicam, piroxicam, and their pharmacological combinations with caffeine.

Materials and Methods: The peripheral analgesic activity of piroxicam, meloxicam, and their combinations with caffeine was studied using the abdominal writhing test. This method was used to induce pain of peripheral origin by intraperitoneal injection of 0.6% acetic acid solution. The investigated drugs, their combinations, and 3% starch mucilage were administrated 1 h before the introduction of the algogen. The cumulative number of writhing responses induced by acetic acid was determined over the subsequent 20 min.

Results: All investigated drugs supplied a decrease in writhing in rats. Meloxicam and caffeine showed peripheral analgesic activity of 63.6% and 64.5%, respectively ($p < 0.05$). The pharmaceutical combination of meloxicam and caffeine showed analgesic potential of 76.4%. Thus, caffeine potentiates the analgesic activity of meloxicam. The results exceeded the corresponding value of diclofenac sodium (67.3%).

Conclusion: Experimental results clearly indicates that caffeine effectively enhances the peripheral analgesic action of meloxicam when combined in a pharmaceutical composition. These results can serve as a basis for the development of new domestic combined drugs.

Key words: Meloxicam, piroxicam, caffeine, pharmaceutical composition, analgesic activity

ÖZ

Amaç: Ağrı sendromlarının tedavisi, ağrı kaynağına maruziyeti, reseptörleri ve periferel lifleri içermektedir. Akut ağrı ve enflamasyonunun tedavisi, nonsteroidal anti-enflamatuvar ilaçların ve narkotik olmayan analjeziklerin kullanımını içerir. Eski analjeziklere bir alternatif kombine bileşimlerdir. Deneysel sonuçlar kafeinin bir analjezik ilaç ile birleştirildiğinde, periferel analjezik aktiviteyi etkin bir şekilde artırdığını açıkça göstermektedir. Bu çalışmanın amacı, meloksikam, piroksikam ve bunların kafeinle farmakolojik bileşimlerinin periferel analjezik aktivitesini değerlendirmektir.

Gereç ve Yöntemler: Piroksikam, meloksikam ve bunların kafeinle bileşimlerinin periferel analjezik aktivitesi abdominal ağrı testi kullanılarak incelenmiştir. Bu yöntem, periferel orijinli ağrının oluşturulmasında %0,6'lık asetik asit çözeltisinin intraperitoneal olarak enjekte edilmesiyle ağrının indüksiyonunu sağlamak için kullanılmıştır. İncelenen ilaçlar, bunların bileşimleri ve %3 nişasta müsilajı, algojenin verilmesinden 1 saat önce uygulanmıştır. Asetik asit tarafından indüklenen kümülatif ağrı cevapları, sonraki 20 dakika boyunca belirlenmiştir.

Bulgular: İncelenen tüm ilaçlar, sıçanlarda ağrı azalması sağlamıştır. Meloksikam ve kafein periferel analjezik aktivitelerini sırasıyla %63,6 ve %64,5 olarak göstermiştir ($p < 0,05$). Meloksikam ve kafeinin farmasötik bileşimi %76,4'lük analjezik potansiyel göstermiştir. Bu nedenle kafein, meloksikamın analjezik aktivitesini potansiyeize etmektedir. Sonuçlar diklofenak sodyumla elde edilen değerden (%67,3) fazladır.

Sonuç: Deneysel sonuçlar açıkça kafeinin meloksikamla farmasötik bileşiminin meloksikamın periferel analjezik etkisini etkin bir şekilde artırdığını göstermektedir. Bu sonuçlar yeni yerli kombine ilaçların geliştirilmesinde temel oluşturabilir.

Anahtar kelimeler: Meloksikam, piroksikam, kafein, farmasötik bileşim, analjezik aktivite

*Correspondence: E-mail: olga.jdan78@gmail.com, Phone: +380577077307 ORCID-ID: orcid.org/0000-0001-9779-7762

Received: 30.09.2018, Accepted: 18.07.2019

©Turk J Pharm Sci, Published by Galenos Publishing House.

INTRODUCTION

Nonsteroidal anti-inflammatory drugs (NSAIDs) and nonnarcotic analgesics (NNAs) are widely used for the treatment of inflammation and pain syndromes. Analysis of the scientific literature has shown that polycomponent compositions are more effective than monopreparations in treating pain. Therefore, the development of new effective domestic multicomponent drugs with a minimum number of side effects is a very important subject.¹⁻⁴

It is known that caffeine improves the analgesic effect of NNAs. The mechanism of potentiation of analgesic effects is associated with an improvement in NNA bioavailability in combinations with caffeine and with the effect of caffeine on adenosine receptors (so-called purine analgesia).⁵⁻⁹ Research on the biological effects of caffeine and its pharmacological combinations showed a positive effect on the central nervous system. Caffeine shows a wide range of action: reduction in adenosine transmission, regulation of excitation processes in the cerebral cortex, and in corresponding doses it enhances positive condition reflexes and increases motor activity.¹⁰⁻¹³

The aim of our work was the experimental investigation of the peripheral analgesic activity of oxicams (meloxicam and piroxicam), caffeine, and their pharmacological combinations.

MATERIALS AND METHODS

An experimental study of analgesic activity was conducted on laboratory animals, namely mature rats. The peripheral analgesic activity was studied by the changes in the nociceptive reactions of the rats. The comparative characteristic of the analgesic activity of meloxicam, piroxicam, caffeine, and their pharmacological combinations was studied using an acetic acid-induced abdominal writhing test. Writhes were caused by a single intraperitoneal injection of 0.6% acetic acid solution (1 mL per 100 g of animal weight) in rats. The investigated drugs, their combination, and 3% starch solution were injected 1 h before the algogen was introduced. Then the number of writhes was counted for 20 min.¹⁴

The animals were divided into 7 groups with 6 animals in each. In the first group 3% starch mucus (2 mL per 200 g of the rats weight) was injected via a gastric tube into intact animals. The experimental drugs and their combinations were administered to the animals in groups 2-7 once via a gastric tube: animals in the second group received piroxicam (1.3 mg per 1 kg of animal weight), the third group meloxicam (0.6 mg per 1 kg of animal weight), the fourth group caffeine (0.6 mg per 1 kg of animal weight), the fifth group the combination of piroxicam (1.3 mg per 1 kg of animal weight) and caffeine (0.6 mg per 1 kg of animal weight), the sixth group the combination of meloxicam (0.6 mg per 1 kg of animal weight) and caffeine (0.6 mg per 1 kg of animal weight), and the seventh group a reference drug, diclofenac sodium (8 mg per 1 kg of animal weight).

Analgesic activity was estimated by the ability of oxicams (meloxicam and piroxicam), caffeine, their pharmacological combinations, and sodium diclofenac to reduce the number of

writhes in the experimental animal groups as compared to the control group and expressed as a percentage by the formula

$$AA = \frac{C_c - C_e}{C_c} \times 100\%$$

where AA: Analgesic activity %;

C_c : The average number of writhes in the control group;

C_e : The average number of writhes in the experimental group (9-10).

In addition, the analgesic activity of oxicams and caffeine was compared with that of their combinations (meloxicam + caffeine and piroxicam + caffeine) and the reference drug.

The study was carried out in accordance with the methodological recommendations of the State Pharmacological Center of the Ministry of Health of Ukraine^{14,15} and approved by the Ethics Committee of Kharkiv National Medical University (KhNMU). An economical approach, bioethical rules, and statistics requirements were considered when choosing the number of animals and their allocation to the treatment groups.

The study was performed on laboratory animals from the experimental biological clinic of KhNMU. The rats were housed under the strict norms for storage, care, and feeding according to the principles of the "European Convention for the Protection of Vertebrate Animals used for Experimental and other Scientific Purposes" (Strasbourg, 1986)^{16,17} and the decision of the First National Congress on Bioethics (Kyiv, 2007).¹⁸ Room temperature was maintained at 23-25°C, room lighting was 100 lx, and the animal cage lighting was 20-40 lx. The laboratory animals were housed for 1.5 months, the acclimatization period was 2 weeks, the main diet was vegetables and fodder beet, and the source of water was settled tap water. The experiments were carried out in the morning, which, according to the literature data, corresponds to the dependence of the main pharmacological parameters and pharmacological activity of investigated drugs on circadian rhythms.¹⁹⁻²¹

Statistical analysis

Statistical calculations were performed by conventional methods using the programs MS Excel and Statgraphics Plus 2.1.²²

RESULTS AND DISCUSSION

A specific pain response was investigated by the method of chemical peritoneal irritation. There are several known methods of specific pain investigation: acetylcholine writhes and acetic acid-induced abdominal writhing tests. "Stretching" of animals in the acetylcholine writhing model caused by activation of the arachidonic acid metabolism with COX results in increased synthesis of prostaglandins under the influence of acetylcholine. The mechanism of acetic acid-induced pathology activates the kinin-kallikrein system, prostaglandins, biogenic amines, and leukotrienes, which are endogenous inflammatory mediators and contribute to the development of the abdominal muscle spasm, accompanied by the retraction of the hind paws and the back flexes. The effect of the investigated substances

on the peripheral component of the nociceptive response was examined by the acetic acid abdominal writhing test, as the most informative method.

In our previous studies, the central analgesic activity of caffeine in combination with piroxicam and meloxicam was studied in order to create a new medicinal composition.

The results of experimental studies have shown that administration of piroxicam, meloxicam, and caffeine monopreparations reduces the number of writhes 2-, 2.6-, and 2.8-fold, respectively, compared to the control group and produces a result similar to that of the reference drug (Figure 1).

Such a result for caffeine peripheral analgesic activity may be associated with inhibition of prostaglandin synthesis and the transient receptor potential channel subfamily A member 1 channel, which acts as the main receptor of neuropathic pain of peripheral origin. Caffeine also helps to eliminate exudate from the area of inflammation and, accordingly, reduces the compression of peripheral nociceptors. This is confirmed by our studies on the anti-exudative effect of the above-mentioned compositions with caffeine.¹³

The analgesic activity of piroxicam (53.6%) and caffeine (64.5%) monopreparations has values similar to that of the reference drug, diclofenac sodium (67.3%). The combination of piroxicam with caffeine shows a reduction in writhes of 1.7-fold and has the lowest value of analgesic activity, 40.9%. Piroxicam, as a nonselective inhibitor of cyclooxygenase (COX-1 and COX-2), has a rapid and pronounced analgesic effect. The selectivity index (inhibition ratio COX-1/COX-2) is 33, i.e. it has the highest potency against COX-1. However, a literature review of nonselective NSAIDs' effects indicates that the concomitant use of piroxicam with a preparation having an antiedemic action (caffeine) might reduce their effect. This effect could be attributed to the NSAID inhibition of renal prostaglandin synthesis and increased fluid retention. Coadministration of piroxicam with caffeine may show antagonism due to their pharmacokinetic properties. Additionally, the high affinity of caffeine to blood proteins could be a reason for the antagonistic effect of this composition component on the peripheral analgesic effect.²

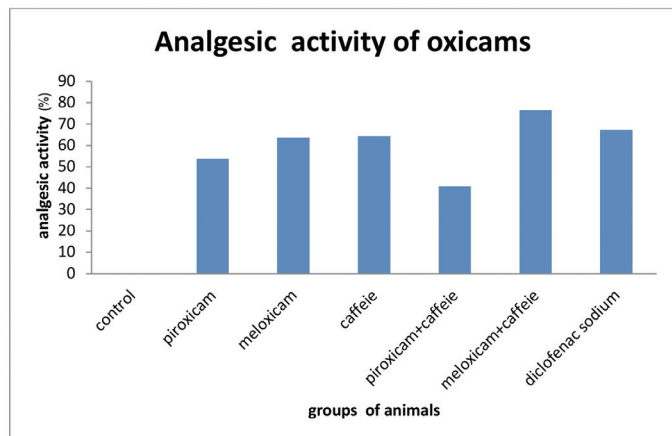


Figure 1. Analgesic activity of oxicams

The addition of caffeine to piroxicam facilitates mitigation of analgesic activity and so this combination shows unpromising results in relation to analgesic activity of peripheral genesis. Contrasting data were obtained by adding caffeine to meloxicam. The meloxicam and caffeine composition has the highest value of analgesic activity, 76.4%, and reduces the number of writhes 4.2-fold.

Meloxicam is a representative of the new generation of NSAIDs, i.e. selective COX-2 inhibitors. The selectivity index (inhibition ratio of COX-1/COX-2) is 0.33; it selectively inhibits the formation of prostaglandins involved in the formation of inflammation and has a much lower effect on the synthesis of prostaglandins that regulate renal blood flow, production of protective mucus in the stomach, and platelet aggregation. It is known that selective COX-2 inhibitors doses in which selectivity is observed do not show a sufficient clinical effect. Increasing the dose leads to a loss of selectivity and the appearance of gastrotoxicity.³

Our research shows that meloxicam and its combination with caffeine in a lower dose (0.6 mg) than piroxicam (1.3 mg) and even the reference drug (8 mg) exhibit higher analgesic activity. The increased analgesic effect of meloxicam combined with caffeine could be explained by the effect of caffeine on the bioavailability of meloxicam and the synergetic effect of these two components. The results indicate potentiation of analgesic activity of the last one; therefore, this composition is considered promising for further study (Table 1).

Table 1. The investigated peripheral analgesic activity of oxicams (meloxicam and piroxicam), caffeine and their pharmaceutical compositions with caffeine

No	Groups of animals	Number of writhes	Analgesic activity, %
1	Control	22.00±0.856	-
2	Piroxicam	10.20±0.167 ^{1/3/4/5/6/7}	53.6
3	Meloxicam	8.30±0.211 ^{1/2/5/6/7}	63.6
4	Caffeine	7.80±0.477 ^{1/2/5/6}	64.5
5	Piroxicam + caffeine	13.00±0.365 ^{1/2/3/4/6/7}	40.9
6	Meloxicam + caffeine	5.20±0.167 ^{1/2/3/4/5/7}	76.4
7	Diclofenac sodium	7.20±0.167 ^{1/2/3/5/6}	67.3

Note: Investigation of peripheral analgesic activity of oxicams and its combination with caffeine shows that the difference is statistically significant:

¹Reliability of results in relation to the control group, $p < 0.05$;

²Reliability of results with respect to the monopreparation of piroxicam, $p < 0.05$;

³Reliability of results with respect to the monopreparation of meloxicam, $p < 0.05$;

⁴Reliability of results with respect to the monopreparation of caffeine, $p < 0.05$;

⁵Reliability of results with respect to the combination of piroxicam with caffeine, $p < 0.05$;

⁶Reliability of results with respect to the combination of meloxicam with caffeine, $p < 0.05$;

⁷Reliability of results with respect to the monopreparation of diclofenac sodium, $p < 0.05$

CONCLUSION

1. Meloxicam (dose: 0.6 mg/kg) shows peripheral analgesic activity (63.6%) at the level of the reference drug (diclofenac sodium) (67.3%).

2. Meloxicam in a lower dose (0.6 mg/kg) than piroxicam (1.3 mg/kg) demonstrates higher peripheral analgesic activity, 63.6% and 53.6%, respectively.

3. The peripheral analgesic activities of piroxicam (53.6%) and caffeine (64.5%) monopreparations have higher values than their pharmaceutical combination (40.9%). Hence, further study of the analgesic activity of piroxicam combined with caffeine is considered inexpedient.

4. The pharmacological combination of meloxicam with caffeine demonstrated pain inhibition of 76.4%, which significantly exceeded the peripheral analgesic activity of the reference drug, diclofenac sodium, 67.3%, i.e. caffeine effectively potentiates the analgesic activity of meloxicam. Thus, the combination of meloxicam with caffeine as a commercial source of a domestic analgesic drug could be subjected to further study.

Conflicts of interest: No conflict of interest was declared by the authors. The authors alone are responsible for the content and writing of the paper.

REFERENCES

1. Laurence DR, Bennett PN, Brown MJ: Inflammation, arthritis and non-steroidal anti-inflammatory drugs (NSAIDs). Moscow: Medicine. 1991;485-523.
2. Bilousov YuB. Clinical pharmacology and pharmacotherapy: A guide for physicians. Moscow: Medical News Agency. 1997;531. <https://www.twirpx.com/file/291957/>
3. Weir MR. Renal effects of nonselective NSAIDs and coxibs. Cleve Clin J Med. 2002;69(Suppl 1):53-58.
4. Kozachok NN, Seluk MN, Bychkova SA. Optimalniy vibor nesteroidnogo protivovospalitel'nogo preparata v sovremennoy klinicheskoy praktike. News of medicine and pharmacy. 2007;8:3-4.
5. Zupanets IA, Nalotov SV, Viktorov AP, editors. Clinical pharmacology. Kharkov: NUPh; 2005.
6. Burchinsky SG. Clinical and pharmacological aspects of the choice of analgesic. Comparative analysis of the paracetamol effectiveness and safety. Pharmacologic Visnik. 2000;354:12-17.
7. Nasonov EL. Nonsteroidal anti-inflammatory drugs: Prospects of use in medicine. Anko. 2000;143:1-2.
8. Chekman I, Gorchakova N, Zvyagintseva T, Syrova G, Nebesna N. Caffeine: Physiological, biochemical and quantum-pharmacological properties. Bulletin of Pharmacology and Pharmacy. 2009;259:2-7.
9. Syrova GO, Zvyagintseva TV. Study of potentiating analgesic properties of caffeine in the experiment. XII Congress of the World Federation of Ukrainian Drug Societies. Ivano-Frankivsk. 2008;454.
10. Sawynok J. Caffeine and pain. Pain. 2011;152:726-729.
11. Sawynok J, Yaksh TL. Caffeine as an analgesic adjuvant: a review of pharmacology and mechanisms of action. Pharmacological Reviews. 1993;45:43-85.
12. Fisone G, Borgkvist A, Usiello A. Caffeine as a psychomotor stimulant: mechanism of action. CMLS. 2004;61:857-872.
13. Syrova GO, Lukianova LV, Chalenko NM. The experimental research on the antiinflammatory action of the new piroxicam-caffeine pharmaceutical composition. Science Review. 2018;4:72-76.
14. Stefanov OV. Preclinical research of medicines: methodological recommendations. Kiiv: Avicenna. 2001;431-432.
15. Trinus FP, Klebanov BM, Kondratyuk VI, editors. Methodical recommendations for the experimental (preclinical) study of non-steroidal anti-inflammatory pharmacological substances. Moscow; 1983.
16. Burkatskaya EN, Beyer VF, editors. Methodical recommendations on the use of behavioral reactions of animals in toxicological studies. Kiev;1980;47.
17. European convention for the protection of vertebrate animals used for experimental and other scientific purposes: Council of European. Strasbourg, 1986;51:29-34.
18. Kundiev YUI, editor. Modern problems of bioethics. Kiev: Akademperiodica, 2009;278:141-173.
19. Drogovoz SM, Rapoport SI, Kononenko AV. Informative chronopharmacology (chronopharmacology in tables and figures): a textbook. Kharkov, Titule. 2014; 128:111-117.
20. Dorogoy AP. To the question of chronopathology, chronotherapy and chronopharmacology in cardiology: Actual problems in modern therapy. Kharkiv. 1992;354:22-25.
21. Zapadnyuk IP, Zapadnyuk VI, Zakharia EA. Laboratory animals: breeding, content, use in experiment (3rd ed). Revised and additional. Kiev: Vishcha skola. Head Publishing House. 1983;383:141-154.
22. Glanc S. Medico-biological statistics. Moscow: Practica. 1998;459:318-323.



Green Synthesis and Characterization of Copper Nanoparticles and Their Effects on Liver Function and Hematological Parameters in Mice

Bakır Nanopartiküllerinin Yeşil Sentezi, Karakterizasyonu, Farelerde Karaciğer İşlevi ve Hematolojik Parametreler Üzerine Etkileri

© Mehrdad KHATAMI¹, © Katrin EBRAHIMI², © Nasrin GALEHDAR³, © Mohammad Nabi MORADI⁴, © Alireza MOAYYEDKAZEMI^{5*}

¹Student Research Committee, Bam University of Medical Sciences, Bam, Iran

²Department of Biology, Payame Noor University, Tehran, Iran

³Social Determinants of Health Research Center, Lorestan University of Medical Sciences, Khorramabad, Iran

⁴Razi Herbal Medicines Research Center, Lorestan University of Medical Sciences, Khorramabad, Iran

⁵Department of Internal Medicine, Lorestan University of Medical Sciences, Khorramabad, Iran

ABSTRACT

Objectives: The present investigation is based on the green synthesis of copper nanoparticles (CuNPs) from aqueous extract of *Capparis spinosa* L. fruit. Their effects on liver function and hematological parameters in mice were evaluated.

Materials and Methods: The green synthesis of CuNPs by means of *C. spinosa* extract was achieved. Ultraviolet-visible spectroscopy, fourier transform infrared (FTIR) spectroscopy, scanning electron microscopy (SEM), and energy dispersive X-ray spectroscopy were used to identify the synthesized nanoparticles. BALB/c mice were orally administrated CuNPs at doses of 1000, 2000, and 5000 µg/kg for 2 weeks. Later, the effects of CuNPs on liver function in the treated mice were evaluated by measuring the serum levels of enzymes such as alanine aminotransferase, aspartate aminotransferase, alkaline phosphatase, and bilirubin as well as hematological parameters including hemoglobin, hematocrit, white blood cell, red blood cell, and platelet counts.

Results: A maximum peak at wavelength 414 nm confirmed the biosynthesis of CuNPs. FTIR spectrum analysis revealed that the factor groups shaped a coating extract on the surface of the nanoparticles. SEM images demonstrated a particle size between 17 and 41 nm. Although some liver enzymes and hematological parameters increased with increasing dose of extract, there was no significant difference ($p>0.05$) between oral administrations of CuNPs at doses of 1000, 2000, and 5000 µg/kg and the control group.

Conclusion: The findings revealed that CuNPs biosynthesized from aqueous extract of *C. spinosa* fruit have no toxic effects on the liver functions and hematological parameters of mice. However, more studies are needed for evaluation of the hepatoprotective effects of CuNPs.

Key words: Nanoparticles, copper, liver, hematology, *Capparis spinosa*, BALB/c mice

ÖZ

Amaç: Bu çalışma *Capparis spinosa* L. meyvesinin sulu ekstrelerinden elde edilen bakır nanopartiküllerinin (CuNP) yeşil sentezi üzerindedir. Bunların karaciğer işlevleri ve hematolojik parametreler üzerine etkileri farelerde değerlendirilmiştir.

Gereç ve Yöntemler: CuNP'lerin *C. spinosa* ekstrelerinden elde edilmesi sağlanmıştır. Fourier dönüşümlü kızılötesi (FTIR) spektroskopisi, taramalı elektron mikroskopu (SEM) ve enerji dağıtıcı X-ışını spektroskopisi ile sentez edilen nanopartiküller belirlenmiştir. BALB/c farelere oral olarak 2 hafta boyunca 1000, 2000 ve 5000 µg/kg dozlarında CuNP uygulanmıştır. Sonrasında, uygulama yapılan farelerde CuNP'lerin karaciğer işlevleri üzerine etkisi alanin aminotransferaz, aspartat aminotransferaz, alkalin fosfataz ve bilirubin ölçülerek karaciğer işlevleri ve hemoglobin, hematokrit, beyaz kan hücreleri, kırmızı kan hücreleri ve trombosit sayıları belirlenerek hematolojik parametreleri ölçülmüştür.

Bulgular: 414 nm'deki maksimum pik CuNP'lerin biyosentezini göstermiştir. FTIR spectrum analizi faktör gruplarının nanopartiküllerin yüzeyinde bir kaplama ekstrelerine şekil verdiğini göstermiştir. SEM resimleri partikül boyutlarının 17 ve 41 nm arasında olduğunu göstermiştir. Her ne kadar karaciğer enzimleri ve hematolojik parametreler artan ekstre dozuyla artsa da, CuNP'lerin 1000, 2000 ve 5000 µg/kg dozlarında oral uygulaması ve kontrol grubu arasında belirgin bir değişiklik görülmemiştir ($p>0,05$).

*Correspondence: E-mail: armokazemi@gmail.com, Phone: +986633120150 ORCID-ID: orcid.org/0000-0002-8522-1093

Received: 25.04.2019, Accepted: 27.06.2019

©Turk J Pharm Sci, Published by Galenos Publishing House.

Sonuç: Bu bulgular *C. spinosa* meyvesinin sulu ekstresinden elde edilen CuNP'lerin farelerde karaciğer işlevleri ve hematolojik parametreler üzerinde toksik etkilerinin olmadığını göstermiştir. Ancak, CuNP'lerin hepatoprotektif etkilerinin değerlendirilmesi için daha çok çalışmaya ihtiyaç vardır.

Anahtar kelimeler: Nanopartiküller, bakır, karaciğer, hematoloji, *Capparis spinosa*, BALB/c fare

INTRODUCTION

Nanotechnology is one of the most useful technologies and it can be applied in many areas including food and nutrition, biomedical science, gene transmission, energy science, electronics, and the space industry. In particular, this technology is implemented in the treatment of cancer, allergies, inflammation, diabetes, and other diseases.¹

There are various physical and chemical methods for the production of nanoparticles, and they are still being investigated for the purpose of obtaining particles with a certain size and lower toxicity.² Green synthesis is considered a new approach to prevent the production of undesired or unsafe by products via reliable, maintainable, and eco-favorable synthesis techniques. Between the current green procedures of synthesis of nanoparticles, use of plant extracts is an appropriate and easy method to harvest nanoparticles on a large scale relative to bacteria and/or fungi mediated synthesis.^{2,3} Recent studies have also shown that the synthesis of metal nanoparticles using plant extracts, i.e. green synthesis, has some benefits such as low cost and low toxic effects for large-scale production.²⁻⁴

Copper (Cu) is one of the most useful elements in medical science because of its numerous anti-inflammatory, anticancer, analgesic, and antimicrobial effects.⁵ In recent years, it has been proven that, because of their high surface-to-volume ratio, Cu nanoparticles (CuNPs) are extremely reactive and simply interact with other particles, leading to a wide range of biological activities.⁵⁻⁷

Previous reviews on laboratory animals have demonstrated that the liver is considered the key target tissue of drug toxicity. Hence, assessing the function of this organ is a very important method to determine drug toxicity.⁸ Nowadays, one of the main criteria to determine liver damage is measuring serum levels of enzymes such as alanine aminotransferase (ALT), aspartate aminotransferase (AST), alkaline phosphatase (ALP), and bilirubin.⁹⁻¹¹ It has been reported that oral consumption of some medicinal agents may affect the hematological parameters and result in anemia, neutropenia, and thrombocytopenia; therefore, it is necessary to evaluate the effects of novel medicinal drugs by measuring hematological parameters.¹⁰ Accordingly, the present study examined the green synthesis of CuNPs from *Capparis spinosa* fruit extract and evaluated their effects on liver function and hematological parameters in mice.

MATERIALS AND METHODS

Green synthesis of copper nanoparticles

Fruits of *C. spinosa* were collected from rural areas in western Iran and then were extracted by percolation procedure by means of methanol (80%) for 3 days at room temperature.¹² In the next step, the green synthesis of CuNPs was performed

according to a method described elsewhere. Briefly, 75 mL of the obtained extract was added to 100 mL of 0.01 M Cu sulfate solution. After stirring, it was kept at 60°C for 1 day. In the next step, to remove all impurities, it was centrifuged twice at 12,000 rpm for 20 min. Nanoparticles started to deposit when the color of the solution changed from green to amber yellow. The synthesized nanoparticles were heat treated in an oven at 60°C for further analyses.

Ultraviolet-visible (UV-Vis) spectroscopy analysis

Transformation of the Cu ions to CuNPs was shown by the surface plasmon resonance (SPR) of the CuNPs. For this purpose, 0.3 mL of the specimens was diluted with 3 mL of normal saline and studied via UV-Vis spectrum analysis by means of a spectrophotometer (JENWAY 6405) in the range of 300-700 nm.¹³

Fourier transform infrared (FTIR) spectroscopy

After pouring and mixing the obtained samples and potassium bromide granules together in a ratio of 1 to 100 (1/100 ratio) and compacting them into tablets, FTIR (model Nicolet 32) analysis was carried out in the range of 400-4000 cm⁻¹ and with the resolution of 1-4 cm⁻¹.¹⁴

Scanning electron microscope (SEM)

To obtain the characteristics of the synthesized nanoparticles, electron microscopy (Mira3, Czech Republic) with 15 kV, magnification of 10x, and resolution of 1 nm was performed.

Animals and study design

A total of 32 male BALB/c mice weighing 25-30 g were provided by the Tehran Pasteur Institute and kept in light/dark cycles of 12:12 h. The room temperature was 22±2°C and the mice had *ad libitum* access to water and food. They were placed in laboratory conditions 30 min before the start of the experiment. The ethical approval required for this study (IR.LUMS.REC.1398.247) was issued by the Ethics Committee of Lorestan University of Medical Sciences, Lorestan, Iran. The mice tested were assigned to the following four groups:

Group i: Received normal saline orally for 14 days;

Group ii: Received CuNPs at a concentration of 1000 µg/kg orally for 14 days;

Group iii: Received CuNPs at a concentration of 2000 µg/kg orally for 14 days;

Group iv: Received CuNPs at a concentration of 5000 µg/kg orally for 14 days.

Sample collection

On day 15 of the experiments, the mice were anesthetized by ketamine-xylazine followed by collection of blood samples from each mouse after the heart was opened. The collected blood samples were put into tubes with or without anticoagulant

to process their clots and then their sera were separated by centrifugation at 5000x g for 10 min.

Evaluation of the serum liver enzymes

To determine the hepatoprotective effects of CuNPs, different clinical chemistry parameters related to liver function such as AST, ALT, ALP, and bilirubin (direct and total) were assayed by commercial diagnostics kits (Roche, Germany).^{10,15}

Hematological parameters

To assess the effects of CuNPs on hematological studies, total collected blood was put into tubes containing ethylenediaminetetraacetic acid. Next, hematological parameters including hemoglobin, hematocrit, white blood cell, red blood cell, and platelet (PLT) counts were measured by Sysmex (KX-21, Japan).

Statistical analysis

SPSS version 17.0 (SPSS Inc., Chicago, IL, USA) was used to analyze the obtained data. One-Way ANOVA and Tukey's post-hoc test were performed to assess the difference between the experimental groups and $p < 0.05$ was considered statistically significant.

RESULTS

Ultraviolet-visible spectrum analysis

The results obtained showed that the highest peak of the synthesized CuNPs was found at a wavelength of 414 nm. The characteristic of the resonance band of the SP happened for CuNPs at 414 nm wavelength (Figure 1).

Fourier transform infrared analysis

The FTIR findings revealed that the biomolecules in the extract decreased the Cu sulfate solution. The bands at 3380, 2928, 1741, 1604, 1400, 1050, and 1271 were indexed to the O-H stretching of alcohol and phenol, C-H stretching of the aliphatic group, C=O stretching of ester carbonyl, C=C stretching of the aromatic ring, and C-O stretching of ester, respectively (Figure 2).

Scanning electron microscope analysis

Following the confirmation of the synthesized nanoparticles through color modification and Vis-UV and FTIR, the

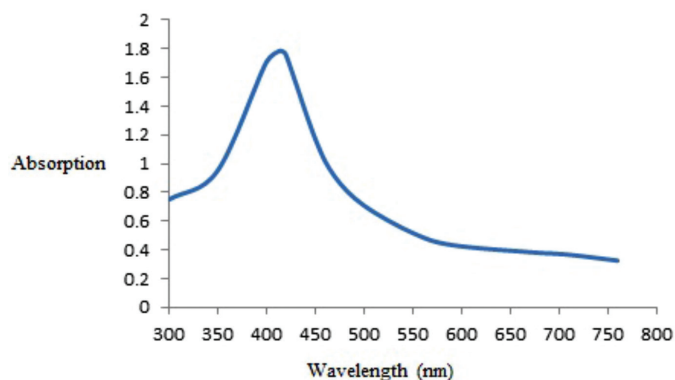


Figure 1. The absorption spectrum of synthesized copper nanoparticles

characterization of nanoparticles was determined with SEM. As shown in Figure 1, the synthesized CuNPs represent spherical morphology, whereas the size of the particles was between 17 and 41 nm (Figure 3).

Hepatoprotective effects of CuNPs

Table 1 shows the results of hepatoprotective effects on serum biochemical parameters in mice receiving CuNPs at doses of 1000, 2000, and 5000 $\mu\text{g}/\text{kg}$ for 14 days. As can be seen, although these parameters increased with increasing doses of extract, there was no statistically significant difference ($p > 0.05$) between oral administrations of CuNPs at doses of 1000, 2000, and 5000 $\mu\text{g}/\text{kg}$ and the control group.

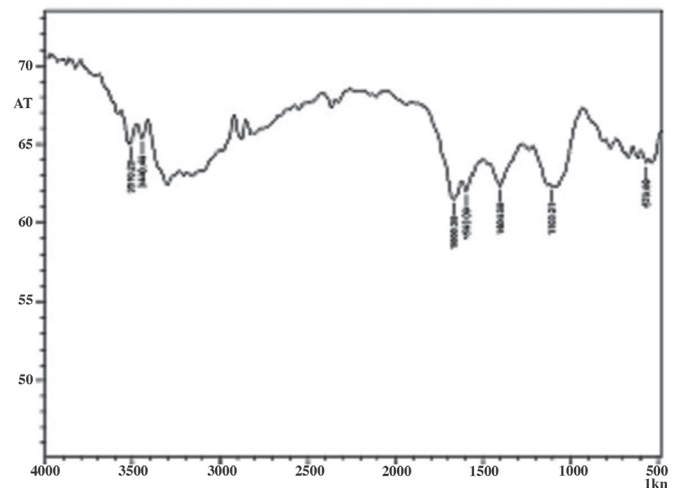


Figure 2. The FTIR spectrum of synthesized copper nanoparticles
FTIR: Fourier transform infrared

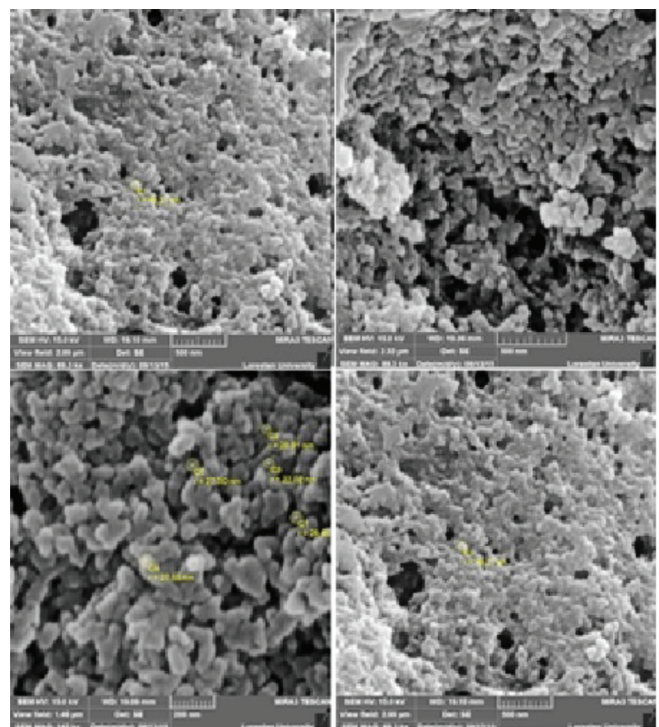


Figure 3. Scanning electron microscope images of copper nanoparticles synthesized using aqueous extract of *Capparis spinosa* fruit x10000

Effect on hematological parameters

As shown in Table 2, following the oral administrations of CuNPs at the employed doses of 1000, 2000, and 5000 µg/kg for 14 days, there was no significant difference ($p < 0.05$) between hematological parameters compared with the control group.

Table 1. Effects of CuNPs on serum liver enzymes after 2 weeks administration in mice. The results are given as mean ± standard deviation

Clinical biochemistry parameters	AST (U/L)	ALT (U/L)	ALP (U/L)	TB
Control	130.6±8.15	38.3±4.31	132.3±8.15	0.12±0.03
CuNPs (1000 µg/kg)	142.4±6.15	40.3±3.15	139.6±6.5	0.15±0.05
CuNPs (2000 µg/kg)	138.8±5.51	39.3±2.51	142.3±5.01	0.14±0.04
CuNPs (5000 µg/kg)	144.3±8.15	42.7±4.36	144.6±6.15	0.17±0.05

CuNPs: Copper nanoparticles, ALT: Alanine aminotransferase, ALP: Alkaline phosphatase, AST: Aspartate aminotransferase, TB: Total bilirubin

Table 2. Hematology parameters in whole blood of mice following oral administration of CuNPs for 2 weeks. The results are given as mean ± standard deviation

Parameters	<i>Curcuma longa</i> essential (µg/kg)			Control
	1000	2000	5000	
RBC ($\times 10^6/\mu\text{L}$)	3.7±0.13	3.2±0.25	2.9±0.41	3.4±0.3
HGB (g/dL)	11.2±0.6	10.5±1.15	10.1±0.6	11.3±0.45
Hct (%)	33.7±3.1	32.12±2.15	30.4±2.51	32.6±2.18
WBC ($\times 10^3/\mu\text{L}$)	3.3±0.45	2.7±0.26	3.1±0.25	2.8±0.2
PLT ($\times 10^3/\mu\text{L}$)	187±15	193±13	175±11	184±17

CuNPs: Copper nanoparticles, RBC: Red blood cell, HGB: Hemoglobin, Hct: Hematocrit, WBC: White blood cell, PLT: Platelet

DISCUSSION

In recent years, studies in the field of nanotechnology have demonstrated that physical and chemical procedures to create nanoparticles, despite having exceptional biological activities, due to having some restrictions like toxicity, are replaced by a number of new methods such as green synthesis.¹ Today, considering that nanoparticles are broadly used by a large proportion of the world's population to treat some diseases, it is necessary to measure the toxicity of these products by different methods. Since recent studies have shown that CuNPs possess a wide range of biological activities,¹⁶ we decided to evaluate their toxicity and hepatoprotective effects in mice.

Recent studies have shown that liver enzyme measurement is one of the key diagnostic tests to evaluate the liver function and also inflammations and damage such as hepatitis and cirrhosis.^{8,10} CuNPs, because of their high surface-to-volume ratio, are extremely reactive and simply interact with other particles.

Therefore, they have numerous biological activities.^{17,18} It has been proven that some medications can cause irreparable complications through reducing white and red blood cells and the number of blood PLTs; thus, it is necessary to evaluate the effects of novel medicinal drugs by measuring hematological parameters.¹⁹

Based on the results of the present study, after oral administration of mice with CuNPs at doses of 1000, 2000, and 5000 µg/kg for 14 days, although some parameters increased with increasing dose of extract, there was no statistically significant difference ($p > 0.05$) between oral administrations of CuNPs at these doses and the control group. Moreover, no statistically significant difference ($p < 0.05$) was observed in hematological parameters between mice treated with CuNPs and the control group.

Considering the study of the hepatoprotective effects of nanoparticles and similar to our findings, Zhang et al.²⁰ demonstrated that silver nanoparticles synthesized using *Rhizophora apiculata* were effective in protecting the liver from harm induced by carbon tetrachloride.

Bhuvaneswari et al.²¹ reported that increased enzymatic levels of AST, ALT, ALP, and bilirubin by CCl_4 returned to normal when treated with silver nanoparticles synthesized using fruit extract of *Embilica officinalis*, indicating potent hepatoprotective effects of these nanoparticles. In the study conducted by Eftekhari et al.²², quercetin nanoparticles showed remarkable hepatoprotective activity via decreasing levels of AST, ALT, and ALP. Ghosh and Gomes²³ also recently showed that gold nanoparticles synthesized by *Trigonella foenum-graecum* extract significantly normalized the increased enzymatic levels of AST, ALT, ALP, and bilirubin induced by CCl_4 , which indicated the hepatoprotective potential of these nanoparticles.

In the present study, we applied *C. spinosa* to facilitate the synthesis of CuNPs. Next, we synthesized CuNPs that were spherical and ranging from 17 and 41 nm in size. To date, a wide range of plants such as *Syzygium aromaticum*, *Nerium oleander*, *Citrus medica* Linn., *Capparis zeylanica*, *Gloriosa superba* L., and *Vitis vinifera* have been applied in the biosynthesis of CuNPs. However, identifying the plant's capacity as biological material for the synthesis of nanoparticles in full detail requires more investigations.^{5,6,17,24-27}

CONCLUSION

The findings revealed that CuNPs biosynthesized from aqueous extract of *C. spinosa* fruit have no toxic effect on the liver of the studied mice, and no significant toxicity was observed in their hematological parameters. However, more studies need to be done for evaluation of the hepatoprotective effect of CuNPs.

ACKNOWLEDGMENTS

The authors are thankful to the staff of Razi Herbal Medicines Research Center, Khorramabad, Iran as well as the staff of Bam University of Medical Sciences, Bam, Iran.

Conflicts of interest: No conflict of interest was declared by the authors. The authors alone are responsible for the content and writing of the paper.

REFERENCES

- Boisseau P, Loubaton B. Nanomedicine, nanotechnology in medicine et nanotechnologies pour la medecine. *Comptes Rendus Physique*. 2011;12:620-636.
- Mano PM, Karunai SB, John Paul JA. Green synthesis of silver nanoparticles from the leaf extracts of *Euphorbia hirta* and *Nerium indicum*. *Digest J Nanomat Biostruct*. 2011;6:869-877.
- Khatami M, Pourseyedi S. *Phoenix dactylifera* (date palm) pit aqueous extract mediated novel route for synthesis high stable silver nanoparticles with high antifungal and antibacterial activity. *IET Nanobiotechnol*. 2015;9:184-190
- Khatami M, Mortazavi SM, Kishani-Farahani Z, Amini A, Amini E, Heli H. Biosynthesis of silver nanoparticles using pine pollen and evaluation of the antifungal efficiency. *Iran J Biotechnol*. 2017;15:95-101.
- Saranyaadevi K, Subha V, Ravindran RS, Renganathan S. Synthesis and caharacterization of copper nanoparticle using *Capparis Zeylanica* leaf extract. *Int J Chem Tech Res*. 2014;6:4533-4541.
- Naika HR, Lingaraju K, Manjunath K, Kumar D, Nagaraju G, Suresh D, Nagabhushana H. Green synthesis of CuO nanoparticles using *Gloriosa superba* L. extract and their antibacterial activity. *J Taibah Uni Sci*. 2015;9:7-12.
- Angrasan J, Subbaiya R. Biosynthesis of copper nanoparticles by *Vitis vinifera* leaf aqueous extract and its antibacterial activity. *Int J Curr Microbiol Appl Sci*. 2014;3:768-774.
- Mahmoudvand H, Fallahi S, Mahmoudvand H, Shakibaie M, Harandi MF, Dezaki ES. Efficacy of *Myrtus communis* L. to Inactivate the Hydatid Cyst Protoscoleces. *J Invest Surg*. 2016;29:137-143.
- Fallahi S, Beyranvand M, Mahmoudvand H, Nayebzadeh H, Kheirandish F, Jahanbakhsh S. Chemical composition, acute and subacute toxicity of *Satureja khuzestanica* essential oil in mice. *J Res Pharm*. 2017;21:515-521.
- Mahmoudvand H, Oliaei RT, Mirbadie SR, Kheirandish F, Kareshk AT, Ezatpour B, Mahmoudvand H. Efficacy and Safety of *Bunium Persicum* (Boiss) to Inactivate Protoscoleces during Hydatid Cyst Operations. *Surg Infect (Larchmt)*. 2016;17:713-719.
- Mahmoudvand H, Mahmoudvand H, Oliaae RT, Kreshk AT, Mirbadie SR, Aflatoonian MR. *In vitro* Protoscolicidal Effects of *Cinnamomum zeylanicum* Essential Oil and Its Toxicity in Mice. *Pharmacogn Mag*. 2017;13(Suppl 3):S652-S657.
- Shiravand M, Ebrahimi K, Mahmoudvand H. Biosynthesis of copper nanoparticles using aqueous extract of *Capparis spinosa* fruit and investigation of its antibacterial activity. *Marmara Pharm J*. 2017;21:866-871.
- Khatami M, Mortazavi SM, Kishani-Farahani Z, Amini A, Amini E, Heli H. Biosynthesis of Silver Nanoparticles Using Pine Pollen and Evaluation of the Antifungal Efficiency. *Iran J Biotechnol*. 2017;15:95-101.
- Soltani Nejad M, Khatami M, Shahidi Bonjar GH. Extracellular synthesis gold nanotriangles using biomass of *Streptomyces microflavus*. *IET Nanobiotechnol*. 2016;10:33-38.
- Mahmoudvand H, Kheirandish F, Dezaki ES, Shamsaddini S, Harandi MF. Chemical composition, efficacy and safety of *Pistacia vera* (var. Fandoghi) to inactivate protoscoleces during hydatid cyst surgery. *Biomed Pharmacother*. 2016;82:393-398.
- Murthy SK. Nanoparticles in modern medicine: State of the art and future challenges. *Int J Nanomedicine*. 2007;2:129-41.
- Gopinath M, Subbaiya R, Selvam MM, Suresh D. Synthesis of copper nanoparticles from *Nerium oleander* leaf aqueous extract and its antibacterial activity. *Int J Curr Microbiol Appl Sci*. 2014;3:814-818.
- Katha U, and Gajera H. Synthesis of copper nanoparticles by two different methods and size comparison. *Int J Pharm Bio Sci*. 2014;5:533-540.
- Muriithi NJ, Maina GS, Mugendi NM, Maina MB, Kiambi MJ, kelvin JK, Umar A, John MK, Ann NW, YA A, Piero NM, Eliud NNM. Determination of Hematological Effects of Methanolic Leaf Extract of *S. incanum* in Normal Mice. *Pharm Anal Acta*. 2015;6:10. doi:10.4172/21532435.1000429
- Zhang H, Jacob JA, Jiang Z, Xu S, Sun K, Zhong Z, Varadharaju N, Shanmugam A. Hepatoprotective effect of silver nanoparticles synthesized using aqueous leaf extract of *Rhizophora apiculata*. *Int J Nanomedicine*. 2019;14:3517-3524.
- Bhuvaneswari R, Chidambaranathan N, Jegatheesan K. Hepatoprotective effect of *Embilica officinalis* and its silver nanoparticles against ccl4 induced hepatotoxicity in Wistar albino rats. *Digest Journal of Nanomaterials and Biostructures*. 2014;9:223-235.
- Eftekhari A, Ahmadian E, Panahi-Azar V, Hosseini H, Tabibiazar M, Dizaj SM. Hepatoprotective and free radical scavenging actions of quercetin nanoparticles on aflatoxin B1-induced liver damage: *in vitro/in vivo* studies. *Artif Cells, Nanomed Biotechnol*. 2018;46:411-420.
- Ghosh S, Gomes A. Hepatoprotective efficacy of gold nanoparticle synthesized by green method using *Trigonella foenum-graecum* seed extract. *Transl Med (Sunnyvale)*. 2016; 6:4.
- Subhankari I, Nayak PL. Synthesis of copper nanoparticles using *Syzygium aromaticum* (Cloves) aqueous extract by using green chemistry. *World J Nano Sci Technol*. 2013;2:14-17.
- Shende S, Ingle AP, Gade A, Rai M. Green synthesis of copper nanoparticles by *Citrus medica* Linn. (Idilimbu) juice and its antimicrobial activity. *World J Microbiol Biotechnol*. 2015;31:865-873.
- Janakiraman M. Protective efficacy of silver nanoparticles synthesized from *Silymarin* on *cisplatin* induced renal oxidative stress in albino rat. *Inter J Appl Pharm*. 2018;10:110-116.
- Nafari A, Cheraghipour K, Sepahvand M, Shahrokhi G, Gabal E, Mahmoudvand H. Nanoparticles: New agents toward treatment of leishmaniasis. *Parasite Epidemiol Control*. 2020;10:e00156.



Molecular Docking Simulation Studies of Curcumin and Its Derivatives as Cyclin-Dependent Kinase 2 Inhibitors

Siklin Bağımlı Kinaz 2 İnhibitörü Olarak Kurkumin ve Türevlerinin Moleküler Kenetlenme Simülasyonları

© Riyadi SUMIRTANURDIN*, © Shafira SUNGKAR, © Yasarah HISPRASTIN, © Kenny Dwi SIDHARTA, © Dea Dian NURHIKMAH

Universitas Padjadjaran, Faculty of Pharmacy, Department of Medicinal Chemistry, Bandung, Indonesia

ABSTRACT

Objectives: Cyclin-dependent kinase 2 (CDK2) is a protein that plays a role in regulating the cell cycle and its overexpression contributes to uncontrolled cell proliferation. Inhibition of CDK2 is known to be a mechanism of action of various anti-cancer drugs. Curcumin is an active compound of *Curcuma longa* and it has been reported to inhibit the activity of cyclin D, cyclin E, CDK2, CDK4, and CDK6. This study aimed to design more active curcumin derivatives as anticancer drugs by targeting CDK2 through a molecular modeling approach.

Materials and Methods: The molecular modeling approach consists of receptor and ligand preparation, method validation, pharmacophore modeling, and docking simulation.

Results: The results of the molecular docking simulation show that the free bonding energy (ΔG) of curcumin and kurkumod 23 and 24 (the best modification of curcumin) are -7.80, -9.15, and -9.36 kcal/mol, respectively. The hydrogen interaction between kurkumod 23 and 24 with CDK occurred on Lys33 residue, which is considered a potential interaction site for CDK2 inhibitor compounds. Pharmacophore modeling showed that kurkumod 23 and 24 have pharmacophore-fit values of 45.20% and 47.26%, respectively.

Conclusion: The results of this study indicate that kurkumod 23 and 24 are the best and most potent modifications of curcumin as CDK2 antagonist, based on the interactions that occur between these two derivatives with amino acid residues from the CDK2 receptor.

Key words: CDK2, curcumin, molecular docking, pharmacophore modeling

ÖZ

Amaç: Siklin bağımlı kinaz 2 (CDK2) hücre siklusunun regülasyonunda rol alan bir proteindir ve yüksek derecede ekspresyonu kontrol edilemeyen hücre proliferasyonuna yardımcı olur. CDK2'nin inhibisyonu birçok anti-kanser ilacının etki mekanizmasıdır. Kurkumin *Curcuma longa*'nın aktif bileşenidir ve siklin D, siklin E, CDK4 ve CDK6'yı inhibe ettiği rapor edilmiştir. Bu çalışmanın amacı bir moleküler modelleme yaklaşımı ile CDK2'yi hedefleyerek daha aktif kurkumin türevlerinin tasarlanmasıdır.

Gereç ve Yöntemler: Moleküler modelleme yaklaşımı bir reseptör ve ligand hazırlanması, yöntem validasyonu, farmakofor modellemesi ve kenetleme simülasyonu içermektedir.

Bulgular: Moleküler kenetleme simülasyonunun sonucu kurkumin, kurkumod 23 ve 24'ün serbest bağlanma enerjilerinin (ΔG) sırasıyla -7,80, -9,15 ve -9,36 kcal/mol olduğunu göstermiştir. Kurkumod 23 ve 24'ün CDK ile hidrojen etkileşimi Lys33 kalıntısı üzerinde olmaktadır ki bu CDK2'yi inhibe eden bileşiklerin potansiyel etkileşim bölgesi kabul edilmektedir. Farmakofor modelleme, kurkumod 23 ve 24'ün farmakofor-uyma değerlerini sırasıyla %45,20 ve %47,26 olarak göstermiştir.

Sonuç: Bu çalışmanın sonuçları CDK2 reseptöründeki amino asit kalıntılarıyla bu iki türevin etkileşimine dayanarak kurkumod 23 ve 24'ün kurkuminin CDK2 antagonisti olan en iyi ve en potent modifikasyonları olduğunu işaret etmektedir.

Anahtar kelimeler: CDK2, kurkumin, moleküler kenetlenme, farmakofor modelleme

*Correspondence: E-mail: riyadidarn@gmail.com, Phone: +088222666852 ORCID-ID: orcid.org/0000-0002-5826-2703

Received: 20.01.2019, Accepted: 28.03.2019

©Turk J Pharm Sci, Published by Galenos Publishing House.

INTRODUCTION

Cancer is a condition of uncontrolled cell growth that can affect the growth of cells and/or other tissues around them through the circulatory system and lymphatic system. Generally, various types of cancer occur due to the overexpression of proteins that play a role in the cell cycle, i.e. cyclin dependent kinase 2 (CDK2). The cell cycle is controlled by several proteins that act as positive and negative regulators. In mammals' cyclin protein groups, especially cyclin D, E, A, and B, expression fluctuates during the cell cycle process. Cyclin proteins together with the protein kinase (CDK) group, specifically CDK 4, 6, and 2, act as positive regulators that spur the occurrence of cell cycles. If a positive regulator experiences overexpression it can trigger acceleration of the cell cycle, thus triggering cell proliferation making the cell cycle difficult to control.¹ Furthermore, cancer is known to be one of the biggest causes of death in most developing countries (<https://www.cancer.gov/about-cancer/understanding/what-is-cancer>). Therefore, research on new therapeutic agents for cancer treatment has always been a critical issue. The aim is to immediately address excessive cell proliferation and immediately prevent the metastatic process. At present, the molecular modeling approach, driven by the rapid development of computational chemistry, plays an important role in drug design and the discovery of new mechanisms from structure-based medicine. This method has been successfully used in many studies to discover new drugs.²

Some natural compounds are known to have the potential to become lead compounds in terms of inhibiting the growth of cancer cells, one of which is curcumin. Curcumin is a hydrophobic polyphenol obtained from turmeric rhizome (*Curcuma longa* L.) and is considered an active anticancer substance.³⁻⁵ Both preclinical and clinical studies have been carried out to learn the anticancer effects of curcumin compounds, including its role in proliferation arrest of MCF7 breast cancer cells, which is associated with their ability to inhibit cyclin D, cyclin E, CDK2, CDK4, and CDK6 activities and its ability to induce apoptosis through the caspase-9 mechanism.⁶ Therefore, the study of curcumin activity and the search for their active derivatives as new anticancer agents targeting CDK2 protein through the molecular modeling approach is thought to be one of the best ways to provide new cancer treatments alternative to the one that is currently available.

MATERIALS AND METHODS

Materials

The hardware used in the present study was a personal computer with the following specifications: Intel® Core™ i5-6600 CPU@3.90 GHz (4CPUs), Nvidia Geforce GTX 970 GPU 4 Gigabyte OC Edition, and 8 Gigabyte DDR4 RAM. The *in silico* testing used the following software:

1. ChemOffice 2010 and ChemDraw Ultra 12.0 to create 2D structures and convert them to 3D structures.
2. LigandScout 4.0 (Wolber and Inte: Ligand GmbH) to conduct pharmacophore modeling.

3. AutoDock 4.2.6 and AutoDockTools 1.5.6 (The Scripps Research Institute, downloaded from <http://www.autodock.scripps.edu/>) to conduct molecular docking simulation.

4. BIOVIA Discovery Studio 2017 for visualizing Protein Data Bank (PDB) complexes, bonds between ligands and cyclic dependent kinase 2, geometry optimization, and overlaying on the validation process.

The three-dimensional structure of the CDK2 protein was downloaded from the PDB (GDP) (<http://www.rcsb.org/>) (ID: 1KE6) as well as the three-dimensional structure of curcumin and its derivatives' structure, which was illustrated using ChemOffice 2010 software.

Receptor and ligand preparation

The CDK2 structure used was downloaded from the PDB website. It was then separated from the ligands and water molecules and added with charges. The standard ligand was obtained from the results of the separation process, while the curcumin and its derivatives were designed by software and then optimized. The curcumin's derivatives' design is based on Lipinski's rule of five (RO5).

Method validation

Validation of the computational methods including validation of the molecular docking process was based on the root mean square deviation (RMSD) values of the standard ligand redocking process, while validation of the pharmacophore modeling process was based on the area under curve 100% (AUC100%) value of the receiver operating characteristic (ROC) curve, which screened 778 active compounds and 2015 inactive compounds obtained from Directory of Useful Decoys, Enhanced (DUDe) from <https://dude.docking.org>.

Pharmacophore modeling

This process was carried out to see the level of similarity between curcumin and its modification with standard ligands where virtual screening was done using a validated structure-based 3D pharmacophore model and utilizing software assistance. The level of similarity of each structure was shown through the value of pharmacophore fit.

Docking simulation

Docking was simulated at the center of the active side of the receptor with the grid coordinates $x=27.440$, $y=10.959$, $z=11.192$ and the dimensions were $40 \times 40 \times 40$ points. The docking parameters were based on the Lamarckian genetic algorithm with 10 runs, 150 population size, 250,000 evaluation energy, gene mutation rate of 0.02, and crossover rate of 0.8. The conformation of the results of molecular docking simulation was clustered using RMSD 1.0 \AA tolerance. Ligand conformation with the lowest free bond energy (ΔG) of the best cluster was used for the next analysis phase. The ligand-receptor complex formed was visualized with the help of software.

RESULTS AND DISCUSSION

CDK2 receptor preparations

CDK2, downloaded from the PDB website with the code ID GDP 1KE6, was used. The CDK2 receptor was complexed with the antagonist ligand N-methyl-4-[2-(7-oxo-6,7-dihydro-8h-[1,3] thiazolo [5,4-e]indol-8-ylidene)hydrazino]phenyl} methanesulfonamide, which was obtained from X-ray diffraction with a resolution of 2.0 Å. Resolution describes the detailed structure of a complex and it illustrates the interaction between the ligand and active site.⁷ A smaller value of resolution will give more accurate results of constituent atom mapping. The ligand receptor complex was separated with the assistance of BIOVIA Discovery Studio software. The water molecules around the structure of receptors resulting from separation were then removed again with the aim of simplifying the docking process later. At the receptor, Kollman charges were added to suit the docking environment and hydrogen was added to polar atoms.

Ligand preparation

The ligand that was determined as the standard was obtained through a separation process with CDK2 receptors with the help of software. Furthermore, the test ligands, namely curcumin and its derivatives (kurkumod), were designed and optimized with the software described above. Table 1 shows the structure and properties of each proposed curcumin derivative. The curcumin derivative design is based on keeping the original pharmacophore that was found in the curcumin compound. Optimization of the ligand includes energy minimization and the addition of the Gasteiger charge and then the hydrogen atom in the polar site of the molecule. The design of the curcumin modification is also based on Lipinski's RO5, which predicts the ability of a compound to penetrate the membrane if given orally. This rule includes a molecular weight of ≤ 500 Da, hydrogen bond donors ≤ 5 , hydrogen bond acceptors ≤ 10 , LogP value ≤ 5 , and molar reactivity in the range between 40 and 130.⁸

Method validation results

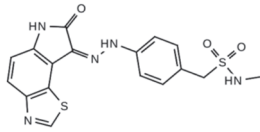
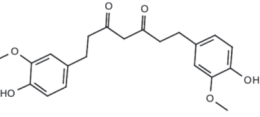
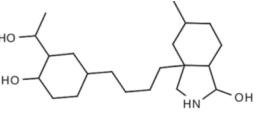
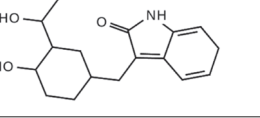
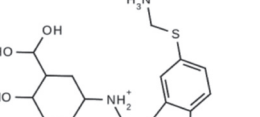
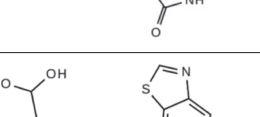
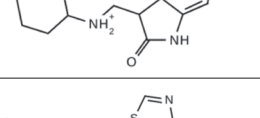
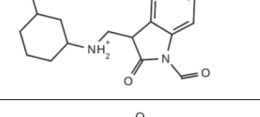
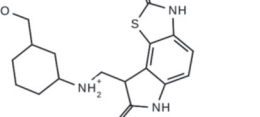
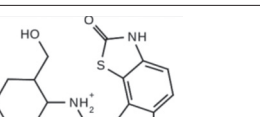
Validation of computational methods is performed to prove and ensure that the method used meets the validity requirements and can be used for testing other molecules and thus minimizing errors.

Validation of the docking simulation method

The docking simulation process was validated by using AutoDock 4.1 and AutoDockTools software through the redocking procedure of ligands that have been previously separated from the receptor. Redocking results are said to be valid if in 10 numbers of a run a minimum of 75% RMSD value ≤ 2 Å. RMSD is the ratio between the distance change and the best ligand conformation from the simulation results with distance and initial ligand conformation.

The results of ligand redocking to CDK 2 receptors produced free energy (ΔG) of -10.53 kcal/mol with an RMSD value of 0.85 Å and all of 10 runs resulted in an RMSD value ≤ 2 Å, as depicted in Figure 1. The redocking results also show that ligands form hydrogen bonds with Leu83, Asp86, and Asp145, in accordance

Table 1. Standard ligand, curcumin, kurkumod structure, and its physicochemical properties

No	Molecule name	Structure	Physicochemical properties
1.	Standard ligand (1ke6)		MW=401.467 LogP=2.349 NHD=3 NHA=5
2.	Curcumin		MW=368.385 LogP=3.62 NHD=2 NHA=6
2.	Kurkumod 11		MW=353.547 LogP=2.763 NHD=4 NHA=3
3.	Kurkumod 17		MW=289.375 LogP=1.994 NHD=3 NHA=0
4.	Kurkumod 18		MW=369.484 LogP=-2.214 NHD=2 NHA=1
5.	Kurkumod 19		MW=348.445 LogP=0.418 NHD=1 NHA=1
6.	Kurkumod 20		MW=360.456 LogP=0.898 NHD=0 NHA=2
7.	Kurkumod 21		MW=348.445 LogP=0.680 NHD=2 NHA=1
8.	Kurkumod 23		MW=348.445 LogP=0.680 NHD=1 NHA=2
9.	Kurkumod 24		MW=348.445 LogP=0.740 NHD=1 NHA=2

MW: Molecular weight, NHD: Number of hydrogen bond donor, NHA: Number of hydrogen bond acceptors

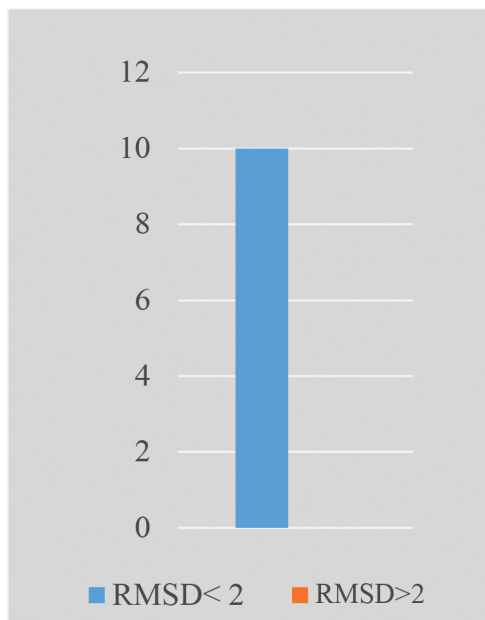


Figure 1. Redocking result of 10 runs of standard ligand to CDK2 receptor
CDK2: Cyclin-dependent kinase 2, RMSD: Root mean square deviation

with the ligand initial bond conditions with the receptors. Figure 2 exhibits superimposition between native and redocked ligand and CDK2 receptor. The validation parameters were fulfilled and so the computational method used is said to be valid and can be used for further testing.

Pharmacophore modeling validation result

This validation aims to see the accuracy of the program in detecting active sets and decoy sets. Validation was carried out through screening 778 active compounds and 2015 inactive compounds obtained from DUDe (<https://dude.docking.org>). The active set is a set of compounds or ligands that are known to be active at certain receptors with known IC₅₀ values from the results of previous studies. Decoy sets are sets of ligands that have a structure similar to that of active sets but are not active against receptors. The screening results show an enrichment factor 100% (EF100%) and AUC100% of 1.825 and 0.67, respectively, on the ROC curve. The greater the AUC value, the better the classification will be. The best results from virtual screening are indicated by the maximum AUC value, i.e. the value equals 1.⁹ The ROC curve is the most common quality validation parameter used for pharmacophore modeling, where this curve consists of the X axis as the rate of inactive compounds on the pharmacophore model and the Y axis as the rate of the active compound on the pharmacophore model.

Pharmacophore modeling result

The results of the pharmacophore modeling will show the level of similarity between the modification of curcumin (kurkumod) and the standard CDK2 ligand (protein 1KE6 ligand). Values of pharmacophore similarity between these two compounds will be shown as pharmacophore-fit values. The test results show that the best modified compounds, namely kurkumod 23 and 24, each have a similarity level of 45.2% and 47.26% to CDK2 standard ligands, as described in Table 2.

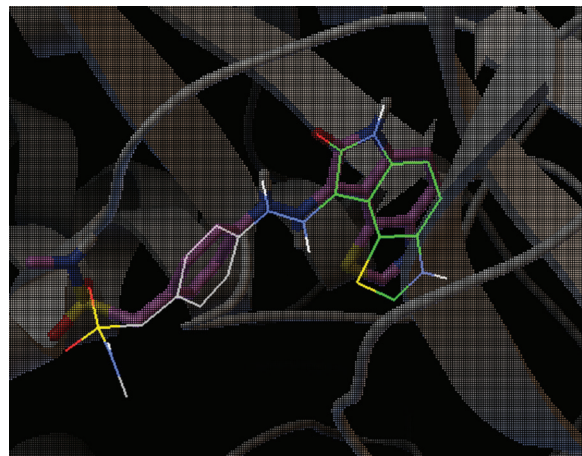


Figure 2. Superimposition illustration of native ligand and redocked ligand to CDK2 receptor (Native ligand shown green with thin line and redocked ligand shown purple with thick line)

CDK2: Cyclin-dependent kinase 2

Docking simulation results

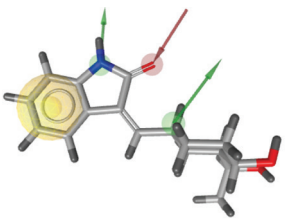
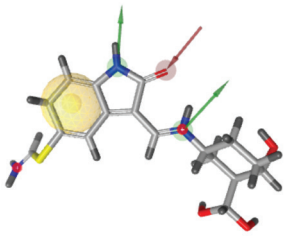
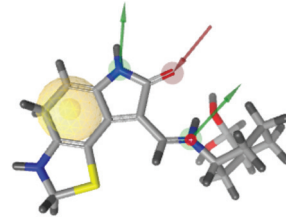
The molecular docking method aims to see the interaction between ligands, i.e. curcumin and its derivatives with the target receptor, CDK2. The results of this process were the Gibbs free energy ΔG , inhibition constant, number of clusters, and types of bonds to amino acid residues. The results of the curcumin docking and its derivative along with the standard CDK2 ligand against the CDK2 receptor itself can be seen in Table 3. Based on the results, modification of kurkumod 23 and 24 shows that the value of ΔG tends to be lower than the modification of kurkumod 11, 17, and 20 although it has not been able to compensate for the free energy values of standard CDK2 ligands (ΔG -10.53) and modification 18, 21, and 19. Lower bond energy indicates that the interaction that occurs has a higher affinity because it tends to be easier (less energy) to interact. The cluster number of derivatives kurkumod 23 and 24 is also at the level where the first ranking cluster has more members than other clusters. More cluster numbers indicate that the poses of the conformation produced are more stable.

The consideration that kurkumod 23 and 24 are the best modifications of curcumin is based on the interactions that occur between these two derivatives with amino acid residues from the CDK2 receptor, as illustrated in Figure 3. Activation of CDK2 through complexation with cyclin A will induce conformational changes on the ATP binding site. The most significant effect is the rotation of helix C, which causes changes in the geometry of the active site in the area of three active site catalyst residues, namely Lys33, Glu51, and Asp145. The Lys33 amino acid residue is considered a potential interaction site for inhibitor compounds. The carboxylic acid molecule, which has been reported as an active CDK2 inhibitor, is known to form hydrogen bonds with Lys-33 on CDK2 receptor residues. Therefore, kurkumod 23 and 24, which both form hydrogen interactions with Lys33, are considered potential CDK2 inhibitors.¹⁰

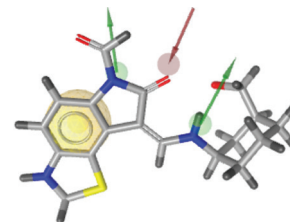
On the other hand, kurkumod 23 also shows hydrogen bonds with amino acid residues Glu81 and Leu83 on CDK2. The NH

hydrogen amide bond with Glu81 and the hydrogen bond from the oxygen carbonyl group with Leu83 are analogous interactions that occur between ATP and CDK2. Hydrophobic interactions also occur between benzene rings from kurkumod 23 and 24 with the hydrophobic environment of CDK2 receptors (Val18 and Leu134).¹⁰

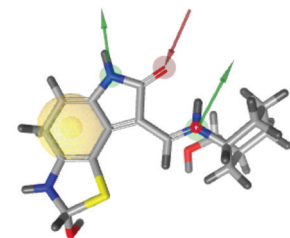
Table 2. Pharmacophore-fit score of curcumin derivatives against CDK2

Name of derivatives	Pharmacophore-fit value	Pharmacophore model
Kurkumod 17	37.90%	
Kurkumod 18	35.27%	
Kurkumod 19	36.29%	

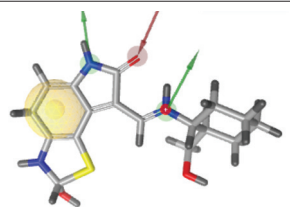
Kurkumod 20 35.01%



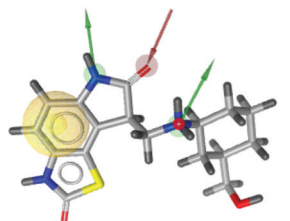
Kurkumod 21 45.06%



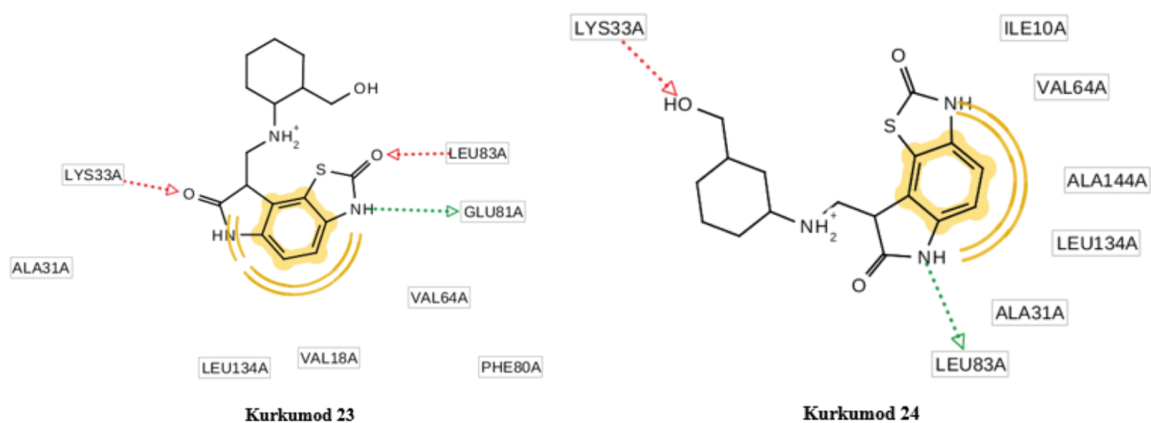
Kurkumod 23 45.20%



Kurkumod 24 47.26%



CDK2: Cyclin-dependent kinase 2



Interactions




-  (Red arrow): Hydrogen bond (acceptor)
-  (Green arrow): Hydrogen bond (donor)
-  (Yellow sphere): Van der Waals interaction

Figure 3. Interaction of kurkumod 23 and 24 with CDK2 active site
CDK2: Cyclin-dependent kinase 2

Table 3. Ligand interaction with CDK2 active site

No	Molecule name	Chemical formula	ΔG (kcal/mol)	Number in cluster	Interaction with amino acids	
					Hydrogen bond	Van der Waals
1.	Standard ligand	$C_{17}H_{15}N_5O_3S_2$	-10.53	10	Glu81A, Leu83A, Asp86A	Ile10A, Val18A, Leu134A, Ala144A, Ala31A, Phe80A, Val64A
2.	Curcumin	$C_{21}H_{20}O_6$	-7.80	1	Glu12A, Leu83A	Val18A, Ile10A
3.	Kurkumod 11	$C_{21}H_{39}N_1O_3$	-8.78	18	Glu81A, Leu83A, Asp145A, Asn132A, Lys129A	Ala31A, Leu134A, Phe82A, Ile10A
4.	Kurkumod 17	$C_{17}H_{23}N_1O_3$	-7.62	5	Gln131A, Asn132A, Asp145A	Leu134A, Phe82A, Val64A, Val18A, Ala31A, Ile10A
5.	Kurkumod 18	$C_{17}H_{27}N_3O_4S_1$	-9.23	9	His84A, Leu83A	Ala31A, Leu134A, Ile10A, Ala144A
6.	Kurkumod 19	$C_{17}H_{22}N_3O_3S_1$	-9.75	1	Leu83A, Glu81A	Val64A, Phe80A, Ala144A
7.	Kurkumod 20	$C_{18}H_{22}N_3O_3S_1$	-8.68	2	Asp86A, Leu83	Val18A, Ile10A, Leu134A, Ala144A, Ala31A Val18A
8.	Kurkumod 21	$C_{17}H_{22}N_3O_3S_1$	-10.04	10	Asp145A, Leu83A, Asp86A	Ile10A, Leu134A
9.	Kurkumod 23	$C_{17}H_{22}N_3O_3S_1$	-9.15	6	Lys33A, Leu83A, Glu81A	Ala31A, Ala144A, Leu134A, Val18A, Phe80A, Val64A
10.	Kurkumod 24	$C_{17}H_{22}N_3O_3S_1$	-9.36	7	Lys33A, Leu83A	Ala31A, Leu134A, Ala144A, Val64A, Ile10A

CDK2: Cyclin-dependent kinase 2

Study Limitation

This was a preliminary study related to the design of derivatives of natural compounds that have potential as anticancer agents. The synthesis of the proposed compound and then *in silico* *in vitro* correlation analysis are expected in the future.

CONCLUSION

Kurkumod 23 and 24 are the best and most potent modifications of curcumin as CDK2 antagonist, based on the interactions that occur between these two derivatives with amino acid residues from the CDK2 receptor.

ACKNOWLEDGEMENTS

The authors would like to thank our team: Hisban Hamid Arifki, Yunistya Dwi Cahyani, Alfia Nursetiani, Traju Ningtyas Dwi Utari, and Jessica Tristi for the great team collaboration.

Conflicts of interest: No conflict of interest was declared by the authors. The authors alone are responsible for the content and writing of the paper.

REFERENCES

- Hamzah N, Najib A, Fatmawati S. Studi Farmakofor Reseptor Estrogen α sebagai Target Terapi Kanker Serviks. *Jurnal Farmasi FIK UIN Alauddin*. 2014;2:133-137.
- de Ruyck J, Brysbaert G, Blossey R, Lensink MF. Molecular docking as a popular tool in drug design, an *in silico* travel. *Adv Appl Bioinform Chem*. 2016;9:1-11.
- Grynkiewicz G, Ślifirski P. Curcumin and curcuminoids in quest for medicinal status. *Acta Biochim Pol*. 2012;59:201-212.
- Borik RM, Fawzy NM, Abu-Bakr SM, Aly MS. Design, Synthesis, Anticancer Evaluation and Docking Studies of Novel Heterocyclic Derivatives Obtained via Reactions Involving Curcumin. *Molecules*. 2018;23:1398.
- Mutiah R. Evidence Based Kurkumin dari Tanaman Kunyit (*Curcuma longa*) sebagai Terapi Kanker pada Pengobatan Modern. *Jurnal Farma Sains*. 2015;1:28-41.
- Li HQ, Jin JL, Wu FF, Li XY, You JS, Cao ZH, Li D, Xu YP. Effect of Curcumin on Proliferation, Cell cycle and caspase and MCF-7 cells. *Afr J Med Med Sci*. 2012;6:864-870.
- Lipinski CA. Lead- and drug-like compounds: the rule-of-five revolution. *Drug Discov Today Technol*. 2004;1:337-341.

8. Kang FN, Simoben CV, KAraman B, Ngwa VF, Judson PN, Sippl W, Mbaze LM. Pharmacophore modeling and in silico toxicity assessment of potential anticancer agents from african medicinal plants. *Drug Des Devel Ther.* 2016;10:2137-2154.
9. Vakser IA. Protein-protein docking: from interaction to interactome. *Biophys J.* 2014;107:1785-1793.
10. Bramson HN, Corona J, Davis ST, Dickerson SH, Edelstein M, Frye SV, Gampe Jr RT, Harris P A, Hassell A, Holmes WD, Hunter RN, Lackey KE, Lovejoy B, Luzzio MJ, Montana V, Rocque, D Rusnak WJ, Shewchuk L, Veal JM, Walker DH, Kuyper LF. Oxindole-based inhibitors of cyclin-dependent kinase 2 (CDK2): design, synthesis, enzymatic activities, and X-ray crystallographic analysis. *J Med Chem.* 2001;44:4339-4358.



Ferulic Acid Prevents Angiogenesis Through Cyclooxygenase-2 and Vascular Endothelial Growth Factor in the Chick Embryo Chorioallantoic Membrane Model

Ferulik Asitin Tavuk Embriyo Koriyoallantoik Membran Modelinde Siklooksijenaz 2 ve Vasküler Endotel Büyüme Faktörü Üzerinden Anjiyojenezi Önlemesi

© Juni EKOWATI^{1*}, © Iwan Sahrial HAMID², © Nuzul Wahyuning DIYAH¹, © Siswandono SISWANDONO¹

¹Airlangga University Faculty of Pharmacy, Department of Pharmaceutical Chemistry, Surabaya, Indonesia

²Airlangga University Faculty of Veterinary Medicine, Department of Basic Veterinary Medicine, Surabaya, Indonesia

ABSTRACT

Objectives: This study was designed to verify the antiangiogenic activity of ferulic acid (FA) and its potency to inhibit cyclooxygenase-2 (COX-2) and vascular endothelial growth factor (VEGF) expression in the chorioallantoic membrane (CAM) model. Moreover, we verified its mechanism of action by docking the molecule on COX-2, tyrosine kinase, and VEGF-2 proteins *in silico*.

Materials and Methods: An antiangiogenesis assay of FA at doses of 30, 60, and 90 µg was performed using the CAM of chicken eggs that were 9 days old and stimulated by 60 ng of basic fibroblast growth factor. Celecoxib (60 µg) was used as the reference drug. The inhibitory activity on VEGF and COX-2 expression was determined by immunohistochemistry assay. Molecular docking of FA was accomplished by Molegro Virtual Docker program ver. 5.5 on COX-2 enzyme (PDB ID 1CX2), tyrosine kinase receptor (PDB ID 1XKK), and VEGF-2 receptor (PDB ID 4ASD).

Results: FA at doses of 30, 60, and 90 µg significantly prevented angiogenesis in the CAM model, which was represented as inhibitory activity against endothelial cells of blood vessels (42.6-70.7%) and neovascularization (43.0-86.6%). The inhibitory activity of FA against VEGF expression was stronger than its action on COX-2 expression. Molecular docking on VEGF-2 receptor resulted in an RS value of FA of -73.844 kcal/mol and for celecoxib it was -94.557 kcal/mol. The RS value on tyrosine kinase of FA was -84.954 kcal/mol, while on celecoxib it was -93.163 kcal/mol. Docking on COX-2 receptor gave an RS value of FA of -73.416 kcal/mol, while for celecoxib it was -118.107 kcal/mol.

Conclusion: Reductions in VEGF-2 and COX-2 expression due to treatment with FA at the dose range 30-90 µg appeared to be related to angiogenesis inhibition, which was shown by two parameters, namely inhibition of neovascularization and endothelial cell growth in blood vessels. It was concluded that FA is a promising antiangiogenic therapeutic agent especially at the early stage, and this activity can arise from inhibitory action on COX-2 and VEGF-2 proteins.

Key words: Ferulic acid, COX-2, VEGF, tyrosine kinase, angiogenesis, chorioallantoic membrane

ÖZ

Amaç: Bu çalışma ferulik asidin (FA)'nın koriyoallantoik membran (CAM) modelinde antianjiyojenik aktivitesini ve siklooksijenaz-2 (COX-2) ve vasküler endotel büyüme faktörünü (VEGF) inhibe etme potensinin doğrulamak üzere tasarlanmıştır.

Gereç ve Yöntemler: FA'nın antianjiyojenik testi dokuz günlük olan ve 3 ng bazik fibroblast faktörü ile stimüle edilen tavuk yumurtalarının CAM'ina 30, 60 ve 90 µg uygulanarak gerçekleştirilmiştir. Referans ilaç olarak selekoksib (60 µg) kullanılmıştır. VEGF ve COX-2 üzerindeki inhibitor aktivitesi immünohistokimya yöntemi ile gerçekleştirilmiştir. FA'nın moleküler kenetlenmesi Molegro Virtual Docker program ver. 5,5 ile COX-2 enzimi (PDB ID 1CX2), tirozin kinaz reseptörü (PDB ID 1XKK) ve VEGF-2 reseptörü (PDB ID 4ASD) üzerinde gerçekleştirilmiştir.

*Correspondence: E-mail: juni-e@ff.unair.ac.id, Phone: +081332041503 ORCID-ID: orcid.org/0000-0002-4402-2039

Received: 04.12.2018, Accepted: 04.04.2019

©Turk J Pharm Sci, Published by Galenos Publishing House.

Bulgular: FA 30, 60 ve 90 µg dozlarla CAM modelinde belirgin bir şekilde anjiyogenezi önlemiştir ve kan damarlarının endotel hücrelerine karşı inhibitor aktivite (%42,6-%70,7) ve neovaskülarizasyon (%43,0-%86,6) göstermiştir. FA'nın VEGF ekspresyonuna karşı inhibitor aktivitesi COX-2 ekspresyonuna karşı olan etkisinden daha güçlü bulunmuştur. FA için VEGF-2 reseptörüne moleküler kenetlenme RS değeri -73,844 kcal/mol ve selekoksib için -94,557 kcal/mol'dür. FA'nın tirozin kinaz üzerine RS değeri -84,954 kcal/mol iken selekoksib üzerine -93,163 kcal/mol'dür. FA'nın COX-2 reseptörü üzerine kenetlenmesinde RS değeri -73,416 kcal/mol iken, selekoksib üzerine kenetlenme değeri -118,107 kcal/mol'dür.

Sonuç: 30-90 µg aralığında FA uygulaması ile VEGF-2 ve COX-2 ekspresyonlarında görülen azalmalar anjiyogenezi inhibisyonuna ilişkili olarak görülmektedir ve bu 2 parametre (neovaskülarizasyon ve kan damarlarında endotel hücre büyümesinin inhibisyonu) ile gösterilmiştir. Sonuç olarak FA'nın özellikle erken evrede ümit vaat eden antiangiyojenik terapötik bir ajan olduğu söylenebilir ve bu aktivite COX-2 ve VEGF-2 proteinleri üzerindeki inhibitör etkisinden kaynaklanıyor olabilir.

Anahtar kelimeler: Ferulic asit, COX-2, VEGF, tirozin kinaz, anjiyogenezi, koryoallantoik membran

INTRODUCTION

The progression of cancer cells depends heavily on angiogenesis, the formation of new blood vessels that supply oxygen and food required for the tumor's cell proliferation and metastasis progression.^{1,2} The development of cancer cells is induced by angiogenesis, which is activated by some growth factors such as vascular endothelial growth factor receptor (VEGFR). Two important growth factor receptors that influence angiogenesis are tyrosine kinase receptor (TKR) and VEGFR-2.^{1,3}

The VEGF signaling pathway is a strategic target for angiogenesis inhibitors.^{4,5} However, there are some clinical problems involving angiogenesis inhibitors in patients (i.e. thromboembolic disorders, intracranial hemorrhage, and bowel perforation).⁶ Other problems are the occurrence of toxicities such as bleeding, fatigue, hypertension, and perforation of the gastrointestinal tract.^{7,8} Therefore, the study of a new antiangiogenic substance that is relatively safe in its pharmaceutical dosage form is an important step in cancer treatment.

Ferulic acid (FA) [3-(4-hydroxy-3-methoxyphenyl)-2-propenoic acid] (Figure 1) is a phenolic acid compound that shows antioxidant^{9,10} and cytotoxic activities in many cancer cell lines.^{11,12} Wang et al.¹³ reported that FA could inhibit the proliferation and induced apoptosis of osteosarcoma cells via the PI3K/Akt pathway. FA also had anti-inflammatory activity and inhibited cyclooxygenase-2 (COX-2) enzyme,¹⁴ which were related to angiogenesis.^{2,15} Koki and Masferrer¹⁶ reported that COX-2 expression increased during the tumorigenesis process and the intensity of its expression was in line with the degree of carcinogenesis. Wu et al.¹⁷ reported that the biosynthesis of PG catalyzed by COX-2 could stimulate the VEGF expression in tumor cells and acted as a positive feedback loop between tumor cells and endothelial cells.

In an effort to improve FA as a drug candidate for cancer chemoprevention, we studied its antiangiogenic activity and inhibitory activity against COX-2 and VEGF expression in the chicken egg chorioallantoic membrane (CAM) model. The CAM assay is a robust and applicable technique to assess a potential drug candidate. The assay has been commonly used to study angiogenesis and tumor invasion in various types of cancer.^{18,19} To verify FA's mechanism in the inhibition of angiogenesis, we conducted molecular docking on COX-2 enzyme, tyrosine kinase, and VEGF-2 receptors.

MATERIALS AND METHODS

Materials

Commercially available materials were used as obtained. FA, Tris-HCl, and basic fibroblast growth factor (bFGF) were purchased from Sigma-Aldrich (St Louis, MO, USA). The chicken eggs were collected from PUSVETMA Surabaya, Indonesia.

Chorioallantoic membrane assay

Twenty-five 9-day-old chicken eggs were incubated at 37°C (60-70% humidity) for 1 day. All of the treatment groups of CAMs were induced by bFGF at a concentration of 1 ng/µL in Tris-HCl solution of pH 7.5. The eggs were divided into five groups; each group consisted of six eggs. Three groups were treated with FA at doses of 30, 60, and 90 µg; the positive control group was treated with celecoxib (60 µg) and one group received no treatment, which was set as the negative control. The egg was perforated to make a hole 1 cm² in diameter to remove the air. Sterile Whatman filter-paper disks 5 mm in diameter with tested compound and bFGF or bFGF alone were dropped into the hole and then were impregnated into the CAM of each embryo. The hole was covered and the egg returned to incubation at 37°C (60% humidity) for 72 h. After incubation, the upper eggshell was opened and the presence of neovascularization from the main blood vessels onto the paper disks was recorded. In addition, we also collected the blood vessels of the CAM in formalin buffer and carried out microscopic observations of the histopathologic slide of the CAM using hematoxylin and eosin staining. To confirm the antiangiogenic activity, this CAM assay was achieved with certain alteration as explained before.^{18,20} The growth of the endothelial cells in the neovascular capillaries was exposed in CAM cross-sections by an inverted phase contrast microscope, a Nikon H600L. The number of endothelial cells in five graphical fields were calculated, whereas each slide was observed at 400x amplification and compared with the positive or negative control groups for the following analysis.

Antibodies

Rabbit polyclonal anti-human COX-2 and VEGF antibodies were obtained from Thermo Scientific™ Lab Vision™ (St Louis, MO, USA).

Immunohistochemical assay

The slides for the immunohistochemical assay were prepared at the Laboratory of Anatomical Pathology, Dr. Sardjito Hospital, Yogyakarta, Indonesia. Paraffin blocks of the CAM

containing blood vessels were cut 3–4 μm thick and placed on the poly-lysine slide, and then they were incubated overnight at 45°C. The next step of VEGF or COX-2 staining for the immunohistochemical assay was carried out as reported in previous research.^{18,19} In the present study, we used Mayer's hematoxylin for counterstaining. Tris-EDTA solution at pH 9 was used in the retrieval step of VEGF staining for 15–20 min, whereas pH 6 citrate buffer was used for retrieval of COX-2 staining for 15–20 min. The slides were divided into six groups. One group consisted of slides of CAM expressing COX-2 protein, which was used as the positive control; three groups contained slides of FA at doses of 30, 60, and 90 μg , one group contained slides of celecoxib at a dose of 60 μg , which was used as the reference drug; and one group was used as a negative control group. The microscopic observation of VEGF expression and COX-2 expression was continued by counting the visible brown cells in five fields for a minimum of 100 cells. This assay was approved by the Ethical Commission of Airlangga University, but it did not involve human participants.

Statistical analysis

The data obtained were subjected to ANOVA and a One-Way Fisher exact test at 95% level of confidence. If there was significant variance among each group, the analysis was continued with Duncan's multiple range test. Statistical significant was set at $p < 0.05$. All statistical analyses were presented using IBM SPSS 21.

Molecular docking equipment

Hardware: Laptop ASUS AMD A8 Vision with CPU @1.9 GHz, 4 GB of RAM.

Software: CS ChemDraw Ultra version 12.00 (Cambridge Soft) was utilized to create the three-dimensional structure (3D) of FA, which was then subjected to energy minimization by MMFF94 method and the 3D structure was saved in SYBYLMol2 format (*.Mol2). Molegro Virtual Docker (MVD) version 5.5 (CLC Bio) was employed as a docking program in this research. The 3D structures of COX-2, TKR, and VEGF-2 proteins were downloaded from the Internet (<http://www.rcsb.org/pdb/home/home.do>)

In silico assay

The 3D structures of the three proteins, which were obtained from a protein data bank (PDB), were: 1) 1XKK, which was TKR containing *N*-(3-chloro-4-[(3-fluorobenzyl)oxy]phenyl)-6-[4-quinazo-linamine) (code FMM-901) as reference ligand, 2) 4ASD, which was VEGFR-2 containing sorafenib (BAX 43-9006) as reference ligand, and (3) 1CX2, which was COX-2 containing [4-(5-(4-bromophenyl)-3-(trifluoro-methyl)-1H-pyrazole-1yl)benzenesulfonamide) (SC58)] as reference ligand. Ligand-protein interactions were prepared by FA molecule MVD version software 5.5. Docking of the FA molecule into each of the 3D structures of proteins was performed as described in our previous study.²⁰ The best docking results can be observed by relating the structure of the docked FA molecule to the crystal structure of the reference ligand at the binding site. The docking results were presented as a rerank score (RS), which

was the total free energy of the ligand-protein interaction. The lowest energy indicated the best pose of binding between the functional group of ligand and amino acid residues of the proteins. The ligand-protein complexes of the lowest score (RS) were used for further visual inspection. The validation of the docking result was performed by redocking the reference ligand into the same cavity in each protein. The redocking result was accepted if the root mean square deviation $< 2.0 \text{ \AA}$.

RESULTS AND DISCUSSION

Antiangiogenic activity of ferulic acid

The antiangiogenesis assay is performed on the CAM of the embryonated chicken egg because the membrane is the site of very high vascularization and is easily observable in line with the process of chicken embryo growth.^{18,21} The CAM is a fusion of chorion and allantois of chicken egg membrane formed after 4 days of incubation.¹⁸ The formation of new blood vessels is derived from the capillaries that arise from the blood vessels.

Angiogenesis in the CAM model through macroscopic observations of new blood vessels induced by bFGF was significantly inhibited ($p < 0.05$) by FA at doses of 30, 60, and 90 μg . The results are represented by inhibition of neovascularization (Figure 2).

Neovascularization is inseparable from the preceding mechanism of growth and the formation of new endothelial cells, whereas one of the angiogenesis stages is endothelial cell migration.²² At this stage, the capillary walls of the blood vessels continue their growth into the lumen of other blood vessels. There are four phases of migration: the growth of two opposite capillary walls, the joining of regulated endothelial cells and bending of the bilayer facilitate growth factors so the cells enter the lumen, and the center of angiogenesis is

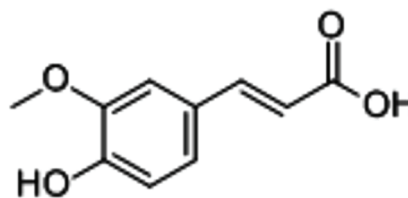


Figure 1. Ferulic acid

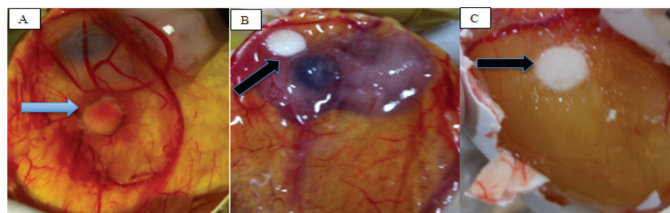


Figure 2. A) Capillary of neovascularization of CAM induced by 60 μg of bFGF (blue arrow) in control positive group, B) capillary of neovascularization of CAM induced by 60 ng of bFGF and treated with 60 μg of celecoxib (black arrow), C) capillary of neovascularization of CAM induced by 60 μg of bFGF and treated with 60 μg of FA (black arrow)

CAM: Chorioallantoic membrane, bFGF: Basic fibroblast growth factor, FA: Ferulic acid

formed between the new blood vessels filled by pericytes and myofibroblasts. The center of angiogenesis is the appearance of smooth muscle fibers that complement the formation of new blood vessels with the development of hematopoiesis as early vascularization.

Figure 2 shows several capillary blood vessels progressing into the impregnated disk of the group without treatment. After treatment with FA and celecoxib, there was a decrease in the number of new blood vessels around the disk on the CAM and endothelial cells of blood vessels. The percentages of inhibition of neovascularization and endothelial cell growth of blood vessels are shown in Table 1.

Based on the statistical analysis by one-way ANOVA, followed by Duncan's multiple range test, it is known that there is no significant difference in potency of the inhibition of neovascularization between celecoxib at 60 µg dose and FA at 60-90 µg dose ($p < 0.05$). However, the potency of FA at 30 µg is smaller than that of FA at 60-90 µg, whereas the potency of FA at 90 µg dose to inhibit endothelial cells of blood vessels is stronger than that of FA at 30-60 µg dose. No significant differences were seen in the potency of inhibition of endothelial cells of blood vessels between FA at 90 µg dose and celecoxib at 60 µg dose ($p < 0.05$). As a reference drug, celecoxib (60 µg) provided 83% new blood vessel growth inhibition in the CAM model.

Ferulic acid inhibited VEGF and COX-2 expression

The microscopic image of VEGF expression in the endothelial cells of the new blood vessels belonging to the positive control group is dominated by the presence of a brown color. It is in sharp contrast to an image from the negative control group, which displays a dominant blue color in the endothelial cell cytoplasm. The brown color in the cytoplasm indicates that VEGF expression of the endothelial cells treated by FA decreases with increasing dose of the substance from 30 µg to 90 µg. The microscopic observation results of VEGF expression in each treatment group are presented in Figure 3.

The microscopic observation results of COX-2 expression in each treatment group are presented in Figure 4. All data of the treatment group are presented in Table 2 and analyzed by SPSS version 21.0 for Windows.

Analysis of percentage inhibition of VEGF expression by FA using the one-sample Kolmogorov-Smirnov test for normality showed probability of $p = 0.398$, whereas percentage inhibition

of COX-2 expression with the one-sample Kolmogorov-Smirnov test showed probability of $p = 0.458$. This means the data are normally distributed because p is greater than 0.05 ($p > 0.05$). Based on statistical analysis by One-Way ANOVA, continued

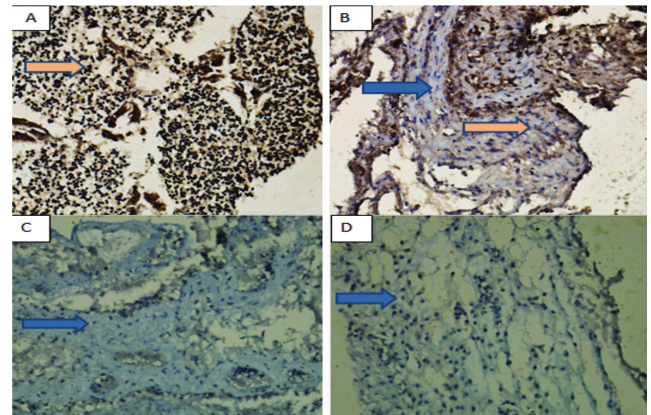


Figure 3. VEGF expression within endothelial cells of blood vessels of the CAM, 400 times magnification: A) positive control group (blank treatment with 60 µg of bFGF), B) group of 60 µg celecoxib treatment, C) group of 60 µg FA treatment, D) group of 90 µg FA treatment. Arrows indicate there is VEGF expression

VEGF: Vascular endothelial growth factor, CAM: Chorioallantoic membrane, bFGF: Basic fibroblast growth factor, FA: Ferulic acid

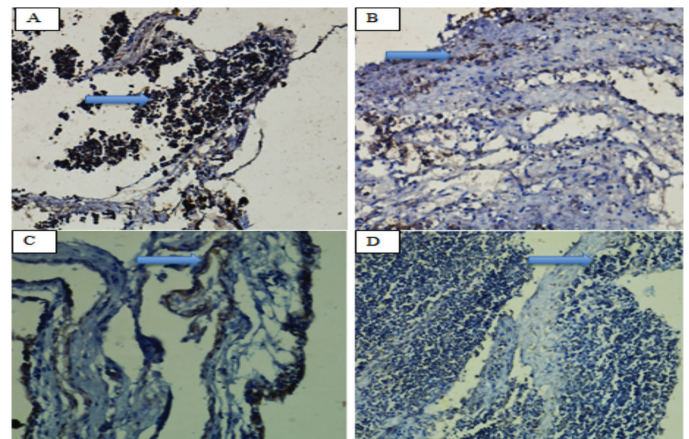


Figure 4. COX-2 expression within endothelial cells of blood vessels of the CAM, 400 times magnification: A) positive control group (blank treatment with 60 µg of bFGF), B) group of 60 µg celecoxib treatment, C) group of 60 µg FA treatment, D) group of 90 µg FA treatment. Arrows indicate there is COX-2 expression

COX-2: Cyclooxygenase-2, CAM: Chorioallantoic membrane, bFGF: Basic fibroblast growth factor, FA: Ferulic acid

Table 1. Antiangiogenesis activity in the CAM model in each group

Treatment	% inhibition of neovascularization	% inhibition of endothelial cells
Celecoxib 60 µg	83.3 ^b ±5.2	79.3 ^c ±2.3
FA 30 µg	43.0 ^a ±4.6	42.6 ^a ±5.9
FA 60 µg	83.4 ^b ±7.4	57.3 ^b ±4.3
FA 90 µg	86.6 ^b ±6.2	70.7 ^c ±3.9

All values are represented as the mean ± SE (n=6) and different superscripts in the same column indicate that there were significant different in each group ($p < 0.05$)
FA: Ferulic acid, CAM: Chorioallantoic membrane, SE: Standard error

with LSD and Duncan's multiple range tests, it is known that there is no significant difference in the potency of inhibition of VEGF expression between celecoxib at 60 μg dose and FA at 60-90 μg dose ($p < 0.05$). The potency of FA inhibiting VEGF expression at 30 μg to 90 μg was dose-dependent. Increasing dose of FA resulted in decreasing VEGF expression of CAM significantly.

Based on the data in Table 2, it is known that giving 30-90 μg of FA decreases VEGF expression in CAM significantly. Reduced VEGF expression due to treatment with FA at 30-90 μg doses is in line with angiogenesis inhibition, which is shown by two parameters, namely neovascularization and resistance to endothelial cell growth of blood vessels in the chick embryo CAM.

The main VEGF receptor in endothelial cells is VEGFR-2, which influences developing and adult cells. VEGFR-2 signaling is better recognized than the other VEGF receptors' signaling. Vascular permeability is an essential *in vivo* consequence of VEGFR-2 activation. Several small-molecular-weight inhibitors of VEGFR-2 kinase activity are employed clinically to block pathological angiogenesis in cancer.¹³

In vitro experiments on capillary endothelial cells showed that VEGF is a powerful stimulator against the occurrence of angiogenesis. This is due to its presence as a growth factor triggering the proliferation and migration of endothelial cells, even the formation of tube formation in a series of capillary vessels.²³ Inhibition of VEGF can occur in several ways; the first is inhibition at the VEGF receptor through kinase activity that contributes to the delivery of growth signals. The second possibility is inhibition through endothelial cell apoptosis induction, whereas the third may involve the incorporation of hematopoiesis and endothelial progenitor cells, and so VEGF is not capable of triggering vasculogenesis.²⁴

According to Di Marco et al.²⁵, binding of VEGFR and VEGF-specific ligand occurs in the transmembrane and cytoplasmic domains. VEGF is known as a promoter of angiogenesis and an endogenous regulator of endothelial integrity. Some anti-VEGF compounds can cause endothelial dysfunction and decreased angiogenesis.

The COX-2 expression in the CAM also presented a brown color in the cell cytoplasm, which is a ligand-receptor complex of COX-2 detected by anti-COX-2 antibodies that are specifically bound to COX-2 ligand. Based on the data in Table 2, it is known that treatment with 30-90 μg of FA can significantly decrease COX-2 expression in the CAM. The inhibitory activity of FA against COX-2 expression is dose-dependent. The inhibitory potency of FA at dose range 30-90 μg is significantly different from that of celecoxib at the 60 μg dose. In our study, the administration of FA appeared to play an important role in angiogenesis inhibition through decreasing COX-2 expression.

The reduction in COX-2 expression due to treatment with FA at the dose range 30-90 μg seems to have been related to angiogenesis inhibition, which is shown by two parameters, namely inhibition of neovascularization and inhibition of endothelial cell growth in blood vessels of chick embryo CAM. Hsu et al.²⁶ reported that prostaglandin-E2 (PGE2) stimulates COX-2 expression in LoVo colon cancer cells. The COX2 expression was interrelated with the elevation in the migration ability of those cancer cells. The experimental data suggested that PGE2 can be a potential therapeutic target in colon cancer metastasis. Yao et al.²⁷ stated that downregulation of COX-2 could significantly diminish the progression of gastric cancer cells and block the replacement and tube formation of human umbilical vein endothelial cells. The results also indicated that downregulation of COX-2 might inhibit VEGF.

Table 2. Inhibition of VEGF and COX-2 expression in the CAM model in each group

Treatment	% inhibition of VEGF expression	% inhibition of COX-2 expression
Celecoxib 60 μg	72.9 \pm 6.8 ^b	84.1 \pm 4.2 ^c
FA 30 μg	46.7 \pm 8.0 ^a	49.9 \pm 6.3 ^a
FA 60 μg	63.7 \pm 4.9 ^b	55.0 \pm 4.6 ^a
FA 90 μg	73.6 \pm 5.3 ^b	66.8 \pm 2.8 ^b

All values are represented as the mean \pm SE (n=6) and different superscripts in the same column indicate that there were significant differences in each treatment ($p < 0.05$)

VEGF: Vascular endothelial growth factor, COX-2: Cyclooxygenase-2, CAM: Chorioallantoic membrane, FA: Ferulic acid

Table 3. The rerank score, type of bonding interactions, and amino acids involved in the interaction of ligands with VEGFR-2 (PDB ID 4ASD)

Compound	Rerank score (kcal/mol)	Number of H-bonds	Amino acid residue	Number of steric interactions	Amino acid residue
FA	-73.844	1	Glu885	6	Ala1050, Glu885, Leu 889, Val 848
Celecoxib	-94.557	2	Gln847 Lys868	24	Asn1033, Cys1045, Gln847, Glu885, Lys868, Phe1047, Val848, Val867, Val914

VEGFR-2: Vascular endothelial growth factor receptor-2, FA: Ferulic acid, FA: Ferulic acid, Lys: Lysine, Met: Methionine, Asp: Aspartic Ala: Alanine, Gly: Glutamine, Ser: Serine, Leu: Leucine, Tyr: Tyrosine, Val: Valine, Phe: Phenylalanine

The COX-2 inhibitor celecoxib²⁸ has been reported to inhibit the growth of prostate, gastric, lung, and breast cancer.^{29,30} The induction of bFGF as pro-angiogenic compounds will lead to inflammation associated with the COX-2 activity.^{31,32} As well as celecoxib, FA also inhibited COX-2 enzyme^{14,30} and so it could obstruct bFGF activity as a pro-angiogenic compound.

Based on the inhibitory mechanism of angiogenesis through the inhibition of VEGF expression examined by other researchers in several studies, it is possible that FA inhibits VEGFR-2 through its inhibitory activity on tyrosine kinase and COX-2. This assumption is studied and proven through *in silico* docking on COX-2, TKR, and VEGFR-2.

Docking study

The best-docked pose of FA, celecoxib, and BAX ligands in the binding site of VEGFR-2 and the interactions between functional groups of FA and celecoxib with amino acid residues in two-dimensional (2D) structures are shown in Figure 5. The docking scores (RS value), the type of bonding interactions with VEGFR-2, and amino acids involved in their interactions are listed in Table 3.

The best-docked pose of FA, celecoxib, and native ligand in the binding site of tyrosine kinase and their interactions with amino acid residues in 2D structures are shown in Figure 6. The RS value, the type of interactions, and amino acids involved in the interaction between ligand and TKR are listed in Table 4.

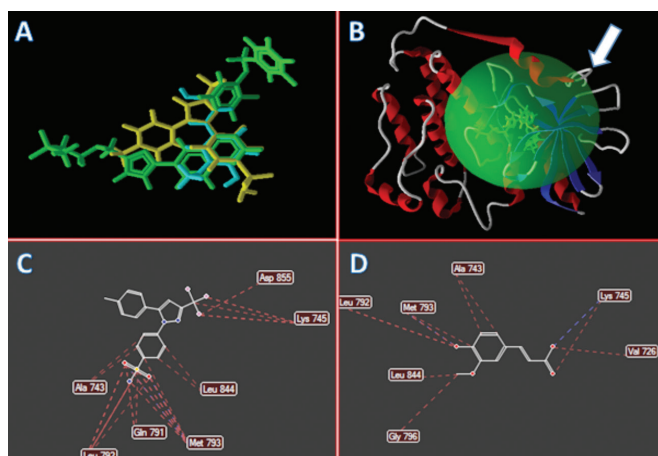


Figure 5. The best docking of FA (yellow)-celecoxib (blue)-BAX (green) ligands A); the three ligands positioned at the active site (cavity-2) of VEGFR-2 B); interaction of celecoxib with amino acids in cavity-2 of VEGFR-2 C); interaction of FA with amino acids in cavity-2 of VEGFR-2 D) FA: Ferulic acid, VEGFR-2: Vascular endothelial growth factor receptor-2

The ligand of PDB ID 1XKK contains a benzylic group (Ar-C-), which acts as a pharmacophore in the ligand-receptor interaction complex. The FA compound contains a similar group, which is also expected to be a pharmacophore. Celecoxib, which produces a lower RS value than FA (Table 3), displays more H-bonds and steric interactions with TKR than FA.

The best-docked pose of FA, celecoxib, native ligand in the binding site of COX-2 and their interactions with amino acid residues of each protein in 2D structures are shown in Figures 5-7. The RS value, the type of bonding interactions with COX-2, and amino acids involved in their interactions are listed in Table 5.

Based on the molecular docking study, the possible interactions can be explained between each compound, i.e. FA and celecoxib, with amino acid residues in each protein enzyme/receptor. The FA-TKR interaction is stronger than FA-VEGFR-2, indicating the possibility that FA worked on growth factor receptors,^{1,31} and it is apparent that FA inhibited VEGF expression in the CAM model.

The ligand binding of VEGFR stimulated strong tyrosine phosphorylation and results in an intense angiogenesis response.³¹ Replacement of the native ligand of VEGFR-2 with FA through the interactions of functional groups of FA with the amino acid residue of VEGFR-2 prevented tyrosine phosphorylation and so decreased angiogenesis.³²

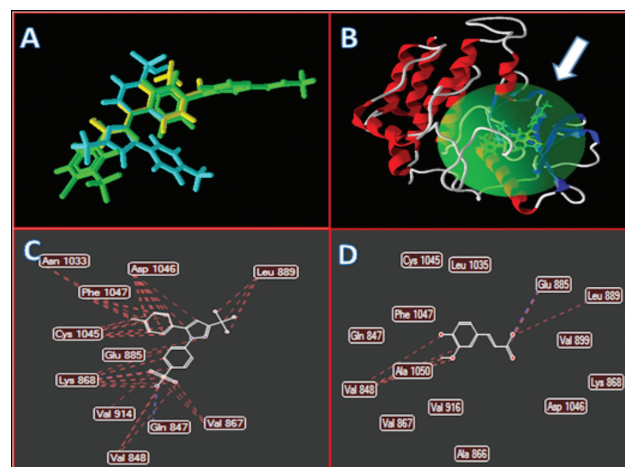


Figure 6. The best docking of FA (yellow)-celecoxib (blue)-FMM (green) A); the three ligands positioned at the active site (cavity-1) of TKR; B); interaction of celecoxib with amino acids of TKR C); interaction of FA with amino acids of TKR D), PDB 1XKK
FA: Ferulic acid, TKR: Tyrosine kinase receptor

Table 4. The rerank score, type of bonding interactions, and amino acids involved in the interaction of ligands with TKR (PDB 1XKK)

Compound	Rerank score (kcal/mol)	Number of H-bonds	Amino acid residue	Number of steric interactions	Amino acid residue
FA	-84.954	1	Lys745	9	Ala743, Gly796, Leu792, Leu844, Lys745, Met793, Val726
Celecoxib	-93.163	2	Met793	24	Ala743, Asp855, Gln791, Leu792, Leu844, Lys745, Met793

TKR: Tyrosine kinase receptor, FA: Ferulic acid, Lys: Lysine, Met: Methionine, Asp: Aspartic Ala: Alanine, Gly: Glutamine, Ser: Serine, Leu: Leucine, Tyr: Tyrosine, Val: Valine

Table 5. The rerank score, type of bonding interactions, and amino acids involved in the interaction of ligands with COX-2 (PDB 1CX2)

Compound	Rerank score (kcal/mol)	Number of H-bonds	Amino acid residue	Number of steric interactions	Amino acid residue
FA	-73.416	3	Ser353, His90	3	Tyr355, Val523, Leu352
Celecoxib	-118.107	5	Arg513 His90 Ser353 Leu352 Gln152	16	Tyr355, Val523, Val349, Ser530, Val116, Ser353, Leu352, Phe518

COX-2: Cyclooxygenase-2, FA: Ferulic acid, Ser: Serine, Arg: Arginine, His: Histidine, Leu: Leucine, Gln: Glutamine, Tyr: Tyrosine, Phe: Phenylalanine, Val: Valine

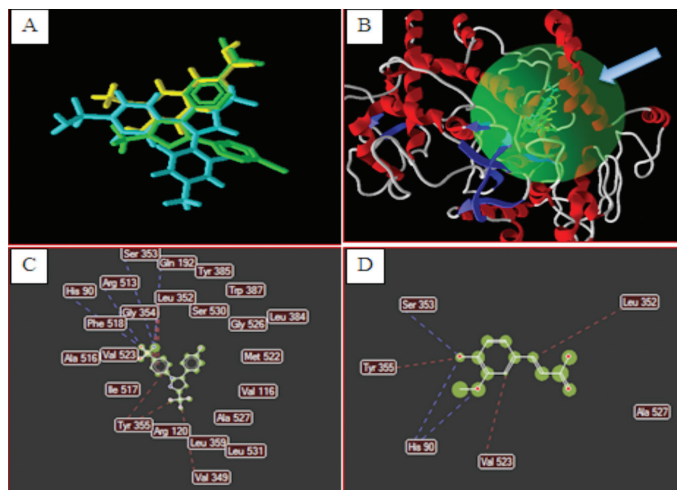


Figure 7. The best docking of FA (yellow)-celecoxib (blue)-SC58 (green) A); the three ligands positioned at the active site (cavity-3) of COX-2 B); the interaction of celecoxib with amino acids COX-2 C); interaction of FA with amino acids COX-2 D), PDB 1CX2

FA: Ferulic acid, COX-2: Cyclooxygenase-2

There are several phases of angiogenesis inhibition, i.e. prevention of endogenous angiogenic factors such as bFGF and VEGF; inhibition of the degradation matrix metalloproteinase (MMP), reducing endothelial cell proliferation; and prevention of endothelial cell movement, inhibiting endothelial cell activation and differentiation.³³

Based on the data and description above, the mechanisms by which FA prevents angiogenesis are by blocking COX-2 activity so that MMP activity, which plays a role in the early formation of branching of blood vessels, will stop, and by obstructing endogenous angiogenic factors, i.e. VEGF and bFGF, in the initial stage of angiogenesis.

Study limitations

In our study, FA inhibits angiogenesis in the CAM model in the earliest process, i.e. endogenous angiogenic factors and kinase activity promoting release of growth signals. Thus, the potency of FA to inhibit angiogenesis at other stages needs further research.

CONCLUSION

FA (at a dose of 30-90 μ g) is a promising antiangiogenic therapeutic agent, especially in an early stage of angiogenesis. It prevents proangiogenic growth factor, which leads to

inflammation (i.e. bFGF), activity of MMP, and development of branching of blood vessels. This activity results from inhibitory action on COX-2 and VEGF-2 proteins.

Conflicts of interest: All authors declare that they have no competing interests.

Financial Disclosure: Publication of this article was funded by PTUPT Grant Airlangga University 2017/2018.

REFERENCES

- Roskoski R. Sunitinib: A VEGF and PDGF receptor protein kinase and angiogenesis inhibitor. *Biochem Biophys Res Commun.* 2007;356:323-328.
- Sahin M, Sahin E, Gümüslü S. Cyclooxygenase-2 in cancer and angiogenesis. *Angiology.* 2015;60:242-253.
- Bikfalvi A, Moenner M, Javerzat S, North S, Hagedorn M. Inhibition of angiogenesis and the angiogenesis/invasion shift. *Biochem Soc Trans.* 2011;39:1560-1564.
- Saha S, Islam MK, Shilpi JA, Hasan S. Inhibition of VEGF: a novel mechanism to control angiogenesis by Withania som-nifera's key metabolite Withaferin A. *In Silico Pharmacol.* 2013;1:11.
- Taylor M, Coleman RL, Sood AK. The Role of Angiogenesis in Cancer. *Target Ther Transl Cancer Res.* 2015:64-71.
- Newton HB. Bevacizumab: Review of Development, Pharmacology, and Application to Brain Tumors. *Clin Med Ther.* 2009;1:1577-1597.
- Gotink KJ, Verheul HMW. Anti-angiogenic tyrosine kinase inhibitors: what is their mechanism of action? *Angiogenesis.* 2010;13:1-14.
- Altun A, Temiz TK, Balci E, Polat ZA, Turan M. Effects of tyrosine kinase inhibitor E7080 and eNOS inhibitor L-NIO on colorectal cancer alone and in combination. *Chin J Cancer Res.* 2013;25:572-584.
- Graf E. Antioxidant potential of ferulic acid. *Free Radic Biol Med.* 1992;13:435-448.
- Itagaki S, Kurokawa T, Nakata C, Saito Y, Oikawa S, Kobayashi M, Hirano T, Iseki K. *In vitro* and *in vivo* antioxidant properties of ferulic acid: A comparative study with other natural oxidation inhibitors. *Food Chem.* 2009;114:466-471.
- Peng CC, Chyau CC, Wang HE, Chang CH, Chen KC, Chou KY, Peng RY. Cytotoxicity of ferulic acid on T24 cell line differentiated by different microenvironments. *Biomed Res Int.* 2013;2013:579859.
- Senawong T, Khaopha S, Misuna S, Komaikul J, Senawong G, Wongphakham P, Yunchalard S. Phenolic acid composition and anticancer activity against human cancer cell lines of the commercially available fermentation products of *Houttuynia cordata*. *Science Asia.* 2014;40:420-427.

13. Wang L, Chen W, Xie X, He Y, Bai X. Celecoxib Inhibits Tumor Growth and Angiogenesis in an Orthotopic Implantation Tumor Model of Human. *Exp Oncol*. 2008;30:42-51.
14. Nile SH, Ko EY, Kim DH, Keum YS. Screening of ferulic acid related compounds as inhibitors of xanthine oxidase and cyclooxygenase-2 with anti-inflammatory activity. *Brazilian J Pharmacogn* 2016, 26:50-5. Available from: <http://dx.doi.org/10.1016/j.bjp.2015.08.013>
15. Rosas C, Sinning M, Ferreira A, Fuenzalida M, Lemus D. Celecoxib decreases growth and angiogenesis and promotes apoptosis in a tumor cell line resistant to chemotherapy. *Biol Res*. 2014;47:1-9.
16. Koki AT, Masferrer JL. Celecoxib: A specific COX-2 inhibitor with anticancer properties. *Cancer Control*. 2002;9(Suppl 2):28-35.
17. Wu GF, Luo J, Rana JS, Laham R, Sellke FW, Li J. Involvement of COX-2 in VEGF-induced angiogenesis via P38 and JNK pathways in vascular endothelial cells. *Cardiovasc Res*. 2006;69:512-519.
18. Ribatti D. The chick embryo chorioallantoic membrane as an *in vivo* assay to study antiangiogenesis. *Pharmaceuticals (Basel)*. 2010;3:482-513.
19. Yuan YJ, Xu K, Wu W, Luo Q, Yu JL. Application of the chick embryo chorioallantoic membrane in neurosurgery disease. *Int J Med Sci*. 2014;11:1275-1281.
20. Ekowati J, Hardjono S, Hamid IS. Ethyl p -methoxycinnamate from *Kaempferia galanga* inhibits angiogenesis through tyrosine kinase. *Universa Med*. 2015;34:43-51.
21. Richardson M, Wong D, Lacroix S, Stanis.z J, Singh G. Inhibition by doxycycline of angiogenesis in the chicken chorioallantoic membrane (CAM). *Cancer Chemother Pharmacol*. 2005;56:1-9.
22. Burri PH, Hlushchuk R, Djonov V. Intussusceptive angiogenesis: Its emergence, its characteristics, and its significance. *Dev Dyn*. 2004;231:474-488.
23. Dannenberg AJ, Lippman SM, Mann JR, Subbaramaiah K, DuBois RN. Cyclooxygenase-2 and epidermal growth factor receptor: Pharmacologic targets for chemoprevention. *J Clin Oncol*. 2005;23:254-266.
24. Kuwano T, Nakao S, Yamamoto H, Tsuneyoshi M, Yamamoto T, Kuwano M, Ono M. Cyclooxygenase 2 is a key enzyme for inflammatory cytokine-induced angiogenesis. *FASEB J*. 2004;18:300-310.
25. Di Marco GS, Reuter S, Hillebrand U, Amler S, König M, Larger E, Oberleithner H, Brand E, Pavenstädt H, Brand M. The soluble VEGF receptor sFlt1 contributes to endothelial dysfunction in CKD. *J Am Soc Nephrol*. 2009;20:2235-2245.
26. Hsu HH, Lin YM, Shen CY, Shibu MA, Li SY, Chang SH, Lin CC, Chen RJ, Viswanatha VP, Shih HN, Huang CY. Prostaglandin E2-Induced COX-2 Expressions via EP2 and EP4 Signaling Pathways in Human LoVo Colon Cancer Cells. *Int J Mol Sci*. 2017;18:1132.
27. Yao L, Liu F, Hong L, Sun L, Liang S, Wu K, Fan D. The function and mechanism of COX-2 in angiogenesis of gastric cancer cells. *J Exp Clin Cancer Res*. 2011;30:13.
28. Klenke FM, Gebhard MM, Ewerbeck V, Abdollahi A, Huber PE, Sckell A. The selective Cox-2 inhibitor Celecoxib suppresses angiogenesis and growth of secondary bone tumors: an intravital microscopy study in mice. *BMC Cancer*. 2006;6:9.
29. Moschona A, Kyriakidis KD, Kleontas AD, Liakopoulou-M. Comparative Study of Natural Phenolic Acids and Flavonols as Antiplatelet and Anti-Inflammatory Agents. *The Grant Med J*. 2017;2:57-66.
30. Manoharan S, Rejitharaji T, Prabhaka MM, Manimaran A, Sing RB. : Modulating Effect of Ferulic Acid on NF- κ B, COX-2 and VEGF Expression Pattern During. 7,12-Dimethylbenz(a)anthracene Induced Oral Carcinogenesis. *The Open Nutraceuticals Journal*. 2014;7:33-38.
31. Schmidt U, Ahmed J, Michalsky E, Hoepfner M, Preissner R. Comparative Vegf Receptor Tyrosine Kinase Modeling for the Development of Highly Specific Inhibitors of Tumor Angiogenesis. *Genome Inform*. 2008;20:243-251.
32. Jeltsch M, Leppanen VM, Saharinen P, Alitalo K. Receptor Tyrosine Kinase-Mediated Angiogenesis. *Cold Spring Harb Perspect Biol*. 2013;5:a009183.
33. Stegmann TJ, Hoppert T, Schneider A, Popp M, Strupp G, Ibing RO, Hertel A. Therapeutic Angiogenesis : Intramyocardial Growth Factor Delivery of FGF-1 as Sole Therapy in Patients with Chronic Coronary Artery Disease:1-14. Available from: <https://citeseerx.ist.psu.edu/viewdoc/download?doi=10.1.1.577.9796&rep=rep1&type=pdf>



Safety Assessment of Vanillic Acid: Subacute Oral Toxicity Studies in Wistar Rats

Vanilik Asitinin Güvenlik Değerlendirmesi: Wistar Sıçanlarında Subakut Oral Toksikite Çalışmaları

© Anwarbaig Chandbaig MIRZA¹, © Shital Sharad PANCHAL^{2*}

¹Anjuman-i-Islams's Kalsekar Technical Campus, School of Pharmacy, Department of Pharmacology, Navi Mumbai, India

²Nirma University Institute of Pharmacy, Department of Pharmacology, Gujarat, India

ABSTRACT

Objectives: Vanillic acid (VA) is a flavoring agent, a phenolic acid, and an intermediary by-product formed during transformation of ferulic acid to vanillin. It has been investigated for diverse pharmacological actions and used in Chinese medicine for decades. However, there is no information in the literature about its mechanism of toxicity or safety with long-term use. The present study will not only supply information on its pharmacological profile but also encourage evidence-based pharmacotherapeutic use. Hence, we performed a subacute toxicity study.

Materials and Methods: According to the Organisation for Economic Co-operation and Development Test Guideline 407 (2008), 3 groups of rats were formed consisting of 12 rats (6 male and 6 female) in each group. For the subacute toxicity, the dose was chosen after a limit test was conducted. VA (1000 mg/kg/day) was orally administered for 2 weeks to the treatment group, whereas the control group received an equivalent volume of the vehicle. To assess reversibility, VA (1000 mg/kg/day, p.o.) was administered to the satellite group for 2 weeks and animals were observed for an additional 2 weeks after treatment. The adverse signs, variation in body weight, and mortality were evaluated throughout the study period. On days 15 and 29, blood was collected to evaluate essential biochemical and hematological parameters. The animals were subsequently weighed and sacrificed. The weights of internal organs were recorded; gross necroscopy and histopathological studies were performed.

Results: The hematological parameters of the satellite group increased and the serum sodium level decreased after the treatment. Satellite groups showed no other major change in biochemical parameters when compared to the control group. In addition, relative organ weights, gross necropsy examinations and histopathological structure of the internal organs showed no major alterations.

Conclusion: VA showed no adverse effect on the process of leukopoiesis, erythropoiesis or on internal organs, as verified by hematological and biochemical evaluations, gross necropsy, and histopathological studies. The decrease in serum sodium is not considered as a major toxic effect.

Key words: Subacute toxicity, vanillic acid, polyphenol, safety

ÖZ

Amaç: Vanilik asit (VA) fenolik asit yapısında tat verici bir ajandır ve ferulik asidin vanilin dönüşümü sırasında oluşan bir ara yan üründür. Çeşitli farmakolojik etkiler için araştırılmış ve yıllardan beri Çin tıbbında kullanılmaktadır. Ancak, uzun süreli kullanımı için toksisite mekanizması veya güvenliliği ile ilgili bilgi literatürde mevcut değildir. Bu çalışma sadece farmakolojik profile hakkında bilgi sağlamakla kalmayacak, aynı zamanda kanıt dayalı farmakoterapötik kullanımı hakkında da bilgi verecektir. Bu nedenle, subakut bir toksisite çalışması yapılmıştır.

Gereç ve Yöntemler: Ekonomik Kalkınma ve İşbirliği Örgütü Test Kılavuzu 407 (2008)'e göre, 12 sıçan (6 erkek ve 6 dişi) rastgele bir şekilde 3 gruba ayrılmıştır. Subakut toksisite için sınır testi yapıldıktan sonra doza karar verilmiştir. VA (1000 mg/kg/gün) uygulama grubuna 2 hafta boyunca oral yoldan uygulanırken kontrol grubuna eşdeğer hacimde taşıyıcı verilmiştir. Tersinirliği değerlendirmek için, uydu grubuna 2 hafta boyunca VA (1000 mg/kg/gün, p.o) uygulanmış ve hayvanlar tedaviden sonra 2 hafta daha gözlenmiştir. Advers belirtiler, vücut ağırlığındaki değişiklik ve mortalite çalışma süresi boyunca değerlendirilmiştir. On beşinci ve 29. günlerde, gerekli biyokimyasal ve hematolojik parametreleri değerlendirmek için kan alınmıştır. Takiben hayvanlar tartılmış ve öldürülmüştür. İç organ ağırlıkları kaydedilmiş, gros nekropsi ve histopatolojik çalışmalar yapılmıştır.

Bulgular: Uydu grubunda hematolojik parametreleri artmış ve serum sodyum düzeyi uygulamadan sonra azalmıştır. Uydu gruplarında kontrol grubuna kıyasla biyokimyasal parametrelerde başka bir önemli değişiklik görülmemiştir. Ayrıca, rölatif organ ağırlığı, gros nekropsi incelemeleri ve iç organların histopatolojik yapısı önemli bir değişiklik göstermemiştir.

*Correspondence: E-mail: shital.panchal@nirmauni.ac.in, Phone: +91 9687626589 ORCID-ID: orcid.org/0000-0003-4211-8202

Received: 13.03.2019, Accepted: 30.05.2019

©Turk J Pharm Sci, Published by Galenos Publishing House.

Sonuç: Hematolojik ve biyokimyasal değerlendirmeler, gros nekropsi ve histopatolojik çalışmalardan da görüldüğü üzere, VA lökopeni, eritropeni ve iç vücut organları üzerinde olumsuz bir etki göstermemiştir. Serum sodyum düzeyindeki düşüş majör bir toksik etki olarak değerlendirilmemiştir

Anahtar kelimeler: Subakut toksisite, vanilik asit, polifenol, güvenlik

INTRODUCTION

Vanillic acid (VA) (4-hydroxy-3-methoxybenzoic acid) is a frequently utilized flavoring agent and an oxidized form of vanillin. It is an intermediary by-product formed during transformation of ferulic acid to vanillin.^{1,2} It is present in large amounts in the roots of *Angelica sinensis*,³ fruits of *Euterpe oleracea*,⁴ wine, and vinegar⁵ and has been used in Chinese medicine for decades.⁶ It was investigated for diverse pharmacological actions in experimental animals and proved to have antidiabetic activity,^{7,8} an anti-inflammatory effect,^{9,10} a strong antioxidant effect,^{11,12} cardioprotectivity,¹³⁻¹⁵ thermal tolerance,¹⁶ and inhibitory effects on Neuro-2A cells.¹⁷ In addition, it ameliorates glomerulonephritis,¹⁸ has a cognitive effect in diabetic mice,¹⁹ and its presence was reported in cerebrospinal fluid.²⁰ It was reported to inhibit carbonic anhydrase isozyme III²¹ and snake venom 5'-nucleotides.²² It controls transgene expression in mammalian cells and mice.²³ It showed a protective effect on ulcerative colitis²⁴ and liver toxicity²⁵ and has a proved analeptic effect.²⁶ Furthermore, it acts as an antifilarial agent²⁷ and respiratory stimulant.²⁸

In the mid 20th century, clinical studies were conducted on excretion of VA in urine. In one study, VA was reported as a metabolic product of 4-hydroxy-3-methoxyphenylglycol and 4-hydroxy-3-methoxymandelic acid.²⁹ It was reported as a metabolite of protocatechuic acid, which is stable at alkaline pH of urine.³⁰ In addition, excretory studies were reported in healthy volunteers, patients with circulatory and liver disorders, and smokers and nonsmokers and during stress.³¹⁻³³

VA is supposed to be administered for long durations to treat chronic disorders; therefore, assessment of its safety or the risk of occurrence of toxic effects becomes crucial. Current scientific research studies revealed undesirable effects of various plant extracts and phytochemicals in rodents at higher dosages, for instance neurotoxicity (*Cannabis sativa*, *Papaver somniferum*, and *Erythroxylum* spp.), hepatotoxicity (*Cimicifuga racemosa*, etc.), genotoxicity (thymol and carvacrol), carcinogenicity (capsaicin, chili powder, safrole), cytotoxicity (*Withania somnifera*, safrole-2', 3'-oxide, etc.), nephrotoxicity (aristolochic acid, turmeric, etc.), teratogenicity (pyrrolizidine alkaloid monster, heliotrine), and gastrointestinal effects (red pepper, fennel, etc.).³⁴ Brown³⁵ discussed case studies of 12 dietary supplements and 21 herbs that give rise to a possible risk of hepatic injuries in certain individuals. These reports are alarming and compelling researchers to assess the safety of phytochemicals in long-term use. Toxicological studies on phytochemicals not only enrich the ethnopharmacology but also augment the careful utilization of phytochemicals and prevent undesirable effects, which seem to be a prime hurdle for the long-term use of modern medications.³⁶ As per the Organisation for Economic Co-operation and Development

(OECD) TG 407 (2008),³⁷ subacute toxicity studies are usually planned and performed after getting early details in acute toxicity studies. It improves understanding of the probable untoward effect on health likely to occur from continuous utilization of medicines over a short period and is considered a foundation for conducting subchronic and chronic toxicological studies.³⁸ Additionally, subacute toxicology studies in experimental animals are thought to be a mandatory stage to start with for clinical trials and thereafter marketing of drug molecules.³⁹

Acute toxicity studies on VA are reported in the literature and the LD50 value was reported as 5020 mg/kg i.p. in rats and 2691 mg/kg i.p. in mice.⁴⁰⁻⁴² However, the currently available scientific literature does not contain enough data on subacute toxicity studies of VA. Hence, it was decided to perform a subacute toxicity study to determine the toxic effect (if any) of VA on physiological processes (such as erythropoiesis and leukopoiesis) and vital internal organs in rodents.

MATERIALS AND METHODS

Chemicals

VA (HSN-29189900) was procured from Sigma (St. Louis, MO, USA). Biochemical kits were purchased from Transasia Bio-Medicals Ltd. and Lab-Care Diagnostics (India) Pvt Ltd. All chemicals and biochemical kits were of analytical grade.

Experimental animals

Wistar albino rats of both sexes were procured from the National Institute of Bioscience, Pune. They were kept in propylene cages and room temperature of 22±1°C was maintained with alternate light and dark cycles. All the rats were allowed to eat high quality pelleted food and drink water *ad libitum*. The Institutional Animal Ethics Committee of AIKTC's, School of Pharmacy, Navi Mumbai, India approved all the experimental protocols.

Limit test

As per the OECD TG 407 (2008),³⁷ this test was carried out by administering one dose of VA (2000 mg/kg) to Wistar rats to make a decision about the dose of the subacute toxicity study. The animals were critically examined for any morbidity as well as mortality.

Subacute toxicity

As per the OECD TG 407 (2008),³⁷ 3 groups of rats were prepared consisting of 12 rats (6 female and 6 male) in each. The VA (1000 mg/kg/day) was orally administered for 2 weeks to the treatment group, whereas an identical volume of vehicle was given to the control group. To check reversibility, the satellite group was orally administered VA (1000 mg/kg/day) for 2 weeks and then kept for a further 2 weeks after treatment for observation. The toxic signs, body weight

changes, water consumption, food intake, and mortality were recorded on a weekly basis. On day 15 the rats in the control and treatment groups were exposed to isoflurane for producing *an anesthetic effect* and blood samples were collected in tubes coated with ethylenediaminetetraacetic acid to determine the complete blood count, which includes hemoglobin (HGB) count, white blood cell (WBC) and red blood cell (RBC) count, etc. For the other biochemical estimations nonheparinized blood samples were collected. Thereafter, all rats were sacrificed and their internal vital organs were dissected for measuring organ weight and to carry out gross anatomical studies. All isolated organs were stored in 10% buffered formaldehyde to carry out histopathological examinations.

Statistical analysis

GraphPad InStat version 3.0 (GraphPad, San Diego, CA, USA) was used to analyze the data. One-Way ANOVA was applied followed by Dunnett's multiple range test. The results were expressed as mean \pm standard deviation and $p < 0.05$ was considered statistically significant.

RESULTS

Limit test

No mortality or signs of toxic effects were observed; hence as per the guideline of OECD 407 (2008), 1000 mg/kg dose was selected for the subacute toxicity study.

Clinical examination, food and water consumption, and body weight

The treatment and satellite groups did not show any signs of toxicity or mortality within the study period. Usual increases in body weights and food and water consumption were observed in the treatment and satellite groups in comparison with the rats in the control group.

Hematological evaluations

Tables 1 and 2 contain the findings of the hematological evaluations. The treatment group showed normal rises in RBC count, HGB, platelet (PLT) count, mean cell hemoglobin (MCH), MCH concentration (MCHC), packed cell volume (PCV), and mean corpuscular cell volume (MCV) in both sexes of Wistar rats but significant increases in all hematological parameters were recorded in the satellite group rats. In addition, the WBC counts of rats in the treatment and satellite groups were within the reference range and were insignificantly different compared to those of the normal control group although the neutrophil count was slightly increased in male rats in the treatment group, which was reversed after 2 weeks in the satellite group (Table 2). The eosinophil, monocyte, and lymphocyte counts in the treated and satellite groups showed no remarkable change in comparison with the rats in the normal control group.

Blood biochemistry

The findings of the clinical biochemistry analysis are shown in Table 3. It involves estimation of lactate dehydrogenase (LDH), total protein (TP), creatinine (CR), total bilirubin (TB), direct bilirubin (DB), blood glucose (BG), serum glutamic-

oxaloacetic transaminase (SGOT), serum glutamine-pyruvic transaminase (SGPT), albumin (ALB), electrolytes [potassium (K), calcium (Ca), chloride (Cl), and phosphate (P)], blood urea nitrogen (BUN), alkaline phosphatase (ALP), and lipid profile [triglycerides (TGs), total cholesterol (TC), and high density lipoprotein (HDL)]. Application of VA to the treatment group rats caused no shift in biochemical parameters in comparison with the normal control rats except for statistically significant decreased sodium levels in the male treatment group, which did not recover in the satellite group to normal levels.

Relative organ weight, gross necropsy, and histopathological findings

Table 4 shows the effect of VA on relative internal organ weight. No significant variation was observed in relative organ weights of the treatment and satellite groups in comparison with the normal control group, although the *liver weight* of treated rats (male) was high in comparison to that of *normal control rats*, but it was reversed in the *respective satellite group*. Gross anatomical examination of vital organs and/or systems of rats

Table 1. Effect of vanillic acid on hematological evaluations at the end of the study

Gender & parameters	Groups		
Male	Control	VA ¹	VA ²
Hb (g %)	13.00 \pm 0.44	12.42 \pm 0.63	14.53 \pm 0.58*
RBC (x10 ⁶ /mm ³)	7.34 \pm 0.23	6.82 \pm 0.12	8.62 \pm 0.43*
WBC (x10 ³ /mm ³)	11.88 \pm 3.74	11.30 \pm 1.61	11.30 \pm 3.89
PLT (x10 ⁵ /mm ³)	9.48 \pm 1.20	7.37 \pm 1.15	9.50 \pm 0.96
PCV (%)	33.86 \pm 1.29	29.40 \pm 5.06	46.71 \pm 2.31*
MCV (fL)	46.06 \pm 0.56	50.50 \pm 1.17*	54.20 \pm 0.91*
MCH (pg)	17.61 \pm 0.23	18.93 \pm 0.79	16.80 \pm 0.38*
MCHC (g/dL)	38.33 \pm 0.42	37.93 \pm 1.97	31.08 \pm 0.65*
Female			
HGB (g %)	12.35 \pm 0.80	12.46 \pm 0.58	14.25 \pm 0.52*
RBC (x10 ⁶ /mm ³)	6.89 \pm 0.40	6.79 \pm 0.27	7.90 \pm 0.38*
WBC (x10 ³ /mm ³)	10.13 \pm 2.91	10.45 \pm 2.77	11.78 \pm 3.60
PLT (x10 ⁵ /mm ³)	8.87 \pm 1.79	7.94 \pm 0.59	9.38 \pm 1.81
PCV (%)	32.73 \pm 1.90	33.61 \pm 1.61	45.31 \pm 2.03*
MCV (fL)	47.58 \pm 0.75	49.58 \pm 1.23*	57.38 \pm 1.17*
MCH (pg)	17.88 \pm 0.33	18.30 \pm 0.37	18.01 \pm 0.41
MCHC (g/dL)	37.66 \pm 0.75	37.05 \pm 0.95	31.4 \pm 0.42*

Values are presented as mean \pm SD, * significantly different from control, $p < 0.05$
VA¹ is a group of rats that received treatment of VA (1000 mg/kg p.o.) for 2 weeks and were then sacrificed

VA² is a group of rats that received treatment of VA (1000 mg/kg p.o.) for 2 weeks, kept under observation for an additional 2 weeks without treatment, and then sacrificed

VA: Vanillic acid, HGB: Hemoglobin, RBC: Red blood cell, WBC: White blood cell, PLT: Platelet, PCV: Packed cell volume, MCV: Mean corpuscular cell volume, MCH: Mean cell hemoglobin, MCHC: Mean cell haemoglobin concentration, SD: Standard deviation

in the treatment and satellite groups did not show any major irregularities in comparison to normal control group rats.

Microscopically, normal histomorphological structures with intact length of nerve fibers and normal cellular details were observed in tissue sections of the sciatic nerve. Sections of the brain showed intact supporting matrix and normal histomorphological structures of neurons. Heart sections of the treatment group revealed no changes in the structures of cardiac muscle fiber, and cardiac fibers were found to be organized in a compact and dense manner, having normal nuclei and cell striation with intact length. Renal tissue slices revealed no major structural alteration in renal tubules and glomeruli. Liver tissue showed normal structures of hepatocytes, central veins, and portal triads in intact hepatic parenchyma. Hepatocytes had normal intact nuclei and cellular borders and were arranged as cords. Histopathological sections did not show any inflammatory or metabolic changes. Representative sections of the histological studies are shown in Figure 1.

DISCUSSION

VA is a flavoring agent and found to have diverse pharmacological actions.⁷⁻²⁸ The safety of VA in future use may be a major concern specifically to make a decision about the optimum dose and to avoid untoward effects, but such information is lacking in the present scientific literature. A subacute toxicity study is preliminary to a chronic study.^{37,43} In addition, the results of the present study will not only enrich the pharmacological profile of VA but also encourage evidence-based pharmacotherapeutic use. In the light of these facts, we conducted a subacute toxicity study. Initially, a limit test was carried out, which helped us to make a decision about

the dose of VA for the subacute toxicity study by oral administration of one dose of 2000 mg/kg. Rats showed no signs of toxicity or mortality. Hence, it can be concluded that VA (1000 mg/kg b.w.) could be safe for use in a subacute toxicity study.

The study was designed by referring to OECD TG 407 (2008).³⁷ All essential examinations were included in the study, such as daily observation for toxic signs, mortality, measurement of weights, water intake, food consumption, all hematological and biochemical estimations within the blood, gross necropsy, and histopathological studies of the vital internal organs. However, we would like to declare that not all examination mentioned in OECD TG 407 were included in the study (such as urine analysis, estimation of T3, T4, TSH hormone, and cholinesterase).

Clinical observation for toxic signs, food and water consumption, and body weight measurements helped us to monitor progression from covert toxicity to overt signs. If the rat is not in a state of well-being it will not consume enough food or drink the necessary quantity of water. Therefore, clinical observation, food and water intake, and body weights are the indicators of general health and relative organ weight indicates organ toxicity, which may be revealed by hypertrophy and/or hyperplasia. Hence, these evaluations are pivotal in subacute toxicity studies.⁴³⁻⁴⁵ Rats in the treatment and satellite groups received VA (1000 mg/kg/day) orally for 2 weeks and they were monitored daily during the dosing period for any mortality or signs of toxicity like physiological activities (e.g., pilomotor reflex, abnormal breathing pattern, pupil size, lacrimation), abnormalities of the skin, mucous membranes, fur, and eyes, and occurrence of secretions. Postural changes and reactions to gait and handling were monitored along with the presence of

Table 2. Effect of vanillic acid on differential leukocyte count at the end of the study

Gender & parameters	Group		
	Control	VA ¹	VA ²
Male			
WBC (x10 ³ /mm ³)	11.88±3.74	11.30±1.61	11.30±1.61
Neutrophil %	44.66±8.80	45.83±10.34	59.12±7.88*
Eosinophil %	2.83±2.85	6.00±7.45	1.00±0.89
Lymphocyte %	51.00±9.71	47.50±15.78	39.00±6.95
Monocyte %	1.50±1.76	0.66±0.51	0.83±0.75
Female			
WBC (x10 ³ /mm ³)	10.13±2.91	10.45±2.77	11.78±1.47
Neutrophil %	44.00±17.29	47.33±11.72	60.00±5.93
Eosinophil %	6.00±4.60	4.00±4.33	0.66±0.81
Lymphocyte %	49.33±21.22	48.00±14.79	38.66±5.35
Monocyte %	0.66±0.51	0.66±0.51	0.66±0.51

Values are presented as mean ± SD, *significantly different from control, p<0.05

VA¹ is a group of rats that received treatment of VA (1000 mg/kg p.o.) for 2 weeks and were then sacrificed

VA² is a group of rats that received treatment of VA (1000 mg/kg p.o.) for 2 weeks, kept under observation for an additional 2 weeks without treatment, and then sacrificed VA: Vanillic acid,

VA: Vanillic acid, SD: Standard deviation, WBC: White blood cell

Table 3: Effect of vanillic acid on biochemical evaluations in wistar rats

Gender & parameters	Group		
	Control	VA ^a	VA ^s
Male			
BG (mg/dL)	89.26±10.42	97.22±9.83	91.58±7.18
BUN (mg/dL)	20.24±1.94	21.44± 2.12	20.82± 1.72
CR (mg/dL)	0.51±0.04	0.52±0.02	0.50±0.09
TP (g/dL)	6.48±0.76	7.21±0.42	7.18±0.41
ALB (g/dL)	4.97±0.23	5.17±0.22	5.02±0.21
TB (mg/dL)	0.21±0.03	0.23 ±0.03	0.22±0.04
DB (mg/dL)	0.062±0.01	0.093±0.07	0.086±0.04
SGOT (U/L)	84.32±7.32	83.62±3.63	81.17±7.23
SGPT (U/L)	32.81±3.73	34.33±3.05	32.58±2.11
ALP (U/L)	262.48±6.69	256.58±31.28	250.24±33.79
Ca (mg/dL)	11.21±0.78	11.19±0.63	10.74±1.09
K (mEq/L)	7.54±1.89	7.41±0.46	8.08±1.18
Cl (mEq/L)	103.76±5.69	110.53±14.61	106.79±7.19
Na (mEq/L)	86.03±4.90	63.66±7.46*	58.33±10.24*
P (mg/dL)	5.93±1.87	5.38±0.69	5.19±0.62
LDH (U/L)	361.44±82.50	408.53±78.92	384.54±34.89
HDL (mg/dL)	20±3.53	20.41±3.68	21.25±4.67
CHL (mg/dL)	81.44±7.92	79.23±6.26	82.27±7.61
TG (mg/dL)	110.66±6.22	113.39±7.29	112.88±5.45
Gender & Parameters	Group		
	Control	VA ^a	VA ^s
Female			
BG (mg/dL)	98.23±13.75	96.35± 8.04	97.52±11.86
BUN (mg/dL)	22.07±11.67	20.16±4.61	21.96 ±2.28
CR (mg/dL)	0.49±0.10	0.50±0.07	0.52±0.05
TP (g/dL)	7.37±0.48	7.24±0.19	7.19±0.35
ALB (g/dL)	4.99±0.39	5.05±0.36	5.12±0.26
TB (mg/dL)	0.24±0.04	0.22±0.04	0.25±0.04
DB (mg/dL)	0.081±0.05	0.11±0.05	0.09±0.04
SGOT (U/L)	73.08±9.29	77.67±4.96	80.121±7.20
SGPT (U/L)	28.80±3.94	30.26±3.77	32.58±3.05
ALP (U/L)	152.77±12.80	156.4±10.98	150.50±18.81
Ca (mg/dL)	11.38±1.02	11.15±1.06	10.99±1.01
K (mEq/L)	8.75±0.85	7.95±0.78	7.62±1.64
Cl (mEq/L)	106.77±7.27	107.5±6.62	110.60±9.49
Na (mEq/L)	82.33±15.46	71.79±9.86	70.17±5.85

P (mg/dL)	6.11±0.73	6.28±0.95	6.27±1.19
LDH (U/L)	473.90±117.43	424.96±11.68	397.71±29.38
HDL (mg/dL)	21.66±4.37	20±3.53	21.25±4.67
CHL (mg/dL)	87.96±4.14	85.83±6.58	86.73±5.66
TG (mg/dL)	108.37±8.08	106.12±5.54	105.27±4.53

Values are presented as mean ± SD. *significantly different from control, p<0.05
 VA^a is a group of rats which received treatment of VA (1000 mg/kg p.o) for 2 weeks and then sacrificed, VA^s is a group of rats which received treatment of VA (1000 mg/kg p.o) for 2 weeks; kept under observation for an additional 2 weeks without treatment and then sacrificed

BG: Blood glucose, BUN: Blood urea nitrogen, CR: Creatinine,TP: Total protein, ALB: Albumin, TB: Total bilirubin, DB: Direct bilirubin, SGOT: Serum glutamic-oxaloacetic transaminase, SGPT: Serum glutamine-pyruvic transaminase, ALP: Alkaline phosphatase, Ca: Calcium, K: Potassium, Cl: Chloride, Na: Sodium, P: Phosphate, LDH: Lactate dehydrogenase, HDL: High density lipoprotein, TG: Triglycerides

activities (e.g., immoderate grooming, continuous circling) or strange actions and clonic/tonic movements.³⁷ The treatment and satellite groups did not show any signs of toxicity or mortality within the course of the study period in comparison with the normal control group. In addition, the treatment and satellite groups showed a normal increment in body weight, water consumption, and food intake. Table 4 shows the effect of VA on relative internal organ weight. *The liver weight* of treated rats (male) was high in comparison to the *normal control rats*, but it was reversed in *the respective satellite group*. Increase in liver weight was considered an adaptive and nonadverse reaction.⁴⁶ Other internal organs in the treatment group did not manifest any remarkable impact on internal organ weight.

Biochemical estimations in the blood and hematological evaluations are important indicators in finding out the mechanism of toxic effects⁴⁷⁻⁴⁹ and the parameters were selected not only to detect target organ toxicity but also to detect pretoxic changes that might predict impending toxicity.^{38,43} The results are shown in Tables 1-3. The RBC, PCV, HGB, MCH, MCV, MCHC, and PLT counts of male and female rats in the treatment group did not reveal any remarkable increase when compared with the normal control group. Significant increases in all the hematological parameters were observed in rats in the satellite group, which were within the reference range, and this cannot be regarded as an undesirable effect of VA.⁵⁰ This can be justified by considering the contrasting situation of the decline in the RBC and HGB counts and other hematological evaluations, which confirmed anemic condition and untoward impact on functioning of erythropoietic stem cells. In addition, the WBC counts of rats in the treatment and satellite groups were within the reference range and had no remarkable difference when compared with the normal control group, although the neutrophil count was slightly increased in the satellite group in both sexes. This, however, cannot be considered a consequence of infection and inflammation. The eosinophil, monocyte, and lymphocyte counts in the treatment and satellite groups showed no remarkable changes when compared with the normal control group. Therefore, it might be concluded that VA is nontoxic and did not alter the function or efficacy of myeloid tissue.

Table 3 shows the effect of VA on biochemical evaluations. The plasma levels of TP, CR, TB, BG, ALB, electrolytes (K, Ca, Cl, P), BUN, ALP, and lipid profile (TG, TC, and HDL) were unaltered. However, some of the biochemical parameters showed nonsignificant alterations in male and female rats, which included DB, SGOT, SGPT, and Na levels. DB, SGOT, SGPT, and ALB levels are important indicators of liver function.⁵¹ In male treated and satellite group rats, an insignificant high level of DB was observed in comparison with the respective control group; even so no major alteration was reported in other liver function tests (SGOT and SGPT). In female rats, DB level was nonsignificantly increased among the treated rats, but reversed within the satellite group with slightly increased SGPT and SGOT levels in the treatment and satellite groups. All the alterations were nonsignificant and not in coordination with the macroscopic and histopathological findings in the liver (Figure 1), conducted to correlate the biochemical findings of the liver.^{39,43} Furthermore, albumin levels were not significantly altered in female and male rats. On the basis of these findings, it can be concluded that VA does not have any subacute toxic effect on the liver.

The effect of VA on renal function was assessed by estimation of BUN, CR, TP, and LDH levels.^{52,53} No statistically remarkable

change was recorded in the renal functional parameters of male and female rats in the treatment and satellite groups. The above evaluations showed that oral administration of VA may not alter the renal function, which is in concurrence with normal renal macroscopic and histopathological findings (Figure 1) of female and male rats in the satellite and treatment groups.

Electrolytes (K, Na, P, and Ca) in serum were evaluated during subacute toxicity studies.^{54,55} In our study, P, K, and Ca evaluation did not show any *statistically* remarkable change within the treatment and satellite groups in comparison with the normal control group. Although a significant decline in Na level was observed in male rats in the treatment and satellite groups, a statistically insignificant high level was reported in female rats in the treatment group in comparison with the normal control group. Based on the available knowledge of electrolyte balance, we can propose the probable mechanism behind reduced serum Na level. Firstly, it could be increased urinary loss and high cellular uptake.⁵⁶ Secondly, the process may be mediated by antidiuretic hormone and atrial natriuretic peptide.⁵⁶ However, this might not be viewed as a serious unsafe effect because a Na level below 20 mEq/L can only indicate Na leakage from damaged renal tubules or hypovolemia⁵⁷ or this effect can be recognized as a side effect as in the case of all classes of antidepressant drugs.⁵⁸ Repeated administration of

Table 4. Effect of vanillic acid on relative organ weights of Wistar rats

Organ weight (g % body weight)			
Treatment group			
Organs	Control	VA ¹	VA ^s
Male			
Lung	0.47±0.01	0.46±0.01	0.48±0.01
Heart	0.37±0.01	0.39±0.05	0.38±0.01
Liver	3.71±0.04	3.76±0.05*	3.69±0.01
Spleen	0.37±0.01	0.37±0.01	0.38±0.01
Kidney	0.47±0.001	0.45±0.02	0.48±0.001
Testis	0.63±0.02	0.61±0.03	0.60±0.03
Adrenal	0.017±0.001	0.016±0.001	0.016±0.001
Female			
Lung	0.49±0.001	0.48±0.004	0.49±0.01
Heart	0.31±0.02	0.26±0.05	0.28±0.01
Liver	2.92±0.11	2.78±0.23	2.82±0.17
Spleen	0.25±0.01	0.23±0.02	0.22±0.02
Kidney	0.46±0.07	0.39±0.03	0.39±0.06
Ovary	0.11±0.01	0.09±0.005	0.091±0.01
Adrenal	0.016±0.001	0.014±0.001	0.016±0.001

Values are presented as mean ± SD. *significantly different from control, p<0.05
VA¹ is a group of rats that received treatment of VA (1000 mg/kg p.o.) for 2 weeks and were then sacrificed, VA^s is a group of rats that received treatment of VA (1000 mg/kg p.o.) for 2 weeks, kept under observation for an additional 2 weeks without treatment, and then sacrificed

SD: Standard deviation, VA: Vanillic acid

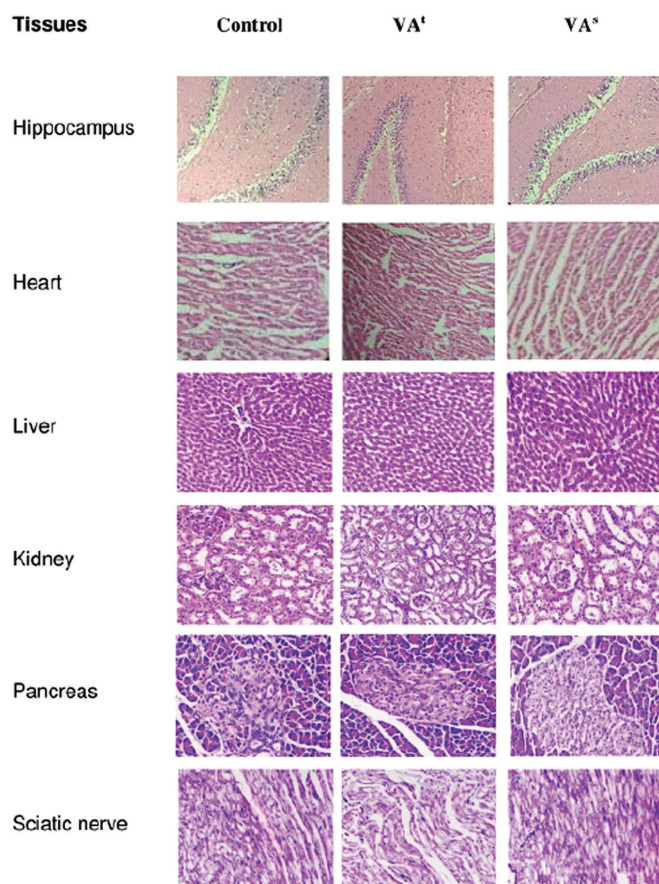


Figure 1. Effect of vanillic acid on the histomorphology of the vital organs of the rat

VA: Vanillic acid

VA does not affect the lipid profile of male and female rats. Thus, it is apparent that oral dosing of VA does not influence the electrolyte balance or the process of lipid metabolism.

Gross necropsy and histopathological studies represent the cornerstone within the process of safety evaluation before trials in human patients, essential to find out any relationship and relevance of treatment-related findings.^{39,43} In our study, the toxic effect on internal vital organs (i.e. brain, heart, liver, kidney, and sciatic nerve) was evaluated by gross necropsy and histopathological studies (Figure 1), which revealed no abnormality in any vital major organs. Thus, the result indicates that the VA is reasonably safe at the selected subacute dose.

CONCLUSION

VA is a polyphenol with diverse pharmacological actions, but no information on subacute toxicity studies is available in the current literature. To enrich its pharmacological profile and encourage its evidence-based pharmacotherapeutic use, a subacute toxicity study was conducted using experimental rats. To summarize, no mortality or clinical toxic signs were recorded during the study period; normal rises in body and internal organ weight were observed. The processes of leukopoiesis, erythropoiesis, and physiology of internal organs were not changed and no structural deformities were detected in the gross necropsy or histopathological studies of vital internal organs. The serum Na level was decreased in male Wistar rats with no major changes in levels of the other electrolytes, and this cannot be categorized as a major toxic effect. Hence, it can be concluded that the VA is safe in experimental rats during subacute toxicity studies. Further subchronic and chronic toxicological research is needed to investigate the safety characteristics of VA.

ACKNOWLEDGEMENTS

The authors really appreciate the assistance provided by NIRMA University and AI's Kalsekar Technical Campus to finish the study. The authors also appreciate the financial support given by Mumbai University to finish the research work.

Conflicts of interest: No conflict of interest was declared by the authors. The authors alone are responsible for the content and writing of the paper.

REFERENCES

- Lesage ML, Delattre M, Haon M, Thibault JF, Ceccaldi BC, Brunerie P, Asther M. A two-step bioconversion process for vanillin production from ferulic acid combining *Aspergillus niger* and *Pycnoporus cinnabarinus*. *J Biotechnol*. 1996;50:107-113.
- Civolani C, Barghini P, Roncetti AR, Ruzzi M, Schiesser A. Bioconversion of ferulic acid into vanillic acid by means of a vanillate-negative mutant of *Pseudomonas fluorescens* strain BF13. *Appl Environ Microbiol*. 2000;66:2311-2317.
- Duke JA. *Database of Phytochemical Constituents of GRAS Herbs and Other Economic Plants*. Boca Raton; CRC Press; 1992.
- Pacheco-Palencia LA, Mertens-Talcott S, Talcott ST. Chemical composition, antioxidant properties, and thermal stability of a phytochemical enriched oil from Acai (*Euterpe oleracea* Mart.). *J Agric Food Chem*. 2008;56:4631-4636.
- Galvez MC, Barroso CG, Pérez-Bustamante JA. Analysis of polyphenolic compounds of different vinegar samples. *Z Lebensm Unters Forch*. 1994;199:29-31.
- Prabhakar PK, Doble M. Effect of Natural Products on Commercial Oral Antidiabetic Drugs in Enhancing 2-Deoxyglucose Uptake by 3T3-L1 Adipocytes. *Ther Adv Endocrinol Metab*. 2011;2:103-114.
- Chang WC, WU JSB, Chen CW, Kuo PL, Chien HM, Wang YT, Shen SC. Protective Effect of Vanillic Acid against Hyperinsulinemia, Hyperglycemia and Hyperlipidemia via Alleviating Hepatic Insulin Resistance and Inflammation in High-Fat Diet (HFD)-Fed Rats. *Nutrients*. 2015;7:9946-9959.
- Klinger W, Kersten L. The effect of vanillic acid diethylamide on the blood sugar in rabbits and ascorbic acid in the liver and adrenal glands in rats. *Acta Biol Med Ger*. 1963;10:689-690.
- Calizto-Compos C, Carvalho TT, Hohmann MSN, Pinho-Ribeiro FA, Fattori V, MAnchope MF, Zarpelon AC, Baracat MM, Georgetti SR, Casagrande R, Verrri Jr WA. Vanillic Acid Inhibits Inflammatory Pain by Inhibiting Neutrophil Recruitment, Oxidative Stress, Cytokine Production, and NFκB Activation in Mice. *J Nat Prod*. 2015;78:1799-1808.
- Kim MC, Kim SJ, Kim DS, Jeon YD, Park SJ, Lee HS, Um JY, Hong SH. Vanillic acid inhibits inflammatory mediators by suppressing NF-κB in lipopolysaccharide-stimulated mouse peritoneal macrophages. *Immunopharmacol Immunotoxicol*. 2011;33:525-532.
- Tai A, Sawano T, Ito H. Antioxidative properties of vanillic acid esters in multiple antioxidant assays. *Biosci Biotechnol Biochem*. 2012;76:314-318.
- Chou TH, Ding HY, Hung WJ, Liang CH. Antioxidative characteristics and inhibition of alpha-melanocyte-stimulating hormone-stimulated melanogenesis of vanillin and vanillic acid from *Origanum vulgare*. *Exp Dermatol*. 2010;19:742-750.
- Dianat M, Radmanesh E, Badavi M, Goudarzi G, Mard SA. The effects of PM10 on electrocardiogram parameters, blood pressure and oxidative stress in healthy rats: the protective effects of vanillic acid. *Environ Sci Pollut Res Int*. 2016;23:19551-19560.
- Dianat M, Hamzavi GR, Badavi M, Samarbafe-zadeh A. Effect of vanillic acid on ischemia-reperfusion of isolated rat heart: Hemodynamic parameters and infarct size assays. *Indian J Exp Biol*. 2015;53:641-646.
- Stanely Mainzen Prince P, Dhanasekar K, Rajakumar S. Vanillic acid prevents altered ion pumps, ions, inhibits Fas-receptor and caspase mediated apoptosis-signaling pathway and cardiomyocyte death in myocardial infarcted rats. *Chem Biol Interact*. 2015;232:68-76.
- Yemiş GP, Pagotto F, Bach S, Delaquis P. Thermal tolerance and survival of *Cronobacter sakazakii* in powdered infant formula supplemented with vanillin, ethyl vanillin, and vanillic acid. *J Food Sci*. 2012;77:M523-M527.
- Huang SM, Hsu CL, Chuang HC, Shih PH, Wu CH, Yen GC. Inhibitory effect of vanillic acid on methylglyoxal-mediated glycation in apoptotic Neuro-2A cells. *Neurotoxicology*. 2008;29:1016-1022.
- Motiram Kakalij R, Tejaswini G, Patil MA, Dinesh Kumar B, Diwan PV. Vanillic Acid Ameliorates Cationic Bovine Serum Albumin Induced Immune Complex Glomerulonephritis in BALB/c Mice. *Drug Dev Res*. 2016;77:171-179.
- Singh JC, Kakalij RM, Kshirsagar RP, Kumar BH, Komakula SS, Diwan PV. Cognitive effects of vanillic acid against streptozotocin-induced neurodegeneration in mice. *Pharm Biol*. 2015;53:630-636.
- Alzweiri M, Al-Hiari Y. Evaluation of vanillic acid as inhibitor of carbonic anhydrase isozyme III by using a modified Hummel-Dreyer method: approach for drug discovery. *Biomed Chromatogr*. 2013;27:1157-1161.

21. Alzweiri M, Al-Hiari Y. Evaluation of vanillic acid as inhibitor of carbonic anhydrase isozyme III by using a modified Hummel-Dreyer method: approach for drug discovery. *Biomed Chromatogr.* 2013;27:1157-1161.
22. Dhananjaya BL, Nataraju A, Raghavendra Gowda CD, Sharath BK, D'Souza CJ. Vanillic acid as a novel specific inhibitor of snake venom 5'-nucleotidase: a pharmacological tool in evaluating the role of the enzyme in snake envenomation. *Biochemistry (Mosc).* 2009;74:1315-1319.
23. Gitzinger M, Kemmer C, Fluri DA, El-Baba MD, Weber W, Fussenegger M. The food additive vanillic acid controls transgene expression in mammalian cells and mice. *Nucleic Acids Res.* 2012;40:e37.
24. Kim SJ, Kim MC, Um JY, Hong SH. The beneficial effect of vanillic acid on ulcerative colitis. *Molecules.* 2010;15:7208-7217.
25. Itoh A, Isoda K, Kondoh M, Kawase M, Watari A, Kobayashi M, Tamesada M, Yagi K. Hepatoprotective effect of syringic acid and vanillic acid on CCl₄-induced liver injury. *Biol Pharm Bull.* 2010;33:983-987.
26. Klinger W, Kersten L. The analeptic effect of vanillic acid diethylamide. *Acta Biol Med Ger.* 1962;9:67-78.
27. Varma RS, Shukla A, Chatterjee RK. Evaluation of vanillic acid analogues as a new class of antifilarial agents. *Indian J Exp Biol.* 1993;31:819-821.
28. Fruhmann G, Specht H. Respiratory stimulation with vanillic acid diethylamide in chronic bronchitis and respiratory insufficiency. *Med Klin.* 1970;65:1570-1576.
29. Mårdh G. Vanillic acid, a metabolite of 4-hydroxy-3-methoxyphenylglycol and 4-hydroxy-3-methoxymandelic acid in man. *J Neurochem.* 1984;43:522-525.
30. Price J. The dependence of vanillic acid excretion on urinary pH. *Clin Chim Acta.* 1969;26:413-418.
31. Schmid E, Tautz NA, Bauersachs E, Krautheim J. The excretion of vanilmandelic acid, vanillic acid, homovanillic acid and 5-hydroxyindoleacetic acid by urine in smokers and non-smokers. *Arzneimittelforschung.* 1968;18:819-821.
32. Brisse B, Bender F. Excretion of vanillin mandelic acid and vanillic acid in healthy subjects and patients with circulatory and liver diseases. *Verh Dtsch Ges Inn Med.* 1967;73:1114-1116.
33. Smith P, Bennett AM. Vanillic acid excretion during stress. *Nature.* 1958;181:709.
34. Guldiken B, Ozkan G, Catalkaya G, Ceylan FD, Ekin Yalcinkaya I, Capanoglu E. Phytochemicals of herbs and spices: Health versus toxicological effects. *Food Chem Toxicol.* 2018;119:37-49.
35. Brown AC. Liver toxicity related to herbs and dietary supplements: Online table of case reports. Part 2 of 5 series. *Food Chem Toxicol.* 2017;107:472-501.
36. Tabasum S, Khare S, Jain K. Subchronic Toxicity Assessment of Orally Administered Methanol (70%) Seed Extract of *Abrus precatorius* L. in Wistar Albino Rats. *Turk J Pharm Sci.* 2019;16:88-95.
37. The Organisation of Economic Co-operation and Development (OECD-2008), Test No. 407: Repeated Dose 28-day Oral Toxicity Study in Rodents, OECD Guidelines for the Testing of Chemicals, Section 4, OECD Publishing, Paris, 1-13.
38. Hayes AW. Principles and Methods of Toxicology (5th ed). Boca Raton; CRC Press.2007;1223-1245.
39. Greaves P. Histopathology of Preclinical Toxicity Studies: Interpretation and Relevance in Drug Safety Evaluation (4th ed). New York. Academic Press. 2012;1-2.
40. Comptes Rendus Hebdomadaires des Seances, Academie des Sciences. 1956;243:609.
41. Ohta S, Furukawa M, Shinoda M. Studies on chemical protectors against radiation. 1984;104:793-797.
42. ChemIDplus chemical Data Bank. Bethesda (MD): National Library of Medicine (US); 2019 [updated 2019 Apr 4; cited 2019 Apr 13]. Vanillic acid; UNII Number: GM8Q3JM2Y8; [about 3 p.]; Available from: <https://chem.nlm.nih.gov/chemidplus/sid/0000121346>
43. Ecobichon, DJ. The Basis of Toxicity Testing. Boca Raton; CRC Press. 1997;94-100.
44. Wang J, Sun F, Tang S, Zhang S, Lv P, Li J, Cao X. Safety assessment of vitacoxib: Acute and 90-day sub-chronic oral toxicity studies. *Regul Toxicol Pharmacol.* 2017;86:49-58.
45. Thanabhorn S, Jaijoo K, Thamaree S, Ingkaninan K, Panthong A. Acute and subacute toxicity study of the ethanol extract from *Lonicera japonica* Thunb. *J Ethnopharmacol.* 2006;107:370-373.
46. Hall AP, Elcombe CR, Foster JR, Harada T, Kaufmann W, Knippel A, Küttler K, Malarkey DE, Maronpot RR, Nishikawa A, Nolte T, Schulte A, Strauss V, York MJ. Liver hypertrophy: a review of adaptive (adverse and non-adverse) changes--conclusions from the 3rd International ESTP Expert Workshop. *Toxicol Pathol.* 2012;40:971-994.
47. Wang J, Sun F, Tang S, Zhang S, Cao X. Acute, mutagenicity, teratogenicity and subchronic oral toxicity studies of diaveridine in rodents. *Environ Toxicol Pharmacol.* 2015;40:660-670.
48. Nyarko AK, Okine LK, Wedzi RK, Addo PA, Ofosuhen M. Subchronic toxicity studies of the antidiabetic herbal preparation ADD-199 in the rat: absence of organ toxicity and modulation of cytochrome P450. *J Ethnopharmacol.* 2005;97:319-325.
49. Han CT, Kim MJ, Moon SH, Jeon YR, Hwang JS, Nam C, Park CW, Lee SH, NA JB, Park CS, Park HW, Lee JM, JAng HS, Park SH, Han KG, Choi YW, Lee HY, Kang JK. Acute and 28-Day Subacute Toxicity Studies of Hexane Extracts of the Roots of *Lithospermum erythrorhizon* in Sprague-Dawley Rats. *Toxicol Res.* 2015;31:403-414.
50. Kanu KC, Ijioma SN, Atiata O. Haematological, Biochemical and Antioxidant Changes in Wistar Rats Exposed to Dichlorvos Based Insecticide Formulation Used in Southeast Nigeria. *Toxics.* 2016;4:28.
51. Mathew S, Dushyant S. Interpretation of abnormal liver function tests. *Hosp Med Clin.* 2014;3:e139-e148.
52. Kluwe WM. Renal function tests as indicators of kidney injury in subacute toxicity studies. *Toxicol Appl Pharmacol.* 1981;57:414-424.
53. Bhargava AS, Khater AR, Gunzel P. The correlation between lactate dehydrogenase activity in urine and serum and experimental renal damage in the rat. *Toxicol Lett.* 1978;1:319-332.
54. Unuofin JO, Otunola GA, Afolayan AJ. Evaluation of acute and subacute toxicity of whole-plant aqueous extract of *Vernonia mespilifolia* Less. in Wistar rats. *J Integr Med.* 2018;16:335-341.
55. Amresh G, Singh PN, Rao CV. Toxicological screening of traditional medicine Laghupatha (*Cissampelos pareira*) in experimental animals. *J Ethnopharmacol.* 2008;116:454-460.
56. Graber M, Corish D. The electrolytes in hyponatremia. *Am J Kidney Dis.* 1991;18:527-545.
57. Pierro A, De Coppi P, Eaton S. Neonatal physiology and metabolic considerations. In: Coran AG, ed. *Pediatric Surgery*. Philadelphia; Saunders. 2012;89-107.
58. Satyakam M, Mnas RS, Neelmadhav R. Amitriptyline induced hyponatremia. *Delhi Psychiatry Journal.* 2014;17:209-210.



The Effect of *Rusa unicolor* Antler Deer Extracts from East Kalimantan in Bone Turnover Cell Models

Doğu Kalimantan'dan *Rusa unicolor* Geyiği Boynuzu Ekstraktlarının Kemik Dönüşümü Hücre Modelleri Üzerine Etkisi

Retno WIDYOWATI^{1*}, Suciati SUCIATI¹, Dewi Melani HARYADI², Hsin-I CHANG³, IPG Ngurah SURYAWAN⁴, Agung Widi UTAMA⁴

¹Airlangga University Faculty of Pharmacy, Department of Pharmacognosy and Phytochemistry, Surabaya, Indonesia

²Airlangga University Faculty of Pharmacy, Department of Pharmaceutics, Surabaya, Indonesia

³National Chiayi University Clinic of Biochemical Science and Technology, Taiwan, China

⁴UPTD Pembibitan dan Inseminasi Buatan, Dinas Peternakan dan Kesehatan Hewan Provinsi Kalimantan Timur, Indonesia

ABSTRACT

Objectives: Osteoporosis is a condition characterized by skeletal degradation of osseous tissue resulting in an escalated chance of broken bones. Traditionally, *Rusa unicolor* horn from East Kalimantan is used to treat many diseases, including conditions associated with bone turnover. The aim of the present research was to analyze the effects of 70% ethanol and aqueous extracts of *R. unicolor* antler's horn from East Kalimantan on nitric oxide inhibition, osteoblast differentiation, and mineralization related to bone turnover.

Materials and Methods: Nitric oxide inhibition of the extracts in lipopolysaccharide-stimulated RAW 264.7 macrophages was evaluated by Griess reagent, while the effects of extracts on osteoblast differentiations were measured by alkaline phosphatase in *p*-nitrophenyl phosphate. Their effects on mineralization was determined using alizarin red staining.

Results: The 70% ethanol and aqueous extracts inhibited cell inflammation (40% and 80%, respectively) and stimulated osteoblast differentiation (65% and 52%, respectively). In the mineralization test, the aqueous extract showed an effect two times higher than that of 70% ethanol extract.

Conclusion: The extracts can effectively degrade inflammatory marker expression and preserve osteoblast functions.

Key words: *Rusa unicolor*, antler, alkaline phosphatase, mineralization, nitric oxide inhibition

ÖZ

Amaç: Osteoporoz artmış kemik kırılmalarıyla sonuçlanan kemik dokusundaki iskelet degradasyonu ile karakterize bir durumdur. Geleneksel olarak, Doğu Kalimantan'dan *Rusa unicolor* boynuzu kemik dönüşümü dahil, birçok hastalığın tedavisinde kullanılır. Bu çalışmanın amacı Doğu Kalimantan *R. unicolor* geyiği boynuzunun %70'lik etanol ve sulu ekstraktlarının nitrik oksit inhibisyonu, osteoblast farklılaşması ve kemik dönüşümüyle ilişkili mineralizasyon üzerine etkilerinin araştırılmasıdır.

Gereç ve Yöntemler: Ekstratların lipopolisakkarit ile stimüle edilen RAW 264,7 makrofajlarında nitrik oksit inhibisyonu Griess belirteciyle değerlendirilirken, ekstraktların osteoblast farklılaşması üzerine etkileri *p*-nitrofenil fosfatta alkalik fosfataz ölçülerek belirlenmiştir. Mineralizasyon üzerine etkileri ise, alizarin kırmızısı kullanılarak belirlenmiştir.

Bulgular: %70'lik etanol ve sulu ekstraktlarının hücre enflamasyonunu inhibe ettiği (sırasıyla %40 ve %80) ve osteoblast farklılaşmasını stimüle ettiği (sırasıyla %65 ve %52) belirlenmiştir. Mineralizasyon testinde, sulu ekstre etanol ekstrelerine göre iki kat daha yüksek etki göstermiştir.

Sonuç: Ekstrelerin etkin bir şekilde enflamasyon belirteci ekspresyonunun degrades etmiş ve osteoblast işlevlerini korumaktadır.

Anahtar kelimeler: *Rusa unicolor*, geyik, alkalik fosfataz, mineralizasyon, nitrik oksit inhibisyonu

*Correspondence: E-mail: rr-retno-w@ff.unair.ac.id, Phone: +6281615886978 ORCID-ID: orcid.org/0000-0003-0572-7551

Received: 18.01.2019, Accepted: 30.05.2019

©Turk J Pharm Sci, Published by Galenos Publishing House.

INTRODUCTION

Osteoporosis is a bone condition characterized by skeletal degradation of osseous tissue leading to an increased chance of broken bones.¹ It is a condition of old age and supposed to increase with rising age and lifespan. At present, more than 200 million people worldwide are estimated to suffer from osteoporosis.² The latest statistical data from the International Osteoporosis Foundation showed that one in three women above 50 years old and one in five men shall suffer osteoporosis for the rest of their lives.³ Indonesia also has the same problem, whereas the number of osteoporosis sufferers is higher than the latest data (>19.7%). In Indonesia, the number of old people is supposed to increase by 14% in 1990-2025, while menopausal women in 2000 contributed to an increase of 15.5 million to 24 million in 2015.⁴

For thousands of years, natural plants and animal resources have played a vital role in the development of pharmaceutical drugs and food supplements for the treatment and prevention of diseases.⁵ One of such resources with great medicinal value is the antler of the deer belonging to the family Cervidae. It is an efficient traditional medicine for strengthening bones and tendons. Researchers assume that the lack of glycosaminoglycans caused disproportion between cartilage erosion and regeneration in osteoarthritis sufferers. These substances have an essential role in cartilage's structural integrity. Glycosaminoglycan is isolated from four parts of the antler of deer (*Cervus elaphus*), namely the tip, upper part, middle, and base, through cellulose acetate electrophoresis, enzymatic digestion, and chromatography. Chondroitin sulfate, which contains 88% uronic acid, is the principal glycosaminoglycan. Apart from chondroitin sulfate, deer antler also contains hyaluronic acid, dermatan sulfate, and keratan sulfate in small quantities.⁶ Several researches also report that deer antler can reduce or even eradicate symptoms related to osteoarthritis.

For decades, Chinese people have traditionally used deer antler extract to strengthen bones, enhance virility, feed blood, supplement vitality, and enhance male and female sexual organs.⁷ A good number of products analogous to deer antler show great potency on illnesses related to aging, infection, and immune dysfunction. However, the active constituents responsible for this mechanism are unclear.⁸⁻¹³ According to some preclinical studies, deer antler products are able to reduce animals osteoporosis.¹⁴⁻¹⁶ Lee et al.¹⁷ showed that facilitation of osteoblast proliferation and mineralization are some of the principal mechanisms of the effects of deer antler products. Furthermore, Choi et al.¹⁸ reported inhibition of osteoclast differentiation by deer antlers. Protein, calcium, lipids, ash, collagen, proteoglycan, testosterone, cholesterol, estradiol, glutamic acid, insulin-like growth factor 1, iron, aspartic acid, and glycine are some of the constituents contained in antler.^{19,20}

In the present study, we evaluated 70% ethanol and aqueous extract of *Rusa unicolor* antler from East Kalimantan Indonesia toward the effect of osteoblast differentiation, mineralization, and expression of inflammatory markers by measuring alkaline phosphatase (ALP), alizarin red staining (ARS), and nitric oxide (NO) inhibition values, respectively.

MATERIALS AND METHODS

Cell culture and reagents

Chemicals such as an acid phosphatase leukocyte kit and ALP colorimetric assay kit were obtained from Sigma-Aldrich Co. (St Louis, MO, USA). Cell culture substances and solvents were bought from Thermo Fisher Scientific (Waltham, MA, USA) and were analytical grade (J.T. Baker, USA). Macrophages (RAW 264.7) and osteoblast cells (7F2) were obtained from the Food Industry Research and Development Institute, Taiwan, and refined in Dulbecco's Modified Eagle's Medium (DMEM). They were further strengthened with 10% v/v fetal bovine serum (FBS), 100 units/mL penicillin, and 100 µg/mL streptomycin. Cells were refined in an incubator with 5% CO₂ at 37°C.

Antler materials

Deer antler of *R. unicolor* was collected in the middle of March 2017 in UPTD (Technical Implementation Service Unit) of East Kalimantan, Indonesia, and voucher specimens were deposited at the UPTD of East Kalimantan, Indonesia.

R. unicolor antler extraction

R. unicolor antler was obtained from UPTD of East Kalimantan, Indonesia. It was powdered (991 g) and extracted with 70% ethanol-aqueous (2.0 Lx3) using maceration. The 70% ethanol solution was concentrated using a rotary evaporator to obtain 70% ethanol extract (Et-TL, 35.0 g). In addition, the deer antler (430 g) was extracted with 100% water (1.0 Lx3) by applying continuous percolation. The aqueous solution was freeze dried to obtain aqueous extract (A-TL, 6.1 g).

Cell viability assay

The RAW 264.7 macrophages were cultured at a density of 5x10⁴ macrophages/well in 96-well plates using DMEM consisting of 10% FBS, 100 units/mL penicillin, and 100 µg/mL streptomycin for macrophage growth studies. After 24 h, the samples (Et-TL and A-TL extracts of *R. unicolor* antler) were incubated at 10, 50, and 100 µg/mL for another 24 h. Afterwards, the medium was discarded and the macrophages were incubated with 200 µL of 3-(4,5-dimethylthiazol-2-yl)- and 100 µL of 2,5-diphenyltetrazolium bromide (MTT) reagents (100 µg/mL) for 4 h. Then 100 µL of dimethyl sulfoxide was added to disperse the formazan crystals. The absorbance was determined at 570 nm using an enzyme-linked immunosorbent assay (ELISA) reader. All treatments were carried out in triplicate and expressed in % macrophage viability of unprocessed control macrophages. A similar method was carried out on 7F2 osteoblast-like cells at 10⁴ cells/well in DMEM containing 10% FBS, 100 units/mL penicillin, and 100 µg/mL streptomycin.²¹

Nitrite measurement

The 5x10⁵ cells/well of RAW 264.7 macrophages were seed in 24-well plates and incubated with DMEM containing 10% FBS, 100 unit/mL penicillin, and 100 µg/mL streptomycin for 24 h. The macrophages were activated with 500 ng/mL lipopolysaccharide (LPS) and evaluated with samples (Et-TL and A-TL extracts) at 10-100 µg/mL for 1 day. The emitted NO was estimated by weighing the nitrite concentration. Then 100

μL of samples were added with 100 μL of Griess reagent to 96-well plates for 15 min at room temperature. An ELISA reader was used to measure the absorbance at 550 nm. Furthermore, curves of standard calibration were processed using NaNO_2 to evaluate nitrite expression of macrophages with sensitivity and linear range values of 2.5 μM and 20-100 μM , respectively.²¹

Differentiation of alkaline phosphatase activity

The 10^4 cells/well of 7F2 osteoblast cells were plated in 24-well plates using DMEM containing 10% FBS, 50 $\mu\text{g}/\text{mL}$ ascorbic acid, and 5 mM β -glycerol phosphate (β -GP) with or without 10-100 $\mu\text{g}/\text{mL}$ Et-TL and A-TL extracts for 4 days of incubation (37°C in a 5% CO_2 atmosphere). Phosphate buffer saline (PBS) was used to wash the extracted supernatants. After that, a percentage of v/v triton solution was added, followed by incubation for 10 min at 37°C. For the ALP assay, the cell lysates were added with 200 μL of *p*-nitrophenyl phosphate and di-ethanolamine buffer to each well for 30 min at room temperature. Then 50 $\mu\text{L}/\text{well}$ NaOH solution was added to end the reaction, while an ELISA reader at 405 nm was used to evaluate the absorbance.²¹

Mineralization of the extracellular matrix

One milliliter of DMEM comprising 5 mM β -GP, 50 $\mu\text{g}/\text{mL}$ ascorbic acid (2GF medium), and 10% FBS was used to seed 10^4 cells/well of 7F2 osteoblast cells for 7 days in an incubator; 10-100 $\mu\text{g}/\text{mL}$ of Et-TL and A-TL extracts were also added to the growth medium. After 7 days, PBS and 75% v/v ethanol were used to wash the samples and they were dried at room temperature. The cells were dyed with 200 μL of 1% ARS for 1 h. A Nikon TI-E microscope and SPOT RT3 camera were used to record images of the cell morphology. Each well received 10% w/v cetylpyridinium chloride (400 μL) and was rocked for 10 min in order to disperse the calcium. The absorbance was finally evaluated at 560 nm using an ELISA reader.²¹

Statistical analysis

The experiments were carried out for three more consecutive times with similar sample. They are presented as mean \pm standard deviations. The paired t-test was used for the data analysis. The differences were significant at $p < 0.05$.

RESULTS

The effect of antler extract on cell viability and nitric oxide production

In the present research, the effects of Et-TL and A-TL extracts against inflammation associated with bone turnover were analyzed. Several researchers have reported the bioactivity impacts of deer bones and antlers from various nations, but there is no information on the pharmacological activity of deer antlers originating from Indonesia (*R. unicolor*).^{7,22-24}

Cytotoxic test samples (Et-TL and A-TL extracts) at different concentrations were incubated with RAW 264.7 macrophages for 1 day and were evaluated using the MTT method. Then the data were represented as the average cell viability. The A-TL extract did not show cytotoxicity compared to Et-TL

extracts (Figure 1), while the macrophage viability in Et-TL extracts (50 and 100 $\mu\text{g}/\text{mL}$) decreased significantly. Thus, the aqueous extract was not toxic toward the macrophages at the concentration series of 10-100 $\mu\text{g}/\text{mL}$ and was able to increase the cellular permeation of constituents therein.

The anti-inflammatory test of samples in RAW 264.7 macrophages stimulated by LPS was conducted by monitoring the NO inhibition. The Griess reagent was used to evaluate the nitrite value directly related to the amount of NO production in RAW 264.7 macrophages. These macrophages were treated with samples, after which the NO produced in the LPS-stimulated RAW 264.7 macrophages deteriorated significantly (Figure 2). The Et-TL extract prevented NO production up to 40% in 10 $\mu\text{g}/\text{mL}$. Similarly, A-TL extract reduced it up to 80% in the same concentration. LPS (500 ng/mL) in macrophages was not used as a control group because it had a total nitrite value of 100%.

The effect on ALP stimulation of 7F2 osteoblasts of 70% ethanol and aqueous extracts of deer antler

The effect of samples (Et-TL and A-TL extracts) on 7F2 osteoblastic cell line proliferation was determined by MTT test. The viability of cells in Et-TL extract decreased significantly (50

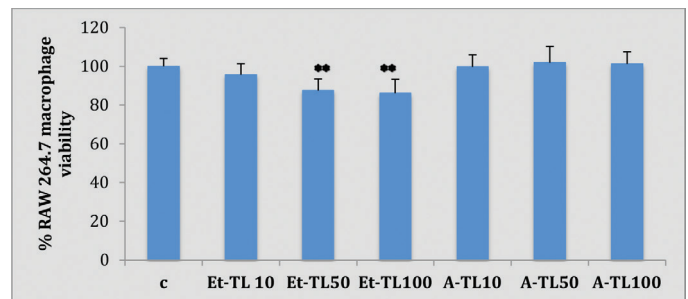


Figure 1. The effects of samples at 10, 50, and 100 $\mu\text{g}/\text{mL}$ on RAW 264.7 macrophage viability; C was the control medium without samples, Et-TL was 70% ethanol extract, A-TL was aqueous extract. Data are shown as the average of % cell viability to control for 24 h \pm standard deviation

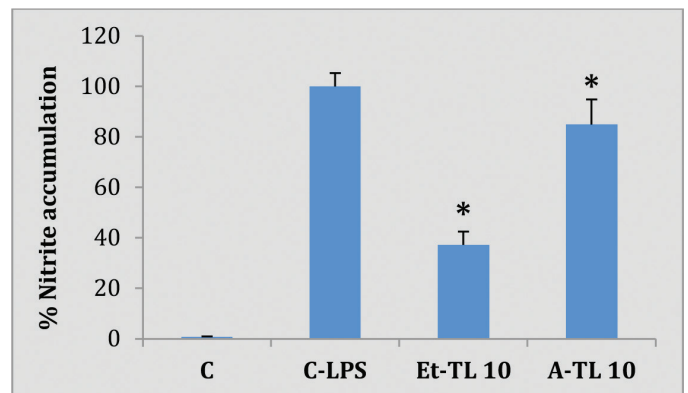


Figure 2. The effects of samples at 10 $\mu\text{g}/\text{mL}$ on NO production in LPS (500 ng/mL)-induced RAW 264.7 macrophages for 24 h; C-LPS was control of LPS, C was cells of the control group were not induced with LPS, Et-TL was 70% ethanol extract, A-TL was aqueous extract. The total nitrite produced by the cells of the LPS group is revealed as 100%. Results are shown as % of average \pm standard deviation. * $p < 0.05$ with respect to control
NO: Nitric oxide LPS: Lipopolysaccharide

and 100 $\mu\text{g}/\text{mL}$), but the value was more than 100%. It showed that a high concentration of Et-TL extract was not toxic even though the cell proliferation value decreased. On the other hand, cell viability of A-TL extract increased significantly (Figure 3). As a result, all deer antler extracts decreased cytotoxicity and raised cellular uptake. Then the ALP and mineralization experiments continued.

The ALP stimulated 7F2 osteoblast cells using Et-TL and A-TL extracts of deer antler were incubated for 4 days. The effects of test samples on the ALP assay increased in the 7F2 osteoblasts as opposed to the 2GF group. After 4 days, the A-TL and Et-TL extracts stimulated ALP activity to 65% and 52%, respectively (Figure 4).

The effect on mineralization of 7F2 osteoblasts of 70% ethanol and aqueous extracts of deer antler

The 7F2 osteoblast cells were cultured in 2GF medium to prompt osteoblast differentiation and mineralization. After 7 days of incubation, the effects of Et-TL and A-TL extracts of deer antler on osteoblast mineralization were examined using ARS, which determined the calcium content in the bone matrix. The Et-TL extract displayed stimulation of cell differentiation (Figure 4) and after 7 days this extract stimulated mineralization. The A-TL extract displayed better stimulation mineralization than 70% ethanol extract of deer antler (Figure 5).

The stains on ARS represented mineral deposits and were quantified by cetylpyridinium chloride extraction. The treated 7F2 osteoblast cells increased the ARS accumulation compared to the 2GF group. Photographs were used to represent the

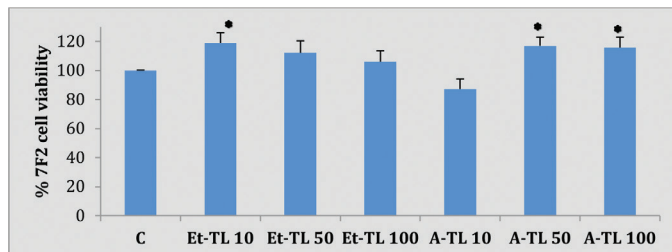


Figure 3. The effects of samples at 10, 50, and 100 $\mu\text{g}/\text{mL}$ on 7F2 cell viability; C was medium without sample, Et-TL was 70% ethanol extract, A-TL was aqueous extract. Data are shown as the average of % cell viability compared to control for 24 h \pm standard deviation

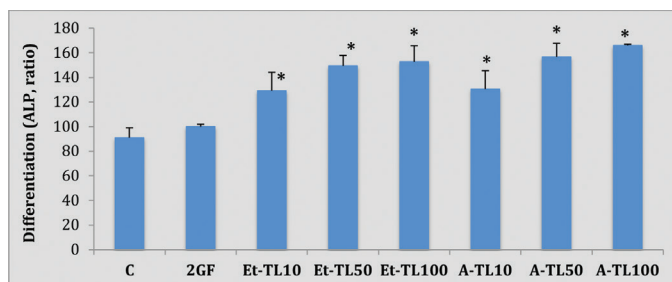


Figure 4. The effects of samples at 10, 50, and 100 $\mu\text{g}/\text{mL}$ on osteoblast differentiation (ALP) during 4 days of incubation; Et-TL was 70% ethanol extract, A-TL was aqueous extract. The 7F2 osteoblast cells were cultured in 2GF medium to produce osteoblast differentiation. Results are shown as % with average \pm standard deviation. * $p < 0.05$ with respect to 2GF
ALP: Alkaline phosphatase

mineralization process of osteoblast cells under a bright field. Mineralized nodule formation (red) was high in 7F2 osteoblast cells treated with Et-TL and A-TL extracts on day 7 under microscope observation (Figure 6). Identical patterns were also observed in ALP activity.

DISCUSSION

Bone metabolism is a lifelong process that occurs because mature bone tissue is lost (osteoclast activity) and new bone tissue is formed (osteoblast activity). Osteoclasts are multinucleated cells and involve nuclear factor kappa-B ligand (RANKL) as a stimulus of receptors and generated by macrophage precursor cells. The RAW 264.7 macrophages have a necessary role in the process of osteoclast formation and function.²⁵ Osteoclast function can be impaired due to degeneration of articular cartilage and synovial inflammation involving tumor necrosis factor- α , chemokines, and a number of inflammatory cytokines and interleukins (IL) such as IL-1 β , IL-6, IL-11, and IL-17. They cause bone loss by reducing osteoprotegerin (OPG) production and stimulating RANKL expression in osteoblasts and stromal cells. The NO inhibition of RAW 264.7 macrophages showed a

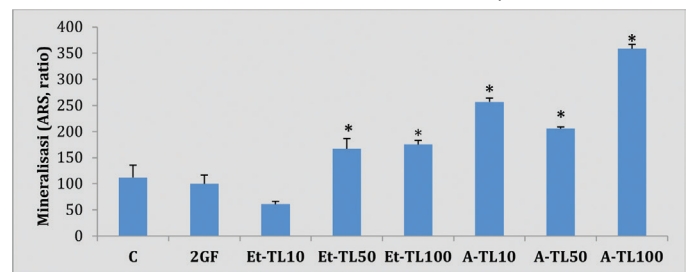


Figure 5. The effects of samples at 10, 50, and 100 $\mu\text{g}/\text{mL}$ on quantification mineralization assay during 7 days of incubation; Et-TL was 70% ethanol extract, A-TL was aqueous extract. ARS dye was measured by cetylpyridinium chloride extraction. The results are shown as % with average \pm standard deviation. * $p < 0.05$ with respect to 2GF
ARS: Alizarin red staining

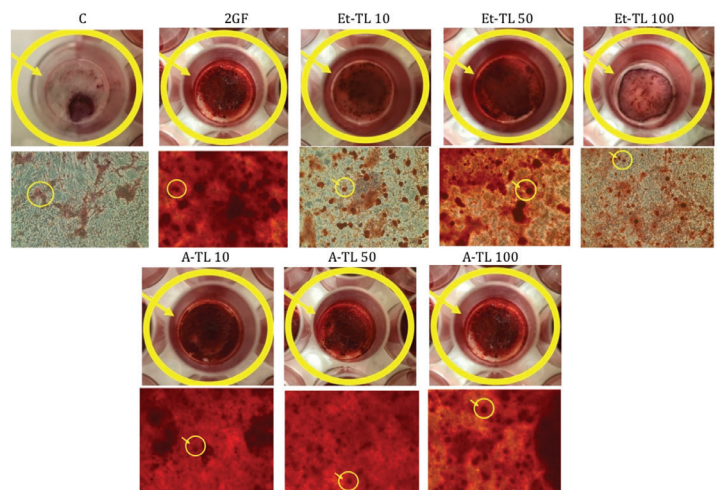


Figure 6. Histochemical staining of mineral deposition of samples at 10, 50, and 100 $\mu\text{g}/\text{mL}$; Et-TL was 70% ethanol extract, A-TL was aqueous extract. They were visualized using ARS staining (100x magnification). Red staining represents mineral deposition
ARS: Alizarin red staining

decrease in cytokine inflammation, thus preventing bone loss by escalating RANKL and OPG levels.²¹

NO inhibition through the p38, JNK, and NF- κ B signaling pathways' retardation is associated with inflammatory response inhibition and osteoclastogenesis suppression. Yeh et al.²¹ showed that Cur liposomes, as samples, inhibited NO production in RAW 264.7 macrophages and prevented osteoclast differentiation by increasing the OPG/RANKL ratio and decreasing cathepsin K regulation and tartrate-resistant acid phosphatase expression. The high NO inhibition and OPG/RANKL ratio lead to a reduction in osteoclast activation and a rise in the number of osteoblasts, so that the effect of osteoporosis can be reduced.

In the present study, we evaluated the NO production of 70% ethanol and aqueous extracts in LPS-stimulated RAW 264.7 macrophages. LPS markedly stimulated NO production in these macrophages compared to in the control group. The 70% ethanol extract of deer antler showed a higher reaction rate in lowering LPS-stimulated RAW 264.7 than that of aqueous extract (Figure 2). Neither of them had any cytotoxic effect on RAW 264.7 macrophages (Figure 1). According to Choi et al.²⁶ the ability of the methanol fraction from deer bone in reducing NO production was the result of decreased regulation and expression of mRNA from pro-inflammatory agents, such as IL-1 β , IL-12 β , and cyclooxygenase. The methanol fraction containing sugar played an essential part in lowering reactions of inflammatory by managing agents and pro-inflammatory cytokines. Pro-inflammatory cytokine production in large quantities can be found in several conditions, such as arthritis, rheumatoid arthritis, osteoarthritis, osteoporosis, and cancer.^{27,28}

The osteoblast phenotype for bone mineralization is obtained in two phases. In the first phase the mature contents and characteristic protein related to the bone cell phenotype such as ALP are detected and in the second phase the contents are mineralized by calcium deposition. A spongy bone layer is formed around the original cartilage and the space between the spongy bones is loaded with bone content and becomes solid bone.

Deer antler is able to stimulate osteoblast proliferation and protein contents in bone such as collagen type 1 and bone sialoprotein and so the antler can trigger osteoblast differentiation through mineralized nodule formation. As expected, the 70% ethanol and aqueous extracts of deer antler increased ALP activity constantly (Figure 4). The result is similar to that in the research reported by Lee et al.¹⁷ in which cells plated in media with aqueous extract had more ALP activity than the 70% ethanol extract. Deer antler significantly increased osteoblast proliferation until 119% of the basic value, stimulated expression of mRNA and ALP activity in the range of 50-100 μ g/mL, and increased type 1 collagen mRNA expression and mineralization to be more than 183%.¹⁷

Interestingly, ALP has been proven to be an enzyme that plays an essential role in the mineralization process. Human bone abnormalities and hypophosphatasia can occur due to the absence of expression of ALP bone form^{29,30} and described by a

lack of bone mineral deposition (rickets). ALP is important for mineralization but its purpose has not yet been fully clarified. We continued to evaluate the effect of 70% ethanol and aqueous extracts of deer antler on mineralization activity (Figure 5).

The new bone tissue formed will be implicated in the mechanism of osteoblast proliferation, osteoblast differentiation, and mineralization. The 7F2 osteoblast cells started differentiating on day 4. The ALP assay is displayed as an initial term marker of differentiated cells. Then the mineralization of 7F2 osteoblast cells produced by ARS was monitored. Figure 6 shows that the extracts stimulated the mineralization of 7F2 osteoblast cells. The stimulation of aqueous extract at 100 μ g/mL was two times higher than that of 70% ethanol extract. This difference may be as a result of a reduction in deer antler extract toxicity or chemical constituents in both extracts.

CONCLUSION

The 70% ethanol and aqueous extracts of *R. unicolor* antler from Kalimantan had a role in bone remodeling. The aqueous extract stimulated higher bone differentiation and mineralization than the 70% ethanol extract with an ALP value of 65% and twice the ARS value. However, the 70% ethanol extract displayed higher NO inhibition activity than aqueous extract with an inhibition value of 40%. Therefore, the extracts can be considered to effectively degrade inflammatory marker expression in osteoblasts and preserve osteoblast functions.

ACKNOWLEDGMENTS

This research was supported by Airlangga University (No. 886/UN3/2018) and was a collaboration between the Faculty of Pharmacy Airlangga University, UPTD of East Kalimantan, and National Chiayi University Taiwan.

Conflict of Interest: No conflict of interest was declared by the authors.

REFERENCES

- Jennifer JW. Methods in molecular biology: Osteoporosis methods and protocol, Human Press; 2008.
- Cooper C, Campion G, Melton LJ 3rd. Hip fractures in the elderly: a world-wide projection. *Osteoporos Int.* 1992;2:285-289.
- Kanis JA, Johnell O, Oden A, Sembo I, Redlund-Johnell I, Dawson A, De Laet C, Jonsson B. Long-term risk of osteoporotic fracture in Malmö. *Osteoporos Int.* 2000;11:669-674.
- Sudoyo SA, Simadibrata S. Osteoporosis. Buku ajar ilmu penyakit dalam II, 4th ed. Jakarta, FKUI; 2006.
- Megraj KVK, Raju K, Balaraman R, Meenakshisundaram K. Biological activities of some Indian medicinal plants. *JAPER.* 2011;1:12-44.
- Sunwoo HH, Nakano T, Hudson RJ, Sim JS. Isolation, characterization and localization of glycosaminoglycans in growing antlers of wapiti (*Cervus elaphus*). *Comp Biochem Physiol B Biochem Mol Biol.* 1998;120:273-283.
- Kawtikwar PS, Bhagwat DA, Sakarkar DM. Deer antler-traditional use and future perspectives. *Indian J Tradit Knowl.* 2010;9:245-251.

8. Mikler JR, Theoret CL, High JC. Effects of topical elk velvet antler on cutaneous wound healing in streptozotocin-induced diabetic rats. *J Altern Complement Med*. 2004;10:835-840.
9. Shi B, Li G, Wang P, Yin W, Sun G, Wu Q, Yu G. Effect of antler extract on corticosteroid-induced a vascular necrosis of the femoral head in rats. *J Ethnopharmacol*. 2010;127:124-129.
10. Dai TY, Wang CH, Chen KN, Huang IN, Hong WS, Wang SY, Chen YP, Kuo CY, Chen MJ. The antiinfective effects of velvet antler of Formosan Sambar Deer (*Cervus unicolor* Swinhoei) on *Staphylococcus aureus*-infected mice. *Evid Based Complement Alternat Med*. 2011;2011:534069.
11. Zhang Z, Liu X, Duan L, Li X, Zhang Y, Zhou Q. The effects of velvet antler polypeptides on the phenotype and related biological indicators of osteoarthritic rabbit chondrocytes. *Acta Biochim Pol*. 2011;58:297-302.
12. Kuo CY, Wang T, Dai TY, Wang CH, Chen KN, Chen YP, Chen MJ. Effect of the velvet antler of Formosan Sambar Deer (*Cervus unicolor* Swinhoei) on the prevention of an allergic airway response in mice. *Evid Based Complement Alternat Med*. 2012;2012:481318.
13. Shao MJ, Wang SR, Zhao MJ, Lv XL, Xu H, Li L, Gu H, Zhang JL, Li G, Cui XN, Huang L. The effects of velvet antler of deer on cardiac functions of rats with heart failure following myocardial infarction. *Evid Based Complement Alternat Med*. 2012;2012:825056.
14. Meng HY, Qu XB, Li N, Yuan S, Lin Z. Effects of pilose antler and antler glue on osteoporosis of ovariectomized rats. *Zhong Yao Cai*. 2009;32:179-182.
15. Li Y, Zhao Y, Tang R, Qu X. Preventive and therapeutic effects of antler collagen on osteoporosis in ovariectomized rats. *Afr J Biotechnol*. 2010;9:6437-6441.
16. Yang JH, Cao Y, Wang RL, Fei YR, Zhang H, Feng P, Liu J. Anti-resorptive effect of pilose antler blood (*Cervus nippon* Temminck) in ovariectomized rats. *Indian J Exp Biol*. 2010;48:554-558.
17. Lee HS, Kim MK, Kim YK, Jung EY, Park CS, Woo MJ, Lee SH, Kim JS, Suh HJ. Stimulation of osteoblastic differentiation and mineralization in MC3T3-E1 cells by antler and fermented antler using *Cordyceps militaris*. *J Ethnopharmacol*. 2011;133:710-717.
18. Choi SW, Moon SH, Yang HJ, Kwon DY, Son YJ, Yu R, Kim YS, Kim SI, Chae EJ, Park SJ, Kim SH. Antiresorptive activity of bacillus-fermented antler extracts: inhibition of osteoclast differentiation. *Evid Based Complement Alternat Med*. 2013;2013:748687.
19. Jeon B, Kim S, Lee S, Park P, Sung S, Kim J, Moon S. Effect of antler growth period on the chemical composition of velvet antler in sika deer (*Cervus nippon*). *Mamm Biol*. 2009;74:374-380.
20. Tseng SH, Sung HC, Chen LG, Lai YJ, Wang KT, Sung CH, Wang CC. Effects of velvet antler with blood on bone in ovariectomized rats. *Molecules*. 2012;17:10574-10585.
21. Yeh CC, Su YH, Lin YJ, Chen PJ, Shi CS, Chen CN, Chang HI. Evaluation of the protective effects of curcuminoid (curcumin and bisdemethoxycurcumin)-loaded liposomes against bone turnover in a cell-based model of osteoarthritis. *Drug Des Dev Ther*. 2015;9:2285-2300.
22. Kuo CY, Cheng YT, Ho ST, Yu CC, Cheng MJ. Comparison of anti-inflammatory effect and protein profile between the water extracts from Formosan sambar deer and red deer. *J Food Drug Anal*. 2018;26:1275-1282.
23. Wu F, Li H, Jin L, Li X, Ma Y, You J, Li S, Xu Y. Deer antler base as a traditional Chinese medicine: a review of its traditional uses, chemistry and pharmacology. *J Ethnopharmacol*. 2013;145:405-415.
24. Suh HJ, Lee H, Min BJ, Jung SU, Jung EY. Effects of gangliosides from deer bone extract on the gene expressions of matrix metalloproteinases and collagen type II in interleukin-1 β -induced osteoarthritic chondrocytes. *Nutr Res Pract*. 2016;10:569-574.
25. Collin-Osdoby P, Osdoby P. RANKL-mediated osteoclast formation from murine RAW 264.7 cells. *Methods Mol Biol*. 2012;816:187-202.
26. Choi HS, Im S, Park Y, Hong KB, Suh HJ. Deer bone oil extract suppresses lipopolysaccharide-induced inflammatory responses in RAW 264.7 cells. *Biol Pharm Bull*. 2016;39:595-600.
27. Landskron G, De la Fuente M, Thuwajit P, Thuwajit C, Hermoso MA. Chronic inflammation and cytokines in the tumor microenvironment. *J Immunol Res*. 2014;2014:149-185.
28. McInnes IB, Schett G. Cytokines in the pathogenesis of rheumatoid arthritis. *Nat Rev Immunol*. 2007;7:429-442.
29. Caswell AM, Russell RG. Identification of ecto-nucleoside triphosphate pyrophosphatase in human articular chondrocytes in monolayer culture. *Biochem Biophys Acta*. 1985;847:40-47.
30. Chuck AJ, Patrick MG, Hamilton E, Wilson R, Doherty M. Crystal deposition in hypophosphatasia: a reappraisal. *Ann Rheum Dis*. 1989;48:571-576.



Cytotoxic, Genotoxic, and Apoptotic Effects of Nickel Oxide Nanoparticles in Intestinal Epithelial Cells

Nikel Oksit Nanopartiküllerinin Bağırsak Epitel Hücreleri Üzerine Sitotoksik, Genotoksik ve Apoptotik Etkileri

© Mahmoud ABUDAYYAK¹, © Elif GÜZEL², © Gül ÖZHAN^{3*}

¹Karadeniz Technical University Faculty of Pharmacy, Department of Toxicology, Trabzon, Turkey

²Istanbul University-Cerrahpaşa, Cerrahpaşa Faculty of Medicine, Department of Histology and Embryology, Istanbul, Turkey

³Istanbul University Faculty of Pharmacy, Department of Pharmaceutical Toxicology, Istanbul, Turkey

ABSTRACT

Objectives: The superior properties of nickel oxide-nanoparticles (NiO-NPs) have led to their wide use in various fields. However, there is little comprehensive knowledge about their toxicity, especially after oral exposure. The toxic effect of NiO-NPs of mean size 15.0 nm was investigated in Caco-2 (human intestinal epithelial) cells as no study has been performed on their intestinal toxicity.

Materials and Methods: Following identification of their particle size distribution and cellular uptake potential, the risk of exposure to NiO-NPs was evaluated by cellular morphologic changes, cyto- and genotoxic potentials, oxidative damage, and apoptotic induction.

Results: NiO-NPs induced a 50% reduction in cell viability at 351.6 µg/mL and caused DNA damage and oxidative damage at 30-150 µg/mL. It appears that apoptosis might be a main cell death mechanism in NiO-NP-exposed intestinal cells.

Conclusion: NiO-NPs might be hazardous to the gastrointestinal system. The results should raise concerns about using NiO-NPs in food-contact appliances and about NiO-NP-containing wastes. Further *in vivo* and *in vitro* research should be conducted to explain the specific toxicity mechanism of these particles and reduce their risk to humans.

Key words: Nickel oxide nanoparticles, intestinal cells, genotoxicity, oxidative stress, apoptosis

ÖZ

Amaç: Nikel oksit-nanopartikülleri (NiO-NP), üstün özellikleri nedeniyle farklı alanlarda geniş kullanıma sahiptir. Ancak, özellikle oral maruziyete NiO-NP'nin toksisitesi hakkındaki yeterli bilgi bulunmamaktadır. NiO-NP'nin intestinal sistem üzerine toksik etkisi ile ilgili herhangi bir çalışma bulunmadığından, bu çalışmada NiO-NP'nin (ortalama boyut 15,0 nm) Caco-2 (insan intestinal epiteli) hücreleri üzerine toksisitesi araştırılmıştır.

Gereç ve Yöntemler: Partikül boyutu dağılımı ve hücre alım potansiyelleri belirlendikten sonra, NiO-NP'ne maruziyetin riski hücre morfolojik değişiklikler, sito- ve genotoksik etkiler, oksidatif hasar ve apoptoz indüksiyonu ile değerlendirilmiştir.

Bulgular: NiO-NP 351,6 µg/mL konsantrasyonda hücre canlılığında %50 azalmaya ve 30-150 µg/mL'de DNA hasarı ve oksidatif hasarın indüksiyonuna neden olmuştur. NiO-NP'ye maruz bırakılan intestinal hücrelerde ana hücre ölüm mekanizması apoptoz olabilir.

Sonuç: NiO-NP gastrointestinal sisteme tehlikeli olabilir. Elde edilen sonuçlar, gıdayla temas eden cihazların yapımında NiO-NP'nin kullanımı ve NiO-NP içeren atıklar nedeniyle endişeler olabileceğini göstermektedir. NiO-NP'in spesifik toksisite mekanizmalarını aydınlatmak ve insan sağlığı üzerine risklerini azaltmak için daha ileri *in vivo* ve *in vitro* araştırmaların yapılması gerekmektedir.

Anahtar kelimeler: Nikel oksit nanopartikülleri, intestinal hücreler, genotoksisite, oksidatif stres, apoptoz

*Correspondence: E-mail: gulozhan@istanbul.edu.tr, Phone: +90 212 440 02 55 ORCID-ID: orcid.org/0000-0002-6926-5723

Received: 11.03.2019, Accepted: 20.06.2019

©Turk J Pharm Sci, Published by Galenos Publishing House.

INTRODUCTION

Nickel oxide-nanoparticles (NiO-NPs) are widely used as catalysts, pigments, and sensors in different medical and industrial applications because of their physicochemical features.^{1,2} NiO and other Ni compounds are regarded as carcinogenic to humans (Group 1).³ Additionally, NiO-NPs are thought to be more toxic than fine particles are because they have high solubility and release higher amounts of ions in medium.⁴ Research has mainly focused on their pulmonary toxicity and reported that the particles induced oxidative stress and inflammatory responses in the airway system.⁵⁻¹⁰ NiO-NPs were detected in intestinal tissue after pulmonary exposure.¹¹ Although it is well known that NiO-NPs could be absorbed through the intestinal tract, there are very few data about the intestinal toxicity of NiO-NPs. NiO-NPs might be harmful to the cells of mucosa.^{12,13} On the other hand, the unabsorbed portion is still considered a risk for intestinal cells following oral exposure.

Therefore, in the present study, the toxicity of NiO-NPs was assessed using various endpoints in the Caco-2 human intestine cell line, a highly differentiated human cell line and extensively used to study apical uptake and absorption of nutrients and chemicals as an *in vitro* model for toxicological studies.^{14,15} Several studies have also reported the chemical permeability to Caco-2 cells to be correlated well with that of the intestinal membrane *in vivo*.¹⁶

MATERIALS AND METHODS

NiO-NPs were obtained from Sigma (St. Louis, MO, USA) and recharacterized using transmission electron microscopy (TEM) (JEM-2100 HR, JEOL, USA) and dynamic light scattering (DLS) (ZetaSizer Nano-ZS, Malvern Instruments, Malvern, UK) in distilled water and cell culture medium.^{17,18}

Human intestinal epithelial cells (Caco-2, HTB-37) were obtained from the American Type Culture Collection (Gaithersburg, MD, USA). The cells were incubated according to the manufacturer's instructions. Cells at a density of 10^5 - 10^6 cells/mL were treated with freshly prepared NiO-NPs for 24 h.

To evaluate the cellular uptake potentials of NiO-NPs, inductively coupled plasma-mass spectrometry [(ICP-MS); Thermo Elemental X series 2, USA] was used, while TEM (Jeol-1011, Tokyo, Japan) with an accelerating voltage of 80 kV and an attached digital camera (Olympus-Veleta TEM Camera, Tokyo, Japan) was used to evaluate both cellular uptake and morphology changes at 50 and 100 $\mu\text{g/mL}$.^{17,18}

The cytotoxic activity of NiO-NPs (50-500 $\mu\text{g/mL}$) was determined using 3-(4,5-dimethylthiazol-2-yl)-2,5-diphenyltetrazolium bromide (MTT) and neutral red uptake (NRU) assays.^{19,20} The optical densities were measured by an enzyme linked immunosorbent assay (ELISA) reader system (Epoch, Germany) at 590 and 540 nm for MTT and NRU, respectively. The enzyme activity inhibition and the accumulation of NR dye in the cells were regarded as cytotoxicity endpoints. The cytotoxicity was calculated compared to that of negative control cells. The median inhibitory concentration (IC_{50}) values

were expressed as the concentration of NiO-NPs that induced inhibition of 50% in enzyme activities in cells.

The genotoxic effects of NiO-NPs were determined at concentrations of 15-120 $\mu\text{g/mL}$ by comet assay.²¹ Hydrogen peroxide (H_2O_2) (100 μM) was the positive control. Caco-2 cells were mixed with premelted low-melting point agarose, layered on slides previously coated with agarose, covered with a cover slip, and allow to solidify at 4°C. Then a lysis solution was used to lyse the cells on the slides (for 1-12 h at 4°C). Electrophoresis was performed for 20 min and the slides were rinsed with neutralization buffer and fixed using 99% ethanol. To score the DNA breaks, ethidium bromide was used to stain the DNA before the examination using a fluorescent microscope supplied with an automated image analysis system (Olympus BX53, Olympus, Tokyo, Japan). The percentage of DNA in the comet tail (tail intensity %) was used to express the DNA damage to individual cells.

Glutathione (GSH), malondialdehyde (MDA), 8-hydroxy-2'-deoxyguanosine (8-OHdG), and protein carbonyl (PC) ELISA oxidative stress determination kits were obtained from Yehua Biological Technology (Shanghai, China), while the dye reagent for the protein assay was purchased from Bio-Rad (Munich, Germany). The oxidative stress parameters in the cells treated with 50-150 $\mu\text{g/mL}$ NiO-NPs were determined according to the manufacturer's instructions and Abudayyak et al.¹⁷ The results were calculated and expressed per gram of protein.

The Annexin V-FITC/propidium iodide (PI) apoptosis/necrosis detection kit was from BioLegend (San Diego, CA, USA). NiO-NP concentrations were 400-700 $\mu\text{g/mL}$. Based on the manufacturer's instructions, the trypsinized cells were adjusted to be 1×10^6 cells/mL. Next, 100 μL of cell suspension were mixed with 5 μL of Annexin V-FITC and 10 μL of PI and the resulting mixture was incubated in the dark for 15 min. A phase-contrast fluorescent microscope (Olympus BX53, Olympus, Tokyo, Japan) was used to count the apoptotic and necrotic cells. The percentages of the cells to the total cell amount were expressed as the results of this parameter.^{17,18}

Statistical analysis

The cytotoxicity tests were performed in triplicate on four different days ($n=12$). The other tests were done in triplicate on three different days ($n=9$). The data were expressed as mean \pm standard deviation. The statistical analysis was conducted using One-Way ANOVA Dunnett t-test by SPSS version 23 for Windows (SPSS Inc., Chicago, IL, USA) and p less than 0.05 was selected as the level of significance.

RESULTS AND DISCUSSION

The results of TEM and DLS evaluations obtained from our previous study indicated that the average sizes of NiO-NPs were 15.0 nm (4.2-38.1 nm) in water and 21.4 nm (7.2-60.5 nm) in the cell culture medium. The increase in the medium group might be due the adsorption of medium proteins in the surface of the particles.^{17,18}

The results of the cellular uptake by ICP-MS indicate that Caco-2 cells took up NiO-NPs after exposure to 50 and 100 µg/mL for 24 h (Table 1). The agglomeration of NiO-NPs at the high concentration could explain the decreases in their cellular uptake at the high exposure concentration in comparison with the lower exposure concentration.

The NiO-NPs were obtained within the cytoplasmic vacuoles at 50 and 150 µg/mL (NPs shown with red arrows). The particle sizes were larger in the exposed cells at 150 µg/mL compared to those at 50 µg/mL. Moreover, the number of particle-containing vacuoles in the exposed cells decreased when the concentration of NiO-NPs was increased. Cytoplasmic organelles appeared normal and nuclear and plasma membranes were intact in the exposed cells, as in the negative control cells. Electron-dense bodies were visible in the cytoplasm of some cells in both treatment groups. The most notable change in the cells included the presence of electron-lucent large vacuoles filled with NPs. In a few cells at 50 µg/mL, the cytoplasmic vacuoles were so large that they induced disruption of the cytoplasm. In addition, abnormal nuclei with indentations in the membrane and chromatin condensation were seen in some cells in both treatment groups (Figures 1A-1C).

In all the cells, lipid droplets were observed to increase with increasing NP concentrations, which could be an indicator or feature of the oxidative stress process.^{22,23} According to TEM pictures and ICP-MS analysis, the NiO-NPs toxicity could be related to the uptake and accumulation of NiO-NPs in the cells.

The results of the cytotoxicity evaluation showed a decrease in cell viability depending on concentration manner. The median IC₅₀ values were 479.15 and 351.6 µg/mL by NRU and MTT tests, respectively (Figure 2). According to previous studies, NiO-

NPs induced cellular death in different human cell lines such as neuron, liver, lung, airway epithelial, and breast cells and rat kidney epithelial cells.^{4,7,23-27} Our results could indicate that the Caco-2 cell line was more vulnerable than other previously studied cell lines to NiO-NP-induced cytotoxic effects.

The genotoxicity of NiO-NPs was estimated using the comet assay (Figure 3). NiO-NPs caused DNA damage (1.2-1.5-fold; p≤0.05). At 120 µg/mL NiO-NPs, the tail intensity was 8.0%, while it was 13.3% (1.85-fold) in the positive control (100 µM H₂O₂). Previously, researchers showed that NiO-NPs could induce DNA damage in different cells.²⁸⁻³² Dumala et al.¹² indicated that NiO-NPs could induce significant DNA damage in the liver, lungs, and kidneys of rats exposed orally to 500 mg/kg bw. Moreover, NiO-NPs caused cell cycle alteration as a consequence of genotoxicity via the nuclear translocation of phospho-ATM and phosphor-ATR in human pulmonary epithelial cell lines.¹² NiO-NPs induced the DNA-damage signaling cascade at 20-100 µg/mL.¹⁸ Li et al.³³ reported DNA damage in pulmonary cells after intratracheal instillation similar to the present results.

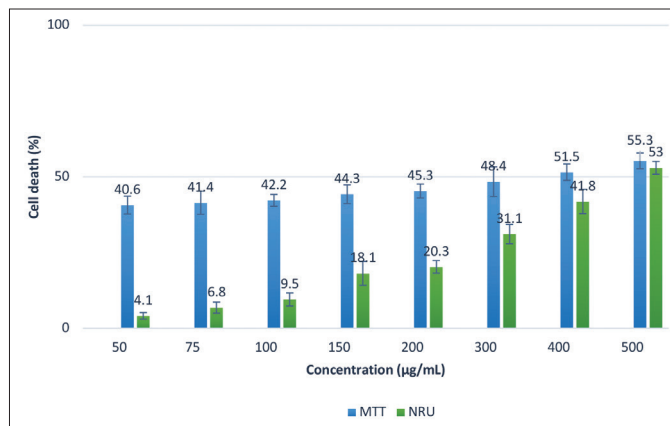


Figure 2. The cytotoxic potential of NiO-NPs

All experiments were done in triplicate and each assay was performed four times. Data are expressed as mean ± SD. The IC₅₀ values were 251.6 µg/mL and 479.2 µg/mL in MTT and NRU, respectively. NiO-NPs: Nickel oxide-nanoparticles, SD: Standard deviation, IC₅₀: Inhibitory concentration, MTT: 3-(4,5-dimethylthiazol-2-yl)-2,5-diphenyltetrazolium bromide, NRU: Neutral red uptake

Table 1. Nickel oxide-nanoparticles taken up by Caco-2 cells

Exposure concentration (µg/mL/10 ⁵ cells)	Ni amount (mg/10 ⁵ cells)
Negative control	0.19±0.05
50	3.29±0.38
100	1.31±0.22

The assay was performed four times. The results are presented as mean ± SD
Ni: Nickel, SD: Standard deviation

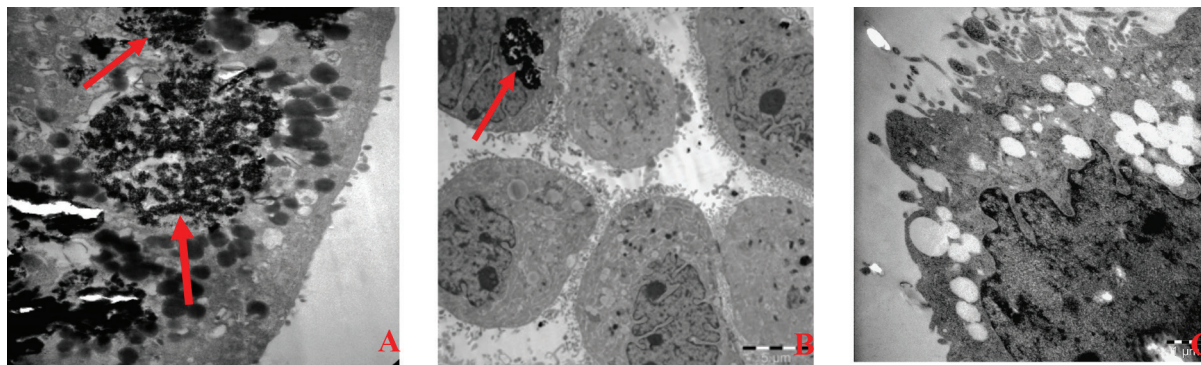


Figure 1. The TEM observations of NiO-NPs uptake by Caco-2 cells

A) Caco-2 cells exposed to NiO-NPs at 50 µg/mL, B) Caco-2 cells exposed to NiO-NPs at 100 µg/mL, C) Caco-2 unexposed cells (negative control)
TEM: Transmission electron microscopy, NiO-NPs: Nickel oxide-nanoparticles

NiO-NP-induced oxidative stress was evaluated with the levels of GSH, MDA, 8-OHdG, and PC (Table 2). NiO-NPs induced oxidative stress as a significant increase in the levels of PC (≤ 1.5 -fold) and a significant decrease in GSH levels (33.1-37.5%) were observed. However, 8-OHdG and MDA levels did not change significantly. In general, the oxidative stress potential of NiO-NPs in Caco-2 cells was statistically significant ($p \leq 0.05$).

The previous data showed that NiO-NPs caused damage in the lung and liver and induce pulmonary inflammation via reactive oxygen species (ROS).^{7,8,11,12} *In vitro* research confirmed with *in vivo* studies that NiO-NPs induced an increase in ROS and caused oxidative damage in different human cell lines such as liver, lung, airway epithelial, and breast cells.^{24,26,31,34} Previous data confirmed our results; oxidative stress could be the mechanism underlying the cyto- and genotoxicity induced by NiO-NPs.

The Annexin V-FITC/PI assay results demonstrate that NiO-NPs led to induction of apoptosis (Figure 4). The rates of apoptotic cells were 84.6-99.6% of the dead cells, while the rates of necrotic cells were 0.4-15.4% of the dead cells (Figure 4). The results indicated that apoptosis might be the main cell death pathway of NiO-NPs. Di Bucchianico et al.²⁴ and Saquib et al.³⁴ observed an increase in the apoptotic cells rate with

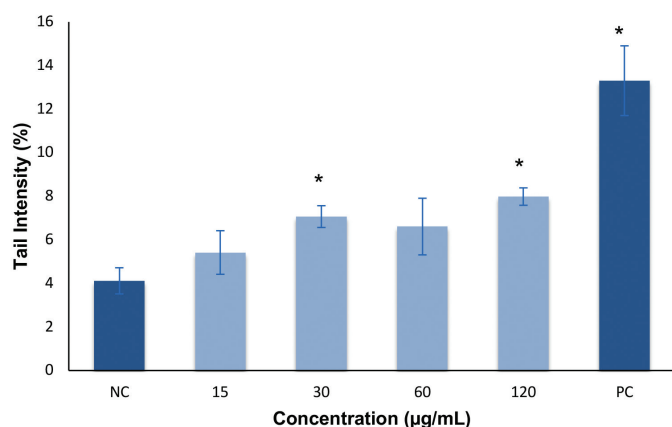


Figure 3. The genotoxic potential of NiO-NPs

All experiments were done in triplicate and each assay was performed three times. The results are presented as mean tail intensity (%) with \pm SD. * $p \leq 0.05$ was selected as the level of significance by One-Way ANOVA Dunnett t-test NiO-NPs: Nickel oxide-nanoparticles, PC: Protein carbonyl, SD: Standard deviation

an increase in NiO-NPs.^{24,34} Similarly, Chang et al.⁶ indicated endoplasmic reticulum stress-related apoptosis in rats exposed to NiO-NPs by intratracheal instillation.

NiO-NPs (25-100 µg/mL) induced apoptosis by functional alterations in mitochondria and lysosomes³⁰ similar to our results. Previously, changes in mRNA levels in the genes related to the apoptosis pathway were reported.^{27,29,34} Duan et al.³⁵ studied the role of apoptosis in NiO-NP-induced toxicity in human bronchial epithelial cells (BEAS-2B) by investigating the impacts of NiO-NPs on sirtuin 1, a NAD-dependent deacetylase. NiO-NPs (5-20 µg/cm²) caused cytotoxicity by an apoptotic process, and showed a suppression effect on sirtuin 1, which could underlie the NiO-NP-induced apoptosis via tumor protein p53 and bcl-2-associated X protein. Similar to previous researchers, we observed that NiO-NPs caused dose-dependent apoptosis. The degree of apoptosis/necrosis corresponded with the severity of cytotoxicity (Figures 2 and 4).

CONCLUSION

The toxic effects of NiO-NPs (15.0 nm) were evaluated in the Caco-2 cell line. Our results indicate cellular uptake of NiO-NPs and show cytotoxic potential by disrupting the mitochondrial and lysosomal functions. The median IC₅₀ values were 251.6 µg/mL and 479.2 µg/mL by MTT and NRU, respectively. Our results also indicate that apoptosis might be the main cell

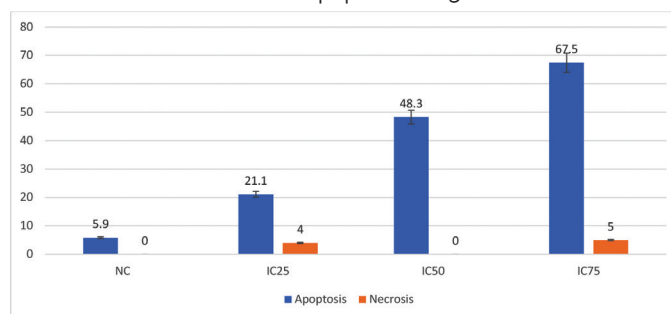


Figure 4. The apoptotic/necrotic potential of NiO-NPs

All experiments were done in triplicate and each assay was performed twice. The results are expressed as the percent of the total cell amount with \pm SD, $p \leq 0.05$ was selected as the level of significance by One-Way ANOVA Dunnett t-test. Apoptotic ratio was significant at all exposure samples NiO-NPs: Nickel oxide-nanoparticles, SD: Standard deviation

Table 2. Nickel oxide-nanoparticle induced oxidative damage to Caco-2 cells

Exposure concentration (µg/mL)	8-OHdG (µg/g protein)	MDA (µmol/g protein)	GSH (µmol/g protein)	PC (µg/g protein)
0	0.917 \pm 0.132	0.350 \pm 0.059	41.142 \pm 2.009	5.160 \pm 0.108
50	0.964 \pm 0.205	0.375 \pm 0.108	25.744 \pm 3.891*	5.435 \pm 0.814
75	0.990 \pm 0.242	0.481 \pm 0.090	27.500 \pm 6.082*	6.667 \pm 1.078*
100	1.111 \pm 0.310	0.408 \pm 0.158	38.092 \pm 3.782	7.115 \pm 0.877*
150	0.985 \pm 0.164	0.442 \pm 0.098	39.099 \pm 2.82	7.907 \pm 1.007*

All experiments were done in triplicate and each assay was performed twice. The results were presented as mean \pm SD.

* $p \leq 0.05$ was selected as the level of significance compared to the negative controls by One-Way ANOVA Dunnett t-test, MDA: Malondialdehyde, GSH: Glutathione, PC: Protein carbonyl

death pathway after treatment with NiO-NPs for 24 h. Oxidative stress could be the reason for DNA damage induced by NiO-NPs at 15-120 µg/mL concentrations. These results should raise concern about the safety of products that contain NiO-NPs. Further studies should be conducted to elucidate the probable toxicity in the gastrointestinal tract and clarify the pathways of apoptosis and DNA damage.

ACKNOWLEDGMENTS

The authors would like to thank to the Research Fund of İstanbul University (Project no: 37785) for supporting this work.

Conflicts of interest: No conflict of interest was declared by the authors. The authors alone are responsible for the content and writing of the paper.

REFERENCES

- Capasso L, Camatini M, Gualtieri M. Nickel oxide nanoparticles induce inflammation and genotoxic effect in lung epithelial cells. *Toxicol Lett.* 2014;226:28-34.
- Martin A, Sarkar A. Overview on biological implications of metal oxide nanoparticle exposure to human alveolar A549 cell line. *Nanotoxicology.* 2017;11:713-724.
- International Agency for Research on Cancer (IARC). Nickel And Nickel Compounds. IARC MONOGRAPHS – 100C. 2018:169-218. <https://monographs.iarc.fr/wp-content/uploads/2018/06/mono100C-10.pdf>
- Horie M, Fukui H, Nishio K, Endoh S, Kato H, Fujita K, Miyauchi A, Nakamura A, Shichiri M, Ishida N, Kinugasa S, Morimoto Y, Niki E, Yoshida Y, Iwahashi H. Evaluation of acute oxidative stress induced by NiO nanoparticles *in vivo* and *in vitro*. *J Occup Health.* 2011;53:64-74.
- Chang X, Zhao H, Gao J, Chen L, Zhu A, Wang C, Yu S, Ren X, Ge P, Sun Y. Pulmonary toxicity of exposure to nano nickel oxide. *Micro Nano Lett.* 2018;13:733-738.
- Chang X, Liu F, Tian M, Zhao H, Han A, Sun Y. Nickel oxide nanoparticles induce hepatocyte apoptosis via activating endoplasmic reticulum stress pathways in rats. *Environ Toxicol.* 2017;32:2492-2499.
- Horie M, Fukui H, Endoh S, Maru J, Miyauchi A, Shichiri M, Fujita K, Niki E, Hagihara Y, Yoshida Y, Morimoto Y, Iwahashi H. Comparison of acute oxidative stress on rat lung induced by nano and fine-scale, soluble and insoluble metal oxide particles: NiO and TiO₂. *Inhal Toxicol.* 2012;24:391-400.
- Marzban A, Seyedalipour B, Mianabadi M, Taravati A. Investigation of the Enzyme activities of Alkaline Phosphatase, Lactate Dehydrogenase, Transaminase and Histopathological Changes of Liver after Exposure to NiO and NiO Nanoparticles in Rats. *JSSU.* 2017;25:381-395.
- Senoh H, Kano H, Suzuki M, Ohnishi M, Kondo H, Takanobu K, Umeda Y, Aiso S, Fukushima S. Comparison of single or multiple intratracheal administration for pulmonary toxic responses of nickel oxide nanoparticles in rats. *J Occup Health.* 2017;59:112-121.
- Yu S, Liu F, Wang C, Zhang J, Zhu A, Zou L, Han A, Li J, Chang X, Sun Y. Role of oxidative stress in liver toxicity induced by nickel oxide nanoparticles in rats. *Mol Med Rep.* 2018;17:3133-3139.
- Shinohara N, Zhang G, Oshima Y, Kobayashi T, Imatanaka N, Nakai M, Sasaki T, Kawaguchi K, Gamo M. Kinetics and dissolution of intratracheally administered nickel oxide nanomaterials in rats. *Part Fibre Toxicol.* 2017;14:48.
- Dumala N, Mangalampalli B, Chinde S, Kumari SI, Mahoob M, Rahman MF, Grover P. Genotoxicity study of nickel oxide nanoparticles in female Wistar rats after acute oral exposure. *Mutagenesis.* 2017;32:417-427.
- Dumala N, Mangalampalli B, Kalyan Kamal SS, Grover P. Biochemical alterations induced by nickel oxide nanoparticles in female Wistar albino rats after acute oral exposure. *Biomarkers.* 2018;23:33-43.
- Käkinen A, Kahru A, Nurmsoo H, Kubo AL, Bondarenko OM. Solubility-driven toxicity of CuO nanoparticles to Caco2 cells and Escherichia coli: Effect of sonication energy and test environment. *Toxicol In Vitro.* 2016;36:172-179.
- Martin KR, Failla ML, Smith JC. Differential susceptibility of Caco-2 and HepG2 human cell lines to oxidative stress. *J Elisha Mitchell Sci Soc.* 1997;113:149-162.
- Yamashita S, Furubayashi T, Kataoka M, Sakane T, Sezaki H, Tokuda H. Optimized conditions for prediction of intestinal drug permeability using Caco-2 cells. *Eur J Pharm Sci.* 2000;10:195-204.
- Abudayyak M, Guzel E, Özhan G. Nickel oxide nanoparticles induce oxidative DNA damage and apoptosis in kidney cell line (NRK-52E). *Biol Trace Elem Res.* 2017;178:98-104.
- Abudayyak M, Guzel E, Özhan G. Nickel oxide nanoparticles are highly toxic to SH-SY5Y neuronal cells. *Neurochem Int.* 2017;108:7-14.
- Repetto G, del Peso A, Zurita JL. Neutral red uptake assay for the estimation of cell viability/cytotoxicity. *Nat Protoc.* 2008;3:1125-1131.
- Van Meerloo J, Kaspers GJL, Cloos J. Cell sensitivity assays: The MTT assay. *Methods Mol Biol.* 2011;731:237-245.
- Collins AR. The comet assay for DNA damage and repair principles, applications, and limitations. *Mol Biotechnol.* 2004;26:249-261.
- Khachadourian A, Maysinger D. Lipid droplets: their role in nanoparticle-induced oxidative stress. *Mol Pharm.* 2009;6:1125-1137.
- Lee J, Homma T, Kurahashi T, Kang ES, Fujii J. Oxidative stress triggers lipid droplet accumulation in primary cultured hepatocytes by activating fatty acid synthesis. *Biochem Biophys Res Commun.* 2015;464:229-235.
- Di Bucchianico S, Gliga AR, Åkerlund E, Skoglund S, Wallinder IO, Fadeel B, Karlsson HL. Calcium-dependent cyto- and genotoxicity of nickel metal and nickel oxide nanoparticles in human lung cells. *Part Fibre Toxicol.* 2018;15:32.
- Lanone S, Rogerieux F, Geys J, Dupont A, Maillot-Marechal E, Boczkowski J, Lacroix G, Hoet P. Comparative toxicity of 24 manufactured nanoparticles in human alveolar epithelial and macrophage cell lines. *Part Fibre Toxicol.* 2009;6:14.
- Mohamed K, Zine K, Fahima K, Abdelfattah E, Sharifudin SM, Duduku K. NiO nanoparticles induce cytotoxicity mediated through ROS generation and impairing the antioxidant defense in the human lung epithelial cells (A549): Preventive effect of Pistacia lentiscus essential oil. *Toxicol Rep.* 2018;5:480-488.
- Siddiqui MA, Ahamed M, Ahmad J, Majeed Khan MA, Musarrat J, Al-Khedairy AA, Alrokayan SA. Nickel oxide nanoparticles induce cytotoxicity, oxidative stress and apoptosis in cultured human cells that is abrogated by the dietary antioxidant curcumin. *Food Chem Toxicol.* 2012;50:641-647.
- Ahamed M. Toxic response of nickel nanoparticles in human lung epithelial A549 cells. *Toxicol In Vitro.* 2011;25:930-936.

29. Ahamed M, Ali D, Alhadlaq HA, Akhtar MJ. Nickel oxide nanoparticles exert cytotoxicity via oxidative stress and induce apoptotic response in human liver cells (HepG2). *Chemosphere*. 2013;93:14-22.
30. A Ahmad J, Alhadlaq HA, Siddiqui MA, Saquib Q, Al-Khedhairi AA, Musarrat J, Ahamed M. Concentration-dependent induction of reactive oxygen species, cell cycle arrest and apoptosis in human liver cells after nickel nanoparticles exposure. *Environ Toxicol*. 2015;30:137-148.
31. Åkerlund E, Cappellini F, Di Bucchianico S, Islam S, Skoglund S, Derr R, Odnevall Wallinder I, Hendriks G, Karlsson HL. Genotoxic and mutagenic properties of Ni and NiO nanoparticles investigated by comet assay, γ -H2AX staining, Hprt mutation assay and ToxTracker reporter cell lines. *Environ Mol Mutagen*. 2018;59:211-222.
32. De Carli RF, Chaves DDS, Cardozo TR, de Souza AP, Seeber A, Flores WH, Honatel KF, Lehmann M, Dihl RR. Evaluation of the genotoxic properties of nickel oxide nanoparticles *in vitro* and *in vivo*. *Mutat Res/Genet Toxicol Environ Mutagen*. 2018;836:47-53.
33. Li YS, Ootsuyama Y, Kawasaki Y, Morimoto Y, Higashi T, Kawai K. Oxidative DNA damage in the rat lung induced by intratracheal instillation and inhalation of nanoparticles. *J Clin Biochem Nutr*. 2018;62:238-241.
34. Saquib Q, Siddiqui MA, Ahmad J, Ansari SM, Faisal M, Wahab Z, Alatar AA, Al-Khedhairi A. Nickel Oxide Nanoparticles Induced Transcriptomic Alterations in HEPG2 Cells. In: Saquib Q, ed. *Cellular and Molecular Toxicology of Nanoparticles* (1st ed). Springer; 2018:163-174.
35. Duan WX, He MD, Mao L, Qian FH, Li YM, Pi HF, Liu C, Chen CH, Lu YH, Cao ZW, Zhang L, Yu ZP, Zhou Z. NiO nanoparticles induce apoptosis through repressing SIRT1 in human bronchial epithelial cells. *Toxicol Appl Pharmacol*. 2015;286:80-91.



Evaluation of the Possible Role of miRNAs in Chemical Allergen Potency

miRNA'ların Kimyasal Alerjen Potansiyellerinin Olası Rollerinin Değerlendirilmesi

© Hatice Gül ANLAR^{1*}, © Valentina GALBIATI², © Emanuela CORSINI², © Nurşen BAŞARAN³

¹Zonguldak Bülent Ecevit University Faculty of Pharmacy, Department of Pharmaceutical Toxicology, Zonguldak, Turkey

²Università degli Studi di Milano, Department of Environmental Science and Policy, Milan, Italy

³Hacettepe University Faculty of Pharmacy, Department of Pharmaceutical Toxicology, Ankara, Turkey

ABSTRACT

Objectives: MicroRNAs (miRNAs) are short, endogenous noncoding RNA molecules that can bind to certain parts of target mRNAs, thereby regulating gene expression. Studies showed that miRNAs could be up- or downregulated in different allergic skin conditions but there is still need for further studies. The aim of this study was to investigate the expression of miRNAs in response to the common contact allergen Bandrowski's base (BB), the principal allergen in patients reacting to p-phenylenediamine (PPD).

Materials and Methods: The human promyelocytic cell line THP-1 was exposed to BB at a concentration of 1 µg/mL for 24, 48, and 72 h. The dose was selected from the results of cytotoxicity assays. RNA was purified and miRNA expression profile and real-time polymerase chain reaction (RT-PCR) were performed to identify up- or downregulated miRNAs and confirm their modulations.

Results: Among the different modulated miRNAs, the upregulation of miRNA-155 and the downregulation of miRNA-21 were found to be important because these are related to immune system. This expression profile of miRNAs was also confirmed by RT-PCR.

Conclusion: These preliminary results showed that miR-155 and miR-21 may play a role in the pathogenesis of allergic contact dermatitis, but further studies are needed to clarify their definite roles.

Key words: MicroRNA, miRNA, immune system, allergic contact dermatitis, skin

ÖZ

Amaç: MikroRNA'lar (miRNA) kısa, endojen ve kodlamayan RNA molekülleri olup hedef mRNA'ların belirli bölgelerine bağlanarak gen ekspresyonunu düzenlerler. Çalışmalar, farklı alerjik deri hastalıklarında miRNA'ların arttığını ya da azaldığını göstermiştir; fakat hala daha ileri çalışmalara ihtiyaç vardır. Bu çalışmada, p-fenilendiamine reaksiyon veren hastalarda sıklıkla rastlana bir temas alerjisi olan Bandrowski bazına (BB) yanıt olan miRNA'ların ekspresyon profillerinin incelenmesi amaçlanmıştır.

Gereç ve Yöntemler: İnsan promiyelositik hücreleri (THP-1) BB'ye 1 µg/mL konsantrasyonda 24, 48 ve 72 saat maruz bırakılmıştır. Bu doz sitotoksitesite deneylerinin sonuçlarına göre seçilmiştir. RNA saflaştırılmış ve miRNA ekspresyon profili ve gerçek zamanlı polimeraz zincir reaksiyonu (RT-PCR) ile artan veya azalan miRNA'ları belirlemek için kullanılmıştır ve sonrasında modülasyonları doğrulanmıştır.

Bulgular: Farklı modüle edilen miRNA'lar arasında, immün sistem ile ilişkili oldukları için, miRNA-155'in düzeyinin artması ve miRNA-21'in ise düzeyinin azalması önemli bulunmuştur. Bu miRNA'ların ekspresyon profilleri aynı zamanda RT-PCR ile doğrulanmıştır.

Sonuç: Bu ön sonuçlar, miR-155 ve miR-21'in alerjik kontakt dermatit patogeneğinde rolü olabileceğini göstermiştir. Ancak, kesin rollerinin açıklanabilmesi için ileri çalışmalara ihtiyaç vardır.

Anahtar kelimeler: MikroRNA, miRNA, immün sistem, alerjik kontakt dermatit, deri

*Correspondence: E-mail: haticegulanlar@gmail.com, Phone: +90 543 868 56 98 ORCID-ID: orcid.org/0000-0002-3623-6176

Received: 21.06.2019, Accepted: 25.07.2019

©Turk J Pharm Sci, Published by Galenos Publishing House.

INTRODUCTION

Immunotoxic agents are xenobiotics that can initiate or exacerbate the adverse immune responses in genetically susceptible persons. Drugs and various chemicals can be classified as immunotoxic compounds.¹ When low molecular weight chemicals come into contact with the skin it can lead to contact allergy and can cause allergic contact dermatitis (ACD) if exposure exceeds the personal threshold. ACD is a more common form of immunotoxic reaction in industrialized countries.² There are more than 4000 chemicals linked to contact allergy and ACD in humans. ACD can be prevented by proper hazard identification and labeling, by characterization of potency, by investigation of human skin exposure, and by the implementation of proper risk assessment and management strategies.³

P-phenylenediamine (PPD) is used commonly in dyeing hair but it is a potential skin allergen. It is found that the mechanism of reaction to PPD is linked to its oxidation products and/or metabolites. Bandrowski's base (BB) (Figure 1), 1,4-benzoquinone, is a trimer that forms quickly upon storage of PPD and it has been suggested as the principal allergen in patients reacting to PPD.⁴

THP-1 is a human leukemia promyelocytic cell line and it has been widely used in immunotoxicology studies that investigated monocyte/macrophage functions, mechanisms, and signaling pathways. This cell line has become a suitable model to estimate the modulation of monocyte and macrophage activities and it is very well suited for *in vitro* studies of chemical allergens.⁵⁻⁷

miRNAs are a class of evolutionarily conserved, single-stranded, noncoding RNA molecules including 19-24 nucleotides that play an important role in various biological processes via regulating gene expression through affecting the transcriptional and translation processes.⁸ miRNAs have also been implicated in several inflammatory and immunological disorders as well as cancer.⁹ It was demonstrated that miR-21 and miR-155 play a significant role in the development of the immune system. miR-21 controls the apoptosis of immune cells and miR-155 is an important factor controlling lymphocyte differentiation and functions.^{10,11} Analysis of microRNAs (miRNAs) has powerful potential for the identification of novel prognostic or predictive biomarkers. Although several studies have evaluated the impact of miRNAs on immunotoxic processes and allergic skin

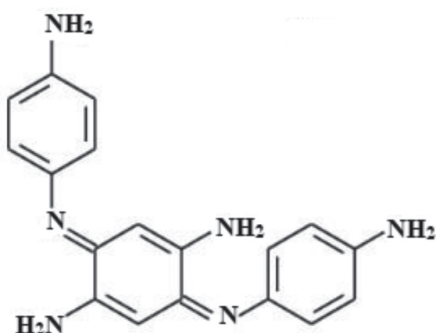


Figure 1. Chemical structure of Bandrowski's base

conditions, these studies are not sufficient to allow a conclusion to be drawn.¹² Therefore, the aim of the present study was to evaluate miRNA profiles that might play a role in chemical allergen potency.

MATERIALS AND METHODS

Cell culture and treatment

The THP-1 cell line was obtained from Istituto Zooprofilattico (Brescia, Italy). The cell culture medium (RPMI-1640) was from Euroclone Diagnostica SpA (Pero, Milano, Italy) and the other substances were from Sigma-Aldrich Co. (St. Louis, MO, USA). First of all, THP-1 cells were diluted to 10^6 cells/mL in RPMI 1640 containing 2 mM L-glutamine, 50 μ M 2-mercaptoethanol, 0.1 mg/mL streptomycin, 100 IU/mL penicillin, and 10% heated-inactivated fetal calf serum. The cells were cultured at 37°C in a 5% CO₂ incubator. The medium was changed every 2-3 days. The cells were treated with BB (Santa Cruz Biotechnology Inc., Dallas, TX, USA; CAS N° 20048-27-5) at a concentration of 1 μ g/mL in dimethyl sulfoxide (DMSO) for 24, 48, and 72 h. The dose was selected from the results of cytotoxicity assays. Cells treated with only DMSO were used as a control (0.2% final concentration).

Total RNA extraction and complementary DNA (cDNA) synthesis

For total RNA extraction, after the treatment, the cells were centrifuged for 5 min at 1200 rpm at room temperature. Then the culture medium was discarded and cell pellets lysed with 700 μ L of TRI Reagent (Sigma-Aldrich, St. Louis, MO, USA). Next, a Qiagen miRNeasy mini kit was used to extract total RNA from the cells following the manufacturer's procedure. The purity and quantity of the total RNA were analyzed with a NanoDrop instrument (NanoVue Plus). After the RNA concentrations were determined, cDNA was synthesized by using a Qiagen script miRNA polymerase chain reaction (PCR) array kit according to the manufacturer's protocol. Then 0.25 μ g and 2.0 μ g of total RNA were retrotranscribed for miRNA expression profile and real-time (RT) PCR analysis, respectively.

miRNA expression profiling

After retrotranscription, miRNA expression profiling (including 86 miRNAs) was determined with Qiagen miScript miRNA PCR Arrays following the manufacturer's procedure with an ABI Prism® 7000 Sequence Detection System. The miRNA expression profiling was done in cells treated with BB (1 μ g/mL) or DMSO as the control for 24 h. The amplification conditions consisted of an initial activation at 95°C for 15 min, then 40 cycles of denaturation at 94°C for 15 s, annealing at 55°C for 30 s, and the extension step for 30 s at 70°C. The data were analyzed with miScript miRNA PCR Arrays (<http://pcrdataanalysis.sabiosciences.com/mirna>)

Real-time PCR for detection of mature miRNA or noncoding RNA

To confirm the expression profile of miRNA, miR-155 and miR-21 were selected as immune system-associated miRNAs,

and their expression was evaluated by RT-PCR using an ABI Prism® 7000 Sequence Detection System with the same amplification conditions as miRNA expression profiling using the miScript SYBR Green PCR Kit (provided by Qiagen). Small nucleolar RNA61 (SNORD61), SNORD68, SNORD72, SNORD95, SNORD96A, and RNA, U6 small nuclear 6, pseudogene (RNU 6P) were used as endogenous miRNA controls in every reaction. All PCR reactions were performed in duplicate in a total of 25 μ L of reaction volume. In the RT-PCR assay, the evaluation was done by calculation of the fluorescent signal. The cycle threshold (Ct) was the required number of cycles for the fluorescent signal to overshoot the threshold, which means to exceed the background level. Ct levels are conversely proportional to the quantity of target nucleic acid in the sample. When normalized gene expression in the test sample is divided by normalized gene expression in the control, fold-change ($2^{-\Delta\Delta CT}$) values are obtained, with values bigger than one indicating a positive or an upregulation and less than one indicating a negative or downregulation.¹³

Statistical analysis

The data were analyzed by SPSS version 23.0 (SPSS, Chicago, IL, USA). Normal distribution and homogeneity of the variances were evaluated by Shapiro-Wilk and Levene's tests, respectively. Student's t-test was used for the comparisons and p values less than 0.05 were considered statistically significant.

RESULTS

miRNA expression profiling

The expression profile of miRNA was evaluated in THP-1 cells treated for 24 h with BB (1 μ g/mL) or DMSO as control. As shown in Figures 2 and 3, the expression of 32 miRNAs was upregulated and the expression of 31 miRNAs was downregulated in the cells after treatment with BB.

Real-time PCR for the detection of miRNAs

Following a search of the literature, we focused on miR-21 and miR-155 because these are thought to be involved in immune responses. THP-1 cells were exposed to BB (1 μ g/mL) or DMSO as a control for 24, 48, and 72 h. After miRNA extraction, miR-

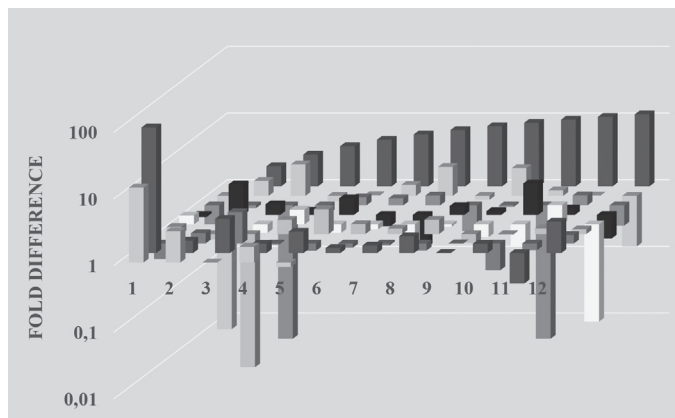


Figure 2. 3D profile of miRNA expression
miRNA: MicroRNA

21 and miR-155 levels were evaluated by RT-PCR. As shown in Figures 4 and 5, the expression of miR-21 was downregulated and the expression of miR-155 was upregulated, confirming the miRNA expression profile data.

DISCUSSION

ACD is a significant disease that occurs after topical exposure to low molecular weight chemicals.^{14,15} It is a delayed-type hypersensitivity reaction that needs previous sensitization by the same chemical.¹⁶ It is crucial to identify potential sensitizing agents because ACD is a common and serious health problem worldwide.¹⁷

It has been shown that miRNAs are involved in the processes of innate and adaptive immune systems. Among all the miRNAs, miR-21, miR-146a, and miR-155 are focused on by scientists. Signal transducer and activator of transcription-3 and nuclear factor kappa-B (NF- κ B) regulate the expression of miR-21.¹⁸ miR-155 is involved especially in proinflammatory processes. It has been observed that the expression of miR-21 is increased by

Upregulated miRNAs	Down-regulated miRNAs
hsa-miR-101-3p	hsa-miR-23a-3p
hsa-miR-223-3p	hsa-let-7g-5p
hsa-miR-30d-5p	hsa-miR-15a-5p
hsa-let-7f-5p	hsa-miR-374a-5p
hsa-miR-32-5p	hsa-miR-425-5p
hsa-miR-30a-5p	hsa-miR-320a
hsa-miR-28-5p	hsa-miR-124-3p
hsa-miR-155-5p	hsa-miR-21-5p
hsa-miR-25-3p	hsa-miR-30c-5p
hsa-miR-24-3p	hsa-miR-191-5p
hsa-miR-22-3p	hsa-let-7a-5p
hsa-miR-181a-5p	hsa-miR-210-3p
hsa-miR-125a-5p	hsa-miR-29a-3p
hsa-miR-140-3p	hsa-miR-19a-3p
hsa-miR-7-5p	hsa-miR-142-3p
hsa-miR-424-5p	hsa-let-7b-5p
hsa-miR-30b-5p	hsa-miR-93-5p
hsa-let-7i-5p	hsa-miR-27a-3p
hsa-miR-15b-5p	hsa-let-7e-5p
hsa-let-7d-5p	hsa-miR-27b-3p
hsa-let-7c-5p	hsa-miR-18a-5p
hsa-miR-126-3p	hsa-miR-16-5p
hsa-miR-23b-3p	hsa-miR-19b-3p
hsa-miR-141-3p	hsa-miR-423-5p
hsa-miR-9-5p	hsa-miR-30e-5p
hsa-miR-20a-5p	hsa-miR-106a-5p
hsa-miR-92a-3p	hsa-miR-17-5p
hsa-miR-128-3p	hsa-miR-181b-5p

Figure 3. Upregulated and downregulated miRNAs
miRNAs: MicroRNAs

vesicular stomatitis virus infection in macrophages.¹⁹ Moreover, miR-155 can suppress the SH2 domain-containing inositol-5-phosphatase that can lead to activation of Akt kinase and upregulation of interferon response genes during the cellular response to lipopolysaccharide.²⁰ In an animal study, it was demonstrated that miR-155 stimulated atherosclerosis in mice via directly suppressing B-cell lymphoma 6 protein, which is a transcription factor that attenuates NF- κ B signaling.²¹ miR-155 is also involved in the development and activation of adaptive immune cells such as effector T-cell subsets.²²

In the present study, we observed upregulation and downregulation in the expression of miR-155 and miR-21 in THP-1 cells after exposure to BB, respectively. The up- and downregulation of the miRNAs were validated by RT-PCR. Similarly, in a study by Sonkoly et al.²³ the expression of miR-155 was found to be highest in the skin samples from patients with atopic dermatitis compared to healthy controls. It was also observed that after the topical exposure of relevant allergens to nonlesional skin of atopic dermatitis patients, miR-155 expression was induced. Cytotoxic T-lymphocyte-

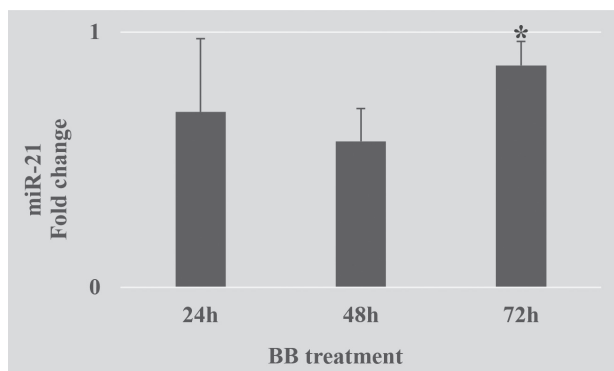


Figure 4. Expression of miR-21 in THP-1 cells following exposure to BB (1 μ g/mL) or DMSO for 24, 48, and 72 h. Fold changes in miR-21 were calculated for each sample for each time point and expressed as mean \pm standard deviation, * p <0.05 vs. control at the different time points of three independent experiments

BB: Bandrowski's base, DMSO: Dimethyl sulfoxide

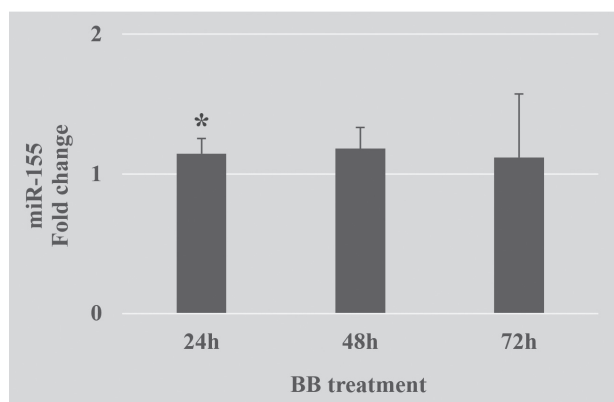


Figure 5. Expression of miR-155 in THP-1 cells following exposure to BB (1 μ g/mL) or DMSO for 24, 48, and 72 h. Fold changes in miR-155 were calculated for each sample for each time point and expressed as mean \pm standard deviation, * p <0.05 vs. control at the different time points of three independent experiments

BB: Bandrowski's base, DMSO: Dimethyl sulfoxide

associated antigen-4 (CTLA-4), a negative regulator of T-cell function, has been repressed by miR-155 and in animal models blocking of CTLA-4 stimulated a much severe allergic reaction and inflammation by increasing the number of eosinophils and immunoglobulin-E, while increases in the expression of CTLA-4 ameliorated the symptoms of allergic pulmonary inflammation in humans.^{24,25} Furthermore, in patients with atopic dermatitis miR-155 has significantly higher expression compared to in healthy subjects and the levels of expression correlated with the severity of atopic dermatitis.²⁶ In contrast to these studies, miR-155 levels were lower in sputum from allergic asthmatics than in healthy subjects.²⁷

miR-21 levels were evaluated in a number of studies. In line with the results obtained from the present study, it was shown that miR-21 was lower in monocytes from children with allergic rhinitis and in patients with metabolic syndrome.^{28,29} In contrast, in an animal study, miR-21 levels were higher in the skin of mice with contact dermatitis and in esophageal tissue in mice with eosinophilic esophagitis, which can reflect interspecies differences between mice and humans in miRNA expression.^{30,31}

In addition to their involvement in various biological processes, miRNAs have potential in disease diagnostics and therapies. Due to their stability, miRNAs could be used as biomarkers. Currently, miRNA panels are used by clinicians in order to determine the origins of cancer cells. The development of miRNA therapeutics has proved more challenging because of delivery problems. In addition, relations between gene expression and miRNAs are complex. As a result, administration or silencing of one miRNA could modify the expression of numerous genes with unknown consequences. In multifactorial diseases, successful silencing of a single gene may not be efficient in clinical practice. Therefore, there is only one miRNA drug in clinical trials (SPC3649: inhibitor/antagomir of miR-122, Santaris Pharma, Denmark) and several more are waiting to enter the clinical phase.³² From this point of view, our study has some limitations. We evaluated only the gene expression profile but protein products made from genes and other immune systems biomarkers such as interleukins and interferons should also be analyzed. These are our aims for future projects.

CONCLUSION

Our results showed that miR-155 expression was upregulated and miR-21 expression was downregulated in THP-1 cells treated with BB. It has been demonstrated that miRNAs are involved in many biological processes and they are important in the pathogenesis of allergic inflammation. However, relations between gene expression and miRNAs are complex and so further investigation of these preliminary results is needed to explain the precise functional roles of these two miRNAs in the regulation of chemical allergen potency and also their potential to serve as novel therapeutic targets.

Conflict of interest: The authors declare that they have no conflicts of interest.

REFERENCES

- Corsini E, Roggen EL. Immunotoxicology: opportunities for non-animal test development. *Altern Lab Anim*. 2009;37:387-397.
- Thyssen JP, Linneberg A, Menné T, Johansen JD. The epidemiology of contact allergy in the general population--prevalence and main findings. *Contact Dermatitis*. 2007;57:287-299.
- Galbiati V, Papale A, Marinovich M, Gibbs S, Roggen E, Corsini E. Development of an *in vitro* method to estimate the sensitization induction level of contact allergens. *Toxicol Lett*. 2017;271:1-11.
- White JM, Kullavanijaya P, Duangdeeden I, Zazzeroni R, Gilmour NJ, Basketter DA, McFadden JP. p-Phenylenediamine allergy: the role of Bandrowski's base. *Clin Exp Allergy*. 2006;36:1289-1293.
- Chanput W, Mes JJ, Wichers HJ. THP-1 cell line: an *in vitro* cell model for immune modulation approach. *Int Immunopharmacol*. 2014;23:37-45.
- Tsuchiya S, Yamabe M, Yamaguchi Y, Kobayashi Y, Konno T, Tada K. Establishment and characterization of a human acute monocytic leukemia cell line (THP-1). *Int J Cancer*. 1980;26:171-176.
- Galbiati V, Mitjans M, Corsini E. Present and future of *in vitro* immunotoxicology in drug development. *J Immunotoxicol*. 2010;7:255-267.
- Wiemer EA. miRNAs and cancer. *J RNAi Gene Silencing*. 2006;2:173-174.
- Sonkoly E, Pivarcsi A. microRNAs in inflammation. *Int Rev Immunol*. 2009;28:535-561.
- Calame K. MicroRNA-155 function in B Cells. *Immunity*. 2007;27:825-827.
- Sheedy FJ. Turning 21: Induction of miR-21 as a Key Switch in the Inflammatory Response. *Front Immunol*. 2015;6:19.
- Bartel DP. MicroRNAs: genomics, biogenesis, mechanism, and function. *Cell*. 2004;116:281-297.
- Livak KJ, Schmittgen TD. Analysis of relative gene expression data using real-time quantitative PCR and the 2(-Delta Delta C(T)) Method. *Methods*. 2001;25:402-408.
- Thyssen JP, Linneberg A, Menné T, Johansen JD. The epidemiology of contact allergy in the general population--prevalence and main findings. *Contact Dermatitis*. 2007;57:287-299.
- Peiser M, Tralau T, Heidler J, Api AM, Arts JHE, Basketter DA, English J, Diepgen TL, Fuhlbrigge RC, Gaspari AA, Johansen JD, Karlberg AT, Kimber I, Lepoittevin JP, Liebsch M, Maibach HI, Martin SF, Merk HF, Platzek T, Rustemeyer T, Schnuch A, Vandebriel RJ, R White I, Luch A. Allergic contact dermatitis: epidemiology, molecular mechanisms, in vitro methods and regulatory aspects. Current knowledge assembled at an international workshop at BfR, Germany. *Cell Mol Life Sci*. 2012;69:763-781.
- Basketter D, Darlenski R, Fluhr JW. Skin irritation and sensitization: mechanisms and new approaches for risk assessment. *Skin Pharmacol Physiol*. 2008;21:191-202.
- Papale A, Kummer E, Galbiati V, Marinovich M, Galli CL, Corsini E. Understanding chemical allergen potency: role of NLRP12 and Blimp-1 in the induction of IL-18 in human keratinocytes. *Arch Toxicol*. 2017;91:1783-1794.
- Iliopoulos D, Jaeger SA, Hirsch HA, Bulyk ML, Struhl K. STAT3 activation of miR-21 and miR-181b-1 via PTEN and CYLD are part of the epigenetic switch linking inflammation to cancer. *Mol Cell*. 2010;39:493-506.
- Wang P, Hou J, Lin L, Wang C, Liu X, Li D, Ma F, Wang Z, Cao X. Inducible microRNA-155 feedback promotes type I IFN signaling in antiviral innate immunity by targeting suppressor of cytokine signaling 1. *J Immunol*. 2010;185:6226-6233.
- O'Connell RM, Chaudhuri AA, Rao DS, Baltimore D. Inositol phosphatase SHIP1 is a primary target of miR-155. *Proc Natl Acad Sci U S A*. 2009;106:7113-7118.
- Nazari-Jahantigh M, Wei Y, Noels H, Akhtar S, Zhou Z, Koenen RR, Heyll K, Gremse F, Kiessling F, Grommes J, Weber C, Schober A. MicroRNA-155 promotes atherosclerosis by repressing Bcl6 in macrophages. *J Clin Invest*. 2012;122:4190-4202.
- Rodriguez A, Vigorito E, Clare S, Warren MV, Couttet P, Soond DR, van Dongen S, Grocock RJ, Das PP, Miska EA, Vetrie D, Okkenhaug K, Enright AJ, Dougan G, Turner M, Bradley A. Requirement of bic/microRNA-155 for normal immune function. *Science*. 2007;316:608-611.
- Sonkoly E, Janson P, Majuri ML, Savinko T, Fyhrquist N, Eidsmo L, Xu N, Meisgen F, Wei T, Bradley M, Stenvang J, Kauppinen S, Alenius H, Lauerma A, Homey B, Winqvist O, Ståhle M, Pivarcsi A. MiR-155 is overexpressed in patients with atopic dermatitis and modulates T-cell proliferative responses by targeting cytotoxic T lymphocyte-associated antigen 4. *J Allergy Clin Immunol*. 2010;126:581-9.e20.
- Hellings PW, Vandenberghe P, Kasran A, Coorevits L, Overbergh L, Mathieu C, Ceuppens JL. Blockade of CTLA-4 enhances allergic sensitization and eosinophilic airway inflammation in genetically predisposed mice. *Eur J Immunol*. 2002;32:585-594.
- Abrams JR, Lebwohl MG, Guzzo CA, Jegasothy BV, Goldfarb MT, Goffe BS, Menter A, Lowe NJ, Krueger G, Brown MJ, Weiner RS, Birkhofer MJ, Warner GL, Berry KK, Linsley PS, Krueger JG, Ochs HD, Kelley SL, Kang S. CTLA4lg-mediated blockade of T-cell costimulation in patients with psoriasis vulgaris. *J Clin Invest*. 1999;103:1243-1252.
- Ma L, Xue HB, Wang F, Shu CM, Zhang JH. MicroRNA-155 may be involved in the pathogenesis of atopic dermatitis by modulating the differentiation and function of T helper type 17 (Th17) cells. *Clin Exp Immunol*. 2015;181:142-149.
- Lu TX, Munitz A, Rothenberg ME. MicroRNA-21 is up-regulated in allergic airway inflammation and regulates IL-12p35 expression. *J Immunol*. 2009;182:4994-5002.
- Chen RF, Huang HC, Ou CY, Hsu TY, Chuang H, Chang JC, Wang L, Kuo H-C, Yang KD. MicroRNA-21 expression in neonatal blood associated with antenatal immunoglobulin E production and development of allergic rhinitis. *Clin Exp Allergy*. 2010;40:1482-1490.
- He QF, Wang LX, Zhong JM, Hu RY, Fang L, Wang H, Gong WW, Zhang J, Pan J, Yu M. Circulating MicroRNA-21 is Downregulated in Patients with Metabolic Syndrome. *Biomed Environ Sci*. 2016;29:385-389.
- Vennegaard MT, Bonefeld CM, Hagedorn PH, Bangsgaard N, Løvendorf MB, Odum N, Woetmann A, Geisler C, Skov L. Allergic contact dermatitis induces upregulation of identical microRNAs in humans and mice. *Contact Dermatitis*. 2012;67:298-305.
- Lu TX, Sherrill JD, Wen T, Plassard AJ, Besse JA, Abonia JP, Franciosi JP, Putnam PE, Eby M, Martin LJ, Aronow BJ, Rothenberg ME. MicroRNA signature in patients with eosinophilic esophagitis, reversibility with glucocorticoids, and assessment as disease biomarkers. *J Allergy Clin Immunol*. 2012;129:1064-75.e9.
- Hydbring P, Badalian-Very G. Clinical applications of microRNAs. *F1000Res*. 2013;2:136.



Toxicological Evaluation of Bisphenol A and Its Analogues

Bisfenol A ve Analoglarının Toksikolojik Değerlendirilmesi

İrem İYİGÜNDOĞDU¹, Aylin ÜSTÜNDAĞ^{2*}, Yalçın DUYDU²

¹Gazi University Faculty of Pharmacy, Department of Toxicology, Ankara, Turkey

²Ankara University Faculty of Pharmacy, Department of Toxicology, Ankara, Turkey

ABSTRACT

Bisphenol A (BPA) is known as one of the oldest synthetic compounds with endocrine disrupting activity. It is commonly used in the production of epoxy resins, polycarbonates, dental fillings, food storage containers, baby bottles, and water containers. BPA is associated with various health problems such as obesity, diabetes, chronic respiratory diseases, cardiovascular diseases, renal diseases, behavior disorders, breast cancer, tooth development disorders, and reproductive disorders. Increasing health concerns have led the industry to seek alternatives to BPA. As BPA is now being excluded from several consumer products, the use of alternative compounds is increasing. However, the chemicals used to replace BPA are also BP analogues and may have similar or higher toxicological effects on organisms. The aim of this review is to focus on the toxicological profiles of different BP analogues (i.e. BPS and BPF) which are increasingly used today as alternative to BPA.

Key words: Bisphenols, bisphenol A, endocrine disruptor, bisphenol S, bisphenol F

ÖZ

Bisfenol A (BPA) endokrin aktiviteye sahip bilinen en eski bileşiklerden biridir. BPA epoksi reçineler, polikarbonatlar, diş dolguları, yemek saklama kapları, bebek biberonları ve su bidonlarının üretiminde yaygın olarak kullanılmaktadır. BPA obezite, diyabet, kronik solunum hastalıkları, kardiyovasküler hastalıklar, renal hastalıklar, davranış bozuklukları, meme kanseri, diş gelişimi bozuklukları ve üreme bozuklukları gibi çeşitli sağlık sorunlarıyla ilişkilendirilmiştir. Artan sağlık endişeleri endüstriyi BPA alternatifleri aramaya yönlendirmiştir. Günümüzde BPA tüketici ürünlerinden çıkarılmaya başlandığı için, alternatif bileşiklerin kullanımı artmaktadır. Ancak, BPA yerine kullanılan kimyasallar da BP analoglarıdır ve organizmalar üzerinde benzer toksikolojik etkileri olabilir. Bu derlemenin amacı günümüzde BPA'ya artan miktarlarda alternatif olarak kullanılan BP analoglarının (BPS ve BPF) toksikolojik profillerine odaklanmaktır.

Anahtar kelimeler: Bisfenoller, bisfenol A, endokrin bozucu, bisfenol S, bisfenol F

INTRODUCTION

Endocrine disruptors, such as pesticides and bisphenol A (BPA), can be defined as exogenous substances that cause different levels of changes in the evolution and function of the endocrine system.¹

BPs are a class of chemicals known as diphenylmethanes. BPs contain two benzene rings separated by a central carbon atom. They mostly have 4-OH substitutes on both benzene rings. Some BPs may have a sulfone group or a sulfide instead of a central carbon atom.²

Regulations and increasing concerns among the public have led the industry to seek alternatives for BPA, and as BPA has begun to be excluded from products due to consumer concern the use of alternative BPs has increased and BPA has begun to be replaced by its chemical analogues.³⁻⁶

The chemicals used to replace BPA also have BP structures and may have similar effects on organisms.⁵ According to research, BPA analogues may result in toxic effects similar to or greater than those of BPA.⁴

Bisphenol

The chemical nomenclature of BPA is 2,2-bis (4-hydroxyphenyl) propane and it has a molecular weight of 228.29 g/mol.^{4,7,8} If its physical properties are examined it is seen that it has water solubility of approximately 120-130 ppm, low volatility, low air emission, and a short photooxidation half-life (<7 h).¹⁸

BPA is known as one of the oldest synthetic compounds with endocrine activity and was first discovered by Dianin in 1891.¹⁹ It is one of the chemicals produced in the largest quantities in the world, with an estimated 5-6.8 million tons produced per year, and it is used in a wide range of areas.^{1,4,10} While 70% of the BPA

*Correspondence: E-mail: dur@pharmacy.ankara.edu.tr, Phone: +90 312 203 32 36 ORCID-ID: orcid.org/0000-0002-8449-1358

Received: 02.08.2019, Accepted: 12.09.2019

©Turk J Pharm Sci, Published by Galenos Publishing House.

produced is used in the production of polycarbonate plastics, 25% is used in the production of epoxy resins.¹⁰

BPA is commonly used in the production of epoxy resins, polycarbonates, baby bottles, food storage containers, dental fillings, and water containers.^{2,8} BPA is also seen in thermographic and pressure-sensitive paper, bank notes, receipts, and toys.^{3,6,8} In addition, it is used in medical devices and health care services such as eye lenses, newborn incubators, and nebulizers.¹

BPA exposure mainly occurs through food.⁴ BPA contamination in foods usually happens as a result of migration from containers including it.¹⁰ Exposure is caused by consuming food and beverages in recycled bottles, cans covered with epoxy resins, and polycarbonate containers that BPA has leaked into.¹ Environmental factors such as temperature, heat, and acidity increase the hydrolysis of ester bonds that bond BPA molecules to epoxy resins and polycarbonates. BPA leakage in polycarbonates happens more often to solutions with low pH values, whereas in epoxy resins higher temperature increases BPA leakage.¹ When exposure concentrations are examined it is seen that in solid canned food mean concentrations of exposure vary from 10 $\mu\text{g kg}^{-1}$ to 70 $\mu\text{g kg}^{-1}$, whereas in liquid canned food they range from 1 $\mu\text{g L}^{-1}$ to 23 $\mu\text{g L}^{-1}$.² Fish, dairy products, meat, canned vegetables, and baby food are examples of goods that may contain BPA.¹⁰ The specific migration limit of BPA is determined as 0.6 mg/kg in the 2002/72/EC Commission Directive and in the Turkish Food Codex.¹⁰

In addition to the sources of exposure mentioned above, dust may also cause significant exposure by inhalation of indoor dust and thermal paper may cause transdermal exposure from the skin.^{4,9,11,12} Dental composite resins may also cause BPA to leak into saliva.¹ Other than these, sources such as water sources in nature, tap water, air, and medical devices are examples of sources of exposure.^{1,11} BPA used in epoxy-based floor materials, adhesives, paints, and electronic devices is another source of exposure.¹ BPA is detected in blood, urine, and sweat in humans.¹¹

Generally it is suggested that BPA is bioactivated by oxidation reactions catalyzed by cytochrome P450 and detoxified by glucuronidation reactions and sulfation reactions. It is shown that the toxic effects of BPA decrease in the presence of ADH, ALDH2, and SULT1E1 and increase in the presence of CYP2E1.¹³

The main mechanism of the toxic effects induced by BPA is endocrine disruption. This property may cause both developmental and reproductive disorders.² BPA is associated with obesity, diabetes, breast cancer, cardiovascular diseases, renal diseases, chronic respiratory diseases, tooth development disorders, behavior disorders, and reproductive disorders.^{9,14}

It is shown in the literature that a low dose of BPA has a negative impact on the endocrine system and may lead to primary endocrine disorders.^{1,10} It affects the cell signaling pathways.¹³ It is reported to have effects on the central nervous system, cardiovascular system, immune system, respiratory system, and renal system.^{1,10} It may be associated with thyroid hormone function disorders.¹⁰ After exposure birth defects may be seen.¹

Pregnant women and fetuses are very sensitive to pathologies induced by BPA due to its penetration of the placenta barrier.¹³ In other research it was shown that BPA can pass to the fetus from the mother and can cause behavior changes and anomalies in the reproductive organs of the fetus.¹⁰ In addition to the effects mentioned above, it is suggested that BPA has mutagenic and genotoxic potential.³

BPA can both bind to $\text{Er}\alpha$ and $\text{Er}\beta$ receptors and affect them by either activating or suppressing their expression.¹⁷ Its relative binding affinity is predicted to be 1000-10,000 times lower than that of estradiol and it is classified as a weak environmental estrogen.⁷

BPA can act as a potential antagonist of endocrine receptors in some cases.⁸ Infertility in men and women, early puberty, and Polycystic Ovary syndrome can be given as examples of endocrine disorders in which BPA plays a pathogenic role.⁸ In addition, it is reported to be associated with low sperm count and motility, spontaneous abortion, and metabolic changes.¹³ When its effects on the reproduction system are examined it is seen that the main target is ovarian granulosa cells. The disruption of these cells by BPA can play an important role in fertility.¹² Based on its effect on the androgen receptor, BPA is a known antagonist.¹⁵

The chemical structures of BPA and thyroid hormone have similarities. BPA has a property of binding to thyroid receptors competitively with thyroid hormone. It is seen to disrupt gene expression by thyroid receptors *in vivo* and *in vitro*.¹⁴

In addition to the mentioned effects, it is observed that BPA activates PXR from nuclear receptors and induces CYP3A4, environmental exposure to BPA can change 25-hydroxy vitamin D level in circulation in adults, and there is a negative correlation between BPA and 25 (OH) D.¹⁶

In other research, it was shown that BPA induces DNA damage in ER-positive MCF-7 cells and its genotoxicity is ER-dependent. It is observed that it induces micronucleus frequencies and chromosomal aberrations in rat bone marrow and causes DNA damage in lymphocytes. In a different study it was suggested that oxidative stress occurs by an increase in 8-hydroxyguanosine plasma levels and in LPO, and reduced glutathione activity in the liver.²

There are controversial results regarding the genotoxicity of BPA. Even though it is found to be negative according to basic genotoxicity tests, research shows that it induces chromosomal aberrations and morphological changes in Syrian hamster embryo (SHE) cells, achromatic lesions and c-mitotic effects in mice bone marrow, its metabolites bind to DNA in SHE cells and rodent liver, and it causes DNA damage in ER-positive MCF-7.² Another study revealed that BPA causes ER-dependent DNA damage by inducing strand breaks in ER-positive MCF-7 cells.⁴ Vahdati Hassani et al.⁷ showed that protein and phosphoprotein levels involved in biological processes related to fatty liver, hepatotoxicity, and carcinoma are affected by BPA exposure. It is also found that BPA induces oxidative stress, an increase in malondialdehyde, and a decrease in glutathione (GSH).⁷

In 2008 concerns about the effects of current BPA exposure in fetuses, adults, and children on brain, behavior, and reproduction were declared in the report by the National Toxicology Program and in 2010 the FDA reported that they shared the same concerns.¹

BPA is banned in Japan, Canada, and most of US. In 2011 the EU forbade the production, marketing, and import of baby bottles containing BPA.² In Turkey baby bottles and other food containers with BPA were collected by the Ministry of Agriculture in 2011.¹

Bisphenol S

BPS is an important analogue of BPA in industrial applications and an increasingly used alternative.⁶ The chemical nomenclature of BPS is bis (4-hydroxyphenyl) sulfone and it has a molecular weight of 250.27 g/mol.^{3,16} BPS is a heat-resistant structural analogue of BPA.¹⁶ It has high thermal stability and is resistant to sunlight.^{16,17}

BPS is mostly used in several consumer products as a replacement for BPA. As the most commonly used alternative to BPA, BPS is commonly used in the production of thermal paper and plastics.^{3,17}

BPS is used as an improver in thermal paper and a stabilizer in canned soft drinks and canned food.^{6,16} In addition, it is used as an electroplating solvent, a fastening agent in cleaning products, and a constituent of epoxy resins in various industrial applications.⁵ As a commonly used analogue of BPA in production, the presence of BPS in nature and food is demonstrated in numerous studies.⁴ It was shown by the National Health and Nutrition Examination Survey that significant concentrations of BPS were detected in canned food, especially in canned vegetables and mushrooms.⁴ In addition, literature findings have shown that significant exposure occurs through dust.⁴ Moreover, the presence of BPS is detected in mud, water, tap water, and sewage.^{5,6,11} In a previous study, BPS was detected in dust samples from various microenvironments and many products produced from thermal paper.¹¹ BPS was detected in human tissues as well.⁶ BPS was found in human urine in concentrations and frequencies comparable to those of BPA.⁵ Especially after its detection in human urine, concerns about its safety were expressed.¹⁶

In addition to the types of exposure mentioned above, BPS was detected in many daily products. These products include personal care products, paper products, and food, with examples such as hair products, toothpaste, currency, mailing envelopes, dairy products, canned food, and cereals.⁵

Skledar et al.¹⁷ showed that glucuronidation is the main pathway in the metabolism and detoxification of BPS and UGT1A9 plays an important role in this process.¹⁷

Cumulative evidence suggests that BPS is toxic to organisms because its chemical structure is similar to that of BPA. Recently it was reported that, similar to BPA, BPS promotes estrogenic activity, proarrhythmic effects, and hypothalamic neurogenesis *in vitro* in cell cultures and in animals *in vivo*. When the estrogenic effects of BPA and BPS were compared in a study it was shown that the genomic estrogenic activity of 40

µM BPS is 15 times lower than that of BPA. It has toxic effects in the rat's endocrine system, adult zebra fish, breast cancer cells, and ovariectomized mice.⁶

BPS is stated to have toxic effects on the endocrine system similar to BPA in the literature.⁴ In other research it was reported that isopropylation of the 4-hydroxy group decreases BPS's estrogenic activity.¹⁷ BPS is also defined as a weak antiandrogenic compound.¹⁶

BPS exposure in zebra fish larvae suggests that oxidative stress parameters and interference of immune response is induced.⁶ In other research it was demonstrated that BPS inhibits pepsin activity, increases reactive oxygen species (ROS) levels in rats, induces lipid peroxidation (LPO), and decreases antioxidant enzyme activity.¹¹

Furthermore, a recent study suggested a link between BPS exposure and obesity and steatosis. It was shown in an *in vivo* study that BPS may alter brain functions in mammals.¹⁷

In addition to the effects mentioned above when its genotoxic potential is examined, a study showed results on BPS exposure and genotoxicity including double strand breaks; however, it is seen that BPS has weaker genotoxic potential compared to BPA.^{3,4} In a study in HepG2 cells it was seen that BPA and BPS cause a significant increase in DNA damage.² Moreover, BPS had effects on hepatic cells, bound to serum albumins, and caused DNA damage.⁵

When the association between BPS and thyroid hormone receptors is examined, it is seen that, similarly to BPA, it binds to thyroid hormone receptors. BPS can bind to both TR α and TR β but its affinity to TR β is higher.¹⁴ In other research, in zebra fish embryos exposed to BPS at concentrations of 10 and 100 µg/L for 75 days, triiodothyronine and thyroxine plasma levels were decreased.¹⁶

BPS exposure caused acute toxicity in *Daphnia magna*, induced uterine growth in rats, and in zebra fish it decreased the weight of gonads, altered plasma estrogen and testosterone, and caused reproductive disorders; it also increased the female ratio over males, decreased the body length, and caused changes in testosterone, estradiol, and vitellogenin concentrations and reproductive disorders.⁵ In nongenomic signal research BPS has a similar potency to BPA. From femtomolar to picomolar concentrations, BPS induced Er α modulated pathways and activities such as membrane MAPK signaling, cell proliferation, and caspase 8 activation. These fast, nongenomic pathways have an important role in optimal cell function, and modulation of proliferation and apoptosis, beside activities such as pancreatic cell function and estrogen-modulated brain function.⁵

Bisphenol F

As an important and increasingly used analogue of BPA, the chemical nomenclature of BPF is 1,1-bis (4-hydroxyphenyl) methane and its molecular weight is 200.23 g/mol.^{3,4,6} BPF is used in the production of polycarbonate resin.² In addition, BPF is used especially in systems that require increasing thickness and durability such as epoxy resins and coatings.⁶

Storage and pipe coatings, industrial floors, structural adhesives, bridge and road deck toppings, electrical varnishes, grouts, and coatings are examples of these systems. In addition, for different consumer products such as water pipes, plastics, food packaging, dental sealants, lacquers, adhesives, varnishes, and liners BPF epoxy resins are used.⁵

Even though it is more biodegradable under aerobic and anaerobic conditions compared to BPA, BPF has become an ubiquitous environmental contaminant.^{2,4} BPF has been detected in nature and food.⁴ The presence of BPF is reported in mud, tap water, indoor dust, water, sewage, and human tissues.^{6,11} In a recent study it was found in dust samples from various microenvironments and many products from thermal paper.¹¹

A recent study showed that this compound accumulates in human urine.⁴ BPF is also detected in personal care products such as lotions and toothpaste, paper products such as tickets and envelopes, and foods such as canned food and cereals.⁵ Active BPF is distributed in many tissues including the placenta, uterus, fetus, and amniotic fluid. The primary elimination form of BPF is seen to be sulfate conjugate.⁵

So far evidence has suggested that, just like BPS, because of its similar chemical structure, BPF is toxic to organisms as BPA is. In studies BPF is reported to cause mild to moderate acute toxicity and weak estrogenic activity.⁶ In *in vivo* studies it is demonstrated to be estrogenic, androgenic, and thyroidogenic, while *in vitro* studies show that it is estrogenic, androgenic, and has other physiological/biochemical effects. There are studies showing that BPF exposure induces uterine growth in rats, which points to estrogenic activity.⁵ Studies show that BPF causes more potent estrogenicity compared to BPA.⁴

BPF exposure causes an increase in thyroid weight and changes in thyroid hormone concentrations.⁵ According to another study BPF can bind to both TR α and TR β , but its affinity to TR β is higher.¹⁴

Furthermore, it causes changes in hematological parameters and enzyme expression. BPF has also shown other *in vitro* effects such as chromosomal aberrations, cytotoxic effects, DNA damage, and cellular dysfunction and decreased *in vitro* adiponectin production and release.⁵

BPF is reported to promote estrogenic activity comparable to BPA, proarrhythmic effects, and hypothalamic neurogenesis *in vitro* in cell lines and *in vivo* in animals. In addition, as a result of BPF exposure concentration-dependent increases in ROS content, nitric oxide and inducible nitric oxide synthase production, superoxide dismutase levels, T-AOC activity, LPO levels, and cytokine and chemokine expression in zebra fish larvae suggest that immune response and oxidative stress in fish are induced.⁶

BPF is reported to result in genotoxic damage that might interfere with DNA replication. In another study it was seen that BPF has weaker genotoxic potential compared to BPA.³ When the genotoxic effects of BPF are examined it is reported that BPF induces DNA damage but does not induce micronuclei frequencies in HepG2 cells. A recent study suggested that the

genotoxic effect of BPF depends on the metabolic capacity of the cell.²

Bisphenol AF

The chemical nomenclature of BPAF is 2,2-bis(4-hydroxyphenyl) hexafluoropropane and its molecular weight is 336.23 g/mol.^{3,4} It is used in the production of polycarbonate resin, is a component of certain plasters, and is used as a rubber bridging material.²

BPAF is detected in the environment, tap water, bottled water, and canned food.^{4,11} In a recent study it was shown that it accumulates in human urine.⁴

When the effects of BPAF are examined, it is seen that BPAF causes more potent toxicity in cells including blood cells. In addition, in the literature it is demonstrated that BPAF binds more strongly to estrogen receptors and has more effects on gene expression compared to BPA. It is also demonstrated that BPAF presents genotoxic and neurotoxic potential.⁴

In their study Mokra et al.⁴ stated that BPA and BPAF have the highest genotoxic potential in incubated cells and they previously reported that BPA and BPAF induced the formation of ROS in peripheral mononuclear blood cells more potently and only BPAF caused a significant increase in OH levels in these cells.⁴ In other studies it was demonstrated that BPAF in high concentrations causes more potent DNA damage in MCF-7 cells compared to BPA. It is also reported to form micronuclei in V79 cells and induce aneuploidy in SHE cells.^{2,4} While causing metaphase arrest in V79 cells, it also causes morphological changes in SHE cells along with aneuploidy.²

In mammalian cells BPAF did not induce chromosomal aberration or gene mutation. Since toxicity data are insufficient and it has a similar structure to BPA, BPAF has been nominated for toxicological characterization by the US NIEHS.²

Bisphenol Z

The chemical nomenclature of BPZ is 1,1-bis(4-hydroxyphenyl) cyclohexane. BP compounds including BPZ have been found in different environmental and human samples. It is reported in different studies that concentrations of BPs in municipal waste water influents and effluents, sewage sludge, water, and sediments are elevated.¹⁸

BPZ may be used in the synthesis of an anesthetic compound.¹⁹ Another area of use of BPZ is to cure highly heat resistant plastic materials and in electrical insulation. Several analogues of BPA, including BPF, BPS, and BPZ, are used in personal care products, food packaging materials, and paper products.²⁰

Schmidt et al.¹⁹ showed that BPZ was biotransformed in highest level of mobility (HLM) in a manner similar to the case of BPAF. According to their research based on the peak areas, hydroxylated BPZ was the main *in vitro* metabolite in HLM in the presence of nicotinamide adenine dinucleotide phosphate and GSH.¹⁹

In their study, Lee et al.²¹ reported that BPZ exposure caused a decrease with varying changes in T3 and T4 levels. Kovačić et al.¹⁸ stated that UV exposure is an effective way of removing

BPF, BPS, and BPZ from water, showing the fastest degradation rate in the case of the photo-Fenton reaction.¹⁸

OTHER BISPHENOLS

The chemical nomenclature of BPC is 2,2-bis (4-hydroxy-3-methylphenyl) propane, of BPM is 4,4'-(1,3-phenylenedii sopropilidene) BP, of BPAP is 4,4'-(1-phenylethylidene) BP, of BPP is 4,4'-(1,4-phenylenedii sopropilidene) bisphenol, and of bisphenol 1 is [sulfonylbis(4,1-phenylene)] bis (oxy) dimethanol.^{2,3} The molecular weight of BPAP is 290.36 g/mol, of BPC is 256.34 g/mol, of BPM is 346.46 g/mol, and of BPP is 346.46 g/mol.³

According to the study by Lee et al.³ some BPs including BPAP, BPM, and BPP showed greater genotoxic potential compared to BPA. BPP is reported to have the greatest genotoxic potency and is suggested to have an association with double strand breaks.³

BP-1 is reported to be a component of polymer bottles. Polybutylene terephthalate modified by BP-1 is seen to improve glass transmission temperature and thermal stability.²

In their research Fic et al.² demonstrated that BPA, BPAF, BPF, BPS, BPZ, BP-1, BP-2, DMBPA, and DMBPS are not mutagenic in the Ames test; however, DMBPA, BP-2, BPZ, and BPAF have toxic effects on *Salmonella typhimurium*.²

Risk Assessment

The current lowest-observable-adverse-effect level of BPA is determined as 50 mg/kg bodyweight per day by the US EPA.²² In hazard assessment protocol by the EFSA it is indicated that the current temporary tolerable daily intake (t-TDI) for BPA is 4 µg/kg bw per day.²³ Mikołajewska et al.²⁴ reported that dietary BPA exposure in children is 1.088-4.492 µg/day, exposure to BPA in 3-month-old infants fed from polycarbonate bottles is 4-11 µg/kg b.w./day, dietary exposure (canned food and beverages) in adults is 1.56-10.453 µg/day, daily exposure to BPA through inhalation is 0.008-0.014 µg/person/day, exposure to BPA from thermal paper is 71 µg/day (exposure by 10 h/day), and exposure from paper currency is 0.0001-1.41 ng/day.²⁴ These data suggest that both children and adults may be exposed to BPA higher than the t-TDI mainly by dietary exposure and might result in toxic health outcomes. Although a t-TDI was not found for BP analogues, Wu et al.²⁵ reported the following values for BP analogues in foodstuffs: BPS <0.01 ng/g, BPA 0.125 ng/g, BPF <0.05 ng/g, BPP <0.025 ng/g, and BPAF <0.01 ng/g in the US between 2008 and 2012, which shows the other analogues to be lower than BPA.²⁵

CONCLUSION

BPA is a widely produced and commonly used chemical. Due to its endocrine disrupting nature, it is associated with many diseases and disorders such as diabetes, breast cancer, obesity, cardiovascular diseases, renal diseases, chronic respiratory diseases, behavior disorders, thyroid hormone function disorders, tooth development disorders, and reproductive disorders. The respiratory system, central nervous system,

cardiovascular system, immune system, and renal system are shown to be affected by BPA. It is also suggested that BPA has genotoxic and mutagenic potentials. Due to its toxic health effects, the use of alternative BPs has increased and BPA has been replaced by its chemical analogues such as BPS, BPF, BPAF, and BPZ. However, these replacing analogues are also BPs and it is suggested that they may pose similar or higher health risks for living organisms. In research BPS is reported to promote estrogenic activity, antiandrogenic activity, proarrhythmic effects, and hypothalamic neurogenesis in cell lines and to possess a potential of endocrine disruption similar to BPA. BPF is demonstrated to be estrogenic, androgenic, and thyroidogenic. BPAF is reported to cause more potent toxicity in cells, binding more strongly to estrogen receptors, and have more effect on gene expression compared to BPA, in addition to its neurotoxic and genotoxic potential. BPZ and other BPs also have structures similar to BPA and may show similar toxic effects. Therefore, it is important to examine the toxicological profile of these compounds and focus on risk assessment of BPA analogues to estimate the relationship between exposure and toxic outcomes. Further studies especially in humans are needed to shed light on the risk from BPA analogues.

Conflicts of interest: No conflict of interest was declared by the authors. The authors alone are responsible for the content and writing of this article.

REFERENCES

1. Ayazgök B, Tüylü Küçükkılınc T. Düşük Doz Bisfenol A'nın Büyük Etkileri. *FABAD J Pharm Sci.* 2017;42:139-150.
2. Fic A, Žegura B, Sollner Dolenc M, Filipič M, Peterlin Mašič L. Mutagenicity and DNA damage of bisphenol A and its structural analogues in HepG2 cells. *Arh Hig Rada Toksikol.* 2013;64:189-200.
3. Lee S, Liu X, Takeda S, Choi K. Genotoxic potentials and related mechanisms of bisphenol A and other bisphenol compounds: a comparison study employing chicken DT40 cells. *Chemosphere.* 2013;93:434-440.
4. Mokra K, Kuźmińska-Surowanec A, Woźniak K, Michałowicz J. Evaluation of DNA-damaging potential of bisphenol A and its selected analogs in human peripheral blood mononuclear cells (*in vitro* study). *Food Chem Toxicol.* 2017;100:62-69.
5. Rochester JR, Bolden AL. Bisphenol S and F: A Systematic Review and Comparison of the Hormonal Activity of Bisphenol A Substitutes. *Environ Health Perspect.* 2015;123:643-650.
6. Qiu W, Shao H, Lei P, Zheng C, Qiu C, Yang M, Zheng Y. Immunotoxicity of bisphenol S and F are similar to that of bisphenol A during zebrafish early development. *Chemosphere.* 2018;194:1-8.
7. Vahdati Hassani F, Abnous K, Mehri S, Jafarian A, Birner-Gruenberger R, Robati RY, Hosseinzadeh H. Proteomics and phosphoproteomics analysis of liver in male rats exposed to bisphenol A: Mechanism of hepatotoxicity and biomarker discovery. *Food Chem Toxicol.* 2018;112:26-38.
8. Kazemi S, Mousavi Kani SN, Rezazadeh L, Pouramir M, Ghasemi-Kasman M, Moghadamnia AA. Low dose administration of Bisphenol A induces liver toxicity in adult rats. *Biochem Biophys Res Commun.* 2017;494:107-112.

9. Eladak S, Grisin T, Moison D, Justine Guerquin M, N'Tumba-Byn T, Pozzi-Gaudin S, Benachi A, Livera G, Rouiller-Fabre V, Habert R. A new chapter in the bisphenol A story: bisphenol S and bisphenol F are not safe alternatives to this compound. *Fertil Steril*. 2015;103:11-21.
10. Er B, Sarımehtemtoğlu B. Gıdalarda bisfenol A varlığının değerlendirilmesi. *Vet Hekim Der Derg*. 2011;82:69-74.
11. Maćczak A, Cyrkler M, Bukowska B, Michałowicz J. Bisphenol A, bisphenol S, bisphenol F and bisphenol AF induce different oxidative stress and damage in human red blood cells (*in vitro* study). *Toxicol In Vitro*. 2017;41:143-149.
12. Molina AM, Abril N, Morales-Prieto N, Monterde JG, Lora AJ, Ayala N, Moyano R. Evaluation of toxicological endpoints in female zebrafish after bisphenol A exposure. *Food Chem Toxicol*. 2018;112:19-25.
13. Lee DW, Oh WY, Yi SH, Ku B, Lee MY, Cho YH, Yang M. Estimation of bisphenol A-Human toxicity by 3D cell culture arrays, high throughput alternatives to animal tests. *Toxicol Lett*. 2016;259:87-94.
14. Zhang YF, Ren XM, Li YY, Yao XF, Li CH, Qin ZF, Guo LH. Bisphenol A alternatives bisphenol S and bisphenol F interfere with thyroid hormone signaling pathway *in vitro* and *in vivo*. *Environ Pollut*. 2018;237:1072-1079.
15. Perera L, Li Y, Coons LA, Rene H, van Beuningen R, Goodwin B, Auerbach SS, Teng CT. Binding of bisphenol A, bisphenol AF, and bisphenol S on the androgen receptor: Coregulator recruitment and stimulation of potential interaction sites. *Toxicol In Vitro*. 2017;44:287-302.
16. Zenata O, Dvorak Z, Vrzal R. Profiling of bisphenol S towards nuclear receptors activities in human reporter cell lines. *Toxicol Lett*. 2017;281:10-19.
17. Skledar DG, Schmidt J, Fic A, Klopčič I, Trontelj J, Dolenc MS, Finel M, Mašič LP. Influence of metabolism on endocrine activities of bisphenol S. *Chemosphere*. 2016;157:152-159.
18. Kovačič A, Gys C, Kosjek T, Covaci A, Heath E. Photochemical degradation of BPF, BPS and BPZ in aqueous solution: Identification of transformation products and degradation kinetics. *Sci Total Environ*. 2019;664:595-604.
19. Schmidt J, Kotnik P, Trontelj J, Knez Ž, Mašič LP. Bioactivation of bisphenol A and its analogs (BPF, BPAF, BPZ and DMBPA) in human liver microsomes. *Toxicol In Vitro*. 2013;27:1267-1276.
20. Lee S, Kim C, Shin H, Kho Y, Choi K. Comparison of thyroid hormone disruption potentials by bisphenols A, S, F, and Z in embryo-larval zebrafish. *Chemosphere*. 2019;221:115-123.
21. Lee J, Kim S, Choi K, Ji K. Effects of bisphenol analogs on thyroid endocrine system and possible interaction with 17 β -estradiol using GH3 cells. *Toxicol In Vitro*. 2018;53:107-113.
22. Mileva G, Baker SL, Konkle AT, Bielajew C. Bisphenol-A: epigenetic reprogramming and effects on reproduction and behavior. *Int J Environ Res Public Health*. 2014;11:7537-7561.
23. European Food Safety Authority (EFSA), Gundert-Remy U, Bodin J, Bosetti C, FitzGerald R, Hanberg A, Hass U, Hooijmans C, Rooney AA, Rousselle C, van Loveren H, Wölfle D, Barizzone F, Croera C, Putzu C, Castoldi AF. Bisphenol A (BPA) hazard assessment protocol. 2017;14:1354E.
24. Mikołajewska K, Stragierowicz J, Gromadzińska J. Bisphenol A - Application, sources of exposure and potential risks in infants, children and pregnant women. *Int J Occup Med Environ Health*. 2015;28:209-241.
25. Wu LH, Zhang XM, Wang F, Gao CJ, Chen D, Palumbo JR, Guo Y, Zeng EY. Occurrence of bisphenol S in the environment and implications for human exposure: A short review. *Sci Total Environ*. 2018;615:87-98.